PATTERN FORMATION IN REACTION-DIFFUSION MODELS FAR FROM THE TURING REGIME

by

THEODORE KOLOKOLNIKOV

B.Math., University of Waterloo, 1997
M.Sci., University of British Columbia, 1999

A THESIS SUBMITTED IN FULFILLMENT OF

THE REQUIREMENTS FOR THE DEGREE OF

DOCTOR OF PHILOSOPHY

in

THE FACULTY OF GRADUATE STUDIES

Department of Mathematics
Institute of Applied Mathematics

We accept this thesis as conforming
to the required standard

THE UNIVERSITY OF BRITISH COLUMBIA

March 2004

Abstract

In this thesis we analyse three different reaction-diffusion models These are: the Gray-Scott model of an irreversable chemical reaction, the Gierer-Meinhardt model for seashell patters, and the Haus model of mode-locked lasers. In the limit of small diffusivity, all three models exhibit localised spatial patterns. In one dimension, the equilibrium state typically concentrates on a discrete number of points. In two dimensions, the solution may consist of stripes, spots, domain-filling curves, or any combination of these. We study the regime where such structures are very far from the spatially homogenous solution. As such, the classical Turing analysis of small perturbations of homogenous state is not applicable. Instead, we study perturbations from the localised spike-type solutions.

In one dimension, the following instbailities are analysed: an overcrowding instability, whereby some of the spikes are annihilated if the initial state contains too many spikes; undercrowding (or splitting) instability, whereby a new spike may appear by the process of splitting of a spike into two; an oscillatory height instability whereby the spike height oscillates with period of $O(1)$ in time; and an oscillatory drift instability where the center of the spike exhibits a slow, periodic motion. Explicit thresholds on the parameters are derived for each type of instability.

In two dimensions, we study spike, stripe and ring-like solutions. For stripe and ring-like solutions, the following instabilities are analysed: a splitting instability, whereby a stripe self-replicates into two parallel stripes; a breakup instability, where a stripe breaks up into spots; and a zigzag instability, whereby a stripe develops a wavy pattern in the transveral direction. For certain parameter ranges, we derive explicit instability thresholds for all three types of instability. Numerical simulations are used to confirm our analytical predictions. Further numerical simulations are performed, suggesting the existence of a regime where a stripe is stable with respect to breakup or splitting instabilities, but unstable with respect to zigzag instabilities. Based on numerics, we speculate that this leads to domain-filling patterns, and labyrinth-like patterns.

For a single spike in two dimensions, we derive an ODE that governs the slow drift of its center. We reduce this problem to the study of the properties of a certain Green's function. For a specific dumbell-like domain, we obtain explicit formulas for such a Green's function using complex analysis. This in turn leads to conjecture that under certain general conditions on parameters, the equilibrium location of the spike is unique, for an arbitrary shaped domain. Finally, we consider another parameter regime, for which the exponentially weak interaction of the spike with the boundary plays a crucial role. We show that in this case there can exist a spike equilibrium solution that is located very near the boundary. Such solution is found to be unstable in the direction that is transversal to the boundary. As the effect of the boundary is increased, the interior spike locations undergo a series of destabilizing bifurcations, until all interior spike equilibria become unstable.

Acknowledgments

I am very grateful to my supervisor, Michael Ward. His expert guidance, support and enthusiasm have been invaluable in seeing this work through completion. I would also like to thank our collaborators, Juncheng Wei and Thomas Erneux. Chapters 1 and 2 are based on joint work with Michael Ward and Juncheng Wei. Chapters 3 and 4 are based on joint work with Michael Ward. Chapter 5 is a joint work with Thomas Erneux.

Table of Contents

List of Figures

Introduction

Reaction-diffusion systems are multi-component models involving diffusion and non-linear interaction among the components. Such systems are commonplace in many areas of physics, chemistry and biology. They are used as a model for such diverse phenomena as cell differentiation, reaction of chemicals, propogation of flame fronts, laser interference patterns and sea shell patterns.

In this thesis we study three different reaction-diffusion models. The first model, studied in §1 and §2, is the Gray-Scott system [28], [29], initially formulated with no diffusion. It models an irreversible reaction involving two reactants in a gel reactor, where the reactor is maintained in contact with a reservoir of one of the two chemicals in the reaction. With diffusion, in dimensionless units it can be written as

$$\begin{cases} V_T = D_V \Delta V - (F + k)V + UV^2 & \text{in } \Omega, \\ U_T = D_U \Delta U + F(1 - U) - UV^2 & \text{in } \Omega, \\ \frac{\partial U}{\partial \nu} = \frac{\partial V}{\partial \nu} = 0 & \text{on } \partial\Omega, \end{cases} \tag{1}$$

where Ω is a bounded domain; the unknowns $U(X,T)$, $V(X,T)$ represent the concentrations of the two biochemicals; D_U, D_V are the diffusion coefficients of U and V respectively; F denotes the rate at which U is fed from the reservoir into the reactor, and k is a reaction-time constant.

This model is known to have a rich solution structure for various parameter ranges. For example spikes, travelling waves, self-replication of pulses, oscillating spikes, and spatio-temporal chaos have all been observed. See [28], [29], [52], [53] for experimental work. For numerical and analytical results, see for instance [18], [20], [35], [53], [52], [57] [58], [59], [63], [64], [65], [66], [67], [79], [80]. [85].

The second model, studied in §3 and §4, is the Gierer-Meinhardt system. Introduced in [54], it is used to model various localization processes including biological morphogenesis and sea-shell patterns (cf. [26], [54], [33]). In dimensionless form, it can be written as:

$$A_t = \varepsilon^2 \triangle A - A + \frac{A^p}{H^q}, \qquad x \in \Omega, \quad t > 0, \tag{2a}$$

$$\tau H_t = D \triangle H - H + \frac{A^r}{H^s}, \qquad x \in \Omega, \quad t > 0, \tag{2b}$$

$$\partial_n A = \partial_n H = 0, \qquad x \in \partial\Omega. \tag{2c}$$

Here Ω is a bounded domain, A and H represent the activator and the inhibitor concentrations, ε^2 and D represent the diffusivity of the activator and inhibitor, τ is the inhibitor time constant, ∂_n denotes the outward normal derivative, and the exponents (p, q, r, s) satisfy

$$p > 1, \qquad q > 0, \qquad r > 0, \qquad s \geq 0, \qquad \frac{p-1}{q} < \frac{r}{s+1}. \tag{3}$$

The last model, studied in §5, is the continious limit of the Haus master equation (see [23] [31],

[41]), which describes the operation of a mode-locked laser:

$$E_T = \left(N - 1 - \frac{a}{1 + b|E|^2} \right) E + E_{\theta\theta} \tag{4a}$$

$$N_T = \gamma \left[A - N - NL^{-1} \int_0^L |E|^2 d\theta \right]. \tag{4b}$$

A common feature of these models is that their solution exhibits *spikes:* a highly localized structure in space, which is concentrated on a discrete number of points of the domain. An example of such a solution is shown in the lower right corner of Figure 1.

Background of Gray-Scott and Gierer-Meinhardt models

The modern theory of pattern formation begins with the seminal 1952 paper by Turing [71], which uses the linear analysis to determine threshold conditions for the instabiloity of spatially homogeneous equilibria of general two-component reaction-diffusion systems. However Turing's method is limited to patterns which are near-homogenous in space. As such, it fails to predict the stability and dynamics of spike-type solutions which are ubiquitous in many reaction-diffusion systems. The stability and dynamics of spike solutions – where Turing's approach is not applicable – is the main topic of this thesis.

A more recent criteria for pattern formation was proposed by Gierer and Meinhardt [26], [43] and independantly by Segel and Jackson [68]. They postulate that the following two conditions are essential for pattern formation: *local self-enhancement* and *long-range inhibition*. Let us illustrate how these two conditions are built into Gierer-Meinhardt (2) and Gray-Scott models (1).

For the Gierer-Meinhardt model, the local self-enhancement of the activator A occurs in the regions where A^p/H^q is sufficently large (i.e. bigger than A). However A cannot increase indefinitely, since eventually the term A^r/H^s will become large, which will induce an increase in the inhibitor H, which in its turn will cancel the destabilizing effect of the A^p/H^q term. Thus the chemical H acts as a long-range inhibitor. For this reason, models of GM type are often referred to as an *activator-inhibitor system*. Note also that the chemical A acts as an autocatalysist, so that the activator is *autocalytic*.

By contrast, The Gray-Scott model is referred to as an *activator-substrate* system. Here, the chemical U can be interpreted as a *substrate* depleted by V. The long-range inhibition here is due to a *depletion* of U. Instead of autocatalysis as in GM model, activation here is due to the presence of the source term in the equation for U.

For the GM model, we suppose that the ratio ε^2/D is small. This implies that H diffuses much slower than A; and so near the region of local self-enhancement, one can assume that H is constant. It then follows from an ODE analysis that A must decay exponentially outside the $O(\varepsilon)$ region of self-enhancement. This is the reason for the occurence of *spikes* in this model. An analogous argument applies to the Gray-Scott model, where spike-type patterns occur provided that D_v/D_u is small. Note that these assumptions are in agreement with the original work of Turing, where the instability was obtained provided that the ratio of diffusivity coefficients is sufficiently large or sufficiently small.

History of Gierer-Meinhardt model

Historically, the Gierer-Meinhardt model was first proposed in a slightly different form as a simple model of a biological morphogenesis in a fresh water polyp *hydra* (see [26], [43]). When the stem of a hydra is cut into two, the part that is left without a head grows one. Moreover, the new head appears on the side of the stem that was the closest to the original head. It was suggested that this process is due to the graduated distribution of the inhibitor inside the stem of the hydra. In addition, Gierer-Meinhadt model in one dimension has been proposed as a model for sea-shell patterns [54]. Many variants of this model have been proposed and studied numerically in [54]. These models involve additional chemical species, saturation effects, etc. The model (2) is the simplest model in this hierarchy.

Mathematically, the first rigorous analysis of the GM model was performed in the so-called *shadow regime*, for which D is assumed to be very large. In such a case, the chemical H becomes slave to A and, to a large degree, the analysis becomes similar to the famous PDE problem,

$$\varepsilon^2 \triangle u - u + u^p = 0, \quad x \in \Omega,$$
$$\partial_n u = 0, \quad x \in \partial\Omega, \tag{5}$$

This problem is by now well understood. In particular, a variational structure can be found in this limit. Using such variational formulation, Gui and Wei [27] have shown that as $\varepsilon \to 0$, the solution to (5) concentrates at a finite number of points, and moreover these points are related to a ball-packing problem: they are the centers of circles of the same size that are tangent to each other and to the boundary of the domain.

Similar equilibrium state exists for the GM model with large D. However such equilibrium state was shown to be unstable in [83] and [84] as long as $D \gg 1$. A more intricate picture emerges as D is decreased. In one dimension Iron, Ward and Wei [40] derived certain thresholds $D_2 > D_3 > \ldots$ such that a K spike symmetric equilibrium solution is stable only if $D < D_K$. Similar therholds were also derived in two dimensions in [77]. Moreover, instead of a ball-packing problem, the locations of spike centers are now related to certain properties of Green's functions.

History of Gray-Scott model

Let us mention some cornerstones in the development of the Gray-Scott model. It was originally introduced in [28], [29] to describe a reaction in a well-stirred tank. The stirring rate was assumed to be large enough to ignore the effects of diffusion, i.e. $D_v = 0 = D_u$. Even in this simple form, the ODE stability analysis reveals the presence of a Hopf bifurcation.

The next major developement was due to Pearson in 1993 [65]. He examined the Gray Scott model in two dimensions, in the limit D_v, D_u small. Using numerical simulations he observed complex pattern formation and reported many possible patterns, including spots, self-replication and labrynthian patterns. As Pearson himself observed, it is doubtful whether the Turing analysis, including the weakly-nonlinear Turing analysis, can predict such patterns, since they appeared to be far from the homogenous state. He suggested that new techniques are needed to study such patterns. Many of these patterns, including self-replicating spots,

were detected experimentally in 1994 by Lee, McCormick, Pearson and Swinney [52], where a gel reactor was used to achieve a large diffusivity ratio D_u/D_v.

The numerical and laboratory experiments Pearson and Swinney et al. have spurred the development of new analytical techniques to understand the these patterns. The first analytical results were derived by Doelman and his co-workers in a series of papers starting with [20]. Their theory explains analytically certain stability properties of spike-type solutions in 1-D in what we shall call here the intermediate regime. See §1.3 for more details. Independently of Doelman's work, Muratov and Osipov have also obtained many similar results for the Gray-Scott model in this regime (see [57]- [60]). In addition, they have developed a theory for pulse-splitting in one, two and three dimensions. In [63] and [64], for a different regime of the Gray-Scott model, Nishuira and Ueyama have proposed a theoretical framework which predicts pulse splitting in one dimension. Central to their theory is a certain alignment property which he demonstrated numerically for certain parameters of the Gray Scott model.

Turing's analysis

Let us now review Turing's approach for the analysis of the stability of spatially homogeneous stead-state solutions to reaction-diffusion systems. This approach is the usual first step for analysing biological and chemical pattern formation in both well-estabilished models such as the Brusselator [62], the Oregonator [25], and in a viriety of other systems, such as described in Murray [61].

We consider a general reaction-diffusion system in 1-D:

$$u_t = Mu_{xx} + F(u).$$

Here, we assume that u is a vector with n components, and M is a matrix of diffusion coefficients. Consider the homogenous solution state u_0 satisfying

$$F(u_0) = 0,$$

and consider a small perturbation from this state

$$u = u_0 + e^{\lambda t}\phi(x), \quad |\phi| \ll 1.$$

We then obtain the following linearized system:

$$\lambda\phi = M\phi_{xx} + \nabla F(u_0)\phi.$$

Substituting $\phi = ve^{mix}$ we then obtain the following n dimensional eigenvalue problem:

$$\lambda v = [-m^2 M + \nabla F(u_0)]v.$$

In particular, we see that when M is a positive definite matrix, $\lambda < 0$ whenever m is large enough. Similarly, if $\nabla F(u_0)$ is a negative definite matrix, $\lambda < 0$ when m is near zero. In between these two extremes, there may exist modes m for which the sign of λ is positive. Such modes correspond to unstable sinusoidal-type perturbations of the homogenous state. When m is of $O(1)$, the sign of λ depends on the balance of the diffusion and the nonlinear terms.
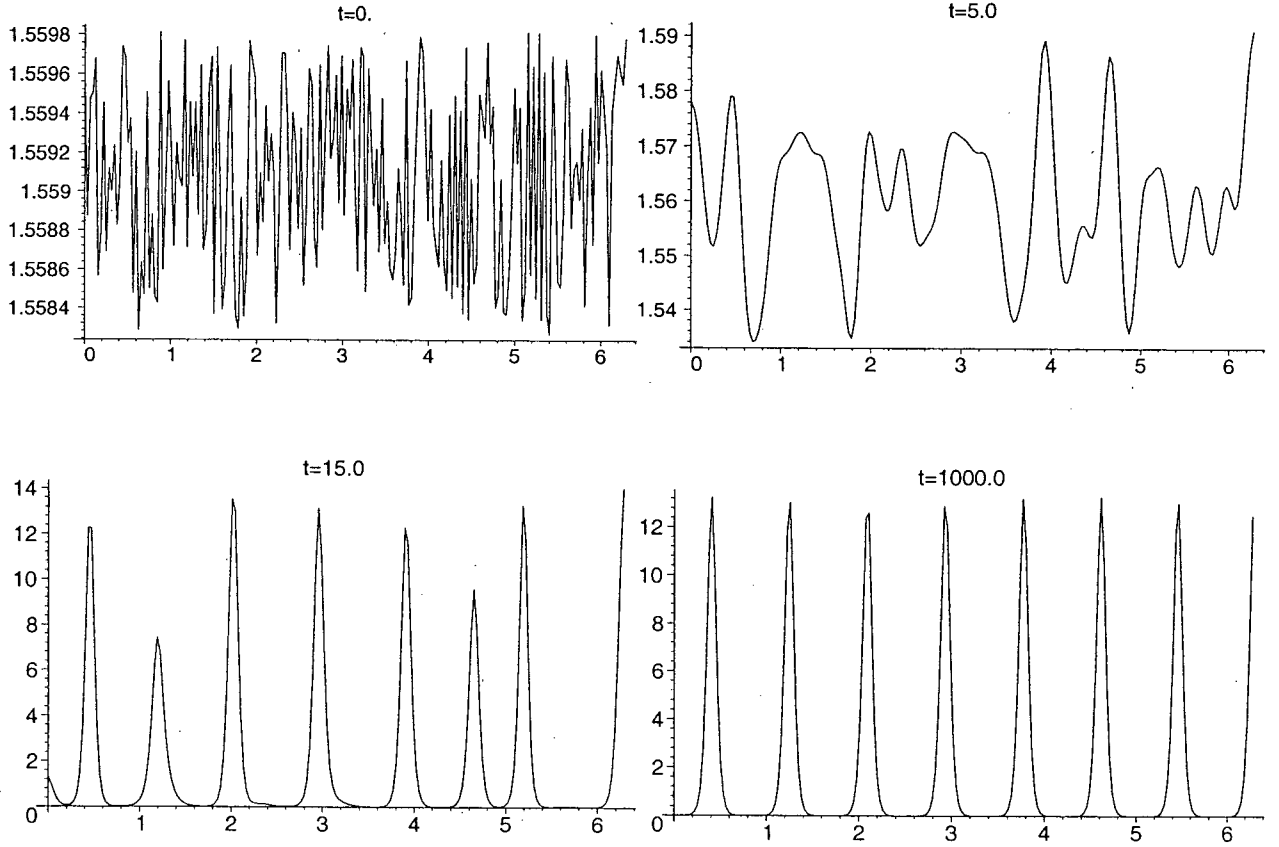
Figure 1: Example of Turing instability. Initial conditions at $t = 0$ consist of the homogenous steady state, with very small random perturbations. After some transient period, the solution converges to spike-type steady state, shown here at $t = 1000$. Note that the final state is very far from the initial homogenous equilibrium. Here, $A = 2.3, \varepsilon = 0.03, D = 1, l = 2\pi$.

Let us now perform Turing's analysis on the one-dimensional Gray-Scott model. We first transform the system (1). Set

$$\varepsilon^2 = \frac{D_V}{(F+k)}, \quad D = \frac{D_U}{F}, \quad A = \frac{\sqrt{F}}{F+k}, \quad \tau = \frac{F+k}{F}, \tag{6}$$

$$T = \frac{1}{F+k}t,$$

$$V(X,T) = \sqrt{F}v(x,t), \quad U(x,t) = u(x,t).$$

It is easy to see that (1) is equivalent to the following

$$\begin{cases} v_t = \varepsilon^2 \triangle v - v + Av^2 u \\ \tau u_t = D \triangle u - u + 1 - v^2 u \quad , \quad x \in \Omega \\ \partial_n v = 0 = \partial_n u, \quad x \in \partial \Omega. \end{cases} \tag{7}$$

First we find the spatially homogenous steady state solution (v_0, u_0). It satisfies:

$$v_0 = v_0^2 u_0 A, \quad u_0 = 1 - v_0^2 u_0.$$

Depending on the parameter A, there are either one or three solutions. A trivial solution is $v_0 = 0, u_0 = 1$. Two other solutions, which exist when $A > 2$, satisfy

$$v_0 u_0 A = 1, \quad v_0^2 - A v_0 + 1 = 0,$$

so that

$$v_0^{\pm} = \frac{A \pm \sqrt{A^2 - 4}}{2}, \quad u_0^{\pm} = \frac{1}{A v_0^{\pm}}.$$

Next, we linearize around these equilibirium states. We let

$$v = v_0 + \phi e^{\lambda t} \cos(mx), \quad u = u_0 + \eta e^{\lambda t} \cos(mx).$$

To satisfy the Neumann boundary condition, we require that $ml = j\pi$ where j is a non-negative integer. We then obtain:

$$\lambda \phi = -\varepsilon^2 m^2 \phi - \phi + 2 u_0 v_0 A \phi + v^2 A \eta,$$
$$\tau \lambda \eta = -D m^2 \eta - \eta - 2 u_0 v_0 \phi - v^2 \eta.$$

This can be written as $\lambda \vec{v} = M \vec{v}$ where $\vec{v} = (\phi, \eta)^t$ and

$$M = \begin{bmatrix} -\varepsilon^2 m^2 - 1 + 2 u_0 v_0 A & v_0^2 A \\ -\frac{1}{\tau} 2 u_0 v_0 & -\frac{1}{\tau}(D m^2 + 1 + v_0^2) \end{bmatrix}.$$

First, we consider the trivial solution $v_0 = 0, u_0 = 1$. Then the eigenvalues of M become $-\varepsilon^2 m^2 - 1, -\frac{1}{\tau}(D m^2 + 1)$. Thus both eigenvalues are negative and so the trivial solution is stable with respect to all modes m. Next, we consider $v_0 = v_0^{\pm}$. Then we obtain:

$$M = \begin{bmatrix} -\varepsilon^2 m^2 + 1 & v^2 A \\ -\frac{1}{\tau} \frac{2}{A} & -\frac{1}{\tau}(D m^2 + 1 + v_0^2) \end{bmatrix}.$$

Note that $\text{tr} M = 1 - \varepsilon^2 m^2 - \frac{1}{\tau}(D m^2 + A v_0)$. There are two cases to consider. First, suppose that $\text{tr} M < 0$ for all m. This occurs provided that

$$\tau < \frac{A^2}{2} \left(1 \pm \sqrt{1 - \frac{4}{A^2}} \right). \tag{8}$$

In additon we have:

$$f(m) \equiv \det M = \frac{1}{\tau} \left\{ \varepsilon^2 D m^4 + m^2 \left((1 + v^2) \varepsilon^2 - D \right) + v_0^2 - 1 \right\}.$$

Assuming the trace is negative, we will have instability whenever $f(m) < 0$. Next, we calculate:

$$f(0) = \frac{v_0^2 - 1}{\tau} = \frac{A v_0 - 2}{\tau} = \frac{\frac{1}{2} A^2 \left(1 \pm \sqrt{1 - \frac{4}{A}} \right) - 2}{\tau}.$$

Since $A > 2$, it follows that $f(0) > 0$ for v_0^+ and $f(0) < 0$ for v_0^-. We conclude that the zero mode is unstable for v_0^-. Thus the v_0^- solution does not generate heterogenous patterns. On the other hand, when $\varepsilon \ll D$ and $m = O(1)$, we have $f(m) \sim -D m^2 + f(0)$. It follows that for

v_0^+, f will become negative at the point when $m^2 = \frac{f(0)}{D} > 0$. This shows the existence of the instability band for v_0^+. Since $f(m) \to \infty$ as $m \to \infty$, we know that all modes m are stable when m is large enough. More precisely, when $m \gg 1$ we have

$$f(m) \sim \varepsilon^2 D m^4 - m^2 D,$$

so the upper bound for the instability band satisfies:

$$m \sim \frac{1}{\varepsilon}.$$

Finally, note from (6) that we must have $\tau > 1$. In particular, since $A > 2$, the condition (8) is satisfied for the v_0^+ solution whenever $\tau \in [1, 2]$.

The second case, when $\mathrm{tr}M > 0$, occurs when τ is sufficiently large. In this case there is always an unstable eigenvalue. In addition, if $f(m) > 0$ then these eigenvalues are purely imaginary when $\mathrm{tr}M = 0$. Thus a Hopf bifurcation occurs when τ is increased past a certain threshold. The corresponding perturbations then oscillate in time.

To conclude, Turing's analysis yields that v_0^+ is unstable with respect to an instability band $m_1 < m < m_2$ where

$$m_1 = \frac{1}{\sqrt{D}} \sqrt{\frac{1}{2} A^2 \left(1 + \sqrt{1 - \frac{4}{A}} \right) - 2}, \quad m_2 = \frac{1}{\varepsilon},$$

whereas v_0^- is unstable with respect to the zero mode. The trivial homogenous state is stable with respect to all modes.

Above we have shown the Turing instability under the assumption that D is large. It is easy to show that the instability band shrinks as D is decreased until it dissapears at some therhold value of $D = D_T$. For values of D near this threshold, it is possible to perform the *weakly non-linear analysis*, by expanding D and m near D_T. This yields the so-called amplitude equations, which are useful to analyse the stability and other properties of the sinusoidal patterns. There is a large body of literature devoted to this topic; see for example [62], [13] for comprehensive reviews.

While Turing's analysis above shows that the Gray-Scott model exhibits patterns, it says nothing about the final state of the destabilized homogenous state. In fact, in the regime $\varepsilon \ll D$, the final equilibrium state is very far from the homogenous state – see Figure 1. Thus Turing's analysis is insufficient to explain the final equilibrium state. The goal of this thesis is to study these far from homogenous state solutions.

Main contributions and comparison to previous work

There has been many related works dealing with localised structures in Gray-Scott system – see Section 1.3 for references. The main difference between these results and the results of Chapter 1 is that the previous works analyse a single spike on the unbounded domain. By contrast, we study K spikes on a bounded or unbounded domains. This introduces several new phenomena which have no counterpart with previous work on the Gray-Scott model.

The first novel result is a simple analytic formula which predicts the minimum number of pulse-splitting events of the Gray Scott model in the high feed regime $A = O(1)$ on a bounded domain. The result is given in Proposition 1.2.1. While the pulse-splitting behaviour has been studied previously on an unbounded domain (see for example [57], [66]), there is no analogue of that formula there, since the boundedness of the domain is essential.

Another new result for the Gray-Scott model is the the overcrowding instability thersholds of multi-spike solutions, as given in Proposition 1.1.7. This result is analogous to the thresholds computed previously for the Gierer-Meinhardt model (see [40]), and again, the boundedness of the domain and allowing for more than one spike solution is essential here.

Finally, the boundedness of the domain is crucial in the analysis of oscillatory travelling spikes. A travelling spike instability was predicted for the infinite domain in [60], where a specific threshold was also derived. However the oscillation in the position of the center of the spike can only occur in the presence of a bounded domain. This oscillation is due to a new type of Hopf bifurcation that is analysed in §1.2.2

The main result of Chapter 2 is the analysis of stripes of the Gray-Scott model in two dimensions. In particular, the technique used to study the zigzag instabilities of Section 2.2.1 is new.

The main contribution of Chapter 3 is an explicit computation of the regular part of the reduced wave Green's function with Neumann boundary condition. We then make a conjecture about uniqueness of the maxima of such a function. The importance and novelty of this conjecture is described in Section 3.4.6. In Chapter 4, one of the main results is the existence and stability analysis of a near-boundary spike equilibria that occurs in the case when the diffusivity coefficient D of the Gierer-Meinhardt is is exponentially large.

The main result of Chapter 5 is the analysis of a Hopf bifurcation in the model (4) of mode-locked lasers. This provides an explanation of oscillations that were numerically found in in [41].

Thesis outline

The outline of this thesis is as follows. In §1 we study the stability of spike solutions in the the one-dimensional Gray-Scott model. We consider four different types of instability that may occur. The first type, analysed in §1.1.2, is an *overcrowding* or *competition* instability. As a result of such an instability, some of the spikes are annihilated if the initial solution profile consists of too many spikes. We derive explicit thresholds on the maximum number of spikes that are stable with respect to such an instability. This number is found to be an increasing function of the domain length. The second type of instability, studied in §1.1.3 and §1.1.4, results in an oscillatory behaviour of a spike, whereby its height oscillates periodically in time. The third type is an *undercrowding* or *splitting* instability. In the presence of such an instability, successive spike replication is observed, until a certain threshold number of the spikes is exceeded. This threshold is found to be an increasing function of domain length. Explicit formulas for this number are given in §1.2.1. In §1.2.2, we study an oscillatory spike drift, whereby the location of the center of the spike oscillates on a slow time scale. In §1.3 we compare our work to previously known results, in particular the work of Doelman and collaborators ([16]-[21], [55]) and the work of Muratov and Osipov [57]-[60]. The results of this chapter have been previously reported in [74] and [44].

In §2 we consider ring-like and stripe-like solutions of the Gray-Scott model in two dimensions. Such solutions are one-dimensional in nature, and many of the techniques from §1 are applicable with some modifications. We focus on two types of instabilities: breakup and zigzag instabilities. When a stripe is unstable with respect to a breakup instability of mode m, it breaks up into m radially symmetric spikes. A zigzag instability on the other hand deforms a stripe into a zigzag-like pattern. These instabilities are illustrated in Figure 2.1. We characterize the instability band for both types of instabilities, and for either a ring or a stripe. In the parameter regime where analysis is possible, we find that the stripe is always unstable with respect to some band of breakup instabilities; and may or may not be stable with respect to zigzag instabilities. We also numerically find a regime where the stripe does not break up but is unstable with respect to zigzag instabilities. We conjecture that this behaviour leads to labrynthian patterns, such as shown on Figure 2.2. The results of §2 were previously reported in [45].

In §3 and §4 we study the slow drift of a single spike solution of the Gierer-Meinhardt model in two dimensions. There are two effects that contribute to this drift: the first is the effect of the boundary, which is typically exponentially small in the distance to the boundary. The second is due to the inhibitor and depends on the diffusivity constant D. In §3 we first consider the latter effect, ignoring the exponentially weak effect of the boundary. For D small with $O(\varepsilon^2) \ll D \ll O(1)$, the spike motion is found to be metastable, with stable equilibrium positions located at points furthest away from the boundary. Thus for a dumbell shaped domain such as shown in Figure 3.2, the equilibria would be located at the centers of lobes of the dumbell. On the other hand for $D \gg O(\ln \frac{1}{\varepsilon})$, the motion depends on the gradient of a modified Green's function for the Laplacian. For a certain class of dumbell-shaped domains, we use complex variables to derive an explicit expression for such a function. Using this formula, we then show that the equilibrium is unique and it is located in the neck of the dumbell. This leads to a general conjecture 3.3.3 about the modified Green's function, that states that its regular part has a unique minimum in the interior of an arbitrary shaped simply-connected domain. Aside our analytical example, several numerical examples are also investigated, all supporting this conjecture. The results of this section were previously presented in [46].

In §4 we consider the limiting case of exponentially large D, when the effect of the boundary cannot be ignored. In the limit $D = \infty$ the Gierer-Meinhardt reduces to a well known shadow problem (see for instance [37]) for which it is known that a single interior spike will drift exponentially slowly towards the nearest boundary. This is in contrast to the dynamics when when D is large enough (but not not exponentially large), in which case a single interior stable equilibrium position exists, as explained in §3. Thus an intricate bifurcation structure occurs in the regime where D is exponentially large. In §4.3 this structure is analysed for a family of dumbell-shaped domains that were introduced in §3. This transition, from a stable interior spike when D is large, to the dynamics driven by the nearest boundary in the case $D = \infty$, is made possible by the existence of what we call *near boundary* spikes, in the transition regime when D is exponentially large. They occur at a distance σ from the boundary, where $\varepsilon \ll \sigma \ll 1$ and

$$D \sim C \left(\frac{\varepsilon}{\pi \sigma} \right)^{1/2} e^{2\sigma/\varepsilon},$$

where C is some positive constant. For our dumbell-shaped domain, we find that their stability is as shown in Figure 4.2. The near-boundary spikes are always unstable in the the direction normal to the boundary. Their stability in the tangential direction depends solely on the

properties of the modified Green's function on the boundary. The results of this section were previously presented in [47].

In the last Chapter 5, we apply some of the techniques of §1 to the the model (4) of mode-locked lasers. In [41], this model was studied numerically. It was found numerically that as the parameter a is increased, the spike starts to exhibit periodic oscillations in height. We show that this behaviour is due to a Hopf bifurcation of the linearized problem. Moreover we are able to accurately predict the threshold value at which this bifurcation occurs. Our theoretical predictions compare favorably with numerical simulations. The results of this section were previously presented in [23].

Chapter 1
Gray-Scott model in one dimension

In this chapter, we consider the one dimensional version of the Gray Scott model (7),

$$
\begin{cases}
v_t = \varepsilon^2 v_{xx} - v + A v^2 u \\
\tau u_t = D u_{xx} - u + 1 - v^2 u \\
v_x(\pm l, t) = 0 = u_x(\pm l, t).
\end{cases}
\quad , \quad x \in [-l, l]
\tag{1.1}
$$

We are concerned with the regime when the ratio of diffusivities is small,

$$
\varepsilon \ll 1, \quad \varepsilon^2 \ll D.
$$

A typical solution is shown on Figure 1.1. The distribution of the chemical v typically consists of k localized spikes, concentrated at certain points of the domain, with negligible amount of v away from these points. The concentration of u vary over the length of the domain.

In one dimension, as we will show, there are three important regimes, depending on the parameter A:

$$
\textit{Low-feed regime:} \quad A = O(\varepsilon^{1/2})
\tag{1.2}
$$

$$
\textit{Intermediate regime:} \quad O(\varepsilon^{\frac{1}{2}}) \ll A \ll O(1)
\tag{1.3}
$$

$$
\textit{High-feed regime:} \quad A = O(1).
\tag{1.4}
$$

The main difference between the low-feed and high-feed regime is that in the low-feed regime, the chemical u changes on a much slower scale than v, both near the center of the spike, and in the region away from the center. Thus (1.1) is *weakly coupled* in the low-feed regime. On the
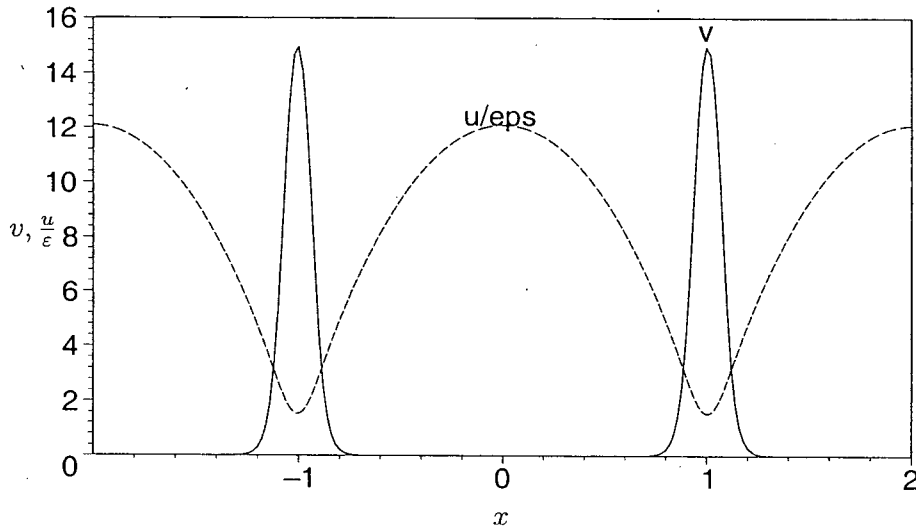
Figure 1.1: Example of an equilibrium two-spike solution to (1.1), in the high-feed regime. Here, $D = 1, \varepsilon = 0.03, l = 2, A = 1.7, \tau = 1$.

other hand, in high-feed regime, u and v are strongly coupled near the core of the spike, but are weakly coupled away from the core. The intermediate region can be viewed as a limit case of between high-feed or low-feed regimes.

Depending on the regime, several different types of instability may occur. In §1.1 we analyse the low-feed regime. There, we study two types of instabilities. First, there exists an *overcrowding* instability: there are thresholds $l_2 < l_3...$ such that if $l < l_k$ then k spikes located symmetrically on the interval $[-l, l]$ are unstable. As a result, some spikes will quickly dissapear until there are k' spikes left, where k' is such that $l > l_{k'}$. Second, we show the existence of an *oscillatory profile* instability. It is manifested by the periodic oscillations of the spike height, when the parameter τ is large enough.

In §1.2 we study the intermediate and high-feed regimes. In these regimes, we study two additional types of instability. We show that in the high-feed regime, an *undercrowding* instability will occur whenever the constant $A \tanh \frac{l}{k\sqrt{D}}$ is above 1.35. This type of instability leads to spike splitting, whereby one spike self-replicates into two spikes. An example of this is shown in

2

Figure 1.2(a). In either the intermediate or the high-feed regime, an *oscillatory drift* instability occurs if τ is sufficiently large. This type of instability results in a slow periodic motion of the centers of the spikes. An example is given on Figure 1.2(b). Finally, as in the low-feed regime, periodic $O(1)$ oscillations of spike height may also occur. In Proposition 1.2.10 we derive a scaling law which predicts whether oscillatory drift or oscillatory profile instability occurs first.

We conclude with §1.3 where we compare the results of this chapter with the existing literature on the Gray Scott model.

(a)

(b)
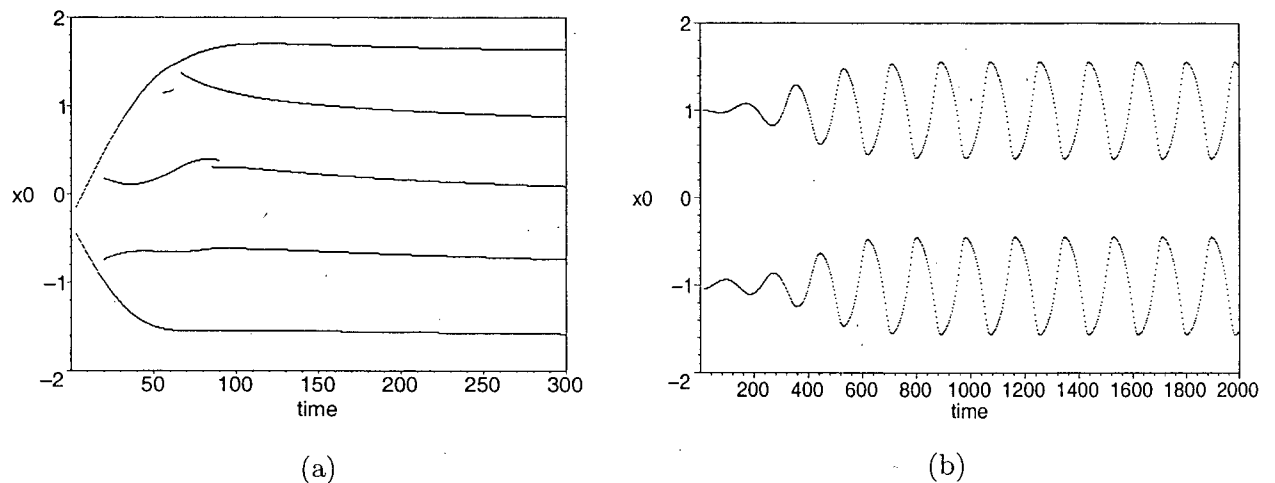
Figure 1.2: (a) Undercrowding effect in Gray-Scott model: Positions of spike's centers are plotted vs. time. Here, $l = 2$, $D = 1$, $A = 3.5, \varepsilon = 0.03$ and $\tau = 1$. (b) Oscillatory drift: two spikes in asynchonious, periodic drift. Here, $l = 2$, $D = 1$, $\varepsilon = 0.03$, $A = 1.64$, $\tau = 88$.

1.1 Low-feed regime of the Gray-Scott model

1.1.1 Symmetric spike Equilibria solutions

We begin by asymptotically calculating the equilibrium spike solution of (1.1). It is convenient to introduce the following scaling:

$$A = \varepsilon^{1/2}\mathcal{A}, \quad v = \varepsilon^{-1/2}\nu.$$

The system (1.1) then becomes:

$$\begin{cases} \nu_t = \varepsilon^2 \nu_{xx} - \nu + \mathcal{A}\nu^2 u \\ \tau u_t = D u_{xx} - u + 1 - \frac{1}{\varepsilon}\nu^2 u \\ \nu_x(\pm l, t) = 0 = u_x(\pm l, t) \end{cases} , \quad x \in [-l, l] \tag{1.5}$$

We seek the equilibrium solution in the form of symmetric k spikes, whose centers are located at

$$x_i = l\left(-1 + \frac{2i-1}{k}\right), \quad i = 1 \dots k. \tag{1.6}$$

Near the core of each spike, we write

$$\nu \sim \xi w\left(\frac{x - x_i}{\varepsilon}\right), \quad u \sim U\left(\frac{x - x_i}{\varepsilon}\right).$$

where w, ξ, U are to be found. We then obtain:

$$w'' - w + w^2 \xi U \mathcal{A} = 0, \quad U'' - \varepsilon^2 U + \varepsilon^2 - \varepsilon \xi^2 w^2 U = 0.$$

Thus, to leading order we obtain: $U \sim u(x_i)$, and choose $\xi = \frac{1}{\mathcal{A}U}$. Then $w(y)$ satisfies

$$w'' - w + w^2 = 0, \quad w'(0) = 0, \quad w(y) \sim Ce^{-|y|} \quad \text{as} \quad |y| \to \infty. \tag{1.7a}$$

The explicit solution of (1.7a) is

$$w = \frac{3}{2}\operatorname{sech}^2\left(\frac{y}{2}\right). \tag{1.7b}$$

To find U, we perform asymptotic matching with the outer solution. We have

$$u(x) = 1 - \frac{1}{\varepsilon}\int_{-l}^{l} G(x, x')u(x')\nu^2(x')\, dx',$$

where G is the Green's function satisfying

$$DG_{xx} - G = -\delta(x - x'), \quad G_x(\pm l, x') = 0.$$

Changing variables, noting that $U(x_i) = U$ and $\xi = \frac{1}{U\mathcal{A}}$ we thus obtain,

$$\frac{1}{\varepsilon}\int_{-l}^{l} lG(x_j, x')u(x')\nu^2(x')\, dx' \sim \sum_{i=1}^{k}\int G(x_j, x_i + \varepsilon y')u(x_i + \varepsilon y')\nu^2(x_i + \varepsilon y')\, dy'$$

$$\sim \sum_{i=1}^{k} G(x_j, x_i)U\xi^2 \int w^2$$

$$\sim 6\sigma\frac{1}{U\mathcal{A}^2},$$

4

where

$$\sigma = \sum_{i=1}^{k} G(x_j, x_i), \tag{1.8}$$

and we have used

$$\int w^2 = 6. \tag{1.9}$$

Here and below, the integration is assumed over entire space unless limits are specified.

It remains to evaluate σ. Rather than doing this directly, we define $u(x) = \sum_i G(x, x_i)$. Then $\sigma = u(x_j)$. Notice that u satisfies

$$Du'' - u = -\sum_{i=1}^{k} \delta(x - x_i), \quad -l < x < l; \quad u'(\pm l) = 0.$$

This problem is equivalent to:

$$Du'' - u = 0, \quad Du'(x_i^+) - Du'(x_i^-) = -1, \quad u'(\pm l) = 0.$$

By symmetry, we obtain: $Du'(x_i^-) = \frac{1}{2}, Du'(x_i^+) = -\frac{1}{2}$. A simple calculation then yields

$$\sigma = \frac{\theta_0}{2} \coth(\frac{l\theta_0}{k}), \quad \text{where} \quad \theta_0 = \frac{1}{\sqrt{D}}. \tag{1.10}$$

From above we have $u(x_j) \sim 1 - \frac{6\sigma}{U\mathcal{A}^2}$. Since $U = u(x_j)$, we get that U satisfies the quadratic equation

$$U = 1 - 6\sigma \frac{1}{U\mathcal{A}^2}. \tag{1.11a}$$

The solution of this equation,

$$U_\pm = \frac{1}{2} \left\{ 1 \pm \sqrt{1 - \frac{12\theta_0 \coth \frac{l\theta_0}{k}}{\mathcal{A}^2}} \right\} \tag{1.11b}$$

exists, with $U_- \in (0, 1/2]$, $U_+ \in [1/2, 1)$, if and only if $\mathcal{A} \geq \mathcal{A}_{ke}$ where

$$\mathcal{A}_{ke} = D^{-1/4} \sqrt{12 \coth l\theta_0/k}, \quad \theta_0 = \frac{1}{\sqrt{D}} \tag{1.12}$$

We summarize our results as follows.

Proposition 1.1.1 *Suppose that $\mathcal{A} > \mathcal{A}_{ke}$, with $\mathcal{A}_{ke}$ given by (1.12). Then there exist two symmetric k-spike equilibria solutions to (1.5). They are given by*

$$\nu_\pm(x) \sim \sum_{i=1}^{k} \frac{1}{\mathcal{A}U_\pm} w\left(\frac{x - x_i}{\varepsilon}\right), \quad u_\pm(x) \sim U_\pm,$$

5

where x_i is given by (1.6), w is given by (1.7) and $U_\pm$ is given by (1.11).

We shall denote (u^+, v^+) the large solution, and (u^-, v^-) the small solution.

1.1.2 Non-local eigenvalue problem

Next, we derive an eigenvalue problem that characterizes the stability of of the symmetric k-spike solution of (1.5), with respect to perturbations that are even functions in the core of each spike. We shall call the corresponding eigenvalues *large eigenvalues*. This is to distinguish them from the *small* eigenvalues which arise from near translation invariance. The stability with respect to small eigenvalues will be discussed in §1.2.2 below. The large eigenvalues are so called because they remain $O(1)$ as $\varepsilon \to 0$. By contrast, the small eigenvalues tend to zero as $\varepsilon \to 0$.

We start by linearizing around the equilibrium state. We let

$$\nu = \nu_\pm(x) + e^{\lambda t}\phi(x), \quad u = u_\pm(x) + e^{\lambda t}\psi(x).$$

The linearized system then becomes

$$\lambda\phi = \varepsilon^2\phi'' - \phi + 2\mathcal{A}\nu_\pm u_\pm\phi + \mathcal{A}\nu_\pm^2\psi, \tag{1.13}$$

$$\tau\lambda\psi = D\psi'' - \psi - \frac{1}{\varepsilon}\left(2\nu_\pm u_\pm\phi + \nu_\pm^2\psi\right). \tag{1.14}$$

Near x_j, we have

$$\phi \sim c_j\Phi\left(\frac{x - x_j}{\varepsilon}\right), \quad \psi \sim \psi_j. \tag{1.15}$$

Here, the constants $c_j, \psi_j, j = 1, \ldots k$ are to be found later by asymptotic matching of the outer and inner solution. We first determine the effect of the inner solution. Near $x = x_j$ we then have using Proposition 1.1.1 that

$$\frac{1}{\varepsilon}\nu_\pm u_\pm\phi \sim \frac{1}{\varepsilon}\frac{c_j}{\mathcal{A}}w\Phi \sim \delta(x - x_j)\frac{c_j}{\mathcal{A}}\int w\Phi,$$

$$\frac{1}{\varepsilon}\nu_\pm^2\psi \sim \delta(x - x_j)\frac{6\psi_j}{\mathcal{A}^2 U_\pm^2}$$

Thus we have:

$$0 = \psi'' - \theta_\lambda^2\psi \sim \delta(x - x_j)\left(\frac{2c_j}{D\mathcal{A}}\int w\Phi + \frac{6\psi_j}{D\mathcal{A}^2 U_\pm^2}\right), \quad \theta_\lambda \equiv \sqrt{\frac{1 + \lambda\tau}{D}}$$

6

The solution may be written as:

$$\vec{\psi} = -\mathcal{G}\left(\left(2\frac{1}{D\mathcal{A}}\int w\Phi\right)\vec{c} + \frac{6}{D\mathcal{A}^2 U_\pm^2}\vec{\psi}\right) .$$

where

$$\vec{\psi} = [\psi_1, \ldots \psi_k]^t, \quad \vec{c} = [c_1, \ldots, c_k]^t, \quad \mathcal{G} = [G(x_i, x_j)].$$

Here $G(x, y)$ is the Green's function satisfying

$$G_{xx} - \theta_\lambda^2 G = -\delta(x - y), \quad G_x(\pm 1, y) = 0.$$

This yields:

$$\vec{\psi} = -\left(1 + \frac{6}{D\mathcal{A}^2 U_\pm^2}\mathcal{G}\right)^{-1}\mathcal{G}\left(\frac{2}{D\mathcal{A}}\int w\Phi\right)\vec{c}$$

Substituting into (1.13) we obtain the nonlocal eigenvalue problem

$$\lambda \vec{c}\Phi = \vec{c}L_0\Phi - M\vec{c}\frac{\int w\Phi}{\int w^2},$$

where

$$L_0\Phi = \Phi'' - \Phi + 2w\Phi, \tag{1.16}$$

and the matrix M is defined as

$$M \equiv \frac{12}{U_\pm^2 D\mathcal{A}^2}\left(6 + \frac{1}{D\mathcal{A}^2 U_\pm^2}\mathcal{G}\right)^{-1}\mathcal{G}.$$

It follows that

$$\lambda\Phi = L_0\Phi'' - \chi\frac{\int w\Phi}{\int w^2},$$

where χ is an eigenvalue of M^t, with $\vec{c}^t$ its corresponding eigenvector. It remains to find the eigenvalues of $M = M^t$. First, we claim that $\mathcal{G}^{-1}$ is the k by k tridiagonal matrix

$$\mathcal{G}^{-1} = \frac{\theta_\lambda}{s}\begin{bmatrix} -1+2c & -1 & & & & \\ -1 & 2c & -1 & & & \\ & -1 & 2c & -1 & & \\ & & \ddots & \ddots & \ddots & \\ & & & -1 & 2c & -1 \\ & & & & -1 & -1+2c \end{bmatrix} \tag{1.17a}$$

7

where

$$s \equiv \sinh(\theta_\lambda d), \quad c \equiv \cosh(\theta_\lambda d), \quad \equiv \frac{2l}{k}. \tag{1.17b}$$

To see this, we consider the system $\mathcal{G}\vec{X} = \vec{B}$, i.e. $\sum_j G(x_i, x_j)X_j = B_i$. But then $B_j = u(x_j)$ where u satisfies

$$u''(x) - \theta_\lambda^2 u(x) = -\sum_j X_j \delta(x_j - x) \quad \text{with} \quad u'(\pm l) = 0.$$

So for $1 < i < K$ we have:

$$B_{i+1} = \frac{1}{\theta_\lambda} u'(x_i^+)s + B_i c,$$

$$u'(x_{i+1}^-) = u'(x_i^+)c + \theta_\lambda B_i s,$$

$$X_i = u'(x_i^-) - u'(x_i^+).$$

It follows that:

$$u'(x_i^+) = \frac{\theta_\lambda}{s}\left(B_{i+1} - B_i c\right),$$

$$\begin{aligned}
X_i &= u'(x_{i-1}^+)c + \theta_\lambda B_{i-1}s - u'(x_i^+) \\
&= \frac{\theta_\lambda}{s}\left(B_i - B_{i-1}c\right)c + \theta_\lambda B_{i-1}s - \frac{\theta_\lambda}{s}\left(B_{i+1} - B_i c\right) \\
&= \frac{\theta_\lambda}{s}\left(-B_{i-1} + 2B_i c - B_{i+1}\right).
\end{aligned}$$

For $i = 1$ we have, on the interval $[-l, x_1]$, $u = \alpha \cos[(x + l)\theta_\lambda]$ where α is some constant. Thus:

$$B_1 = \alpha \cosh \frac{d}{2}\theta_\lambda,$$

$$u'(x_1^-) = \alpha\theta_\lambda \sinh \frac{d}{2}\theta_\lambda,$$

$$\begin{aligned}
X_1 &= \alpha\theta_\lambda \sinh \frac{d}{2}\theta_\lambda - u'(x_1^+) \\
&= \frac{B_1}{\cosh\left(\frac{d}{2}\theta_\lambda\right)}\theta_\lambda \sinh \frac{d}{2}\theta_\lambda - \frac{\theta_\lambda}{s}\left(B_2 - B_1 c\right), \\
&= \frac{\theta_\lambda}{s}\left(B_1(2c - 1) - B_2\right),
\end{aligned}$$

where we have used the identity

$$\frac{\sinh(\frac{x}{2})}{\cos(\frac{x}{2})} = \frac{\cosh(x) - 1}{\sinh(x)}.$$

This proves (1.17a). Next we note by direct computation that the eigenvalues of the $k \times k$ matrix

$$
A = \begin{bmatrix}
-1 & -1 & & & & \\
-1 & 0 & -1 & & & \\
& -1 & 0 & -1 & & \\
& & \ddots & \ddots & \ddots & \\
& & & -1 & 0 & -1 \\
& & & & -1 & -1
\end{bmatrix},
$$

are given by

$$
-2\cos(\frac{\pi(j-1)}{k}), \quad j = 1 \cdots k
$$

with the corresponding eigenvectors

$$
v_{mj} = \cos\left(\frac{\pi(j-1)}{k}(m - \frac{1}{2})\right), \quad m = 1 \cdots k
$$

It follows that the eigenvalues of $\mathcal{G}^{-1}$ are:

$$
\mu_j = \frac{\theta_\lambda}{s}\left(2c - 2\cos\frac{\pi(j-1)}{k}\right)
$$
$$
= 2\theta_\lambda\left[\tanh(\theta_\lambda/k) + \left(1 - \cos\frac{\pi(j-1)}{k}\right)\operatorname{csch}(2\theta_\lambda/k)\right], \quad j = 1 \cdots k,
$$

with the corresponding eigenvectors

$$
c_{mj} = \cos\left(\frac{\pi(j-1)}{k}(m - 1/2)\right).
$$

Thus we obtain the eigenvalues of M, which we write in the following form:

$$
\chi_j = \frac{2s}{s + \mu_j \sigma D}
$$

where

$$
s = \frac{U_\pm - 1}{U_\pm}.
$$

We summarize.

Proposition 1.1.2 *In the limit $\varepsilon \to 0$, the large eigenvalues of (1.13) satisfy:*

$$
\lambda\Phi = L_0\Phi - \chi\frac{\int w\Phi}{\int w^2}, \tag{1.18a}
$$

9

where $\Phi(r) = \phi(\varepsilon x)$,

$$L_0\Phi = \Phi'' - \Phi + 2w\Phi, \tag{1.18b}$$

and $\chi = \chi_j$, $j = 1 \ldots k$ *given by*

$$\chi_j \equiv \frac{2s}{s + \frac{\theta_\lambda}{\theta_0}\left[\tanh(l\theta_\lambda/k) + \left(1 - \cos\frac{\pi(j-1)}{k}\right)\text{csch}(2l\theta_\lambda/k)\right]\coth(l\theta_0/k)}, \quad j = 1 \ldots k \tag{1.18c}$$

where

$$\theta_\lambda \equiv \sqrt{\frac{1 + \tau\lambda}{D}}, \quad \theta_0 \equiv \sqrt{\frac{1}{D}}, \tag{1.18d}$$

$$s = \frac{U_\pm - 1}{U_\pm} \tag{1.18e}$$

We shall refer to (1.18) as a non-local eigenvalue problem (NLEP).

The non-local eigenvalue problem (1.18) has been extensively studied in a series of papers. In [18], a computer algebra assisted approach was developed to determine the spectrum of of (1.18). However their approach relies on manipulation of hypergeometric functions, and requires the use of computer algebra. Here, we will use a different method that does not require hypergeometric functions, developed in a series of papers [78], [77], and [74].

The basic result, shown in [78] and [77], is the following.

Theorem 1.1.3 *(See [78]) Consider the problem (1.18a), and suppose that* χ *is a constant independent of* λ. *Let* λ *be an eigenvalue of (1.18a) with largest real part that corresponds to an even eigenfunction* Φ. *Then* $\text{Re}(\lambda) < 0$ *if* $\chi > 1$, $\lambda = 0$ *with* $\Phi = w$ *if* $\chi = 1$, *and* $\text{Re}(\lambda) > 0$ *if* $\chi < 1$.

Suppose that $\chi = \chi(\tau\lambda)$ *is continuous and defined on* $\mathbb{R}^+$. *If* $\chi(0) < 1$ *then* $\text{Re}(\lambda) > 0$.

Note that the threshold case $\chi = 1$ follows from the observation that $L_0 w = w$ and $\int w^2 = \int w$. The proof for non-constant χ is deferred until Proposition 1.1.6. For the rest of the proof, see [78], Theorem 2.12.

Note also that the assumption that Φ is even is necessary, since $\lambda = 0, \Phi = w'$ satisfies (1.18) for any χ.

For the case $\chi = 0$, the following result is known:

Lemma 1.1.4 *(From [50]): The problem $L_0\Phi = \lambda\Phi$ admits a positive eigenvalue $\lambda_0 = 5/4$, with the corresponding eigenfunction $\Phi = \operatorname{sech}^3(y/2)$, a zero eigenvalue with eigenfunction $\Phi = w'$ and a negative eigenvalue $\lambda = -3/4$ with the corresponding eigenfunction $5\operatorname{sech}^2(y/2) - 4\operatorname{sech}(y/2)$.*

We now study the case where χ depends on λ. This analysis first appeared for the Gierer Meinhardt model in [77], [74]. By scaling Φ, we may write (1.18) as
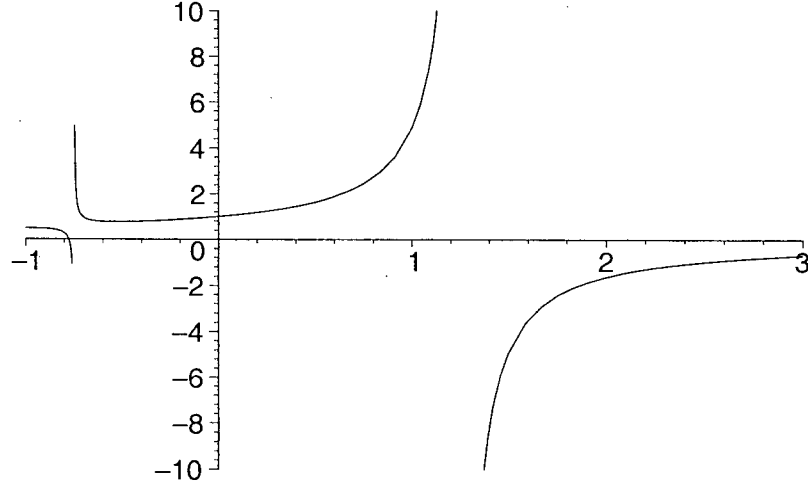
Figure 1.3: The function f, given by (1.21), for real values of λ

$$\frac{\int w\Phi}{\int w^2} = \frac{1}{\chi_j}, \quad (L_0 - \lambda)\Phi = w^2.$$

Thus the NLEP problem (1.18) is equivalent to finding the roots of

$$C_j(\lambda\tau) = f(\lambda) \quad \text{where} \quad f(\lambda) = \frac{\int w(L_0 - \lambda)^{-1}w^2}{\int w^2} \quad \text{and} \quad C_j(\lambda\tau) = \frac{1}{\chi_j}. \tag{1.19}$$

Explicitly, we have:

$$C_j = \frac{1}{2} + \frac{1}{2s}\frac{\theta_\lambda}{\theta_0}\left[\tanh(l\theta_\lambda/k) + \left(1 - \cos\frac{\pi(j-1)}{k}\right)\operatorname{csch}(2l\theta_\lambda/k)\right]\coth(l\theta_0/k), \quad j = 1\ldots k. \tag{1.20}$$

The following lemma summarizes some properties of f.

Lemma 1.1.5 *(see [77]) The behaviour of f near the origin is:*

$$f(\lambda) \sim 1 + \frac{3}{4}\lambda + \kappa_c \lambda^2 + O(\lambda^3), \quad where \quad \kappa_c = \frac{\int (L^{-1}w)^2}{\int w^2} > 0. \tag{1.21}$$

In addition we have the global behaviour:

$$f'(\lambda) > 0, \quad f''(\lambda) > 0, \quad \lambda \in (0, 5/4).$$

Moreover f has a singularity at $\lambda = 5/4$ with $f \to \pm\infty$ as $\lambda \to 5/4^{\pm}$. On the other side of the singularity we have

$$f(\lambda) < 0, \quad \lambda > 5/4,$$

and

$$f(\lambda) \sim -\frac{5}{6\lambda} \quad as \quad \mathrm{Re}(\lambda) \to \infty.$$

The graph of f for real λ is shown on Figure 1.3. Note the singularities at $5/4$ and $-3/4$, which are the discrete eigenvalues of the L_0.

The first result with C_j non-constant concerns instability. We show the following:

Proposition 1.1.6 *(See also [77]) Let*

$$B_j \equiv \frac{1}{\chi_j(0)} = \frac{1}{2} + \left[\frac{1}{2s} + \frac{1}{4s \sinh^2 l\theta_0/k} \left(1 - \cos \frac{\pi(j-1)}{k} \right) \right] \tag{1.22}$$

Suppose that $B_j > 1$ for some j. Then the NLEP problem (1.18) is admits a purely positive eigenvalue. Thus a k-spike equilibrium derived in Proposition 1.1.1 is unstable.

In the inner region near the mth spike, the perturbation of the v-component of the equilibrium solution that corresponds to j-th large eigenvalue has the following form:

$$\nu(x,t) \sim \left(\frac{1}{\mathcal{A}U_{\pm}} w \left(\frac{x - x_m}{\varepsilon} \right) + \beta c_{mj} \Phi \left(\frac{x - x_m}{\varepsilon} \right) e^{\lambda t} \right), \quad |x - x_m| = O(\varepsilon) \tag{1.23}$$

where $\beta \ll 1$ is some small constant, Φ is an even function defined in (1.15), and

$$c_{mj} = \sin \left(\frac{\pi j}{k} (m - 1/2) \right). \tag{1.24}$$

12

Proof. We have $f(0) = 1$. Thus $f(0) < B_j$. But f blows up at 5/4. It follows that by the intermediate value theorem that f and C_j intersect at some $\lambda \in (0, 5/4)$. $\square$

It is easy to see that we have the following ordering principle: $B_1 < B_2 < \ldots < B_k$. Therefore the first node that undergoes an instability in Proposition 1.1.6 is B_k. The threshold case $B_k = 1$ corresponds to the value

$$s = s_k = 1 + \frac{1 + \cos \pi/k}{2 \sinh^2 l\theta_0/k} \tag{1.25}$$

or equivalently,

$$l = l_k = \sqrt{D}k \operatorname{arcsinh} \sqrt{\frac{1 + \cos \pi/k}{2(s-1)}}. \tag{1.26}$$

Using the identity:

$$\frac{\mathcal{A}}{\mathcal{A}_{ke}} = \frac{1 + s}{2\sqrt{s}}, \tag{1.27}$$

this threshold is also equivalent to

$$\mathcal{A} = \mathcal{A}_k = \mathcal{A}_{ke} \left\{ \frac{2 + \frac{1 + \cos \pi/k}{2 \sinh^2 l\theta_0/k}}{2\sqrt{1 + \frac{1 + \cos \pi/k}{2 \sinh^2 l\theta_0/k}}} \right\}. \tag{1.28}$$

In addition, in view of Lemma 1.1.3 and the ordering principle, we have stability whenever $B_k < 1$ and $\tau = 0$. Next, note that $B_1 = \frac{1}{2} + \frac{1}{2s}$. It follows that we have instability whenever $s < 1$. But from (1.18e), we have $s < 1$ for U^+, $s > 1$ for U^-.

We summarize the results as follows.

Theorem 1.1.7 *The large equilibrium solution ν^+, u^+ given in Proposition 1.1.1 is always unstable. A one-spike negative solution is always stable provided that $\tau = 0$.*

The small k-spike equilibrium solution ν^-, u^- is unstable, provided that $k \geq 2$ and $\mathcal{A} < \mathcal{A}_k$ or $l < l_k$, where $\mathcal{A}_k$ and l_k are given by (1.28) and (1.26) respectively. The converse is true when $\tau = 0$.

Note that the small and large k-spike solutions are connected through a saddle-node structure, as illustrated by solid curves in Figure 1.11. For a single-spike solution, since $s_1 = 1$, this
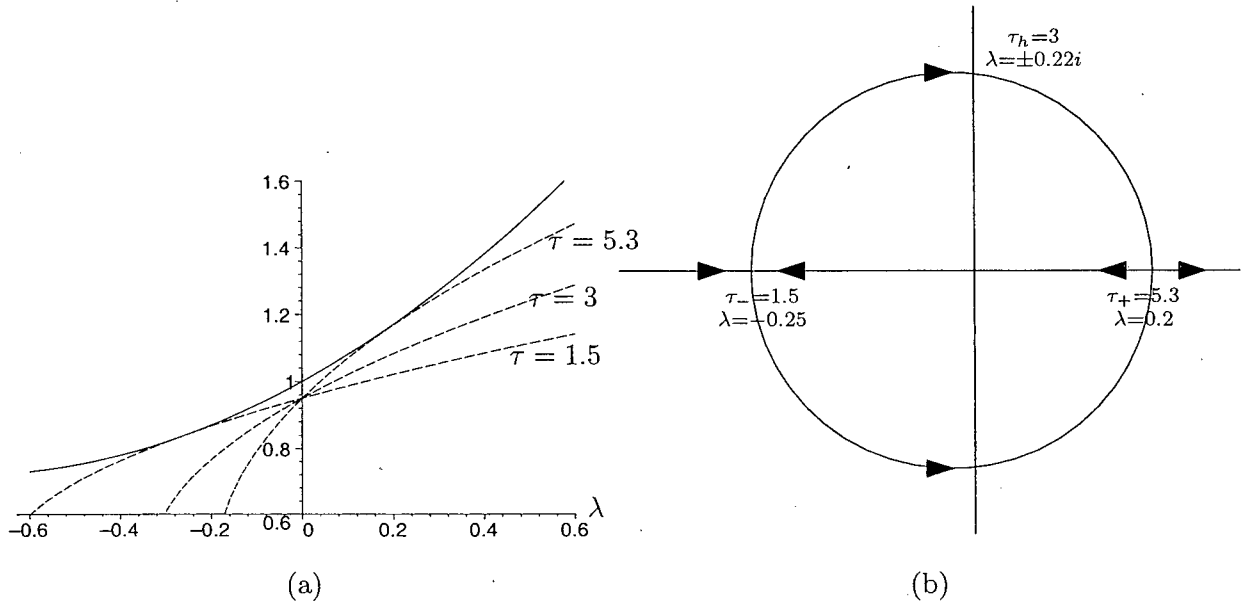
Figure 1.4: (a) The plot of $f(\lambda)$ (solid curve) and $C_1(\lambda)$ (dashed curves) for three different values of τ as indicated, with $C_1(0) = 0.9$. (b) The path traced by λ in the complex plane for different positive values of τ. The arrows indicate the direction of the path as τ is increased. Note that λ is negative real when $\tau < 1.5$, λ is complex for $\tau \in [1.5, 5.3]$ and λ is positive real when $\tau > 5.3$. A Hopf bifurcation occurs at $\tau = 3$.

theorem shows that the small solution branch is stable. For $k > 1$, part of the small branch near the fold point is also unstable.

A consequence of this theorem is that a domain of a given length $2l$ can support at most k spikes where k is some increasing function of l. If the initial condition consists of more than k spikes, then numerical simulations indicated that some of them will be annihilated until at most k are left. We thus refer to such an instability as *competition* or *overcrowding* instability. The name *competiton*

We next study the effect of τ on stability. In general, if τ is sufficiently large, the system can be destabilized via a Hopf bifurcation. This was first proved in [77] for the Gierer-Meinhardt model, and in [74] for the Gray-Scott model. In general, there is no explicit formulae for the threshold τ_h at which the Hopf bifurcation occurs (although rigorous estimates have been derived in [77]). However explicit formula is available when s is slightly above s_k. For clarity, we will only treat the case of a single spike here.

The existence of a Hopf bifurcation in such a case is easily seen geometrically, as shown in

14

Figure 1.4, and explained below. When s is slightly above $s_1 = 1$, $C_1(0)$ will be slightly below 1, and since f has a positive slope at the origin, it follows that for f will fall below $C_1(0)$ when λ is sufficiently negative. Note that increasing or decreasing τ corresponds to compressing or expanding the curve $C_1(\tau\lambda)$ along the x-axis, respectively. Moreover, $C_1 \to \infty$ as $\lambda \to \infty$. It follows that f and C_1 will intersect tangentially at some $\lambda < 0$ for some $\tau = \tau_-$ sufficiently small; and again at some $\lambda > 0$ for some $\tau = \tau_+ > \tau_-$. In between τ_- and τ_+, the intersections occur in complex plane; thus by continuity they must intersect the imaginary axis at some $\tau_h \in [\tau_-, \tau_+]$.

Next we compute the precise value of $\tau_h, \tau_\pm$. for s near 1. Assume that

$$s = 1 + \delta, \quad 0 < \delta \ll 1.$$

After some algebra, we obtain:

$$\frac{\tanh l\theta_\lambda}{\tanh l\theta_0} = 1 + zl\theta_0 \operatorname{csch} 2l\theta_0 - z^2\left(l\theta_0\frac{1}{4}\operatorname{csch}2l\theta_0 + \frac{1}{4}l^2\theta_0^2\operatorname{sech}^2 l\theta_0\right) + O(z^3), \quad z = \lambda\tau,$$

from which

$$C_1(\lambda) = 1 - \frac{\delta}{2} + \beta z - \gamma z^2 + O(z^2, \delta^2, z\delta), \quad \text{where}$$

$$z = \lambda\tau, \quad \beta = \frac{1}{4} + \frac{l\theta_0}{2}\operatorname{csch}2l\theta_0, \quad \gamma = \frac{1}{8} - \frac{1}{4}l\theta_0\operatorname{csch}2l\theta + \frac{1}{8}l^2\theta^2\operatorname{sech}^2 l\theta_0 \quad (1.29)$$

Moreover, using some calculus, one can show that γ always positive. It follows that the eigenvalue λ, given by the intersection of C_1 and f, satisfies:

$$\frac{\delta}{2} + \lambda(\frac{3}{4} - \beta\tau) + (\kappa_c + \gamma\tau^2)\lambda^2 = 0.$$

These curves intersect tangentially provided that in addition,

$$(\frac{3}{4} - \beta\tau) + (\kappa_c + \gamma\tau^2)2\lambda = 0.$$

This yields an equation for τ,

$$\delta = (\frac{3}{4} - \beta\tau)^2/(\kappa_c + \gamma\tau^2),$$

whose solution is

$$\tau_\pm = \frac{3}{4\beta} \pm \sqrt{\delta}\frac{\sqrt{\kappa_c + \gamma\left(\frac{3}{4\beta}\right)^2}}{\beta} + O(\delta)$$

15

The corresponding λ is negative for τ_- and positive for τ_+. When $\tau \in [\tau_-, \tau_+]$, the two curves f and C_1 do not intersect, and so λ is complex-valued. In particular, it is purely imaginary precisely when $\tau = \tau_h = \frac{3}{4\beta}$. This shows the existence of the Hopf bifurcation.

Next, the formula (1.27) yields: $\mathcal{A} = \mathcal{A}_{1e} \left(1 + \frac{1}{8}\delta^2\right)$. Finally for the infinite domain case $l = \infty$, we have $\beta = 4$, $\gamma = \frac{1}{8}$. We have shown the following:

Proposition 1.1.8 *Suppose that*

$$\mathcal{A} = \mathcal{A}_{1e} \left(1 + \frac{1}{8}\delta^2\right), \quad where \ \ 0 < \delta \ll 1. \tag{1.30}$$

Let

$$\tau_h = \frac{3}{4\beta} \quad and \ \ \tau_\pm = \tau_h \pm \sqrt{\delta}\frac{\sqrt{\kappa_c + \gamma\left(\frac{3}{4\beta}\right)^2}}{\beta},$$

where β and γ are defined in (1.29) and κ_c is defined in (1.21). Then the small equilibria solution (v_-, u_-) given by Proposition 1.1.1 with $k = 1$, is stable if and only if $\tau < \tau_h$, and undergoes a Hopf bifurcation at $\tau = \tau_h$. Moreover, the corresponding eigenvalue λ is purely imaginary at $\tau = \tau_h$, purely real and positive for $\tau \geq \tau_+$ and purely real and negative for $\tau < \tau_-$. For the case of an infinite domain $l = \infty$, we have

$$\tau_h = 3, \quad \tau_\pm = 3 \pm \sqrt{\delta}\frac{1}{4}\sqrt{\kappa_c + 9/8}.$$

When $\tau \in [\tau_h, \tau_+]$, due to the eigenvalue being complex, instability is manifested as small oscillations in the spike height. However when $\tau > \tau_+$, the eigenvalue is purely real, and numerical experiments indicate that the corresponding instability results in the monotinic decrease of spike height, until the spike is annihilated in $O(1)$ time. Thus the range of τ for which oscillatory behaviour occurs is of $O(\sqrt{\delta})$ when (1.30) is satisfied.

Due to the scaling of the Gray-Scott model (see (6)) τ must satisfy $\tau > 1$. It is easy to show that τ_h is an increasing function of θ_0 with $\tau_h = \frac{3}{2}$ when $\theta_0 = 0$ and $\tau_h = 3$ when $\theta_0 = \infty$. Thus the single spike solution that is near the threshold $\mathcal{A}_{1e}$ is always stable when $\tau = 1$.

16

1.1.3 Hopf bifurcation away from the saddle node point

In the previous section we have studied the occurence of the Hopf bifurcation using local analysis near the saddle node bifurcation point. Here, we study the more general case. We proceed as in [77] and [74]. The main result is the following.

Theorem 1.1.9 *Consider the k-spike small solution (ν_-, u_-) given by Proposition 1.1.1. Then for each $1 < j < k$, there exists a value $\tau_h > 0$ and $\tau_+ > \tau_h$ such that the j-th large eigenvalue of (1.18) is stable for τ just below τ_h, and unstable for all $\tau > \tau_h$. At $\tau = \tau_h$, this eigenvalue undergoes a Hopf bifurcation so that (1.18) admits purely imaginary eigenvalues. For $\tau \in [\tau_h, \tau_+]$ there are complex eigenvalues which merge with the positive real axis at $\tau = \tau_+$. For $\tau > \tau_+$, there are purely real, positive eigenvalues.*

We first show the existence of τ_h. We substitute $\lambda = i\lambda_i$ into (1.18) and collect real and imaginary parts. We obtain:

$$\widehat{C}_r(\tau\lambda_i) = \hat{f}_r(\lambda_i), \quad \widehat{C}_i(\tau\lambda_i) = \hat{f}_i(\lambda_i) \text{ where} \tag{1.31a}$$

$$\widehat{C}(\tau\lambda_i) = C(i\tau\lambda_i), \quad \hat{f}(\lambda_i) = f(i\lambda_i), \quad \widehat{C} = \widehat{C}_r + i\widehat{C}_i, \quad \hat{f} = \hat{f}_r + i\hat{f}_i, \text{ and } C = C_j \tag{1.31b}$$

with C_j given by (1.20). The key properties of these functions, derived in [77] and [74], are summarized below.

Lemma 1.1.10 *(see [77] and Proposition 3.7, [74]) The functions $\hat{f}_i, \hat{f}_r$ satisfy*

$$\hat{f}_r(\lambda_i) = \frac{\int wL_0[L_0^2 + \lambda_i^2]^{-1}w^2}{\int w^2}, \quad \hat{f}_i(\lambda_i) = \frac{\lambda_i \int w[L_0^2 + \lambda_i^2]^{-1}w^2}{\int w^2}.$$

They have the following asymptotic behaviour:

$$\hat{f}_r(\lambda_i) \sim 1 - \kappa_c\lambda_i^2 + O(\lambda_i^4) \text{ as } \lambda_i \to 0; \quad \hat{f}_r(\lambda_i) \sim \frac{7}{5}\lambda_i^{-2} + O(\lambda_i^{-4}) \text{ as } \lambda_i \to \infty, \tag{1.32a}$$

$$\hat{f}_i(\lambda_i) \sim \frac{3}{4}\lambda_i + O(\lambda_i^3) \text{ as } \lambda_i \to 0; \quad \hat{f}_i(\lambda_i) = \frac{5}{6}\lambda_i^{-1} + O(\lambda_i^{-2}) \text{ as } \lambda_i \to \infty. \tag{1.32b}$$

Here κ_c is given in (1.21). Moreover, the functions $\hat{f}_r(\lambda_i)$ and $\hat{f}_i(\lambda_i)$ have the following global behaviour:

$$\hat{f}_r'(\lambda_i) < 0, \quad \hat{f}_i(\lambda_i) > 0 \text{ for } \lambda_i > 0.$$

For $\lambda_i > 0$ and $\tau > 0$, the functions $\widehat{C}_r$ and $\widehat{C}_i$ given by (1.31) satisfy:

$$\widehat{C}_r(0) = B_j, \quad \widehat{C}_r'(\tau\lambda_i) > 0; \quad \widehat{C}_i(0) = 0, \quad \widehat{C}_i'(\tau\lambda_i) > 0, \tag{1.33a}$$

$$\frac{d}{d\lambda_i}\widehat{C}_r(\tau\lambda_i) = O(\tau^{1/2}), \quad \frac{d}{d\lambda_i}\widehat{C}_i(\tau\lambda_i) = O(\tau^{1/2}) \quad as \quad \tau \to \infty, \tag{1.33b}$$

$$\widehat{C}_r(\lambda_i\tau) = B_j + O(\tau\lambda_i), \quad \widehat{C}_i(\lambda_i\tau) = O(\tau\lambda_i) \quad as \quad \tau \to 0. \tag{1.33c}$$

Here, $B_j = C_j(0)$ whose properties are given in (1.22).

We now return to proof of Theorem 1.1.9. Let

$$g = C - f, \quad \hat{g} = \widehat{C} - \hat{f},$$

so that the number of unstable eigenvalues M of the mode j of (1.18) corresponds to the number of zeroes of g in the positive half-plane. To determine M, we use the argument principle. Consider a counterclockwise contour composed of the imaginary axis $[-iR, iR]$ and the semi-circle $Re^{i\theta}, \theta \in [-\frac{\pi}{2}, \frac{\pi}{2}]$. From (1.20) we have $C \sim O(\sqrt{\lambda})$ as $\lambda_r \to \infty$. Moreover $f \to 0$ as $\lambda_r \to \infty$. It follows that the change in argument of g over the semi-circle is $\frac{\pi}{2}$ as $R \to \infty$. In addition, the function g has a simple pole at the eigenvalue $5/4$ of the local operator L_0. On the imaginary axis, we use $g(\overline{\lambda}) = \overline{g(\lambda)}$. We thus obtain the following formula for the number of zeroes M of g in the right half-plane:

$$M = \frac{5}{4} + \frac{1}{\pi}\triangle_{[i\infty, 0]}g$$

where $\triangle_{[i\infty, 0]}g$ denotes the change in argument of g along the semi-infite imaginary axis $[0, i\infty]$ traversed in the downwards direction.

From Lemma 1.1.10 we have $\hat{g}_r(0) < 0$, $\hat{g}_r' > 0$ and $\hat{g}_r \to \infty$. It follows that $\hat{g}_r$ has a unique root $\lambda_i^* \in \hat{f}_r^{-1}([C(0), 1])$, for any given $\tau > 0$. Next, note that $\hat{g} \sim b\sqrt{\lambda_i}e^{i\pi/4}$ as $\lambda_i \to \infty$ where b is some positive constant, whereas $\hat{g}_r(0) < 0$, $\hat{g}_i(0) = 0$. Thus $\triangle_{[i\infty, 0]}g$ is either $-\frac{5}{4}\pi$ or $\frac{3}{4}\pi$, depending on whether the $\hat{g}_i(\lambda_i^*)$ is positive or negative, respectively. But by scaling, $\widehat{C}_i(\lambda_i\tau) \to 0$ as $\tau \to 0$ and $\widehat{C}_i(\lambda_i\tau) \to \infty$ as $\tau \to \infty$, with $\lambda_i \neq 0$. Thus we have: $\hat{g}_i(\lambda_i^*) > 0$ for τ sufficiently small and $\hat{g}_i(\lambda_i^*) < 0$ when τ is sufficiently large. In particular this shows the existence of τ_h at which $\hat{g}(\lambda_i^*) = 0$. Moreover, this shows that $M = 0$ for small enough

18

τ and $M = 2$ for large enough τ. Note that this does not show the uniqueness of τ_h. That is, we cannot rule out the possibility of $\hat{g}_i(\lambda_i^*)$ changing sign more than once as τ is changed. Nonetheless, by choosing the largest such τ_h, this shows the existence of τ_h for which λ is purely imaginary, and such that there are two positive eigenvalues for all $\tau > \tau_h$.

To show the existence of τ_+, some algebra shows that $C''(\tau\lambda) < 0$. It follows from convexity of f and the fact that $C \to \infty$ as $\tau\lambda \to \infty$ and $C(0) < 1$, that for small enough τ, the curves C and f do not intersect, and for large enough τ, they intersect twice. Thus by continuity, there must be a value of $\tau = \tau_+$ where these two curves intersect tangentially. Moreover, this value is unique because of convexity. For $\tau \geq \tau_+$, these intersections are clearly positive. This concludes the proof of Theorem 1.1.9. $\qquad\square$
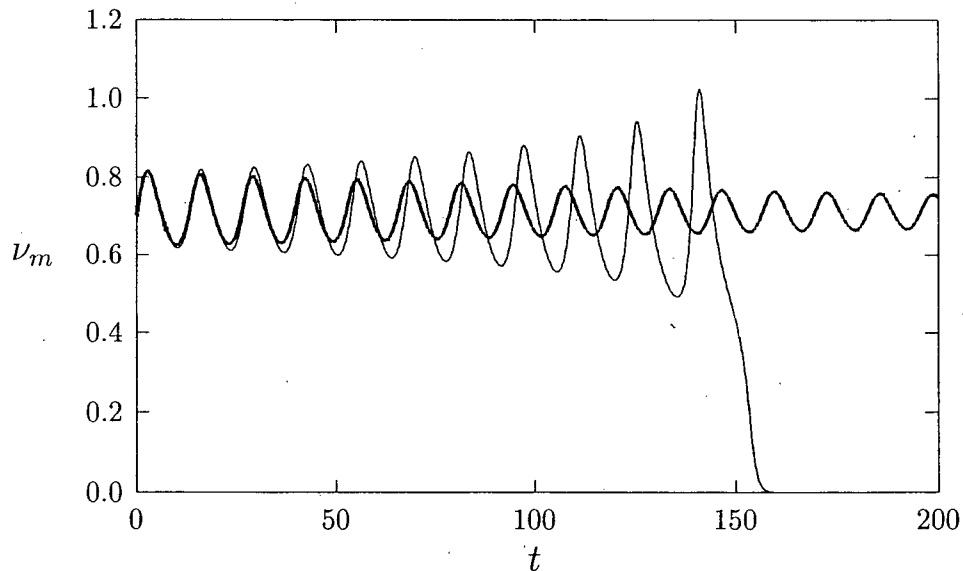
Figure 1.5: Plot of $\nu_m = \nu(0)$ versus t for a one-spike solution with $\varepsilon = 0.01, l = 1, D = 0.1, \mathcal{A} = 6.59$. The heavy curve corresponds to $\tau = 8.6$, the lighter to $\tau = 8.8$.

Note that the proof of this theorem is constructive: it gives a method for computing τ_h provided that $\hat{f}_i, \hat{f}_r$ are available. To verify this theorem, we took a one-spike solution with parameter values $l = 1, D = 0.1$, $\mathcal{A} = 6.59$ with $\varepsilon = 0.01$. For this parameter set, we have computed numerically that $\tau_h = 8.7$. We then plotted the evolution of the one-spike solution in time

for $\tau = 8.6$ and $\tau = 8.8$. The result is shown on Figure 1.5. For $\tau = 8.6$ we get decaying oscillations in spike height, and for $\tau = 8.8$ the oscillations start to increase in magnitude, eventually leading to the collapse of the spike. Thus the theory gives a correct prediction for the Hopf bifurcation value. Moreover, the increase of amplitude for $\tau > \tau_h$ suggests that the Hopf bifurcation is subcritical. Unfortunately the linear theory is insufficient to explain this.

1.1.4 Hopf bifurcation in the intermediate regime

Next we consider the intermediate regime (1.3), $1 \ll \mathcal{A} \ll \varepsilon^{-1/2}$. From (1.27) we obtain, for the small solution u^-, v^-:

$$s \sim 4\frac{\mathcal{A}^2}{\mathcal{A}_{ke}^2} \gg 1.$$

First, note that if $\lambda\tau = 0(1)$ then we have $C_j \sim \frac{1}{2}$ in which case the NLEP problem (1.18) is stable by Lemma 1.1.3. On the other hand, if θ_λ is large, (1.20) becomes: $C_j \sim \frac{1}{2} + \frac{1}{2s}\sqrt{\tau\lambda}\coth(l\theta_0/k)$. This suggests the following scaling for τ:

$$\tau = \tau_0 s^2 \tanh^2(l\theta_0/k)$$

so that C_j becomes:

$$C_j \sim \frac{1 + \sqrt{\tau_0\lambda}}{2},$$

and is independent of j. The proof of Theorem 1.1.9 then goes through as before, and shows the existence of the Hopf bifurcation $\tau_0 = \tau_{0h}$, as well as the existence of $\tau_0 = \tau_{0+}$ at which the eigenvalue merges with the real positive axis. Numerically, we find:

$$\tau_{0h} = 1.748, \quad \lambda_{ih} = 0.534; \quad \tau_{0+} = 8.567; \quad \lambda_+ = 0.300. \tag{1.34}$$

We summarize.

Proposition 1.1.11 *Consider the k spike small solution in the intermediate regime $1 \ll \mathcal{A} \ll \varepsilon^{-1/2}$, with $\frac{l}{\sqrt{D}} \gg 0$. Such solution is stable with respect to large eigenvalues whenever $\tau \ll O(\mathcal{A}^4)$. It undergoes a Hopf bifurcation at*

$$\tau_h = \mathcal{A}^4 D/9 \tanh^4(l\theta_0/k)\tau_{0h} \tag{1.35}$$

20

where τ_{0h} is given by (1.34). At that value of τ, $2k$ large eigenvalues cross the imaginary axis at asymptotically the same time.

Note that since the Hopf bifurcation for all the different nodes j occurs simultaneously, and since the corresponding k eigenvectors c_{mj} given by (1.24) span all of $\mathbb{R}^k$, the oscillating motion of the different spikes is independent of each-other.

While the expression (1.35) is valid asymptotically as $\varepsilon \to 0$, numerically we find that it provides a poor approximation for moderate values of ε such as $\varepsilon = 0.05$. A better agreement with numerics is obtained by finding the second term in the asymptotic expansion for τ_h. This calculation was performed in [74] with the following result:

$$\tau_h = \mathcal{A}^4 D/9 \tanh^4(l\theta_0/k)\tau_{0h} \left(1 - \frac{6l\theta_0 \tanh(\theta_0)}{\mathcal{A}^2}\right)^2.$$

1.2 High-feed and intermediate regime

We continue our study of Gray-Scott model (1.1), but this time we consider intermediate and high-feed regimes (1.3), (1.4). We find two types of instabilities that occur there, which are not present in the low-feed regime. The first type is an *undercrowding* or *pulse-splitting* instability. That is, when A is increased past a certain threshold, some of the spikes will be split into two spikes that start moving away from each other. This process may repeat a number of times, until sufficiently many spikes have been generated, at which time the system reaches an equilibrium. An example of such instability is shown on Figure 1.2:a. The pulse-splitting occurs only in the high-feed regime, and corresponds to the dissapearence of the steady-state solution as A is increased past a certain threshold. In §1.2.1, we derive the minimum number of pulse splittings that will occur before the spikes settle to a new equilibria.

The second type of instability is the slow oscillatory drift instability, as shown on Figure 1.2b. This instability occurs in both intermediate and high-feed regimes, when τ is of $O(\frac{1}{\varepsilon})$. The cause of such an instability is the existence of small eigenvalues of $O(\varepsilon)$ which cross the imaginary axis into the positive half-plane as τ is increased past a certain threhold. In §1.2.2 we derive

an expression for this threshold.

For the rest of this section, by scaling $x = \hat{x}\sqrt{D}$, we will assume without loss of generality that

$$D = 1.$$

To obtain results for an arbitrary D, it suffices to replace ε by $\frac{\varepsilon}{\sqrt{D}}$ and l by $\frac{l}{\sqrt{D}}$ in the results that follow.

1.2.1 Equilibria in high-feed and intermediate regime

We begin with the analysis of equilibria solutions of (1.1) with $D = 1$:

$$\begin{cases} 0 = \varepsilon^2 v_{xx} - v + Av^2 u \\ 0 = u_{xx} - u + 1 - v^2 u \quad , \quad x \in [-l, l] \\ v'(\pm l) = 0 = u'(\pm l) \end{cases} \tag{1.36}$$

We have the following result:

Proposition 1.2.1 *Let*

$$B = \tanh\left(\frac{l}{k}\right) A. \tag{1.37}$$

Suppose $A \gg \varepsilon^{1/2}$ and $B < 1.35$. Then there exists a spike solution to (1.36) of the form

$$v \sim \frac{1}{\varepsilon} V_0(r), \quad u \sim \frac{\varepsilon}{A} U_0(r), \quad r = \frac{x}{\varepsilon}.$$

where $V_0(r)$, $U_0(r)$ satisfy (1.42) below with boundary conditions

$$V_0(0) = 0 = U_0(0), \quad V_0(\infty) = 0, \quad U_0'(\infty) = B. \tag{1.38}$$

Conversely, if $B > 1.35$, then the k-spike solution of this form does not exist.

Thus, for any given k, the k-spike solution will dissapear if A is sufficiently increased. Conversely, for any given A or domain size l, there will be a k spike solution if k is large enough. For this reason, we refer to this instability as *undercrowding* or *pulse-splitting* instability. This

type of instability is in some sense the opposite of the overcrowding instability discussed in Theorem 1.1.7, where the equilibrium solution becomes unstable if k is too big.

Before showing Proposition 1.2.1, we consider a numerical example. Consider the case $l = 2$, $A = 3.5$, $D = 1$, $\varepsilon = 0.03$, $\tau = 1$. Letting $B_k = A \tanh \frac{l}{k}$, we obtain: $B_1 = 3.34$, $B_2 = 2.66$, $B_3 = 2.03$, $B_4 = 1.61$, $B_5 = 1.32$. We see that $B_4 > 1.35$ but $B_5 < 1.35$. So for the equilibrium to exist, we must have $k \geq 5$. Indeed, starting with the initial conditions of one spike whose center is located slightly asymmetrically at $x_0 = 0.1$, the system undergoes 4 additional spike splittings, and then settles to a 5-spike equilibrium, as shown on Figure 1.2a.

To show Proposition 1.2.1, we start by constructing a single-spike solution on $[-l, l]$. Because of the Neumann boundary condition, we can then glue together k copies of such a solution to obtain a k-spike solution on $[-lk, lk]$. By redefining $l \to l/k$ we will then obtain a k spike solution on the interval $[-l, l]$.

Near the core of the spike, we make the following rescaling:

$$v = \frac{1}{\varepsilon} V(r), \quad u = \frac{\varepsilon}{A} U(r), \quad r = \frac{x}{\varepsilon}. \tag{1.39}$$

The steady state solution then satisfies:

$$0 = V'' - V + V^2 U \tag{1.40a}$$

$$0 = U'' - \varepsilon^2 U + A\varepsilon - V^2 U. \tag{1.40b}$$

Therefore we expand:

$$v = \frac{1}{\varepsilon} \left(V_0(r) + A\varepsilon V_1(r) + \cdots \right), \quad u = \frac{\varepsilon}{A} \left(U_0(r) + A\varepsilon U_1(r) + \cdots \right) \tag{1.41}$$

to obtain:

$$0 = V_0'' - V_0 + V_0^2 U_0 \tag{1.42a}$$

$$0 = U_0'' - V_0^2 U_0 \tag{1.42b}$$

and

$$0 = V_1'' - V_1 + 2V_0U_0V_1 + V_0^2U_1 \tag{1.43a}$$

$$0 = U_1'' + 1 - 2V_0U_0V_1 - V_0^2U_1. \tag{1.43b}$$

Next, we expand the outer solution as:

$$u = u_0(x_1) + \varepsilon u_1 + \ldots$$

to obtain:

$$u_0'' - u_0 = -1 + v^2 u$$

from where

$$u_0(x_1) = 1 - \int_{-l}^{l} G(x_1, x_1')v^2(x_1')u(x_1')dx_1'$$

where G is the Green's function with Neumann's boundary conditions:

$$G_{xx} - G = -\delta(x - x'), \tag{1.44a}$$

$$G_x(-l, x') = 0 = G_x(l, x'). \tag{1.44b}$$

It is easy to see that

$$G(x, x') = \frac{1}{J_1'(x')J_2(x') - J_1(x')J_2'(x')} \begin{cases} J_1(x)J_2(x') & \text{if} \quad x < x' \\ J_1(x')J_2(x) & \text{if} \quad x' < x \end{cases} \tag{1.45a}$$

where $\quad J_1(x) = \cosh(l + x), \quad J_2(r) = \cosh(l - x). \tag{1.45b}$

Thus we have:

$$J_1'(0)J_2(0) - J_1(0)J_2'(0) = 2l\sinh(l)\cosh(l),$$

$$G(0, 0) = \frac{1}{2}\coth(l).$$

and so:

$$u(\varepsilon r) = 1 - \frac{1}{A}\int_{-\frac{l}{\varepsilon}}^{\frac{l}{\varepsilon}} G(\varepsilon r, \varepsilon r')\left[V_0^2U_0 + \varepsilon A\left(2V_0U_0V_1 + V_0^2U_1\right)\right]dr'; \tag{1.46a}$$

$$u_0(0) = 1 - \frac{1}{A}G(0, 0)\int_{-\infty}^{\infty} V_0^2U_0, \tag{1.46b}$$

$$u_0'(0^{\pm}) = -\frac{1}{A}G_x(0^{\pm}, 0)\int_{-\infty}^{\infty} V_0^2U_0, \tag{1.46c}$$

$$u_0''(0^{\pm}) = -\frac{1}{A}G_{xx}(0^{\pm}, 0)\int_{-\infty}^{\infty} V_0^2U_0 = -\frac{1}{A}G(0, 0)\int_{-\infty}^{\infty} V_0^2U_0. \tag{1.46d}$$

24

We also have the following matching condition:

$$u_0(\varepsilon r) + \varepsilon u_1(\varepsilon r) \sim \frac{\varepsilon}{A} U_0(r) + \varepsilon^2 U_1(r). \tag{1.47}$$

This yields:

$$u_0(0) = 0, \tag{1.48a}$$

$$U_0'(\pm\infty) = A u_0'(0^\pm), \tag{1.48b}$$

$$U_1''(\infty) = u_0''(0^+) \tag{1.48c}$$

Next, we define:

$$B = \frac{1}{2} \int_{-\infty}^{\infty} V_0^2 U_0. \tag{1.49}$$

Equations (1.46b) and (1.48a) then yields:

$$B = \frac{A}{2G(0,0)} = \tanh(l) A. \tag{1.50}$$

and from (1.48c), (1.48a), (1.46d) we obtain:

$$U_1''(\infty) = u_0''(0^+) \sim u_0(0) - 1 \sim -1 \tag{1.51}$$

Integrating (1.42b) (or alternatively, using (1.46c, 1.48b) and $G_x(0^+, 0) = -\frac{1}{2}$) we obtain:

$$U_0'(\infty) = \int_0^{\infty} V_0^2 U_0 = B.$$

Next, we argue numerically that the solution to the problem (1.42) with boundary conditions $V_0(0) = U_0(0) = 0$, $V_0(\infty) = 0$, $U_0'(\infty) = B$, exists only when $B < 1.35$. Multiplying (1.42a) by V_0', integrating and using $V_0'(0) = 0$ yields:

$$V_0^2(0) - \frac{1}{3} V_0^3(0) U(0) = \int_0^{\infty} \frac{1}{3} V_0(r)^3 U_0'(r) dr.$$

Assuming $V_0 > 0$ and integrating (1.42b), we see $U_0' > 0$ so that that $\int_0^{\infty} \frac{1}{3} V_0(r)^3 U'(r) dr > 0$. Therefore letting

$$\gamma = V_0(0) U_0(0), \tag{1.52}$$

we obtain $0 \le \gamma \le \frac{3}{2}$. For each value of γ in that range, we compute numerically the corresponding value of B. The resulting plot is shown in Figure 1.6. This graph has a fold point
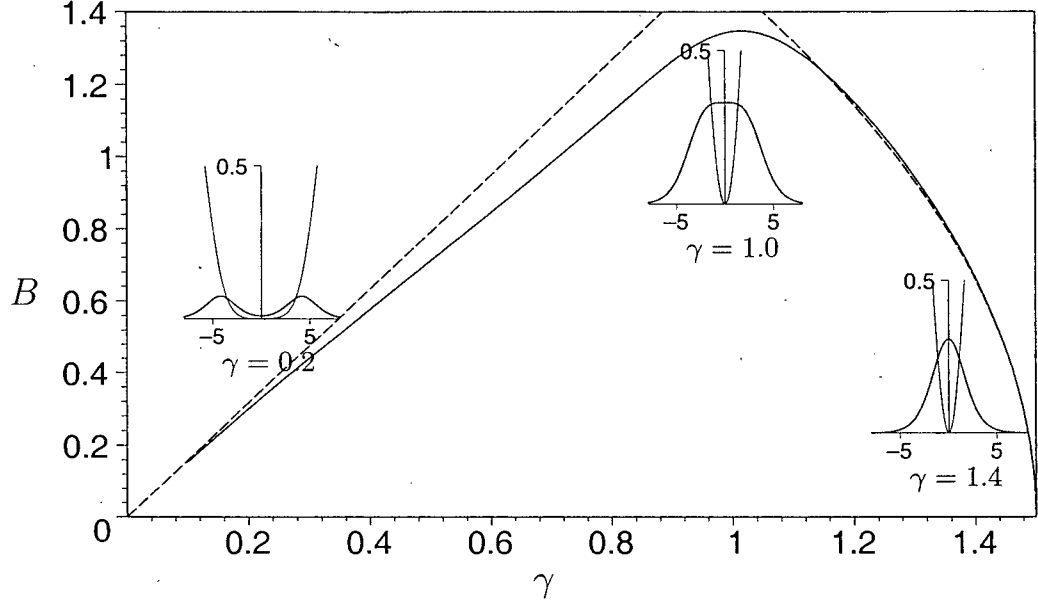
Figure 1.6: The graph of $\gamma = V(0)U(0)$ vs. $B = U'(\infty)$. The fold point occurs at $\gamma = 1.02$, $B = 1.35$. The dashed curves represent asymptotic approximations, derived in Propositions 1.2.2 and 1.2.3. Subfigures show the actual solution for three different values of γ as indicated. In subfigures, the thicker curve represents V_0 and the thinner $U_0(r) - U_0(0)$. Note that near the left endpoint, the solution looks like two well-separated bumps, whereas near the right endpoint the solution consists of a single bump. At $\gamma = 1$, the solution is flat at the top.

at $\gamma = 1.02$, at which point $B = 1.35$. Beyond $B = 1.35$, no single-spike solution exists. This concludes the proof of Proposition 1.2.1 $\qquad\qquad\square$

In general, the problem (1.42, 1.38) must be solved numerically. However asymptotic expansion is available in the intermediate regime, when B is small. We first study the limiting behavior $U(0) \gg 1$. We introduce a small parameter δ by $\delta = 1/U(0)$, and expand the solution to (1.42) in terms of δ as

$$V = \delta\left(v_0 + \delta^2 v_1 + \cdots\right), \qquad U = \delta^{-1}u = \delta^{-1}\left(u_0 + \delta^2 u_1 + \cdots\right), \qquad \text{with} \quad u(0) = 1.$$

$$(1.53)$$

Since $\int_0^\infty V^2 U \, dr = B$ from (1.49), the expansion (1.53) yields that $B = O(\delta)$. Hence, we write $B = \delta B_0$. Substituting (1.53) into (1.42), and collecting powers of δ, we obtain the leading-order

26

problem

$$v_0'' - v_0 + v_0^2 u_0 = 0\,, \qquad u_0'' = 0\,, \tag{1.54}$$

with $v_0'(0) = 0$, $u_0(0) = 1$, $v_0 \to 0$ as $r \to \infty$, and $u_0' \to 0$ as $r \to \infty$. Therefore, we obtain $u_0(r) = 1$ and $v_0(r) = w(r)$, where w satisfies (1.7). From collecting terms of order $O(\delta^2)$, we see that v_1 and u_1 satisfy

$$Lv_1 \equiv v_1'' - v_1 + 2wv_1 = -w^2 u_1\,, \quad 0 < r < \infty\,; \qquad v_1'(0) = 0\,, \quad v_1 \to 0\,, \quad \text{as} \quad r \to \infty\,, \tag{1.55a}$$

$$u_1'' = w^2\,, \quad 0 < r < \infty\,; \qquad u_1'(0) = 0\,, \quad u_1(0) = 0\,, \quad u_1' \to B_0\,, \quad \text{as} \quad r \to \infty\,. \tag{1.55b}$$

By integrating (1.55b) over $0 < r < \infty$, we get that $B_0 = \int_0^\infty w^2\, dr = 3$.

Next, we multiply (1.55a) by w' and integrate over $0 < r < \infty$. Then, using $Lw' = 0$ and $w'(0) = v_1'(0) = 0$, we get

$$\int_0^\infty w' Lv_1\, dr = w''(0)v_1(0) = -\int_0^\infty w^2 w' u_1\, dr\,. \tag{1.56}$$

Integrating the last term in (1.56) by parts, and noting that $u_1(0) = 0$, we get

$$w''(0)v_1(0) = \frac{1}{3} \int_0^\infty w^3 u_1'\, dr\,. \tag{1.57}$$

To calculate $v_1(0)$, we must determine $u_1'(r)$. To do so, we substitute $w(r) = \frac{3}{2}\,\text{sech}^2\,(r/2)$ and $w^2 = w - w''$ directly into (1.55b) to get

$$u_1'' = w - w'' = \frac{3}{2}\,\text{sech}^2\,(r/2) - w''\,. \tag{1.58}$$

Integrating this equation twice, and using $u_1'(0) = 0$, $u_1(0) = 0$, we readily obtain

$$u_1(r) = 6\ln\left[\cosh\left(\frac{r}{2}\right)\right] - \frac{3}{2}\,\text{sech}^2\left(\frac{r}{2}\right) + \frac{3}{2}\,. \tag{1.59}$$

To determine $v_1(0)$, we integrate (1.58) once to get

$$u_1' = 3\tanh\left(\frac{r}{2}\right) - w' = -\frac{3w'}{w} - w'\,. \tag{1.60}$$

Finally, substituting (1.60) into (1.57), integrating the resulting expression by parts, and using the explicit form of w, we obtain

$$v_1(0) = \frac{1}{3w''(0)} \int_0^\infty \left(-3w^2 w' - w' w^3\right)\, dr = \frac{1}{3w''(0)} \left[w^3(0) + \frac{w^4(0)}{4}\right] = -\frac{33}{16}\,. \tag{1.61}$$

27

Since $\gamma \equiv U_0(0)V_0(0)$, we use (1.53) to get $\gamma = w(0) + \delta^2 v_1(0)$. We summarize the result of this calculation in the following formal proposition:

Proposition 1.2.2 *Consider the intermediate regime $B = 3\delta$, with $\delta \ll 1$, where $B = A\tanh(l/k)$. Then the core problem (1.42) admits a solution with $\gamma \equiv U_0(0)V_0(0) \to 3/2^-$ as $\delta \to 0$. This solution is given asymptotically by*

$$V_0 \sim \delta \left(w(r) + \delta^2 v_1(r) + \cdots \right), \qquad U_0 \sim \delta^{-1} \left(1 + \delta^2 u_1(r) + \cdots \right), \tag{1.62a}$$

where $w(r)$ satisfies (1.7), $u_1(r)$ is given in (1.59), and v_1 satisfies:

$$v_1'' - v_1 + 2wv_1 = -w^2 u_1, \quad v_1'(0) = 0, \quad v_1 \to 0 \ as \ r \to \infty. \tag{1.62b}$$

Moreover, we have $v_1(0) = -\frac{33}{16}$,

$$\gamma \sim \frac{3}{2} - \frac{33}{16}\delta^2 + \cdots. \tag{1.62c}$$

The asymptotic curve $B \sim 3\delta, \gamma \sim \frac{3}{2} - \frac{33}{16}\delta^2$ is shown as the dashed parabola in Figure 1.6. As seen from that figure, it provides a good approximation to the actual solution of the core problem (1.42) in the limit $\gamma \to 3/2^-$.

Next we construct a solution that corresponds to the regime $\gamma \to 0$. First, note that $V_0''(0) = 0$ at $\gamma = 1$ and $V_0''(0) > 0$ when $\gamma < 1$. This suggests that in the limit $\gamma \to 0$, the solution has the shape of two bumps. To analyze this regime, we again label $\delta = 1/U_0$, with $U_0 \equiv U(0)$, except that now we make a two-spike approximation for V with spikes located at $r = r_1 > 0$ and $r = -r_1$. As $\delta \to 0$, we will show that $r_1 \sim -\ln\delta \gg 1$. Therefore, the separation between the spikes grows as δ decreases. The analysis below to calculate r_1 is similar in essence to the analytical construction of multi-bump solutions to the Gierer-Meinhardt model (cf. [26]) given in [12].

We look for a two-bump solution to (1.42) in the form

$$V_0 = \delta \left(w_1 + w_2 + R + \cdots \right), \quad U_0 = \delta^{-1}u = \delta^{-1} \left(1 + \delta^2 u_1 + \cdots \right) \quad \text{with} \quad u_1(0) = 0. \tag{1.63}$$

28

Here we have labelled $w_1(r) \equiv w(r - r_1)$, $w_2(r) \equiv w(r + r_1)$, and we assume $R \ll 1$. Substituting (1.63) into (1.42), we obtain that u_1 and the residual R satisfy

$$LR \equiv R'' - R + 2(w_1 + w_2)R = -2w_1w_2 - \delta^2 \left(w_1^2 + w_2^2 + 2w_1w_2 \right) u_1 , \quad -\infty < r < \infty ,$$

(1.64a)

$$u_1'' = w_1^2 + w_2^2 + 2w_1w_2 , \quad -\infty < r < \infty ,$$

(1.64b)

with $u_1'(0) = 0$. Notice that w_1w_2 is small when the bumps are widely separated. In particular, when $r_1 = O(-\ln \delta)$, the two terms on the right hand-side of (1.64a) are both of order $O(\delta^2)$. This is compatible with R being small, indeed it shows $R = O(\delta^2)$.

To determine r_1 we use a solvability condition. Assuming that the spikes are well-separated so that $r_1 \gg 1$, we multiply (1.64a) by w_1', and then integrate by parts over $-\infty < r < \infty$ to obtain the solvability condition

$$0 = \int w_1' LR \, dr \sim -2 \int w_1 w_1' w_2 \, dr - \delta^2 \int w_1^2 w_1' u_1 \, dr .$$

(1.65)

The dominant contribution to the first integral on the right hand-side of (1.65) arises from the region where $r = r_1$. In this region, we use $w(r) \sim 6e^{-r}$ to get $w(r + 2r_1) \sim 6e^{-r-2r_1}$. In this way, we calculate

$$I_1 \equiv 2 \int w_1 w_1' w_2 \, dr \sim 2 \int w(r) w'(r) w(r + 2r_1) \, dr \sim 12e^{-2r_1} \int e^{-r} w(r) w'(r) \, dr .$$

(1.66)

Integrating the last expression in (1.66) by parts, and then using $w^2 = w - w''$, we obtain

$$I_1 \sim 6e^{-2r_1} \int e^{-r} \left(w - w'' \right) dr = 6e^{-2r_1} \lim_{r \to -\infty} \left[e^{-r} \left(w + w' \right) \right] = 72e^{-2r_1} .$$

(1.67)

To calculate the other integral on the right hand-side of (1.65) we integrate by parts once and use $u_1(0) = 0$ to get

$$I_2 \equiv \delta^2 \int w_1^2 w_1' u_1 \, dr = -\frac{\delta^2}{3} \int w_1^3 u_1' \, dr = -\frac{\delta^2}{3} \int [w(r)]^3 u_1'(r + r_1) \, dr .$$

(1.68)

Next, by integrating (1.64b) with $u_1'(0) = 0$, we get

$$u_1'(r) \sim \int_0^r [w(s - r_1)]^2 \, ds .$$

(1.69)

29

We can then write $u_1'(r + r_1)$ as

$$u_1'(r + r_1) \sim \int_{-r_1}^{0} [w(s)]^2 \, ds + \int_{0}^{r} [w(s)]^2 \, ds \sim 3 + \int_{0}^{r} [w(s)]^2 \, ds \,. \tag{1.70}$$

Here we have used $\int_{-r_1}^{0} w^2 \, dr \sim \int_{-\infty}^{0} w^2 \, dr = 3$ for $r_1 \gg 1$. The integral on the right hand-side of (1.70) is odd. Therefore, upon substituting (1.70) into (1.68), we get an integral that is readily evaluated as

$$I_2 \sim -\delta^2 \int [w(r)]^3 \, dr = -\frac{36\delta^2}{5} \,. \tag{1.71}$$

Finally, substituting (1.71) and (1.67) into (1.65), we obtain that r_1 satisfies

$$72 e^{-2r_1} \sim \frac{36\delta^2}{5} \,. \tag{1.72}$$

The product $\gamma \equiv U_0 V_0$ is calculated as $\gamma \sim [w_1(0) + w_2(0)] = 2w(r_1)$. Since $r_1 \gg 1$, we use $w(r) \sim 6e^{-r}$ to get $\gamma \sim 12 e^{-r_1}$, where r_1 satisfies (1.72). Finally, B is determined by $B = \delta \int_{0}^{\infty} [w_1^2 + w_2^2] \, dr \sim 6\delta$. This formal construction of a two-bump solution is summarized as follows:

Proposition 1.2.3 *Let $\delta = 1/U_0(0) \ll 1, \gamma = U_0(0)V_0(0)$. Then the core problem (1.42) admits a two-bump solution with $\gamma \to 0^+$ as $\delta \to 0^+$. This solution is given asymptotically by*

$$V_0 \sim \delta \left[w(r - r_1) + w(r + r_1) \right] \qquad U_0 \sim \frac{1}{\delta} \left(1 + \delta^2 \left[u_1(r - r_1) + u_1(r + r_1) \right] \right) , \tag{1.73a}$$

where $w(r)$ satisfies (1.7), and $u_1(r)$ is given explicitly in (1.59). The constants γ, r_1, and B, are given for $\delta \ll 1$ by

$$B = 6\delta + \cdots , \qquad \gamma \equiv U_0 V_0 \sim \frac{6\delta\sqrt{2}}{\sqrt{5}} , \qquad r_1 \sim -\ln \delta + \frac{1}{2} \ln 10 \,. \tag{1.73b}$$

This implies the following local behavior for the $B = B(\gamma)$ curve:

$$\gamma \equiv U_0 V_0 \sim \sqrt{2} B / \sqrt{5} , \qquad as \quad B \to 0 \,. \tag{1.73c}$$

Numerically, the single-bump solution found in Proposition 1.2.2 joins with the double-bump solution of Proposition 1.2.3. Since $B \to 0$ at the endpoints $\gamma = 3/2$, 0, this necessitates the

existence of the fold point corresponding to the maximum of the $B = B(\gamma)$ curve. However it is an open question to show this rigorously.

Next, we argue numerically that the existence of a connection between a single and double-bump solution graph causes the pulse to split into two when B is increased beoynd the the fold point at $B = 1.35$. We first show the existence of the zero eigenvalue at the fold point. We introduce a perturbation around the equilibrium state:

$$v(x) = \frac{1}{\varepsilon}\left(V(r) + e^{\lambda t}\Phi(r)\right),$$
$$u(x) = \frac{\varepsilon}{A}\left(U(r) + e^{\lambda t}N(r)\right) \quad \text{where } r = \frac{x}{\varepsilon}$$

to obtain:

$$\lambda\Phi = \Phi'' - \Phi + V^2 N + 2VU\Phi \tag{1.74}$$
$$\tau\varepsilon^2\lambda N = N'' - \varepsilon^2 N - V^2 N - 2VU\Phi.$$

At the fold point $\gamma_0 = 1.02, B = 1.35$, we have $\frac{dB}{d\gamma} = 0$. Using this identity and differentiating (1.42) with respect to γ, we obtain a leading-order solution to (1.74) given by

$$\lambda = 0, \quad \Psi = \frac{dV_0}{d\gamma_0}, \quad N = \frac{dU_0}{d\gamma_0}.$$

Next, we compute the function $\frac{dV_0}{d\gamma_0}$ numerically, using the approximation $\frac{dV_0}{\gamma_0} \sim 200(V_0|_{\gamma_0+0.01} - V_0|_{\gamma_0-0.01})$. As can be seen from the resulting graph on Figure 1.7, this eigenfunction has a dimple-like shape. As a consequence, when B is increased just above 1.35, the equilibrium solution dissapears, but the *shadow* of the dimple eigenfunction will control the resulting dynamics. Its shape has the effect of splitting the spike into two. Numerically, immediately after splitting the two spikes start to move away from each-other. As they move far enough apart, the equilibrium state may again dissapear and the whole process can repeat itself.

1.2.2 Slow drift and oscillatory drift instabilities

So far, we have studied instabilities which occur on a fast time scale, due to an unstable eigenvalue of $O(1)$. Next, we study instabilities with respect to small eigenvalues. Such eigenvalues

31
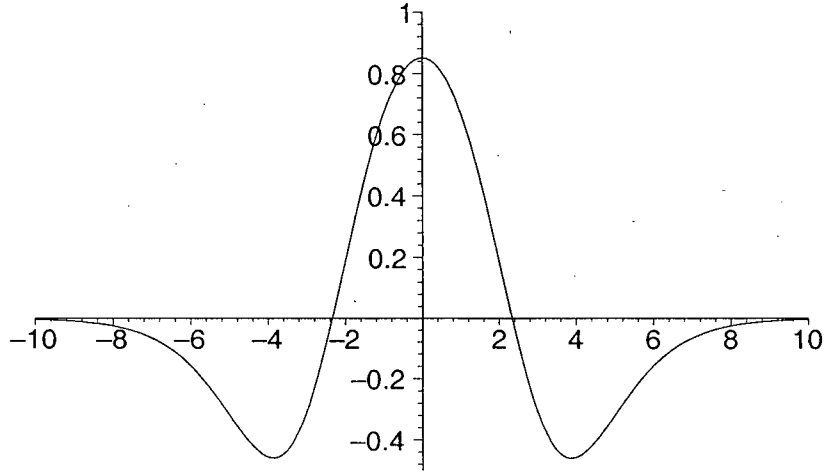
Figure 1.7: The graph of the dimple eigenfunction $\Phi = \frac{dV_0}{d\gamma_0}$ at the fold point $\gamma_0 = 1.02$.

exist because of translation invariance of the Gray-Scott model. The corresponding perturbation is the derivative of the profile to the leading order. The main result of this section is the following.

Theorem 1.2.4 *Let* $\varepsilon A \ll 1$, $A \gg \varepsilon^{1/2}$ *and* $\varepsilon \ll 1$. *Then the small eigenvalues* λ *associated with drift instabilities of the k-spike equilibrium solution of Proposition 3.1 are of order* $O(\varepsilon A)$, *and satisfy the k transcendental equations,*

$$\lambda \sim \alpha \varepsilon A \left[\theta_\lambda \tanh \left(\frac{l}{k} \right) \left(\coth \left(\frac{2l\theta_\lambda}{k} \right) + \operatorname{csch} \left(\frac{2l\theta_\lambda}{k} \right) \cos \left(\frac{\pi j}{k} \right) \right) - 1 \right], \qquad j = 1, \ldots, k,$$
$$(1.75)$$

where

$$\theta_\lambda = \sqrt{1 + \lambda \tau}$$

and α *is some positive constant that is defined in (1.102) below. This constant depends only on the bifurcation parameter* γ *associated with the core solution, and is listed in Table (1.80). The constant* α *is found to be positive numerically. In the inner region near the* m^{th} *spike, the perturbation of the v-component of the equilibrium solution that corresponds to j-th small eigenvalue (1.75) has the following form:*

$$v(x,t) \sim \frac{1}{\varepsilon} \left(V_0 \left(\frac{x - x_m}{\varepsilon} \right) + \beta c_{mj} V_0' \left(\frac{x - x_m}{\varepsilon} \right) e^{\lambda t} \right), |x - x_m| \ll 1 \qquad (1.76)$$

where $\beta \ll 1$ is some small constant, V_0 is defined in Proposition 1.2.1, and

$$c_{mj} = \sin\left(\frac{\pi j}{k}(m - 1/2)\right). \tag{1.77}$$

In the intermediate regime

$$A \sim 3\coth(l/k)\delta \quad with \ \delta \ll 1, \tag{1.78}$$

the constant α is given asymptotically as

$$\alpha \sim 2\delta \sim \frac{2}{3}A\tanh(l/k) \tag{1.79}$$

γ	B	$\int \Psi_1^\dagger V_r$	α
1.48	0.30	-10.01	0.20
1.46	0.40	-7.51	0.27
1.44	0.50	-6.00	0.33
1.42	0.60	-4.98	0.40
1.39	0.70	-4.24	0.47
1.36	0.80	-3.67	0.56
1.32	0.90	-3.20	0.63
1.28	1.00	-2.79	0.72
1.23	1.10	-2.41	0.83
1.17	1.20	-2.01	1.00
1.14	1.25	-1.77	1.13
1.10	1.30	-1.48	1.35
1.02	1.347	-0.74	2.70

$$\tag{1.80}$$

We begin by linearizing around the equilibrium v_e, u_e:

$$v = v_e + e^{\lambda t}\phi, \qquad u = u_e + e^{\lambda t}\eta. \tag{1.81}$$

Substituting (1.81) into (1.1) with $D = 1$ we obtain the eigenvalue problem

$$\varepsilon^2 \phi_{xx} - \phi + 2Au_e v_e \phi + A\eta v_e^2 = \lambda\phi, \qquad -1 < x < 1, \tag{1.82a}$$

$$\eta_{xx} - \eta - \eta v_e^2 - 2u_e v_e \phi = \tau\lambda\eta, \qquad -l < x < l. \tag{1.82b}$$

We begin by examining (1.82) in the jth inner region where $r = \varepsilon^{-1}(x - x_j)$. Since we use the scaling (1.39) for the equilibrium solution, we also rescale the eigenfunctions as

$$\phi(x) = \frac{A}{\varepsilon}\Phi(r; \varepsilon), \qquad \eta(x) = \varepsilon N(r; \varepsilon). \tag{1.83}$$

33

to obtain (1.74). Next, we expand Φ, N and λ in εA:

$$\Phi = \Phi_0 + A\varepsilon\Phi_1, \quad N = N_0 + A\varepsilon N_1, \quad \lambda = A\varepsilon\lambda_0.$$

Note that

$$V^2 = V_0^2 + 2\varepsilon A V_0 V_1, \quad UV = U_0 V_0 + \varepsilon A(V_0 U_1 + U_0 V_1)$$

where U_m, V_m are defined in (1.42) and (1.43). Thus we obtain:

$$0 = \Phi_0'' - \Phi_0 + V_0^2 N_0 + 2V_0 U_0 \Phi_0, \tag{1.84a}$$

$$0 = N_0'' - V_0^2 N_0 - 2V_0 U_0 \Phi_0. \tag{1.84b}$$

and:

$$\lambda_0 \Phi_0 = \Phi_1'' - \Phi_1 + V_0^2 N_1 + 2V_0 V_1 N_0 + 2V_0 U_0 \Phi_1 + 2(V_0 U_1 + U_0 V_1)\Phi_0 \tag{1.85a}$$

$$0 = N_1'' - \left[V_0^2 N_1 + 2V_0 V_1 N_0 + 2V_0 U_0 \Phi_1 + 2(V_0 U_1 + U_0 V_1)\Phi_0 \right]. \tag{1.85b}$$

Differentiating (1.42), we see that (1.84) admits a solution:

$$\Phi_0 = c_j V_0', \quad N_0 = c_j U_0', \tag{1.86}$$

where c_j will be determined below through asymptotic matching. Substituting (1.86) into (1.85), we then express the result in matrix form as

$$\mathcal{L}\Psi = c_j \begin{pmatrix} \lambda_0 & 0 \\ 0 & 0 \end{pmatrix} \begin{pmatrix} V_r \\ U_r \end{pmatrix} + c_j \begin{pmatrix} -2(UV_1 + U_1 V) & -2VV_1 \\ 2(UV_1 + U_1 V) & 2VV_1 \end{pmatrix} \begin{pmatrix} V_r \\ U_r \end{pmatrix}, \tag{1.87a}$$

where $\Psi \equiv (\Phi_1, N_1)^t$, and the operator $\mathcal{L}$ is defined by

$$\mathcal{L}\Psi \equiv \begin{pmatrix} \Phi_{1rr} \\ N_{1rr} \end{pmatrix} + E \begin{pmatrix} \Phi_1 \\ N_1 \end{pmatrix}, \quad E \equiv \begin{pmatrix} -1 + 2UV & V^2 \\ -2UV & -V^2 \end{pmatrix}. \tag{1.87b}$$

To determine the solvability condition for (1.87), we let $\Psi^\dagger$ denote the solution of the homogeneous adjoint equation

$$\mathcal{L}^\dagger \Psi^\dagger \equiv \begin{pmatrix} \Psi_{1rr}^\dagger \\ \Psi_{2rr}^\dagger \end{pmatrix} + E^t \begin{pmatrix} \Psi_1^\dagger \\ \Psi_2^\dagger \end{pmatrix} = 0, \tag{1.88}$$

where t denotes transpose. We look for an odd solution to (1.88) where $\Psi_1^\dagger \to 0$ and $\Psi_{2r}^\dagger \to 0$ as $|r| \to \infty$.

To determine the solvability condition for (1.87a), we multiply (1.87a) by $\Psi^{\dagger t}$ and integrate by parts to get

$$\int \Psi^{\dagger t} \mathcal{L} \Psi \, dr = \left(\Psi^{\dagger t} \Psi_r - \Psi^t \Psi_r^\dagger \right) \big|_{-\infty}^\infty = c_j \lambda_0 I_2 + c_j I_1 \,, \tag{1.89a}$$

where I_1 and I_2 are defined by

$$I_1 \equiv \int \left(\Psi_2^{\dagger t} - \Psi_1^{\dagger t} \right) \left[2(UV)_r V_1 + (V^2)_r U_1 \right] \, dr \,, \qquad I_2 \equiv \int \Psi_1^\dagger V_r \, dr \,. \tag{1.89b}$$

Since Ψ and $\Psi^\dagger$ are odd functions and $\Psi_r^\dagger \to 0$ as $r \to \infty$, (1.89a) can be reduced to

$$c_j \lambda_0 I_2 = -c_j I_1 + \Psi_2^\dagger(\infty) \left(N_{1r}(+\infty) + N_{1r}(-\infty) \right) \,. \tag{1.89c}$$

The next step in the analysis is to calculate I_1 explicitly. To do so, we introduce W by $W = (V_{1r}, U_{1r})^t$. Upon differentiating the system (1.43) for V_1 and U_1 with respect to r, it follows that

$$\mathcal{L} W = \begin{pmatrix} -2(UV)_r V_1 - (V^2)_r U_1 \\ 2(UV)_r V_1 + (V^2)_r U_1 \end{pmatrix} \,. \tag{1.90}$$

Therefore, I_1 in (1.89b) can be written in terms of W. Integrating the resulting expression by parts, we get

$$I_1 = \int \Psi^{\dagger t} \mathcal{L} W \, dr = \left(\Psi^{\dagger t} W_r - \Psi_r^{\dagger t} W \right) \big|_{-\infty}^\infty + \int W^t \mathcal{L}^\dagger \Psi^\dagger \, dr \,. \tag{1.91}$$

Using $\mathcal{L}^\dagger \Psi^\dagger = 0$, with $\Psi_1^\dagger \to 0$ and $\Psi_{2r}^\dagger \to 0$ as $|r| \to \infty$, (1.91) reduces to

$$I_1 = 2\Psi_2^\dagger(\infty) U_{1rr}(\infty) = -2\Psi_2^\dagger(\infty) \,. \tag{1.92}$$

Here we have used $U_{1rr}(\infty) = -1$ as seen from (1.51). Finally, substituting (1.92) into (1.89c), we obtain a compact expression for λ_0

$$c_j \lambda_0 \int \Psi_1^\dagger V_r \, dr = 2\Psi_2^\dagger(\infty) \left[\frac{1}{2} \left(N_{1r}(+\infty) + N_{1r}(-\infty) \right) + c_j \right] \,, \qquad j = 1, \ldots, k \,. \tag{1.93}$$

This completes the analysis of the jth inner region.

Next, we match this j^{th} inner solution constructed above to the outer solution for (1.82). This will determine $N_{1r}(\pm\infty)$ and the constants c_j, for $j = 1, \ldots, k$. In the outer region, we have:

$$\eta_{xx} - (1 + \tau\lambda)\eta = \eta v_e^2 + 2u_e v_e \phi\,. \tag{1.94}$$

Away from $O(\varepsilon)$ regions centered at the spike equilibrium locations, v_e is exponentially small. Therefore we have:

$$\eta_{xx} - (1 + \tau\lambda)\eta \sim 0, \quad x \neq x_j \tag{1.95}$$

Matching the inner and outer solution, we have:

$$\varepsilon\left(c_j U_r(\pm\infty) + \varepsilon A N_1\right) \sim \eta(x_j^{\pm}) + \varepsilon r \eta_x(x_j^{\pm}) + \cdots\,. \tag{1.96}$$

Using $U_r(\pm\infty) = B$ we therefore obtain:

$$\eta(x_j^{\pm}) = \pm\varepsilon c_j B\,, \tag{1.97a}$$

$$N_{1r}(\pm\infty) = \frac{1}{\varepsilon A}\eta_x(x_j^{\pm})\,. \tag{1.97b}$$

We now solve (1.95) on each subinterval and we use the condition (1.97a) for $\eta(x_j^{\pm})$ and the boundary condition $\eta_x(\pm 1) = 0$. This yields,

$$\eta(x) = \begin{cases} -\varepsilon B c_1 \frac{\cosh[\theta_\lambda(1+x)]}{\cosh[\theta_\lambda(1+x_1)]}\,, & -l < x < x_1\,, \\[2mm] \varepsilon B c_j \frac{\sinh[\theta_\lambda(x-x_{j+1})]}{\sinh[\theta(x_j-x_{j+1})]} - \varepsilon B c_{j+1}\frac{\sinh[\theta_\lambda(x-x_j)]}{\sinh[\theta_\lambda(x_{j+1}-x_j)]}\,, & x_j < x < x_{j+1}\,, \quad j = 1, \ldots, k-1\,, \\[2mm] \varepsilon B c_k \frac{\cosh[\theta_\lambda(1-x)]}{\cosh[\theta_\lambda(1-x_k)]}\,, & x_k < x < l\,. \end{cases} \tag{1.98}$$

Here θ_λ is defined by

$$\theta_\lambda \equiv \sqrt{1 + \tau\lambda}. \tag{1.99}$$

Combining (1.98) and (1.96) we obtain, for $j = 1$:

$$\frac{(N_{1r}(+\infty) + N_{1r}(-\infty))}{2} = \frac{B\theta_\lambda}{2A}\left[-c_1\left(\coth\left(\frac{2l\theta_\lambda}{k}\right) + \tanh\left(\frac{l\theta_\lambda}{k}\right)\right) - c_2 \operatorname{csch}\left(\frac{2l\theta_\lambda}{k}\right)\right]\,. \tag{1.100a}$$

For $j = 2, \ldots, k-1$, we get

$$\frac{(N_{1r}(+\infty) + N_{1r}(-\infty))}{2} = \frac{B\theta_\lambda}{2A} \left[-c_{j-1} \operatorname{csch}\left(\frac{2l\theta_\lambda}{k}\right) - 2c_j \coth\left(\frac{2l\theta_\lambda}{k}\right) - c_{j+1} \operatorname{csch}\left(\frac{2l\theta_\lambda}{k}\right) \right].$$
(1.100b)

Similarly for $j = k$, we get

$$\frac{(N_{1r}(+\infty) + N_{1r}(-\infty))}{2} = \frac{B\theta_\lambda}{2A} \left[-c_{k-1} \operatorname{csch}\left(\frac{2l\theta_\lambda}{k}\right) - c_k \left(\coth\left(\frac{2l\theta_\lambda}{k}\right) + \tanh\left(\frac{l\theta_\lambda}{k}\right) \right) \right].$$
(1.100c)

Substituting (1.100) into (1.93), and using the relation $B/A = \tanh(l\theta_0/k)$ from (1.37), we obtain the following matrix problem for $c = (c_1, \ldots, c_k)^t$ and λ_0:

$$\lambda_0 c = \alpha \left[\frac{\sqrt{1+\tau\lambda}}{2} \tanh\left(\frac{l}{k}\right) \mathcal{B} - I \right] c.$$
(1.101)

Here α is defined by

$$\alpha \equiv -\frac{\Psi_2^\dagger(\infty)}{\int_0^\infty \Psi_1^\dagger V_r \, dr},$$
(1.102)

and $\mathcal{B}$ is the tridiagonal matrix

$$\mathcal{B} \equiv \begin{pmatrix} d & f & 0 & \cdots & 0 & 0 & 0 \\ f & e & f & \cdots & 0 & 0 & 0 \\ 0 & f & e & \ddots & 0 & 0 & 0 \\ \vdots & \vdots & \ddots & \ddots & \ddots & \vdots & \vdots \\ 0 & 0 & 0 & \ddots & e & f & 0 \\ 0 & 0 & 0 & \cdots & f & e & f \\ 0 & 0 & 0 & \cdots & 0 & f & d \end{pmatrix},$$
(1.103a)

with matrix entries d, e, and f defined by

$$d \equiv \coth\left(\frac{2l\theta_\lambda}{k}\right) + \tanh\left(\frac{l\theta_\lambda}{k}\right), \qquad e \equiv 2\coth\left(\frac{2l\theta_\lambda}{k}\right), \qquad f \equiv \operatorname{csch}\left(\frac{2l\theta_\lambda}{k}\right).$$
(1.103b)

The spectrum of $\mathcal{B}$ can be calculated explicitly as was done in Appendix D of [40]. This leads to the following result:

Lemma 1.2.5 *The eigenvalues* ζ_j, *ordered as* $0 < \zeta_1 < \ldots < \zeta_k$, *of* $\mathcal{B}$ *and the associated eigenvectors* $\mathbf{c}_j$ *of* $\mathcal{B}$ *are*

$$\zeta_j = 2 \coth\left(\frac{2\theta_\lambda}{k}\right) + 2 \operatorname{csch}\left(\frac{2\theta_\lambda}{k}\right) \cos\left(\frac{\pi j}{k}\right), \qquad j = 1, \ldots, k, \tag{1.104a}$$

$$\mathbf{c}_k^t = \left(1, -1, 1, \ldots, (-1)^{k+1}\right); \quad c_{m,j} = \sin\left(\frac{\pi j}{k}(m - 1/2)\right), \quad j = 1, \ldots, k-1. \tag{1.104b}$$

Here $\mathbf{c}^t$ *denotes transpose and* $\mathbf{c}_j^t = (c_{1,j}, \ldots, c_{k,j})$.

Substituting (1.104) into (1.101) leads to (1.75).

As shown in Table (1.80), the constant α is always positive for the primary branch $\gamma > 1.02$. For general B, this constant is determined numerically. However in the intermediate regime $B = 3\delta \ll 1$ this constant can be determined analytically. In this limit, we recall from Proposition 1.2.2 that $V_0 \sim \delta w$, and $U_0 \sim \delta^{-1}$. Here w is the spike profile given in (1.7). Therefore, for $\delta \ll 1$, the homogeneous adjoint problem (1.88) reduces to

$$\psi_{1rr}^\dagger + (-1 + 2w)\psi_1^\dagger - 2w\psi_2^\dagger \sim 0, \qquad \psi_{2rr}^\dagger + \delta^2 w^2\left(\psi_1^\dagger - \psi_2^\dagger\right) \sim 0. \tag{1.105}$$

The solution to this limiting system is odd and is given, up to a normalization constant, by

$$\psi_1^\dagger = w_r + O(\delta^2), \qquad \psi_2^\dagger = -\frac{\delta^2}{3}\int_0^r [w(s)]^3 \, ds + O(\delta^4). \tag{1.106}$$

Therefore, for $\delta \ll 1$, we have

$$\alpha \equiv -\frac{\Psi_2^\dagger(\infty)}{\int_0^\infty \Psi_1^\dagger V_r \, dr} \sim \frac{\delta}{3}\left(\frac{\int_0^\infty w^3 \, dr}{\int_0^\infty w_r^2 \, dr}\right). \tag{1.107}$$

To calculate the integral in (1.107) we use $w(r) = \frac{3}{2}\operatorname{sech}^2(r/2)$ to obtain $\alpha = 2\delta$. This concludes the proof of Theorem 1.2.4. $\qquad\qquad \square$

Note that if $\tau \ll \frac{1}{\varepsilon}$ then $\theta_\lambda \sim 1$ in (1.75), as $\lambda = O(\varepsilon)$. In this case it is easy to show that (1.75) reduces to

$$\lambda \sim -\varepsilon \alpha A \operatorname{sech}^2(l/k)\left[1 - \frac{1}{2}(1 + \cos(\pi j/k))\right], \quad j = 1 \ldots k. \tag{1.108}$$

We thus have the following corollary:

38

Corollary 1.2.6 *Suppose that $\tau \ll \frac{1}{\varepsilon}$. Then the small eigenvalues in the high-feed or intermediate regime, as given by Theorem 1.2.4, are all stable, and are given explicitly by (1.108), where $\alpha > 0$ is defined in Theorem 1.2.4.*

We now show that when $\tau = O(\frac{1}{\varepsilon})$, the small eigenvalues can be destabilized via a Hopf bifurcation.

To analyze (1.75) it is convenient to introduce the new variables τ_d, ω, and ξ, defined by

$$\lambda = \varepsilon \alpha A \omega, \qquad \tau = \left(\frac{1}{\varepsilon \alpha A}\right)\tau_d, \qquad \xi = \tau_d \omega. \tag{1.109}$$

Substituting (1.109) into (1.75), we obtain that ξ satisfies:

$$\frac{\xi}{\tau_d} = G(\xi) \equiv z\frac{\tanh(\beta/2)}{\sinh(\beta z)}\left(\cosh(\beta z) + \gamma\right) - 1, \quad j = 1 \ldots k, \text{ where} \tag{1.110a}$$

$$z = \sqrt{1 + \xi}, \quad \beta = 2l/k, \quad \gamma = \cos\left(\frac{\pi j}{k}\right) \tag{1.110b}$$

Elementary calculus yields the following facts about G, $j = 1 \ldots k$:

$$G(0) < 0, \quad G'(\xi) > 0, \quad G_j''(\xi) < 0. \tag{1.111}$$

It follows that (1.110) has a negative double root for some $\tau_d = \tau_{d-}$ sufficiently small and positive, and has a positive double root for some $\tau_d = \tau_{d+}$ sufficiently large and positive. For $\tau_d \in (\tau_{d-}, \tau_{d+})$, the two roots are therefore complex conjugate; and by continuity, they must cross the imaginary axis at some $\tau_d = \tau_{dh}$. This shows the existence of the Hopf bifurcation. Moreover, the following theorem shows uniqueness of τ_{dh} for each j:

Theorem 1.2.7 *Suppose $\varepsilon \alpha A \ll 1$ and $A \gg O(\varepsilon^{1/2})$, where α is given in Theorem 1.2.4. Then for each $j = 1 \ldots k$, there exists a unique positive $\tau = \tau_h = \frac{1}{\varepsilon \alpha A}\tau_{dh}$ where $\tau_{dh} = O(1)$ such that the corresponding small eigenvalue λ given by Theorem 1.2.4 is purely imaginary. Moreover, $\operatorname{Re}\lambda < 0$ if $\tau < \tau_h$ and $\operatorname{Re}\lambda > 0$ if $\tau > \tau_h$.*

Proof. We set $\xi = i\xi_i$ in (1.110). Taking real and imaginary parts of (1.110a) we obtain:

$$\operatorname{Re}(G(i\xi_i)) = 0, \quad \tau_d = \frac{\xi_i}{\operatorname{Im}G(i\xi_i)} \tag{1.112}$$

39

Some algebra shows that

$$\frac{d}{d\xi_i}\text{Re}(G(i\xi_i)) > 0, \quad \frac{d}{d\xi_i}\text{Im}(G(i\xi_i)) > 0. \tag{1.113}$$

In addition we have

$$\text{Re}(G(i0)) < 0, \quad \text{Im}(G(i0)) = 0. \tag{1.114}$$

It follows that the solution to (1.112) is unique with the corresponding $\tau_d > 0$. This proves the uniqueness of τ_d. The fact that $\text{Re}\,\lambda > 0$ if and only if $\tau > \tau_d$ follows from uniqueness of τ_d and from the continuity argument discussed before the statement of Theorem 1.2.7 $\qquad\square$

If τ_d is increased just to the right of τ_{dhj}, the k spike solution is destabilized by a perturbation of the form (1.76). In the case of $k = 1$, this corresponds to slow oscillations of the spike around the equilibria location. In the case $k = 2, j = 2$, the corresponding eigenvector is $c_2 = (-1, 1)$ and the shape of the perturbation causes a slow asynchronous oscillation of the two spikes around their equilibria. An example of such behaviour is shown in Figure 1.2b. By contrast, if $k = 2, j = 1$, then the oscillations around equilibria are synchronous. However we were unable to observe this type of oscillation numerically. Indeed, numerical computations suggest that the the asynchronous oscillation corresponding to the node $j = k$ is always triggered before any other nodes. We state this as a conjecture:

Conjecture 1.2.8 *Let τ_{hj} be the Hopf bifurcation values as found in Theorem 1.2.7. Then the following monotonicity property holds:*

$$\tau_{h1} > \tau_{h2} > \ldots > \tau_{hk}.$$

It follows that as τ is increased, the asynchronous drift corresponding to the node $j = k$ becomes unstable first.

Thus we do not expect to observe synchronous drift in the absence of asynchronous drift.

We have the following evidence for this conjecture. Write G from (1.110a) as

$$G = a(b + \gamma) - 1 \quad \text{where} \quad a = z\frac{\tanh(\beta/2)}{\sinh(\beta z)}, \quad b = \cosh(\beta z).$$

Then ξ_i and τ_{dh} satisfy:

$$\operatorname{Re} G = a_r(b_r + \gamma) - a_i b_i - 1 = 0, \tag{1.115a}$$

$$\operatorname{Im} G = a_i \gamma + a_r b_i + b_r a_i = \frac{\xi_i}{\tau_{dh}} \tag{1.115b}$$

Solving for γ in (1.115a) and substituting into (1.115b), we obtain:

$$\frac{1}{\tau_{dh}} = \frac{a_i + b_i |a|^2}{\xi_i a_r}. \tag{1.116}$$

As will be shown in the proof of Lemma 1.2.9 below, $\xi_i \in [0, \xi_i^\star)$, where $\xi_i^\star$ is the first root of $a_r(i\xi_i)$. Now in Lemma 1.2.9 below we will show that $\xi_i = \xi_{ihj}$ is an increasing function of j. Thus we would have the proof of the conjecture if we can show that the right hand side of (1.116) is an increasing function of ξ_i, at least for $\xi_i \in [0, \xi_i^\star)$. Using a computer, we have verified this condition for various values of β. It remains to show:

Lemma 1.2.9 *The following monotonicity property holds:*

$$\xi_{ih1} < \xi_{ih2} < \ldots < \xi_{ihk}.$$

Here, ξ_{ihj} is the unique purely imaginary solution $\xi = i\xi_{ihj}$ of (1.110).

Proof. Let ξ_{ih} be the unique root of $\operatorname{Re} G(i\xi_i) = 0$ as found in Theorem 1.2.7. We need to show that ξ_{ih} is a decreasing function of γ. The proof is illustrated on Figure 1.8, and is explained below.

From (1.115a), it follows that the curves $\operatorname{Re} G(i\xi_i)$ for different values of γ all intersect at the same point whenever $a_r = 0$, and do not intersect at all otherwise. Label the first such point by $\xi_i^\star$. But then $\operatorname{Re} G(i\xi_i^\star) > 0$ since $\operatorname{Re} G(i\xi_i)|_{\gamma=1}$ is always positive due to (1.113) and because of the fact that $\operatorname{Re} G(i0)|_{\gamma=1} = 0$. Thus $\xi_{ih} \in (0, \xi_i^\star)$ for all $\gamma \in (-1, 1)$. But $a_r(i\xi_i) > 0$ on this interval since $a_r > 0$ when $\xi_i = 0$. It follows that for $\xi_i \in [0, \xi_i^\star)$, $\operatorname{Re} G$ is an increasing function of γ. This proves that its root ξ_{ih} is a decreasing function of γ. $\qquad \square$

Finally, consider $\tau_d = \tau_{d+}$ for which the eigenvalue λ given by Theorem 1.2.4 merges with the positive real axis. Since $G(z)$ is increasing in γ, τ_{d+} is a decreasing function of γ. Thus τ_{d+}
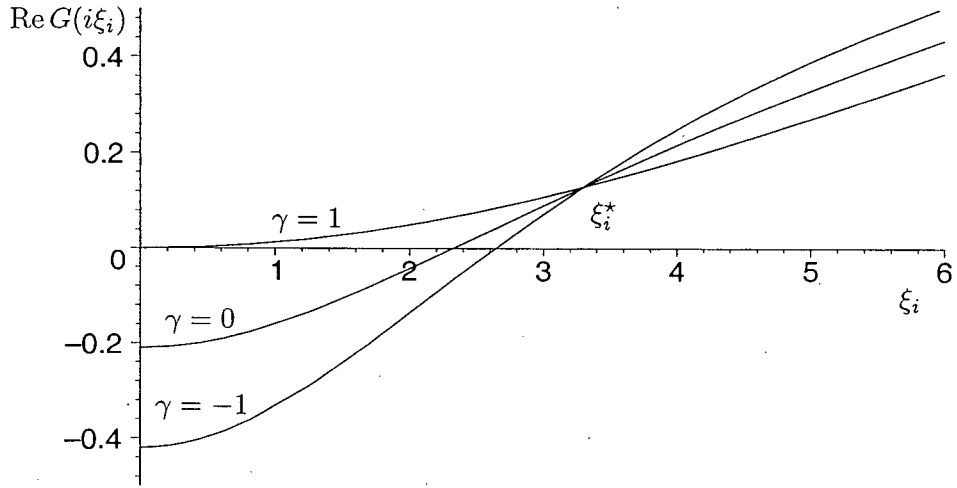
Figure 1.8: Plot of $\operatorname{Re} G(i\xi_i)$ for three values of γ as indicated, and with $\beta = 2$. All three curves intersect at a the same point $\xi_i^\star$ with $\operatorname{Re} G(i\xi_i^\star) > 0$.

corresponding to $\gamma = -1$ i.e. $j = k$, is the first value of τ for which there exist purely positive small eigenvalues.

The following table lists the value of τ_{dh}, computed numerically, for various values of γ and β, as well as the value τ_{d+} for $k = j$.

β	τ_{dh} $\gamma = -1$	τ_{dh} $\gamma = \cos(\pi 2/3)$	τ_{dh} $\gamma = 0$	τ_{dh} $\gamma = \cos(\pi/3)$	τ_{d+} $\gamma = -1$
0.1	663	735	828	957	1688
0.2	167	185	208	240	423
0.3	74.7	82.78	93.19	107.6	189
0.4	42.5	47.12	53.00	61.14	107
0.5	27.66	30.62	34.40	39.64	69.20
0.6	19.58	21.65	24.30	27.95	48.59
0.7	14.71	16.25	18.21	20.91	36.16
0.8	11.55	12.75	14.26	16.34	28.09
0.9	9.39	10.35	11.56	13.21	22.56
1.0	7.84	8.631	9.623	10.97	18.61
1.5	4.21	4.595	5.065	5.691	9.240
2.0	2.990	3.221	3.502	3.868	5.965
2.5	2.461	2.619	2.808	3.047	4.452
3.0	2.207	2.322	2.457	2.622	3.633
4.0	2.021	2.085	2.156	2.240	2.826
5.0	1.9831	2.018	2.056	2.097	2.461
6.0	1.9835	2.001	2.020	2.040	2.271
10	1.9989	1.9996	2.0003	2.0011	2.037

$$(1.117)$$

This table provides a more direct numerical verification to Conjecture 1.2.8.

Note also that $\tau_d, \tau_+ \to 2$ as $l \to \infty$, for all values of γ. This is easily seen as in this case, we have $G(0) \sim 0$ and $G'(0) \sim \frac{1}{2}$.

Recall from Proposition 1.1.11 that profile instabilities in the intermediate regime may occur when $\tau \gg 1$. Whether drift or profile instability occurs first depends on the scaling of A as we now show. For the profile instability in the intermediate regime, we have from Proposition 1.1.11:

$$\tau_{hl} = \frac{A^4}{9\varepsilon^2} \tanh^4(l/k)\tau_{0h}.$$

On the other hand, we derived that the drift instabilities in the high regime regime occur when τ is increased beyond

$$\tau_{hs} = \frac{1}{\varepsilon \alpha A}\tau_{dh}.$$

Using (1.79), in the intermediate regime this reduces to:

$$\tau_{hs} = \frac{3}{2\varepsilon A^2} \coth(l/k)\tau_{dh}$$

Equating $\tau_{hs} = \tau_{hl}$ leads to the following threshold.

Proposition 1.2.10 *Let*

$$A_c = \frac{\sqrt{3}}{2^{1/6}} \varepsilon^{1/6} \coth^{5/6}(l/k) \tau_{dh}^{1/6} \tau_{0h}^{1/6} = 1.404 \varepsilon^{1/6} \coth^{5/6}(l/k) \tau_{dh}^{1/6}$$

where τ_{dh} is defined in Theorem 1.2.7 and is listed in 1.117.

If $A < A_c$ then oscillatory profile instability occurs before the drift instability. If $A > A_c$ then the drift instability occurs before the oscillatory profile instability.

For the infinite line case $l = \infty$, we have

$$A_c = 1.578 \varepsilon^{1/6}.$$

Full numerical simulations indicate that the Hopf bifurcation corresponding to oscillatory profile instability is subcritical, and as such, leads to the eventual collapse of the spikes. Thus in order to observe drift instability, we must take $A > A_c$.

To verify the correctness of our theory, we consider several numerical examples. To perform numerical simulations in 1D, we have discretized the problem in space, reducing it to n ODE's that are to be solved in time. We then used a code of [34] that implements an explicit Runga-Kutta code of order 4-5 with stepsize control.

Example 1. We consider a one-spike solution with $k = 1$, $A = 1.3$, $l = 2$, $\varepsilon = 0.03$, $D = 1$. For our initial condition, we took a spike slightly off-center, centered at $x = 0.1$. From (1.50) we have $B = 1.25$ and from Table 1.80 we find $\alpha = 1.13$. From (1.110b) we have $\beta = 4$. From Table 1.117 we find that

$$(\tau_{dh})_{j=1} = 2.02, \tau_{d+} = 2.8.$$

From (1.109) we have $\tau = 22.7\tau_d$ so that that the theoretical prediction for the oscillatory drift and the merging bifurcation is:

$$\tau_h \sim 46, \tau_+ \sim 64$$

Using direct numerical simulation of (1.1) with these parameter values, we observe that the spike is stationary for $\tau < 55$, whereas the slow oscillatory drift is observed for $58 < \tau < 73$, settling into a periodic motion. For $\tau > 73$, the spike the drift instability causes an eventual extinction of the spike. See Figure 1.9. An interesting behaviour is observed when $\tau = 72$. In this case, the amplitude of the drift is rather large. When the spike center approaches the edge of the domain, it triggers an oscillatory profile instability, so that fast oscillations in spike height are observed at that point. While the analysis of the oscillatory profile instability given in §1.1.3 was done for the spike at equilibrium position – and so is insufficient to explain the observed oscillations – it is possible to extend this analysis for spikes at arbitrary positions, as was done in [39] for the Gierer-Meinhardt model.
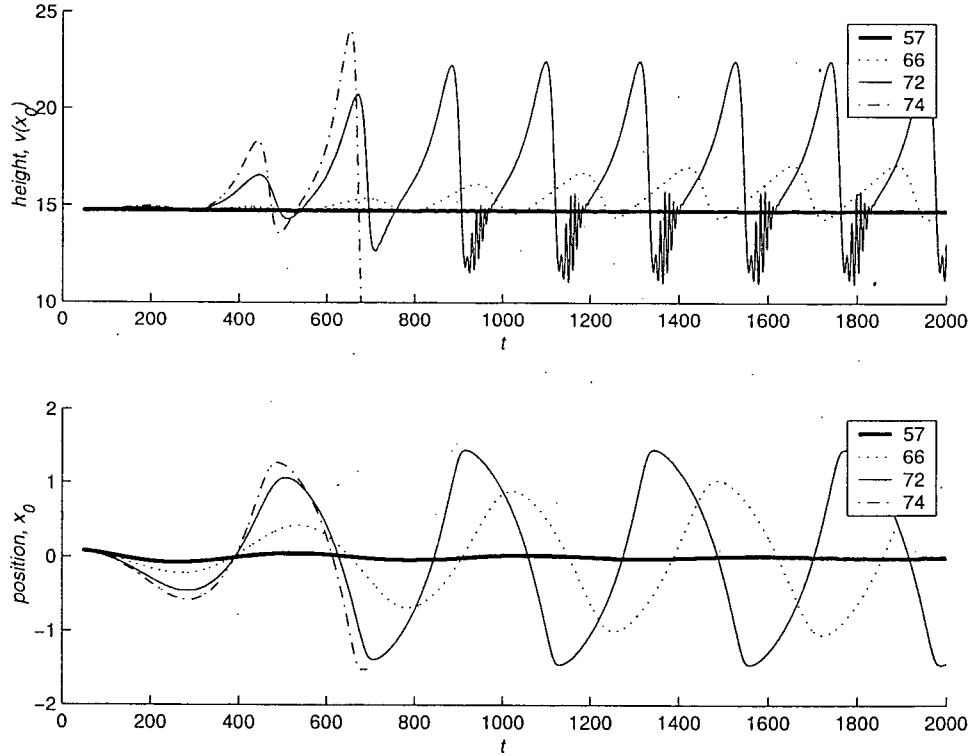
Figure 1.9: Example 1. Plots of the height and center of a single spike vs. time for four different values of τ. Top figure: the height $v(x_0)$ plotted vs. time, where x_0 is the center of the spike. Bottom figure: x_0 vs. time. Here, $k = 1$, $A = 1.3$, $l = 2$, $\varepsilon = 0.03$, $D = 1$ and τ is taken to be 57, 66, 72, 74, as indicated in the legend.
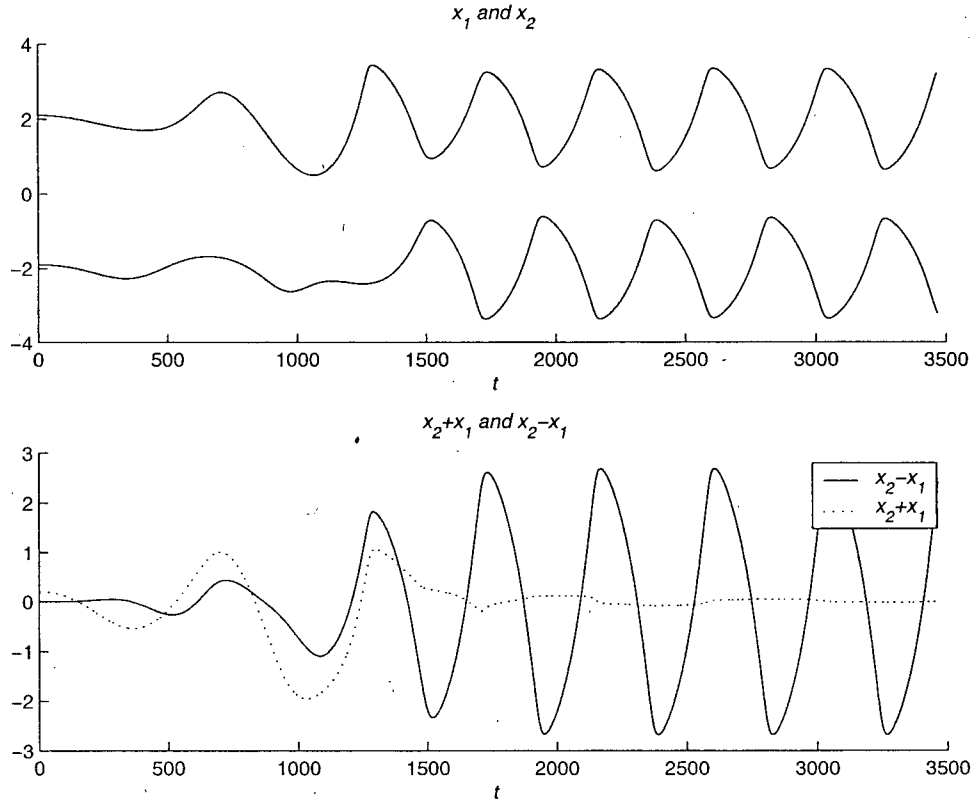
Figure 1.10: Example 2. Here, $k = 2$, $l = 4, \tau = 70$ and the other parameters are as in Example 1.

Example 2. Next, we consider a two-spike solution with $k = 2$, $l = 4$ and other parameters as in Example 1. The equilibrium state is then the same as in Example 1, but copied twice. Thus we obtain, as in Example 1,

$$\left(\tau_{dh}\right)_{j=2} = 2.02, \left(\tau_{dh}\right)_{j=1} = 2.16, \tau_{d+} = 2.8$$

Here, $j = 2$ corresponds to the asynchronous mode and $j = 1$ corresponds to the synchronous mode. Therefore we obtain:

$$\tau_{h,asynchronous} \sim 46, \tau_{h,synchronous} \sim 49, \tau_+ \sim 64$$

In Figure 1.10 we plot the solution for $\tau = 70$. The top subfigure shows the positions of the centers x_1 and x_2 as a function of time. Initial configuration was taken to be two spikes located at 2.1 and -1.9. In the bottom subfigure we plot the sum and the difference in the position

46

of the spikes, respectively. A changing sum or difference indicates instability with respect to synchronous or synchronous mode, respectively. Since $\tau_{h,asynchronous}$ and $\tau_{h,synchronous}$ are within 3 units of each other, and since $\tau = 70$ was found about 13 units away from $\tau_h = 57$ of example 1, we expect that both synchronous and asynchronous modes are unstable with $\tau = 70$. Indeed, for $t < 1300$, this appears to be the case as the amplitude of both $x_1 - x_2$ and $x_1 + x_2$ increases over time. However at a later time, the synchronous mode appears to die out, and asynchronous mode dominates. This appears to contradict the theory. A resolution of this paradox is that the oscillations happen far from the asynchronous bifurcation point and therefore linear theory is only applicable for relatively small values of t/ε.

1.3 Discussion

Most of the results presented in this chapter have been previously reported in [74] and [44]. The methods used in §1.1 were first derived in [40] and [77] to analyse instabilities in the Gierer-Meinhardt model. In addition to the large eigenvalue analysis of the low-feed regime of §1.1, it is also possible to carry out the small eigenvalue analysis as was done in [44] for the GS model, or [40] for the GM model. Unlike the intermediate and high-feed regime, the small eigenvalues can be unstable in the low-feed regime even with $\tau = 0$, when $\mathcal{A}$ is near the saddle-node point $\mathcal{A}_{ke}$ and $k > 1$. Moreover, they become unstable through a saddle-node bifurcation, not through a Hopf bifurcation as in high or intermediate-feed regime. The corresponding small eigenvalues are always real, so one does not observe the oscillatory drift in such a case.

In the low-feed regime, there also exists asymmetric equilibria, whereby the k-spike solution at equilibrium may have spikes of precisely two different heights. As was shown in [74], asymmetric solutions bifurcate from the symmetric solution through a saddle-node bifurcation at precisely the same point where the small eigenvalues change their sign. These bifurcations are illustrated in Figure 1.11

Finally, the following equivalence principle between the one-dimensional Gierer-Meinhardt model (2) and the low-feed regime of the Gray-Scott model (1.1) is shown in [74].
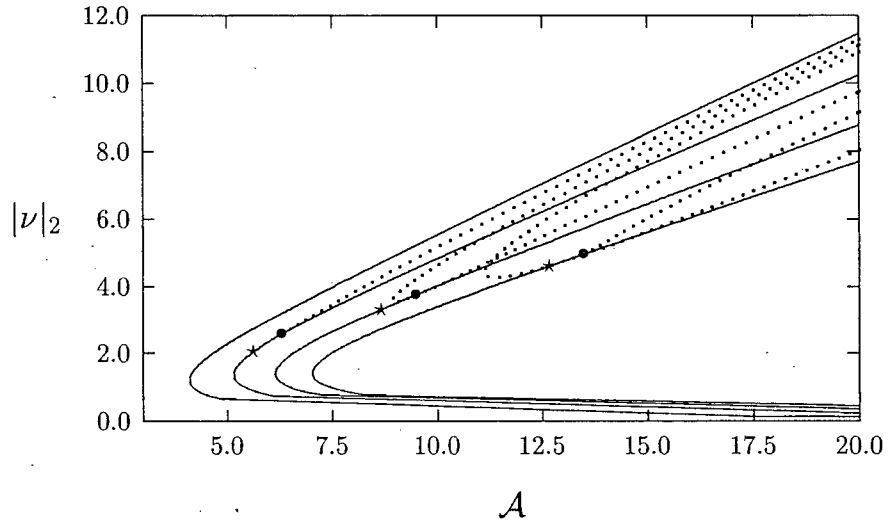
Figure 1.11: Bifurcation diagram of symmetric and asymmetric spike patterns in the low-feed regime, for $k = 1, 2, 3, 4$. Solid curves represent symmetric solution branch and dotted curves represent asymmetric solutions bifurcating from the symmetric branch at the points •. The saddle-node values $\mathcal{A}_{ke}$, represented by $\star$, increase with k. The part of the solid curve below (above) $\star$ is unstable (stable) with respect to large eigenvalues. The part of the solid curve below (above) • is unstable (stable) with respect to small eigenvalues.

Proposition 1.3.1 *Consider a k-spike equilibria solution to the Gray Scott model in the low-feed regime, as derived in Proposition 1.1.1. The eigenvalues of the linearized problem of the Gray Scott model are exactly the same as the eigenvalues of the k spike solution to the Gierer-Meinhardt model (2) with $\Omega = [-l, l]$ and with the exponent set $(p, q, m, s) = (2, s, 2, s)$, where s is defined in (1.18e).*

However the intermediate and high-feed regime of the Gray Scott model exhibit certain phenomena that have not been observed in the Gierer Meinhardt model.

There have been several related works on Gray Scott model before [74] and [44]. Of particular interest to us is the work of Doelman and collaborators ([16]-[21], [55]) and the work of Muratov and Osipov [57]-[60]. The main difference between their work and [44], [74] is that they only consider the case of a single spike $k = 1$ on an entire space $l = \infty$, whereas we also consider a bounded domain. Below we review and compare their results with ours.

We start with low-feed and intermediate regimes. The k spike symmetric equilibria corresponds to periodic solutions on the entire space. Existence of such periodic solutions has been rigorously proven in the low-feed and intermediate feed regime in [55] using dynamical system techniques. However their stability analysis is restricted to a single spike on the entire domain. In particular, they do not have the overcrowding instability threholds l_k derived in Theorem 1.1.7. This instability is specific to having multiple spikes on a bounded domain in a low-feed regime, whose stability neither Doelman et al. nor Muratov and Osipov consider. In [18] and [19] Doelman et al also study the oscillatory profile instabilities for a single spike on the entire space, in the intermediate regime. They use the hypergeometric functions in their analysis of the corresponding eigenvalue problem. They also show the existence of the Hopf bifurcation which initiates the oscillatory profile instability, as we have done in Proposition 1.1.11. However their proof relies on the properties of hypergeometric functions. Our approach does not require their use. In addition we also consider multiple spikes, which they do not. The possibility of asynchronous profile instability (for example in the case of two spikes) is is specific to multiple spikes and does not occur with a single spike.

Next we compare the results in the high-feed regime. The pulse-splitting has been numerically observed in [15, 17, 66]. However no analysis of it is given there. The first analysis appears in [57] where they also derive the dimple eigenfunction of Figure 1.7 at the fold point $B = 1.35$. In [57] they also observe numerically the connection between one and two-bump solution which we beleive is the underlying cause of pulse-splitting. However the Proposition 1.2.1, which predicts the minimum number of pulse-splitting events is new, as [57] only considers a single spike on an entire space.

Finally, the drift instability in the intermediate regime has been analysed in [60], for a single spike on the entire space. In [16], Doelman, Eckhaus and Kaper also derive the equation of motion of the center of the spike in the intermediate regime, for the case of two spikes on the entire space moving away from each other. However in both of these, the drift is not oscillatory, because in the limit $l \to \infty$, the Hopf bifurcation is replaced by a saddle-node bifurcation as $\tau_{dh} \sim 2 \sim \tau_+$ (see discussion after Table (1.117)). The oscillatory drift is specific to having

a finite domain. In addition, we also analyse the small eigenvalues for the high-feed regime, giving a hybrid analytic-numerical result of Theorem 1.2.4.

Several open problems remain. In [77], the existence of the Hopf bifurcation with respect to oscillatory profile instabilities was proven. Numerical evidence indicates that it is unique, but we cannot show this at the moment. Another open problem is to prove Conjecture 1.2.8, which states that asynchronous drift instabilities always occur before the synchronous ones. Indeed, numerical simulations suggest a stronger result is true: the the end state is always an asynchronous oscillation, even with the synchronous mode unstable.

A central open problem in the high-feed regime is to show the connection between one and two bump solutions, which would prove the dissapearence of the equilibria state, leading to pulse splitting. This connection seems to be a generic phenomenon. It is also present in the Gierer-Meinhardt model (2) when the ratio of diffusivities D/ε^2 is of $O(1)$ [69] as well as in the Gray-Scott model when $O(D) = O(\varepsilon^2)$ [63].

Chapter 2

Stripe and ring-like solutions of the Gray-Scott model in two dimensions

In this chapter we continue our study of the Gray Scott model (7). As in §1, we assume without loss of generality that $D = 1$.

$$
\begin{cases}
v_t = \varepsilon^2 \triangle v - v + Av^2 u \\
\tau u_t = \triangle u - u + 1 - v^2 u \\
\partial_n v = 0 = \partial_n u,
\end{cases}
\begin{aligned}
& , \quad x \in \Omega \\
& \quad x \in \partial\Omega.
\end{aligned}
\tag{2.1}
$$

We consider stripe and ring-like solutions, where the domain is either a rectangle or a disk, respectively. Such solutions are one-dimensional in nature, and many of the techniques from Chapter 1 are then applicable with some modifications. We consider three types of instabilities of such solutions. First, a *breakup* instability, which results in a breakup of a ring or a stripe into m spots. Second, a *zigzag* instability, which causes the formation of a zigzag pattern. Finally, a *splitting* instability, causing a stripe or a ring to split into two. These instabilities are illustrated in Figure 2.1.

We show that breakup and zigzag instabilities always exist for either the low, intermediate or high-feed regimes, whereas the splitting instability occurs only in the high-feed regime. The method of analysis of the zigzag instability is similar to the analysis of the slow oscillatory drift instability discussed in Chapter 1. Alternatively, the breakup instabilities on the other hand, are similar to the overcrowding instability for the low-feed regime, which was also discussed in Chapter 1.
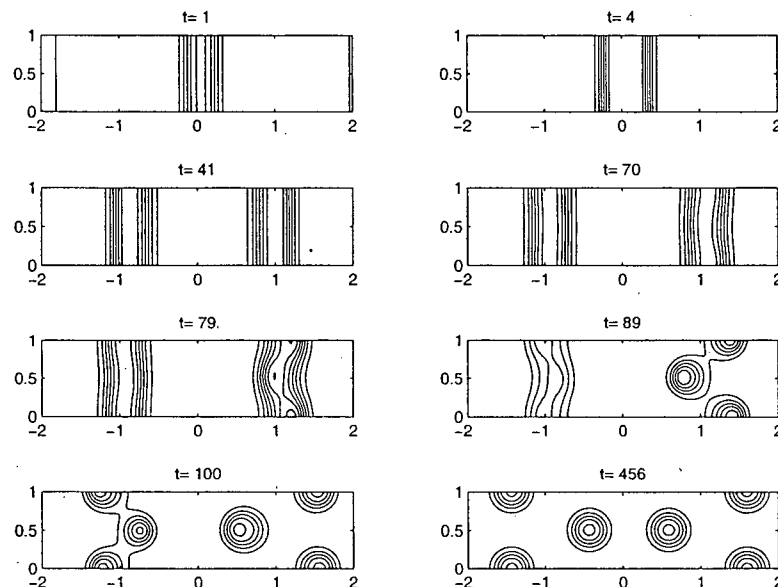
Figure 2.1: Three different instabilities of a stripe: a single stripe splits into two at $t \sim 0$; a zigzag instability is visible at $t \sim 70$; followed by a breakup instability at $t \sim 80$. The end steady state consists of two spots and four half-spots. The domain size was set to $[-2, 2] \times [0, 1]$, with $\varepsilon = 0.07, A = 2, \tau = 1$.

The results for the splitting instability for a stripe are equivalent to the corresponding results for a splitting instability of a one-dimensional spike. A similar technique also yields a corresponding result for ring splitting. In contrast to stripe splitting, the ring radius enters into the formula which involves Bessel functions.

We also perform numerical computations in the regime where the ratio of the diffusivities is of $O(1)$. We find the existence of labyrinth-like patterns and space-filling curves, such as shown in Figure 2.2.

This chapter is organized as follows. In §2.1 we study the low-feed regime $A = O(\varepsilon^{1/2})$. In §2.1.1 we derive the equations of motion for a ring radius in the low-feed regime, using a Melnikov-type calculation. We then prove the existence of a ring radius r_0 for which the ring is at equilibrium. In §2.1.2 we study the breakup instability of ring and stripe solutions in the low-feed regime. Stripe solutions in the intermediate and high-feed regimes are considered in §2.2. We characterize both zigzag and breakup instability bands for stripes in §2.2.1 and
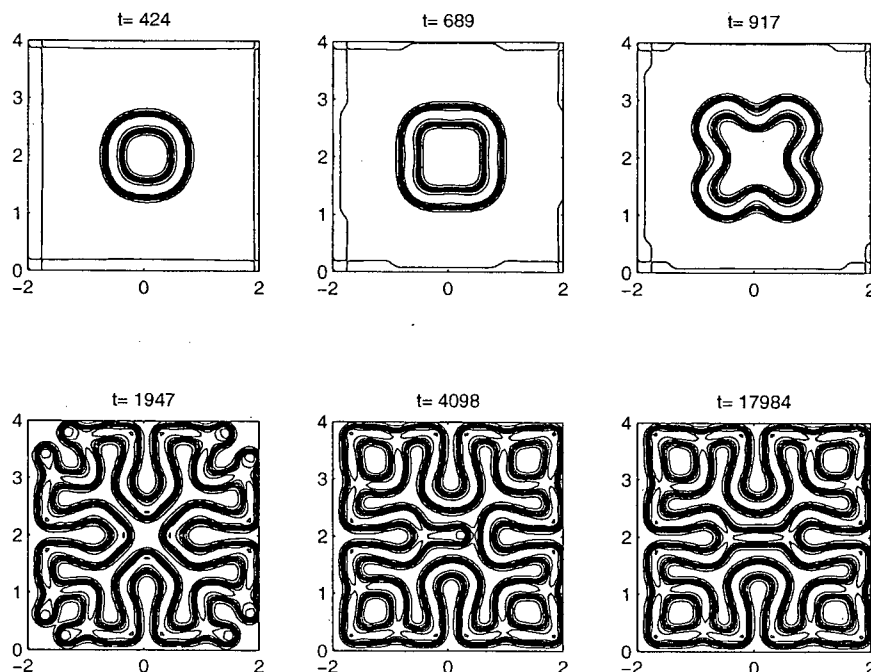
Figure 2.2: Development of a labyrinth-type pattern in the Gray-Scott model. Here, we take $\varepsilon = 0.5, \Omega = [0, 40]^2, A = 2, \tau = 1$.

§2.2.2, respectively. For the intermediate regime explicit thresholds are derived whereas in the high-feed regime we present hybrid numeric-analytic results. In §2.3 we derive the analogous results for a ring in the high-feed and the intermediate regime. In the high-feed regime, we also derive a threshold on A above which the equilibria solution ceases to exist and ring splitting occurs. Some numerical simulations are given in §2.4. We conclude with a brief discussion section §2.5.

2.1 Ring and stripe solutions in the low-feed regime

In this section we study the equilibria and stability of stripes and rings for the two-dimensional Gray Scott model in the low-feed regime $A = O(\varepsilon^{1/2})$. Using the same scaling as in (1.5) and setting as before $D = 1$, our starting point is the following system:

$$
\begin{cases}
\nu_t = \varepsilon^2 \triangle \nu - \nu + A\nu^2 u \\
\tau u_t = \triangle u - u + 1 - \frac{1}{\varepsilon}\nu^2 u \\
\partial_n \nu = 0 = \partial_n u,
\end{cases}
\quad
\begin{aligned}
& x \in \Omega \\
& \\
& x \in \partial\Omega
\end{aligned}
\tag{2.2}
$$

53

where $\mathcal{A} = \varepsilon^{-1/2}A$. As usual, we proceed by first describing the equilibrium state and then looking at its perturbations.

2.1.1 Ring equilibria solutions

We first consider the equilibria solutions. Since the stripe equilibria is simply a trivial extension of a one-dimensional spike solution, in this section we concentrate on the less trivial case of a ring solution. We assume that the domain is a ball of radius R in $\mathbb{R}^N$, $N \geq 2$:

$$\Omega = B_R = \{x = (x_1, x_2, \cdots, x_N) \; : \; |x| < R\}.$$

We will also allow the case of entire space $R = \infty$. A *ring solution* is a solution that concentrates on a ring $\{|x| = r_0\}$ of radius r_0, as $\varepsilon \to 0$. In this section we derive an ODE which describes the slow evolution of r_0 in time. We then show that such ODE always admits an equilibrium in the case $R < \infty$. When $R = \infty$, the equilibrium may or may not exist, depending on the value of the parameter $\mathcal{A}$.

To derive the ODE for the ring radius r_0, we start with the following anzatz for the solution:

$$\nu = \frac{1}{\mathcal{A}U_0(0)} \left(w(y) + \varepsilon V_1(y) + \ldots\right), \quad y = \frac{r - r_0}{\varepsilon}, \quad r = |x|, \quad r_0 = r_0(\varepsilon^2 t), \qquad (2.3)$$

$$u = U_0(y) + \varepsilon U_1(y) + \ldots. \qquad (2.4)$$

The leading order equation for u is $U_0'' = 0$. Thus $U_0(y) = U_0$ is constant. The equation for w on $-\infty < y < \infty$ then becomes

$$w'' - w + w^2 = 0, \quad w'(0) = 0, \quad w(0) > 0. \qquad (2.5)$$

It follows that $w = \frac{3}{2} \operatorname{sech}^2(y/2)$ as in (1.7). At next order, we obtain the following system:

$$L_0 V_1 = -r_0' w' - \frac{N-1}{r_0} w' - \frac{w^2 U_1}{U_0} \quad \text{where} \quad L_0 V_1 = V_1'' - V_1 + 2w V_1, \qquad (2.6a)$$

$$U_1'' = \frac{w^2}{\mathcal{A}^2 U_0}. \qquad (2.6b)$$

Using the self-adjointness property of L_0, the solvability condition for (2.6a)

$$\int w' L_0 V_1 = 0,$$

54

and therefore we have

$$\left(r_0' + \frac{N-1}{r_0}\right)\int w'^2 = -\int \frac{w^2 U_1 w'}{U_0} = \frac{1}{3U_0}\int w^3 U_1'. \tag{2.7}$$

Note that U_1 may be discontinuous at the origin. To evaluate the integral on the right hand side of (2.7), we obtain

$$\int w^3 U_1' = \left(\frac{U_1'(-\infty) + U_1'(\infty)}{2}\right)\int w^3. \tag{2.8}$$

This is seen as follows. Integrating (2.6b) and using the even symmetry of w, we have:

$$U_1'(y) = \begin{cases} \frac{1}{U_0 \mathcal{A}^2}\left(\int_0^y w^2 - \int_0^\infty w^2\right) + U_1'(\infty), & y > 0, \\ \frac{1}{U_0 \mathcal{A}^2}\left(\int_0^y w^2 + \int_0^\infty w^2\right) + U_1'(-\infty), & y < 0 \end{cases}$$

Thus

$$\int w^3 U_1' = \left(\int_{-\infty}^0 + \int_0^\infty\right)w^3 U_1' = \int w^3 \left(\frac{1}{U_0 \mathcal{A}^2}\int_0^y w^2 + \frac{U_1'(-\infty) + U_1'(\infty)}{2}\right)$$

Using the fact that $w^3(y)\left(\int_0^y w^2\right)$ is an odd function yields (2.8). This shows the claim. Finally, using (1.7) we have

$$\int w'^2 = \frac{6}{5}, \quad \int w^3 = \frac{36}{5}.$$

This leads to the following ODE for the ring radius r_0:

$$r_0' + \frac{N-1}{r_0} = \frac{U_1'(-\infty) + U_1'(\infty)}{U_0}. \tag{2.9}$$

We now evaluate the right hand side by using the asymptotic matching with the outer solution. We obtain

$$U_0 = u(r_0), \quad U_1'(\pm\infty) \sim u'(\pm r_0) \tag{2.10}$$

and,

$$u_{rr}(r) + \frac{N-1}{r}u_r(r) - u(r) \sim -1 + \frac{1}{\varepsilon}\frac{1}{\mathcal{A}^2 U_0^2}w^2(y)u(y) \sim -1 + \frac{1}{\mathcal{A}^2 U_0}\delta(r - r_0)\int w^2$$

where δ is the delta function. Using $\int w^2 = 6$, we may then write:

$$u \sim 1 - \frac{6}{\mathcal{A}^2 U_0}G(r, r_0), \tag{2.11}$$

where G is the Green's function satisfying

$$G_{rr} + \frac{N-1}{r}G_r - G = -\delta(r - r_0) \qquad (2.12\text{a})$$

with boundary conditions

$$G_r(0, r_0) = 0 = G_r(R, r_0). \qquad (2.12\text{b})$$

It is easy to see that

$$G(r, r_0) = \frac{1}{\mathcal{W}} \begin{cases} J_1(r)J_2(r_0) & \text{if } r < r_0 \\ J_1(r_0)J_2(r) & \text{if } r_0 < r, \end{cases} \qquad (2.13\text{a})$$

where $\mathcal{W}$ is defined by

$$\mathcal{W} = J_1'(r_0)J_2(r_0) - J_1(r_0)J_2'(r_0) \qquad (2.13\text{b})$$

and where J_1, J_2 satisfy

$$J_{rr} + \frac{N-1}{r}J_r - J = 0 \text{ with } J_1'(0) = 0 \text{ and } J_2'(R) = 0. \qquad (2.13\text{c})$$

We write the solution to (2.13c) as

$$J_1(r) = I(r), \quad J_2(r) = K(r) - \frac{K'(R)}{I'(R)}I(r), \qquad (2.13\text{d})$$

where I and K satisfy (2.13c) but with R replaced by ∞. Note that in the case $N = 2$, I, K are Bessel's functions of order 0. We may always scale J_1 and J_2 so that

$$\mathcal{W} = J_1'(r_0)J_2(r_0) - J_1(r_0)J_2'(r_0) = \frac{N-1}{r_0}. \qquad (2.14)$$

In particular, when $N = 2$, (2.14) is satisfied with J_1, J_2 as given in (2.13d). With the above scaling for $N \geq 2$, we obtain

$$G(r_0, r_0) = \frac{r_0}{N-1}J_1(r_0)J_2(r_0). \qquad (2.15)$$

Therefore, from (2.10) and (2.11) we obtain

$$U_0 = 1 - \frac{6}{\mathcal{A}^2 U_0}\frac{J_1(r_0)J_2(r_0)}{\mathcal{W}}, \qquad (2.16\text{a})$$

$$U_1'(\infty) + U_1'(-\infty) = -\frac{6}{\mathcal{A}^2 U_0}\frac{(J_1(r_0)J_2(r_0))'}{\mathcal{W}}, \qquad (2.16\text{b})$$

$$\frac{U_1'(\infty) + U_1'(-\infty)}{U_0} = -s\frac{(J_1(r_0)J_2(r_0))'}{J_1(r_0)J_2(r_0)} \text{ where } s = \frac{1 - U_0}{U_0}. \qquad (2.16\text{c})$$

Substituting (2.16c) into (2.9) we then obtain the following proposition:

Proposition 2.1.1 *Let $\Omega = B_R$ be the ball of radius R. In the low-feed regime $\mathcal{A} \ll \infty$, the Gray-Scott model (2.2) admits a solution of the form*

$$\nu \sim \frac{1}{\mathcal{A}U_0}w\left(\frac{r-r_0}{\varepsilon}\right), \quad r = |x|, \quad r_0 = r_0(\varepsilon^2 t), \quad u \sim U_0, \ for \ |r - r_0| = O(\varepsilon) \qquad (2.17)$$

where w is given by (1.7), U_0 satisfies (2.16a) and r_0 satisfies the following ODE:

$$\frac{d}{dt}r_0 = -\varepsilon^2\left\{\frac{N-1}{r_0} + s\frac{(J_1(r_0)J_2(r_0))'}{J_1(r_0)J_2(r_0)}\right\} \quad where \quad s = \frac{1-U_0}{U_0}. \qquad (2.18)$$

Here, J_1, J_2 are defined in (2.13).

We now study the existence of equilibria of the ODE (2.18). We set $r_0' = 0$ in (2.18) and eliminate U_0 using (2.16a). This yields

$$\mathcal{A}^2 = -6G(r_0, r_0)\frac{(1-\gamma)^2}{\gamma} \quad where \quad \gamma = \frac{r_0}{N-1}\frac{(J_1(r_0)J_2(r_0))'}{J_1(r_0)J_2(r_0)}, \qquad (2.19a)$$

$$U_0 = \frac{\gamma}{\gamma - 1}. \qquad (2.19b)$$

A graph of r_0 versus $\mathcal{A}^2$ for $N = 2$ and $R = 5, \infty$ is given in Figure 2.3. When $R = 5$, the graph shows that $\mathcal{A}^2$ blows up as $r_0 \to r_R$ where $r_R = 3.943$ is a root of γ. Moreover, $\mathcal{A}^2 > 0$ for $r_0 \in (0, r_R)$ and all values of $\mathcal{A}$ are attained on that interval. On the other hand, when $R = \infty$, $\mathcal{A}$ remains bounded for any r_0, as shown on Figure 2.3. We show the following:

Proposition 2.1.2 *Suppose that $R < \infty$, $N \geq 2$. Then there exists an $r_R \in (0, R)$ which satisfies*

$$[J_1(r_R)J_2(r_R)]' = 0. \qquad (2.20)$$

Moreover, for any $\mathcal{A} > 0$ with $\mathcal{A} = O(1)$, there exists $r_0 \in (0, r_R)$ and $U_0 \in (0, \frac{1}{2})$ such that

$$\nu \sim \frac{1}{\mathcal{A}U_0}w\left(\frac{r-r_0}{\varepsilon}\right), \quad r = |x|, \quad u \sim U_0 \qquad (2.21)$$

and r_0, U_0 satisfies (2.19).

Suppose that $R = \infty$, $N \geq 2$. Then there exists $\mathcal{A}_c \geq \sqrt{12}$ such that for any $\mathcal{A} \in (0, \mathcal{A}_c)$, the solution to (2.19) with $r_0 > 0, U_0 \in (0, \frac{1}{2})$ exists, and (2.21) holds.

57
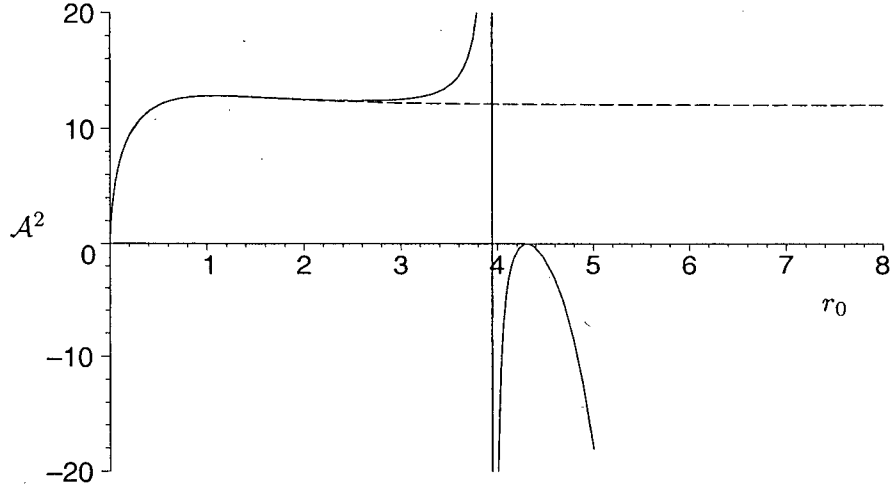
Figure 2.3: Plot of r_0 versus $\mathcal{A}^2$, with $R = 5$ (solid curve) and $R = \infty$ (dashed curve). In the case $R = 5$, note the singularity at $r_R = 3.943$.

Proof. To show the existence of r_R for finite R, note that $(J_1 J_2)'(R) = J_1'(R) J_2(R) > 0$ whereas $(J_1 J_2)'(0) = J_1(0) J_2'(0) < 0$. Thus $(J_1 J_2)'$ has a root in $(0, R)$. Let r_R be the first such root. Thus $\gamma < 0$ for $r_0 \in (0, r_R)$.

We next show that when $\mathcal{A}$ satisfies the conditions of the proposition, there exists a solution r_0 to (2.19a) with $\gamma < 0$ at that point. There are two cases to consider.

- *Case $R < \infty$* : Since $\gamma \to 0^-$ as $r_0 \to r_R^-$, we see that $\mathcal{A}^2$ blows up as $r_0 \to r_R^-$. Moreover, using (2.15) and (2.19a), it is easy to show that $\mathcal{A} \to 0$ as $r_0 \to 0$. This shows the existence of solution $r_0 \in (0, r_R)$ to (2.19a) for any given $\mathcal{A} > 0$ when R is finite, and the corresponding value of γ satisfies $\gamma < 0$.

- *Case $R = \infty$* : In this case, we first claim that $\gamma < 0$ for all $r_0 > 0$. Since $J_1, J_2 > 0$, this is equivalent to showing that $u(r) = r(J_1(r) J_2(r))'$ is always negative. After some algebra, we obtain

$$u''(r) + \frac{N-1}{r} u'(r) - 4u(r) = 2N J_1(r) J_2(r). \tag{2.22}$$

58

Note that $J_1 J_2 > 0$, $u(y) \sim -(N-1)C\frac{1}{y^{N-1}}$ as $y \to \infty$, and

$$u \sim \begin{cases} -C, & N = 2 \\ -(N-2)Cy^{2-N}, & N > 2 \end{cases} \quad \text{as} \quad y \to 0.$$

In the equation above, C is some positive constant that may change from line to line. Thus u is negative on the boundary of an annulus $\{x : \varepsilon < |x| < R\}$, for any R big enough and any ε small enough. It then follows from the positivity of $J_1 J_2$ and the comparison principle that u is negative everywhere on that annulus. Since ε and R are arbitrary, $u(r) < 0$ for all $r > 0$.

A simple calculation shows that for $R = \infty$,

$$\gamma(r) \sim -1 + \frac{N-3}{4r^2} + O(\frac{1}{r^3}), \quad r \to \infty,$$

$$G(r,r) \sim 1, \quad r \to \infty$$

But then $\mathcal{A}^2 \to 12$ as $y \to \infty$. This shows the existence of $\mathcal{A}_c \geq \sqrt{12}$, as well as the existence of $r_0 \in (0, \infty)$ satisfying (2.19a) whenever $\mathcal{A} \in (0, \mathcal{A}_c)$.

This establishes the existence of $r_0 > 0$ solving (2.19a) with $\gamma < 0$. Next, note that $\gamma < 0$ implies that $\frac{\gamma}{\gamma-1} \in (0, 1)$. Therefore (2.19b) admits a solution with $U_0 \in (0, 1)$. $\square$

2.1.2 The breakup instability in the low-feed regime

In this section we study the breakup instabilities of stripe and ring solutions in the low-feed regime. The analysis here parallels the analysis of the large eignevalues in §1.1.2. First, consider the stripe solution on the rectangular domain

$$\Omega = [-l, l] \times [0, d].$$

Start with a one-dimensional single spike solution on $x_1 \in [-l, l]$, as derived in Proposition 1.1.1, then extend it trivially in the x_2 direction. This yields the leading-order equilibria stripe solution in the inner region

$$\nu_e \sim \frac{1}{\mathcal{A}U} w(\frac{x_1}{\varepsilon}), \quad u_e \sim U, \tag{2.23}$$

where $U = U_\pm$ is given by (1.11). We consider the following perturbations from the steady state:

$$\nu = \nu_e + \cos(mx_2)e^{\lambda t}\phi(x_1), \quad u = u_e + \cos(mx_2)e^{\lambda t}\psi(x_1). \tag{2.24}$$

where, to satisfy the Neumann boundary condition, the mode m is an integer multiple of π/d. We obtain the following linearized problem:

$$\lambda\phi = \varepsilon^2\phi'' - m^2\varepsilon^2\phi - \phi + 2\mathcal{A}\nu_e u_e\phi + \mathcal{A}\nu_e^2\psi, \tag{2.25a}$$

$$\tau\lambda\psi = \psi'' - m^2\psi - \psi - \frac{1}{\varepsilon}\left(2\nu_e u_e\phi + \nu_e^2\psi\right). \tag{2.25b}$$

Near the core of the stripe, where $x_1 \ll 1$, we have

$$\phi \sim \Psi(\frac{x_1}{\varepsilon}), \quad \psi(x_1) \sim \phi(0) = \psi_0, \tag{2.26}$$

$$\mathcal{A}\nu_e u_e\phi \sim w\Phi, \quad \frac{1}{\varepsilon}\nu_e u_e\phi \sim \delta(x_1)\frac{1}{\mathcal{A}}\int w\Phi,$$

$$\mathcal{A}\nu_e^2\psi \sim \frac{1}{\mathcal{A}U^2}w^2\psi_0, \quad \frac{1}{\varepsilon}\nu_e^2\psi \sim \delta(x_1)6\psi_0\frac{1}{\mathcal{A}^2U^2},$$

so that

$$\psi'' - (1 + m^2 - \tau\lambda)\psi \sim 2\delta(x_1)\frac{1}{\mathcal{A}}\int w\Phi + \delta(x_1)6\psi_0\frac{1}{\mathcal{A}^2U^2}, \tag{2.27}$$

$$\lambda\Phi = L_0\Phi + \frac{1}{\mathcal{A}U^2}w^2\psi_0 \tag{2.28}$$

From (2.27) we obtain:

$$\psi_0 \sim G_m(0,0)\left\{\frac{2}{\mathcal{A}}\int w\Phi + 6\psi_0\frac{1}{\mathcal{A}^2U^2}\right\} \tag{2.29}$$

where G_m is the Green's function satisfying

$$G_{mx_1x_1} - (1 + m^2 + \tau\lambda)G_m = -\delta(x_1' - x_1) \tag{2.30a}$$

with Neumann boundary conditions at $x_1 = \pm 1$. We thus have

$$G_m(0,0) = \frac{1}{2\theta}\coth(l\theta), \quad \theta = \sqrt{1 + m^2 + \tau\lambda}. \tag{2.30b}$$

60

Combining (2.29) and (2.28) we obtain the following non-local eigenvalue problem:

$$\lambda \Phi = L_0 \Phi + \chi w^2 \frac{\int w \Phi}{\int w^2} = 0, \quad \chi = \frac{2}{\frac{\sigma}{G_m(0,0)s} + 1}, \quad (2.31)$$

where $s = \frac{1-U}{U}$ and σ is given by (1.10) with $D = 1$. As with Proposition 1.1.6, we therefore obtain the following instability result:

Proposition 2.1.3 *Suppose* $m\varepsilon \ll 1$. *Let*

$$s_m = \frac{\sqrt{1+m^2} \tanh(l\sqrt{1+m^2})}{\tanh(l)}, \quad s = \frac{1-U}{U},$$

where U is given by (1.11). If $s < s_m$ then a single stripe solution given by (2.23) is unstable with respect to the mode m perturbation given by (2.24). Here, ϕ is an even function.

If $s > s_m$ and $\tau \ll 1$ then the mode m is stable.

As shown numerically, an instability of this type leads to a breakup of the stripe into m spots. We therefore refer to this instability as a *breakup instability of mode m*.

Since s_m can be made arbitrary large by choosing large enough m, we have deduced the following result:

Corollary 2.1.4 *The stripe in a low-feed regime is always unstable with respect to breakup instabilities for large enough m.*

The analysis for a ring in two dimensions is the same, except σ in (2.31) is replaced by $G_R(r_0, r_0)$ as given by (2.13), and $G_m(0,0)$ is replaced by $G_{Rm}(r_0, r_0)$, where G_{Rm} is the radial Green's function of order m, satisfying

$$\frac{d^2}{d^2 r} G_{Rm} + \frac{1}{r}\frac{d}{dr} G_{Rm} - \frac{m^2}{r^2} G_{Rm} - (1 + \tau\lambda) G_{Rm} = -\delta(r' - r).$$

This yields

$$G_{Rm}(r_0, r_0) = J_{1m}(r_0) J_{2m}(r_0) r_0,$$

where

$$J_{1m}(r) = I_m(\mu r), \quad J_{2m}(r) = K_m(\mu r) - \frac{K'_m(\mu R)}{I'_m(\mu R)} I_m(\mu r), \quad \mu = \sqrt{1 + \tau\lambda}, \tag{2.32}$$

where K_m, I_m are Bessel functions of order m. Thus we obtain the next result.

Proposition 2.1.5 *Consider the equilibrium ring solution of radius r_0 of Proposition 2.1.2, in two dimensions, and consider the breakup perturbation of the form*

$$\nu(r) + \cos(m\theta)e^{\lambda t}\phi(r) \tag{2.33}$$

with ϕ even, and $m\varepsilon \ll O(1)$. Let

$$s_m = \frac{J_1(r_0)J_2(r_0)}{J_{1m}(r_0)J_{2m}(r_0)}, \quad s = \frac{1 - U_0}{U_0},$$

where

$$J_{1m}(r) = I_m(r), \quad J_{2m}(r) = K_m(r) - \frac{K'_m(R)}{I'_m(R)} I_m(r), \quad J_1 = J_{10}, \quad J_2 = J_{20},$$

and U_0 is given in (2.16a). Then the equilibrium solution ν_e is unstable with respect to the breakup mode m (2.33) if $s < s_m$. Conversely, if $s > s_m$ and $\tau \ll 1$ then the mode m is stable.

Note that $J_{1m}(r_0)J_{2m}(r_0) = O(1/m)$ as $m \to \infty$. Therefore, as with stripes, we have

Corollary 2.1.6 *The ring solution in a low-feed regime is always unstable with respect to breakup instabilities for large enough m.*

We remark that from our numerical computation, we find that in the case $R = \infty$, the mode $m = 1$ is always unstable.

Finally, we consider the case $m \doteq \frac{m_0}{\varepsilon}$ with $m_0 = O(1)$. Then the linearized problem (2.25) for the stability of the stripe stripe becomes

$$(\lambda + m_0^2)\phi = \varepsilon^2 \phi'' - \phi + 2\mathcal{A}\nu_e u_e \phi + \mathcal{A}\nu_e^2 \psi, \tag{2.34a}$$

$$\tau\lambda\psi = \psi'' - \frac{m_0^2}{\varepsilon^2}\psi - \psi - \frac{1}{\varepsilon}\left(2\nu_e u_e \phi + \nu_e^2 \psi\right). \tag{2.34b}$$

It follows from (2.34b) that $\psi \sim 0$ in the inner region, and after changing variables as in (2.26) we obtain

$$(\lambda + m_0^2)\Phi = L_0\Phi,$$

where L_0 is defined in (1.16). From Lemma 1.1.4, L_0 has a single positive eigenvalue $\frac{5}{4}$. Thus we obtain $\text{Re}\,\lambda \leq \frac{5}{4} - m_0^2$. The calculation for a ring is identical except that m_0^2 gets replaced by $\frac{m_0^2}{r_0^2}$. The result is summarized as follows:

Proposition 2.1.7 *The stripe solution in the low-feed regime is stable with respect to breakup instabilities of mode $m = \frac{m_0}{\varepsilon}$ for all m_0 satisfying $m_0^2 > \frac{5}{4}$.*

The ring solution of radius r_0 is stable with respect to breakup instabilities of mode $m = \frac{m_0}{\varepsilon}$ for all m_0 satisfying $\frac{m_0^2}{r_0^2} > \frac{5}{4}$.

Corollaries 2.1.4, 2.1.6 and Proposition 2.1.7 establish the existence of a wide instability band for the breakup instabilities in the low-feed regime, for either stripes or rings. The upper bound is $m = O(\frac{1}{\varepsilon})$ and the lower bound is of $O(1)$. As we will see below, an instability band also exists for the intermediate and high-feed regime.

2.2 Stripe in the Intermediate and high-feed regime

In this section we discuss the stability of a stripe solution in high and intermediate regimes of the Gray Scott model in two dimensions 2.1.

The equilibria stripe solution in the high-feed or intermediate regime is constructed by taking the one-dimensional pulse solution constructed in §1.2.1 and trivially extending it in the x_2 direction. In this way we obtain the following equilibrium state:

Proposition 2.2.1 *Let $\Omega = [-l, l] \times [0, d]$. Let*

$$B = \tanh(l)A.$$

Suppose $A \gg O(\varepsilon^{1/2})$ and $B < 1.347$. Then there exists a stripe solution to (2.1) of the form

$$v \sim \frac{1}{\varepsilon}V_0(y), \quad u \sim \frac{\varepsilon}{A}U_0(y), \quad y = \frac{x_1}{\varepsilon},$$

where $V_0(y)$, $U_0(y)$ satisfy (1.42) with boundary conditions

$$V_0(0) = 0 = U_0(0), \quad V_0(\infty) = 0, \quad U_0'(\infty) = B. \tag{2.35}$$

In the intermediate regime $B = 3\delta$ where $\varepsilon^{1/2} \ll \delta \ll 1$, U_0 and V_0 are given in Proposition 1.2.2.

2.2.1 Zigzag instabilities of a stripe

We now study the stability with respect to the small eigenvalues of the stripe equilibrium solution constructed in Proposition 2.2.1. The shape of these instabilities causes the stripe to develop a zigzag-type pattern in the transversal direction.

We introduce a perturbation around the equilibrium state:

$$v(x) = \frac{1}{\varepsilon} \left(V(y) + e^{\lambda t} e^{imx_2} \Phi(y) \right),$$

$$u(x) = \frac{\varepsilon}{A} \left(U(y) + e^{\lambda t} e^{imx_2} N(y) \right) \quad \text{where } y = \frac{x_1}{\varepsilon}.$$

Here, V, U satisfy (1.40), and m is an integer multiple of π/d. The equations for Φ, N on $-\infty < y < \infty$ become:

$$\lambda \Phi = \Phi'' - m^2 \varepsilon^2 \Phi - \Phi + V^2 N + 2VU\Phi, \tag{2.36}$$

$$\tau \varepsilon^2 \lambda N = N'' - m^2 \varepsilon^2 N - \varepsilon^2 N - V^2 N - 2VU\Phi.$$

From (2.36), it is clear that there are several cases to consider, depending of the magnitude of m. First we consider the case $m = O(1)$. Then, for small eigenvalues, we expand

$$\Phi = \Phi_0 + A\varepsilon \Phi_1 + \dots, \quad N = N_0 + A\varepsilon N_1 + \dots, \quad \lambda = A\varepsilon \lambda_0 + \dots.$$

The equations for Φ_0, N_0 and Φ_1, N_1 are then exactly the same as in §1.2.2 and are given by (1.84) and (1.85), respectively. Therefore the analysis of the inner region is exactly the same as in the proof of Theorem 1.2.4 up to (1.93). In particular we obtain as before $\Phi_0 = V_0'$, $N_0 = U_0'$, and the mode m plays no effect there. For the outer region, we set

$$v = v_e(x_1) + e^{\lambda t} \cos(mx_2)\phi(x_1), \qquad u = u_e(x_1) + e^{\lambda t} \cos(mx_2)\eta(x_1), \tag{2.37}$$

64

where v_e, u_e is the equilibrium stripe solution to (2.1), to obtain the following problem for the η in the outer region:

$$\eta_{xx} - (1 + \tau\lambda + m^2)\eta = \eta v_e^2 + 2u_e v_e \phi. \tag{2.38}$$

Comparing this with (1.94), we see that the only difference is that $1 + \tau\lambda$ gets replaced by $1 + \tau\lambda + m^2$. Following the rest of the computations with this replacement, we have therefore shown the following result regarding the small eigenvalues for a stripe:

Proposition 2.2.2 *Consider a single stripe equilibrium solution (U_0, V_0), of (2.1) in the high-feed and intermediate regimes, as given by Propositions 1.2.1 and 1.2.2, respectively. There exists an instability the form*

$$U \sim U_0(y + ce^{mx_2}e^{\lambda t}), \quad V \sim V_0(y + ce^{mx_2}e^{\lambda t}),$$

where $m = O(1)$, $y = \frac{x_1}{\varepsilon}$, c is a small constant, and λ is given by:

$$\lambda \sim -\varepsilon A \alpha \left(1 - \theta \tanh \theta l \tanh l\right), \tag{2.39}$$

where

$$\theta = \sqrt{1 + \lambda\tau + m^2},$$

and α is a positive constant whose definition is given in Proposition 1.2.4.

Assuming $\tau \ll O(\frac{1}{\varepsilon})$, (2.39) reduces to:

$$\lambda = -A\varepsilon\alpha \left(1 - \sqrt{m^2 + 1}\tanh(l)\tanh(l\sqrt{m^2 + 1})\right). \tag{2.40}$$

Thus λ is negative for small m but is positive if m is big enough. The threshold of stability occurs for $m = m_l$, satisfying

$$1 - \sqrt{m^2 + 1}\tanh(l)\tanh(l\sqrt{m^2 + 1}) = 0. \tag{2.41}$$

The graph of l versus the first unstable mode m_l is shown in Figure 2.4.

In particular, the lowest unstable mode m_l is $m_l \sim 0$ as $l \to \infty$. Additionally, it easy to see that $m_l \sim \frac{z}{l}$ as $l \to 0$ where $z = 1.1997$ is the unique root of $z \tanh z = 1$.
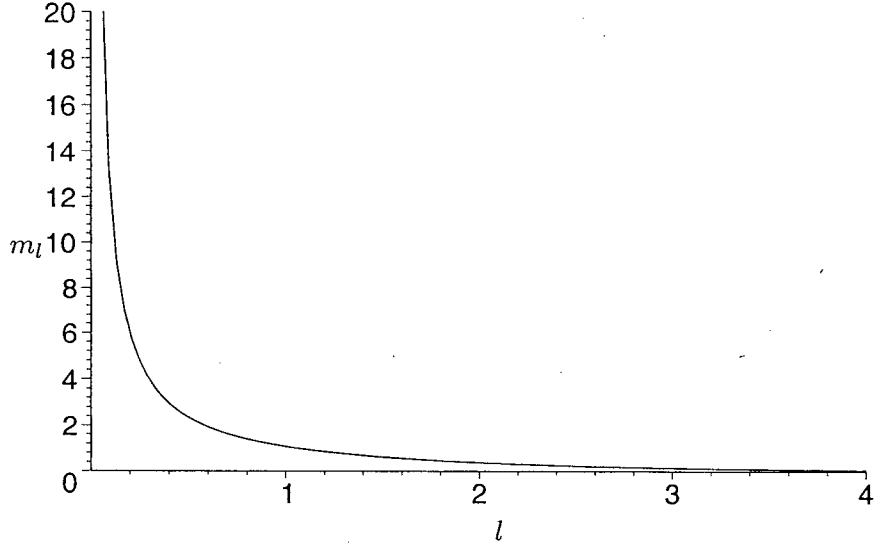
Figure 2.4: Plot of the domain half-length l versus the lowest unstable mode m_l. Above this curve we have instability.

Next, we consider the case $O(1) \ll m \ll O(\frac{1}{\varepsilon})$. Then in the inner region, we expand the solution to (2.36) as

$$\lambda = m\varepsilon\lambda_0 + \ldots, \quad \Phi = V_0' + \varepsilon m\Phi_1 + \ldots, \quad N = U_0' + \varepsilon m N_1 + \ldots. \tag{2.42}$$

We then obtain that Ψ_1, N_1 satisfy the following system of $-\infty < y < \infty$:

$$\lambda_0 V_0' = \Phi_1'' - \Phi_1 + V_0^2 N_1 + 2V_0 U_0 \Phi_1, \tag{2.43a}$$

$$0 = N_1'' - N_1 V_0^2 - 2V_0 U_0 \Phi_1. \tag{2.43b}$$

To determine λ_0, we multiply (2.43a) by the adjoint solution $\Psi^\dagger$ which satisfies (1.88). By integrating over the domain, we obtain that

$$\int \Psi^\dagger L\Psi = \Psi_2^\dagger(\infty) \left[N_1'(\infty) + N_1'(-\infty) \right] = \lambda_0 \int \Psi_1^\dagger V_0'. \tag{2.44}$$

To determine $N_1(\pm\infty)$, we match the inner solution N with the outer solution η, as in (1.96)-(1.97b). We have:

$$\eta(x_1) = \varepsilon \left(U_0' \left(\frac{x_1}{\varepsilon} \right) + \varepsilon m N_1 \left(\frac{x_1}{\varepsilon} \right) \right),$$

$$\eta'(x_1) = \left(U_0'' \left(\frac{x_1}{\varepsilon} \right) + \varepsilon m N_1' \left(\frac{x_1}{\varepsilon} \right) \right),$$

66

and also $U_0''(\pm\infty) = 0$. It follows that

$$N_1'(\pm\infty) = \frac{1}{\varepsilon m}\eta'(\pm 0). \tag{2.45}$$

Note that η satisfies (2.38). Assuming that $\lambda\tau \ll O(m^2)$, we therefore obtain

$$\eta'' - m^2\eta \sim 0, \quad x_1 \neq 0$$

and

$$\eta(0^\pm) \sim \pm\varepsilon B = \pm\varepsilon A \tanh(l), \quad \eta'(\pm l) = 0.$$

Since m is large, we obtain that

$$\eta \sim \varepsilon B e^{-m|x|}. \tag{2.46}$$

Combining (2.45) and (2.46) we obtain

$$N_1'(\infty) + N_1(-\infty) = -2B.$$

Recalling (2.44), (2.42) and (1.102) we finally obtain

$$\lambda_0 \sim \alpha A \tanh l, \tag{2.47a}$$

$$\lambda \sim \alpha m\varepsilon A \tanh l. \tag{2.47b}$$

This computation shows that in the high-feed regime, all of the modes m with $O(1) \ll m \ll O(\frac{1}{\varepsilon})$ are indeed unstable, whenever $\alpha > 0$. As a remark, (2.47b) can be obtained formally by taking the limit $m \gg 1$ in (2.39).

Equation (2.47b) is valid uniformly in the high-feed regime $A = O(1)$, for $1 \ll m \ll \frac{1}{\varepsilon}$. However in the intermediate regime, this computation is not uniformly valid. This is because we have not included the term $\varepsilon^2 m^2 \Phi_0$ in the second order equations (2.43a). However as m is increased, the order of this term will eventually balance $O(\varepsilon m \Phi_1)$. To see when this balance occurs, we formally rewrite (2.43a), but include the term $\varepsilon^2 m^2 \Phi_0 = \varepsilon^2 m^2 V_0'$:

$$\lambda_0 V_0' = \Phi_1'' - m\varepsilon V_0' - \Phi_1 + V_0^2 N_1 + 2V_0 U_0 \Phi_1.$$

Proceeding as before, this leads to (2.47a) but with λ_0 replaced by $\lambda_0 + m\varepsilon$:

$$\lambda_0 + m\varepsilon \sim \alpha A \tanh l. \tag{2.48}$$

Using (1.79), (1.50) this can be written as

$$\lambda \sim m\varepsilon(6\delta^2 - m\varepsilon). \tag{2.49}$$

Thus (2.47a) is valid in the intermediate regime only when $O(1) \ll m \ll O(\frac{\delta^2}{\varepsilon})$. However (2.48) is valid uniformly for $O(1) \ll m \leq O\left(\frac{\delta^2}{\varepsilon}\right)$. Equation (2.48) also yields the upper threhold m_u on the instability band:

$$m_u \sim \frac{6\delta^2}{\varepsilon}. \tag{2.50}$$

Recall that $\delta \gg O(\varepsilon^{1/2})$; thus we indeed have $m_u \gg 1$.

Finally, we consider the case $m = O(\frac{1}{\varepsilon})$. We set

$$m = m_0 \frac{1}{\varepsilon}$$

with $m_0 = O(1)$. The leading order linearized equations then become:

$$(\lambda + m_0^2)\Phi_0 = \Phi_0'' - \Phi_0 + V_0^2 N_0 + 2V_0 U_0 \Phi_0, \tag{2.51a}$$

$$m_0^2 N_0 = N_0'' - V_0^2 N_0 - 2V_0 U_0 \Phi_0. \tag{2.51b}$$

We first consider the intermediate regime. Using (1.62) we obtain:

$$V_0 U_0 = w + \delta^2(v_1 + u_1 w) + \ldots$$

$$V_0^2 = \delta^2 w^2 + \delta^4 2wv_1 + \ldots$$

Thus we expand:

$$\Phi_0 = \Phi_{00} + \delta^2 \Phi_{01} + \ldots,$$

$$N_0 = N_{00} + \delta^2 N_{01} + \ldots$$

Since we are looking for odd solutions, we must also assume

$$m_0 = \delta\mu + \ldots, \quad \lambda = \lambda_0 \delta^2 \ldots.$$

The leading order equation for Φ_{01} then becomes:

$$0 = L_0\Phi_{00}, \quad 0 = N''_{00} - 2w\Phi_{00},$$

where $L_0\Phi = \Phi'' - \Phi + 2w\Phi$. Thus we obtain:

$$\Phi_{00} = w', \quad N_{00} = u'_1.$$

Equation for Ψ_{01} at next order is then

$$(\mu^2 + \lambda_0)w' = L_0\Phi_{01} + w^2 u'_1 + 2(v_1 + u_1 w)w'. \tag{2.52}$$

Multiplying by w', integrating, and using the self-adjointness of L_0, we obtain:

$$(\mu^2 + \lambda_0)\int w'^2 = \int w^2 u'_1 w' + 2(v_1 + u_1 w)w'^2.$$

Next, we differentiate (1.62b) to obtain:

$$L_0 v'_1 = -w^2 u'_1 - 2(v_1 + u_1 w)w'.$$

Multiplying this expression by w' and integrating, we obtain that the right hand side of (2.52) is zero. This yields

$$\lambda_0 \sim -\mu^2, \quad \lambda \sim -(\varepsilon m)^2. \tag{2.53}$$

This shows the stability of the higher modes $m = O(\frac{\delta}{\varepsilon})$. As a remark, note that (2.53) can also be obtained by taking a limit $m\varepsilon \gg \delta^2$ in (2.48). Thus (2.48) is valid uniformly for all $O(1) \ll m$. Combining together (2.48) and (2.39) we can write a uniformly valid formula for the small eigenvalues in the intermediate regime:

Proposition 2.2.3 *Consider a single stripe equilibrium solution* $(U_0(x_1), V_0(x_1))$, *of (2.1) in the intermediate regimes, as given by Proposition 1.2.2, and suppose that* $\tau \leq O(1)$. *Then the small eigenvalue* λ *corresponding to the mode* m *as in Proposition 2.2.2 is given by:*

$$\lambda \sim m\varepsilon \left\{ 6\delta^2 \left[\frac{\sqrt{m^2+1}}{m} \tanh(\sqrt{m^2+1}l) - \frac{\coth l}{m} \right] - m\varepsilon \right\} \tag{2.54}$$

69

Here, δ is as in Proposition 1.2.2, and (2.54) is valid for all $0 \le m \le O\left(\frac{\delta}{\varepsilon}\right)$. This eigenvalue is unstable if and only if $m_l < \lambda < m_u$, where m_l is the root of the transcendental equation

$$1 = \sqrt{m_l^2 + 1}\,\tanh(l)\tanh(l\sqrt{m_l^2 + 1}), \tag{2.55}$$

and

$$m_u \sim \frac{6\delta^2}{\varepsilon}.$$

The graph of l versus m_l is shown on Figure 2.4.

In the high-feed regime, the system (2.51) can only be solved numerically. To do so, we discretize (2.51) on a long interval $[0, L]$ using centered finite differences, ensuring that Φ_0 and N_0 are odd functions so that $N_0(0) = \Phi_0(0) = 0$. Choosing a meshsize $h = L/n$, where $n > 1$, we label $y_1 = h$ and $y_n = L$. This leads to the discrete eigenvalue problem

$$\left(\mathcal{M} - \left(1 + m_0^2\right)I + \Lambda_2\right)\Phi_0 + \Lambda_1 N_0 = \lambda\Phi_0, \qquad \left(\mathcal{M} - m_0^2 I - \Lambda_1\right)N_0 = \Lambda_2\Phi_0, \tag{2.56a}$$

so that

$$\left(\mathcal{M} - \left(1 + m_0^2\right)I + \Lambda_2 + \Lambda_1\left(\mathcal{M} - m_0^2 I - \Lambda_1\right)^{-1}\Lambda_2\right)\Phi_0 = \lambda\Phi_0. \tag{2.56b}$$

Here $\Phi_0 = (\Phi_0(y_1), \dots, \Phi_0(y_n))^t$, $N_0 = (N_0(y_1), \dots, N_0(y_n))^t$, and the matrices Λ_1, Λ_2, and $\mathcal{M}$, are defined by

$$\Lambda_1 \equiv \begin{pmatrix} V_0^2(y_1) & 0 & \cdots & 0 \\ 0 & \ddots & \cdots & 0 \\ \vdots & \vdots & \ddots & \vdots \\ 0 & 0 & \cdots & V_0^2(y_n) \end{pmatrix}, \quad \Lambda_2 \equiv \begin{pmatrix} 2U_0(y_1)V_0(y_1) & 0 & \cdots & 0 \\ 0 & \ddots & \cdots & 0 \\ \vdots & \vdots & \ddots & \vdots \\ 0 & 0 & \cdots & 2U_0(y_n)V_0(y_n) \end{pmatrix},$$

$$\tag{2.56c}$$

and

$$\mathcal{M} \equiv \frac{1}{h^2} \begin{pmatrix} -2 & 1 & 0 & \cdots & 0 & 0 & 0 \\ 1 & -2 & 1 & \ddots & \ddots & 0 & 0 \\ 0 & \ddots & \ddots & \ddots & \ddots & \ddots & 0 \\ \vdots & \ddots & \ddots & \ddots & \ddots & \ddots & \vdots \\ 0 & \ddots & \ddots & \ddots & \ddots & \ddots & 0 \\ 0 & 0 & \ddots & \ddots & 1 & -2 & 1 \\ 0 & 0 & 0 & \cdots & 0 & 2 & -2 \end{pmatrix}. \tag{2.56d}$$

Our computational results show that there is a critical value m_{0u} of m_0 for which $\text{Re}(\lambda) < 0$ for $m_0 > m_{0u}$ and $\text{Re}(\lambda) > 0$ for $m_0 < m_{0u}$. This re-stabilization value m_{0u} is computed numerically from the discrete eigenvalue problem using LAPACK [2] on a domain with $L = 12$ and $n = 200$ meshpoints. Increasing the number of meshpoints and the domain length did not change the results significantly. In Fig. 2.5 we plot the critical mode m_{0u}, corresponding to $\lambda = 0$, for each point along the primary branch of the γ versus B curve of Figure 1.6 (i.e. that part of the curve for which $\gamma > 1.02$). Notice that the critical mode m_{0u} tends to zero as $B \to 0$. This agrees with our analysis of the re-stabilization value m_u in the intermediate regime.

We summarize our stability results obtained so far in the following statement:

Proposition 2.2.4 *Using the notation of Proposition 2.2.2, suppose $l \geq O(1)$. Then there exists a band of unstable zigzag modes m satisfying*

$$m_l \leq m \leq m_u,$$

where $m_l = O(1)$ is given by by the root of (2.55) and $m_u \gg 1$ depends on $B = tanh(l)A$. In the intermediate regime $B = 3\delta \ll 1$ we have $m_u \sim \frac{6\delta^2}{\varepsilon}$. In the high-feed regime, $m_u = \frac{m_{0u}}{\varepsilon}$ where m_{0u} depends only on B. Numerically, this dependence is given by the graph of Figure 2.5.

As was mentioned after (2.41), m_l is proportional to l^{-1} for small l. On the other hand, we

71
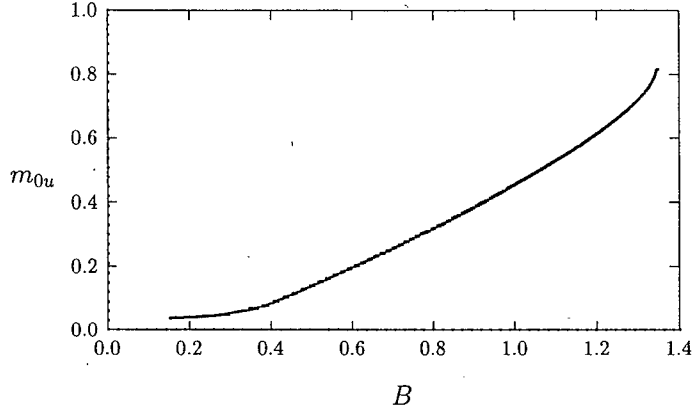
Figure 2.5: Plot of the re-stablization value m_{0u} (with $m_u = \varepsilon^{-1} m_{0u}$) versus B computed from (2.51) at each point along the primary branch of the γ versus B bifurcation diagram. Above this curve we have stability with respect to zigzag perturbations.

have $B = \tanh lA \sim lA$ for small l. Thus when $A = O(1)$ and l is small we have $B \ll 1$, which corresponds to the intermediate regime. We then obtain:

$$m_l \sim \frac{1.1997}{l}, \quad m_u \sim \frac{1}{\varepsilon} \frac{2}{3} l^2 A^2.$$

In addition, we require that the $O(\varepsilon)$ extent of the core of the spike be much small than the domain size, so that $\varepsilon \ll l$. Moreover, the intermediate regime requires the condition $\delta^2 \gg \varepsilon$. Equating $m_l = m_u$, we obtain the following condition for the stability with respect to all zigzag modes.

Proposition 2.2.5 *Using the notation of Proposition 2.2.2, suppose that*

$$l \ll 1, \quad A^2 l^2 \gg \varepsilon, \quad l \gg \varepsilon \tag{2.57a}$$

and

$$\frac{l^3 A^2}{\varepsilon} < \frac{3z}{2}, \tag{2.57b}$$

where $z = 1.1997$ is the unique root of $z \tanh z = 1$. Then the stripe solution is stable with

72

respect to all zigzag instability modes m. In particular, (2.57) are satisfied when $A = O(1)$ and

$$l^3 \ll \varepsilon \ll l^2.$$

In our analysis, we have assumed that $\tau \leq O(1)$ as $\varepsilon \to 0$. If we were to allow $\tau = O(\varepsilon^{-1})$, then for each fixed value of m we could get a zigzag instability due a Hopf bifurcation when τ is increased past some threshold. We will not consider the case of asymptotically large τ here.

2.2.2 Breakup Instabilities of a Stripe

In this section we study the stability with respect to the large eigenvalues of the stripe equilibrium solution constructed in Proposition 2.2.1. Numerically, these instabilities are found to be the mechanism through which a stripe equilibrium breaks up into a sequence of spots.

As in the study in §2.2.1 of the small eigenvalues, we look for a normal mode solution in the inner region $x_1 = O(\varepsilon)$ in the form

$$v = \frac{1}{\varepsilon}\left(V(y) + e^{\lambda t}e^{imx_2}\Phi(y)\right), \qquad u = \frac{\varepsilon}{A}\left(U(y) + e^{\lambda t}e^{imx_2}N(y)\right), \qquad (2.58)$$

where $y = \varepsilon^{-1}x_1$, U, V satisfy (1.40), and U, V, Φ, and N, have power series expansions in powers of εA. We now look for even functions Φ and N. Assuming that $\tau = O(1)$, we obtain, as in §2.2.1, the following leading-order eigenvalue problem on $-\infty < y < \infty$:

$$\lambda\Phi_0 = \Phi_0'' - (1 + \mu)\Phi_0 + V_0^2 N_0 + 2V_0 U_0 \Phi_0, \qquad (2.59a)$$

$$0 = N_0'' - \mu N_0 - V_0^2 N_0 - 2V_0 U_0 \Phi_0. \qquad (2.59b)$$

Here we have defined μ by

$$\mu \equiv \varepsilon^2 m^2.$$

To determine the instability band for (2.59), we discretise (2.59) on a long interval $[0, L]$ using centered finite differences, ensuring that Φ_0 and N_0 are even functions and that $N_{0y} = 0$ at $y = L$. The resulting matrix eigenvalue problem is similar to that in (2.56), except for slight differences in the matrix structure due to the different parity of the breakup eigenfunction. Our

73

computational results show that there are values μ_1 and μ_2 for which $\mathrm{Re}(\lambda) > 0$ for $\mu_1 < \mu < \mu_2$, and $\mathrm{Re}(\lambda) < 0$ for $0 < \mu < \mu_1$ and $\mu > \mu_2$. This instability band is determined from numerical computations of the discrete eigenvalue problem using LAPACK [2] on a domain with $L = 12$ and $n = 200$ meshpoints. Increasing the number of meshpoints and the domain length did not change the results significantly. In Fig. 2.6 and in Table 2.1, we give numerical results for μ_1 and μ_2 versus B along the primary branch of the γ versus B curve.
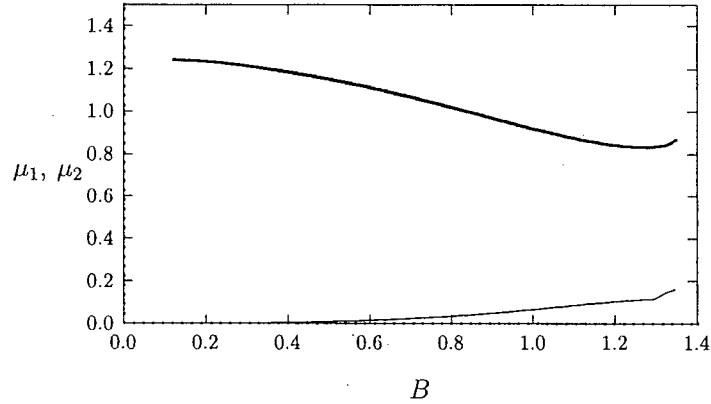
Figure 2.6: Plot of μ_1 (heavy solid curve) and μ_2 (solid curve) versus B computed from (2.59) at each point along the primary branch of the γ versus B bifurcation diagram. In terms of m, the thresholds are $m_j = \sqrt{\mu_j}/\varepsilon$ for $j = 1, 2$.

Although we are not able to calculate μ_1 and μ_2 analytically in the high-feed-rate regime, we can asymptotically calculate these critical values, at which $\lambda = 0$, in the intermediate regime where $B = 3\delta \ll 1$ with $O(\varepsilon^{1/2}) \ll \delta \ll O(1)$.

In the intermediate regime we use Proposition 1.2.2 for V_0 and U_0. In this way, (2.59) reduces to

$$(\mu + \lambda)\Phi_0 \sim \Phi_0'' - \Phi_0 + 2\left(w + O(\delta^2)\right)\Phi_0 + \left(\delta^2 w^2 + O(\delta^4)\right) N_0, \qquad (2.60a)$$

$$\mu N_0 \sim N_0'' - 2\left(w + O(\delta^2)\right)\Phi_0 - \left(\delta^2 w^2 + O(\delta^4)\right) N_0. \qquad (2.60b)$$

The balance of the various terms in the first equation gives rise to two possibilities: either $O(N_0)\delta^2 \ll O(\Phi_0)$ or $O(N_0)\delta^2 = O(\Phi_0)$. In the former case, the leading-order equation for Φ_0

γ	B	μ_1	μ_2
1.464	0.40	0.003713	1.188
1.443	0.50	0.007010	1.154
1.419	0.60	0.01249	1.113
1.390	0.70	0.02093	1.069
1.357	0.80	0.03277	1.020
1.319	0.90	0.04796	0.9700
1.277	1.00	0.06588	0.9208
1.220	1.12	0.08830	0.8695
1.140	1.25	0.1096	0.8345
1.100	1.30	0.1156	0.8358
1.020	1.347	0.1617	0.8724

Table 2.1: The values of μ_2 and μ_1 as defined in Proposition 2.2.6 along the primary branch of the γ versus B bifurcation diagram.

on $-\infty < y < \infty$ is

$$(\mu + \lambda)\Phi_0 = \Phi_0'' - \Phi_0 + 2w\Phi_0 \,, \tag{2.61}$$

with $\Phi_0 \to 0$ as $|y| \to \infty$. From Lemma 1.1.4, this problem has a unique positive eigenvalue $\mu + \lambda = \frac{5}{4}$. This gives the upper bound of $\mu_2 = \frac{5}{4}$ for the instability band.

For the second possibility, we must expand

$$N_0 = \frac{1}{\delta^2}\left(N_{00} + \delta^2 N_{01} + \cdots\right)\,, \qquad \mu = \delta^2\mu_0 + \cdots\,, \qquad \Phi_0 = \Phi_{00} + \delta^2\Phi_{01} + \cdots\,. \tag{2.62}$$

Substituting this expansion into (2.60), we get that N_{00} satisfies $N_{00}'' = 0$. Therefore, N_{00} is a constant to be determined. The leading-order equation for Φ_0 is

$$\lambda\Phi_{00} = \Phi_{00}'' - \Phi_{00} + 2w\Phi_{00} + N_{00}w^2 \,, \tag{2.63}$$

with $\Phi_{00} \to 0$ as $|y| \to \infty$. To determine N_{00}, we must match the inner solution to the outer solution. In the outer region, we have:

$$v = v_e(x_1) + e^{\lambda t}e^{imx_2}\phi(x_1)\,, \qquad u = u_e(x_1) + e^{\lambda t}e^{imx_2}\eta(x_1)\,, \tag{2.64}$$

75

where u_e, v_e are the equilibrium solutions to (2.1), and

$$\phi(x_1) = \frac{1}{\varepsilon}\Phi(\frac{x_1}{\varepsilon}), \quad \eta(x_1) = \frac{\varepsilon}{A}N(\frac{x_1}{\varepsilon}).$$

Substituting (2.64) into (2.1), we obtain the following eigenvalue problem on $-l < x_1 < l$:

$$\lambda\phi = \varepsilon^2\phi_{x_1x_1} - \varepsilon^2 m^2\phi - \phi + 2Au_e v_e\phi + Av_e^2\eta\,, \qquad (2.65\text{a})$$

$$\eta_{x_1x_1} - \left(1 + m^2 + \tau\lambda\right)\eta = 2u_e v_e\phi + v_e^2\eta\,, \qquad (2.65\text{b})$$

with $\eta_{x_1}(\pm l) = 0$. The right-hand side of (2.65b) is localized near $x_1 = 0$. Using Proposition 1.2.2 for solutions in the intermediate regime we obtain that

$$2u_e v_e\phi + v_e^2\eta \sim \frac{2w}{\varepsilon A}\Phi_{00} + \frac{w^2}{\varepsilon A}N_{00}\,. \qquad (2.66)$$

Therefore, we obtain the following problem for $\eta(x_1)$:

$$\eta_{x_1x_1} - \left(1 + m^2 + \tau\lambda\right)\eta = \left(\frac{2}{A}\int w\Phi_{00}\,dy + \frac{N_{00}}{A}\int w^2\,dy\right)\delta(x_1)\,, \qquad -l < x_1 < l\,, \quad (2.67)$$

with $\eta_{x_1}(\pm l) = 0$. The solution for η is

$$\eta(x_1) = -\left(\frac{2}{A}\int w\Phi_{00}\,dy + \frac{N_{00}}{A}\int w^2\,dy\right)G_m(x_1, 0)\,, \qquad (2.68)$$

where $G_m(x_1, x_1')$ is as given in (2.30). The matching condition for the inner and outer solutions is that

$$\frac{\varepsilon}{A}\left(\delta^{-2}N_{00} + \cdots\right) \sim \eta(0) + \cdots\,. \qquad (2.69)$$

This yields that $\eta(0) = \varepsilon\delta^{-2}N_{00}/A$. Evaluating (2.68) at $x_1 = 0$, we obtain an equation for the unknown constant N_{00},

$$N_{00}\left(\frac{G_m(0,0)}{A}\int w^2\,dy + \frac{\varepsilon}{A\delta^2}\right) = -\frac{2}{A}\left(\int w\Phi_{00}\,dy\right)G_m(0,0)\,. \qquad (2.70)$$

Solving (2.70) for N_{00}, noting that $\int w^2\,dy = 6$, and substituting the result into (2.63), we obtain the following nonlocal eigenvalue problem for Φ_{00} on $-\infty < y < \infty$:

$$\Phi_{00}'' - \Phi_{00} + 2w\Phi_{00} - \chi w^2\frac{\int w\Phi_{00}\,dy}{\int w^2\,dy} = \lambda\Phi_{00}\,, \qquad (2.71)$$

with $\Phi_{00} \to 0$ as $|y| \to \infty$. Here χ is defined by

$$\chi \equiv 2 \left[1 + \frac{\varepsilon}{6\delta^2 G_m(0,0)} \right]^{-1} . \tag{2.72}$$

Here, $G_m(0,0)$ is given in (2.30). From Lemma 1.1.3, we obtain the following sufficient condition for instability:

$$2 \tanh(l\sqrt{1+m^2})\sqrt{1+m^2} \geq \frac{6\delta^2}{\varepsilon} . \tag{2.73}$$

This condition is also necessary provided that χ is asymptotically independent of τ; i.e. when $m^2 \gg O(\tau)$. But since $\delta \gg O(\varepsilon^{1/2})$, (2.73) implies $m \gg 1$. By assumption $\tau \leq O(1)$, it then follows that (2.73) is also a necessary condition. Assuming $l \geq O(1)$, (2.73) then becomes

$$m \geq \frac{3\delta^2}{\varepsilon} . \tag{2.74}$$

This yields the lower limit of the breakup instability band in the intermediate regime. We summarize our result for breakup instabilities in the following statement:

Proposition 2.2.6 *Let $\varepsilon \to 0$, $\tau \leq O(1)$ and $l \geq O(1)$. In the intermediate regime, the stripe equilibrium solution is unstable with respect to breakup instabilities if and only if the following inequality holds:*

$$3\delta^2 < \varepsilon m < \frac{\sqrt{5}}{2} . \tag{2.75}$$

In the high-feed-rate regime, the instability band along the primary solution branch of the γ versus B curve is given by

$$\sqrt{\mu_1} < \varepsilon m < \sqrt{\mu_2} , \tag{2.76}$$

where $\mu_1 = \mu_1(B)$ and $\mu_2 = \mu_2(B)$ are given in Fig. 2.6 and in Table 2.1.

2.3 Stability of a Ring Solution in intermediate and high-feed regimes

In this section we modify the methods of §2.2 to obtain analogous results for the stability of an equilibrium ring solution for the Gray-Scott model (2.1) in the disk domain

$$\Omega = \{x : |x| \equiv r < R\}.$$

2.3.1 Ring radius and splitting in the high-feed regime

We first study the equilibria ring solutions in the intermediate and high-feed regime $A \gg O(\varepsilon^{1/2})$. The results of §1.2.1 concerning a pulse-splitting instability in the high-feed regime readily generalize to stripe or ring splitting. For a stripe, the threshold on A for the rectangular domain $[-l, l] \times [0, d]$ is the same as for a one dimensional spike splitting on a domain $[-l, l]$, as given in Proposition 1.2.1. Similar analysis also applies for ring solutions, as we now show. In analogy with (1.39), we assume that the ring profile has the shape

$$v(x) = \frac{1}{\varepsilon} V(y), \quad u(x) = \varepsilon \frac{U(y)}{A}, \quad y = \frac{|x| - r_0}{\varepsilon},$$

where both V, U are of order 1, and r_0 is the radius of the ring to be determined. We then obtain on $-\infty < y < \infty$ that

$$V'' + \varepsilon \frac{V'}{r_0 + \varepsilon y} - V + V^2 U = 0,$$

$$\frac{1}{\varepsilon^2} U'' + \frac{1}{\varepsilon} \frac{U'}{r_0 + \varepsilon y} - U + \frac{A}{\varepsilon} - \frac{V^2 U}{\varepsilon^2} = 0.$$

Expanding as in (1.41), the leading term equations are then (1.42). Outside the core region of the ring, we have:

$$u(r_0) = 1 - \int_0^R G(r, r_0) v^2(r) u(r) dr \tag{2.77a}$$

$$\varepsilon \frac{U_0(0)}{A} \sim 1 - \frac{G(r_0, r_0)}{A} \int V_0^2 U_0, \tag{2.77b}$$

where G is the radial Green's function on the disk of radius R, given by (2.13). Since $U(0)$ is of order 1, we obtain:

$$\int_{-\infty}^{\infty} V_0^2 U_0 = \frac{A}{G(r_0, r_0)}.$$

From (1.42b), this yields:

$$U_0'(\infty) - U_0'(-\infty) = \frac{A}{G(r_0, r_0)}.$$

Normally, U_0 will not be symmetric. However, on a disk of radius R, it is symmetric for the special case when $r_0 = r_R$, i.e. when the following condition holds:

$$(J_1(r_0) J_2(r_0))' = 0, \tag{2.78}$$

78

as we now show.

From (2.77) we obtain:

$$u'(r_0^\pm) \sim -\frac{1}{A}\frac{d}{dr_0^\pm}\left(G(r,r_0^\pm)\right)\big|_{r=r_0} \int_{-\infty}^{\infty} V_0^2(y)U_0(y)dy.$$

But the matching condition of the outer solution u and the inner solution U is:

$$U'(\pm\infty) = Au'(r_0^\pm).$$

For U_0 to be symmetric, we must have $U_0'(\infty) + U_0'(-\infty) = 0$ which is equivalent to

$$0 = \frac{d}{dr_0^-}\left(G(r,r_0^-)\right)\big|_{r=r_0} + \frac{d}{dr_0^+}\left(G(r,r_0^+)\right)\big|_{r=r_0} = \frac{1}{\mathcal{W}}J_1'(r_0)J_2(r_0) + \frac{1}{\mathcal{W}}J_1(r_0)J_2'(r_0)$$

This shows (2.78).

Note that r_0 given by (2.78) agrees with the limiting case $\mathcal{A} \to \infty$ (see (2.19a)).

Assuming that U_0 is symmetric, we thus obtain the following boundary conditions for U_0 and V_0:

$$U_0'(0) = 0 = V'(0), \quad U_0'(\infty) = \frac{A}{2G_R(r_R, r_R)}, \quad V_0 \to 0 \text{ as } y \to \infty. \tag{2.79}$$

As was argued in §1.2.1, the solution to the boundary problem (2.79) and (1.42) exists if and only if $U_0'(\infty) < 1.35$. We therefore obtain the following result:

Proposition 2.3.1 *Let r_R be a root of*

$$(J_1(r_R)J_2(r_R))' = 0, \tag{2.80}$$

and let

$$B = \frac{A}{2G(r_R, r_R)}. \tag{2.81}$$

Suppose that

$$O(\varepsilon^{1/2}) \ll B < 1.35, \tag{2.82}$$

where J_1, J_2 are given by (2.13d) and G is given by (2.13). Then there exists an equilibrium ring solution to (2.1) given by

$$v(x) \sim \frac{1}{\varepsilon} V_0(y), \quad u(x) \sim \varepsilon \frac{U_0(y)}{A}, \quad y = \frac{|x| - r_R}{\varepsilon}, \tag{2.83}$$

where U_0, V_0 satisfy (1.42) with the boundary condition (2.79).

Numerically, when B is given by (2.81) is just above 1.35, ring splitting is observed (see §2.4).

Next we look at the zigzag instabilities of a ring. Expand V and U as in (1.41) to obtain the following equations for U_1, V_1 on $-\infty < y < \infty$:

$$V_1'' - V_1 + 2V_0 U_0 V_1 + V_0^2 U_1 = -\frac{V_0'}{Ar_0}, \tag{2.84a}$$

$$U_1'' + 1 - 2V_0 U_0 V_1 - V_0^2 U_1 = -\frac{U_0'}{Ar_0}. \tag{2.84b}$$

The asymptotic boundary conditions for U_1 as $y \to \pm\infty$ are to be obtained by matching.

Next, we introduce a perturbation around the equilibrium state in the form

$$v = v_e(r) + e^{\lambda t} e^{im\theta} \phi(r), \qquad u = u_e(r) + e^{\lambda t} e^{im\theta} \eta(r), \tag{2.85}$$

where $\phi \ll 1$, $\eta \ll 1$, and m is a non-negative integer. Substituting (2.85) into (2.1), we obtain, in place of (2.65), the following eigenvalue problem on $0 < r < R$:

$$\lambda\phi = \varepsilon^2 \left(\phi_{rr} + \frac{1}{r}\phi_r \right) - \frac{\varepsilon^2 m^2}{r^2}\phi - \phi + 2Au_e v_e \phi + Av_e^2 \eta, \tag{2.86a}$$

$$\tau\lambda\eta = \eta_{rr} + \frac{1}{r}\eta_r - \frac{m^2}{r^2}\eta - \eta - 2u_e v_e \phi - v_e^2 \eta. \tag{2.86b}$$

We will study this problem in the inner region where $y = \varepsilon^{-1}(r - r_0) = O(1)$, and in the outer region where $r - r_0 = O(1)$.

In the inner region, we write

$$v_e(r) = \frac{V(y)}{\varepsilon}, \quad u_e(r) = \frac{\varepsilon}{A}U(y), \quad \phi(r) = \frac{1}{\varepsilon}\Phi(y), \quad \eta(r) = \frac{\varepsilon}{A}N(y), \quad y = \varepsilon^{-1}(r - r_0). \tag{2.87}$$

In terms of these variables, (2.86) reduces to an eigenvalue problem on $-\infty < y < \infty$:

$$\lambda \Phi = \Phi'' + \frac{\varepsilon}{r_0 + \varepsilon y}\Phi' - \frac{\varepsilon^2 m^2}{(r_0 + \varepsilon y)^2}\Phi - \Phi + V^2 N + 2VU\Phi, \qquad (2.88a)$$

$$\tau \varepsilon^2 \lambda N = N'' + \frac{\varepsilon}{r_0 + \varepsilon y}N' - \frac{\varepsilon^2 m^2}{(r_0 + \varepsilon y)^2}N - \varepsilon^2 N - V^2 N - 2VU\Phi. \qquad (2.88b)$$

We first assume that $m = O(1)$ as $\varepsilon \to 0$. By expanding V, U, Φ, and N, in powers of εA, and writing $\lambda = \varepsilon A \lambda_0$, we derive (1.84) for Φ_0 and N_0. Thus, $\Phi_0 = V_0'$ and $N_0 = U_0'$. The system for Φ_1 and N_1 is (1.85), with the terms $-\Phi_0'/(Ar_0)$ and $-N_0'/(Ar_0)$ added to the right-hand sides of (1.85a) nd (1.85b), respectively. Since these additional terms are even functions, they do not contribute to the solvability condition that determines λ_0. Therefore, the entire analysis of (1.87-1.89) can be repeated, and we obtain that λ_0 satisfies

$$\lambda_0 = -\alpha\left(\frac{N_1'(+\infty) + N_1'(-\infty)}{2} + 1\right), \qquad \alpha \equiv \frac{-\Psi_2^\dagger(+\infty)}{\int_0^\infty \Psi_1^\dagger V_0' \, dy}. \qquad (2.89)$$

Here $\Psi_j^\dagger$ for $j = 1, 2$ is the solution to the adjoint problem (1.88).

To determine $N_1'(\pm\infty)$ we must consider the outer region. By repeating the analysis of (1.94)–(1.96), we obtain that the outer solution for η on $0 < r < R$ satisfies

$$\eta_{rr} + \frac{1}{r}\eta_r - \frac{m^2}{r^2}\eta - (1 + \tau\lambda)\eta \sim 0, \quad r \neq r_0 \qquad (2.90)$$

with $\eta_r(R) = 0$ and $\eta_r(0) = 0$. The matching condition of the inner and outer solutions for η is

$$\frac{\varepsilon}{A}(N_0 + \varepsilon A N_1 + \cdots) \sim \eta\left(r_0^\pm\right) + \varepsilon y \eta_r\left(r_0^\pm\right) + \cdots. \qquad (2.91)$$

Since $N_0 = U_0'$ satisfies $N_0(\pm\infty) = \pm B$, we get from this matching condition that

$$\eta\left(r_0^\pm\right) = \pm\frac{\varepsilon B}{A} = \pm\frac{\varepsilon}{2G(r_0; r_0)}, \qquad N_1'(\pm\infty) = \varepsilon^{-1}\eta_r\left(r_0^\pm\right)., \qquad (2.92)$$

where $G(r, r')$ is the radial Green's function satisfying $G_{rr} + \frac{1}{r}G_r - (1 + \tau\lambda)G = -\delta(r - r')$. Solving (2.90) for $\eta(r)$, we obtain that

$$\eta(r) = \begin{cases} \eta\left(r_0^+\right) J_{2,m}(r)/J_{2,m}(r_0), & r < r_0 < R, \\ \eta\left(r_0^-\right) J_{1,m}(r)/J_{1,m}(r_0), & 0 < r < r_0. \end{cases}$$

Here $J_{1,m}$ and $J_{2,m}$ are defined in (2.32). Using (2.92) and the Wronskian relation

$$J'_{1,m}(r_0)J_{2,m}(r_0) - J_{1,m}(r_0)J'_{2,m}(r_0) = \frac{1}{r_0},$$

we obtain the compact formula

$$\frac{N'_1(+\infty) + N'_1(-\infty)}{2} = -\frac{1}{4r_0^2 J_1(r_0)J_2(r_0)J_{1,m}(r_0)J_{2,m}(r_0)}. \tag{2.93}$$

where $J_1 = J_{1,0}, J_2 = J_{2,0}$. Substituting (2.93) into (2.89), and recalling that $\lambda \sim \varepsilon A \lambda_0$, we obtain the following result for λ:

Proposition 2.3.2 *Consider an equilibrium ring solution of radius r_0 for the Gray-Scott model in a disk of radius R as constructed in Proposition 2.3.1. Suppose that $m = O(1)$ as $\varepsilon \to 0$. Then, for a perturbation of the form (2.85), λ satisfies the transcendental equation*

$$\lambda \sim -\varepsilon A \alpha \left(1 - \frac{1}{4r_0^2 J_1(r_0)J_2(r_0)J_{1,m}(r_0)J_{2,m}(r_0)} \right). \tag{2.94}$$

The constant α is as in Theorem 1.2.4 and is positive along the primary branch of the γ versus B curve. The functions $J_{1,m}$, $J_{2,m}$ are defined in (2.32) and $J_1 = J_{1,0}, J_2 = J_{2,0}$.

We will only consider the case where $\tau = O(1)$ as $\varepsilon \to 0$. Since $\lambda = O(\varepsilon)$, we get $\theta \sim 1$. Therefore, from (2.94) we conclude that λ is positive, and hence we have a zigzag instability, if and only if

$$4r_0^2 J_1(r_0)J_2(r_0)J_{1,m}(r_0)J_{2,m}(r_0) < 1. \tag{2.95}$$

Using the asymptotic expansion for large m and fixed R, it is easy to show that $J_{1,m}J_{2,m} = O(\frac{1}{m})$ for $m \gg 1$ and r_0 fixed (see below). Therefore, from (2.95), we have an instability if m is large enough. In Fig. 2.7 we show the numerical computation of the first unstable mode $m = m_l$ versus the ring radius r_0. The corresponding disk radius R can be determined in terms of r_0 from (2.78). From this figure we notice that the first two modes $m = 1, 2$ are stable for any r_0. Also note that the first unstable mode increases as the ring radius r_0 is increased. This is in contrast to the result for stripes in §2.2.1, where the first unstable mode tends to zero as the domain half-length l is increased.
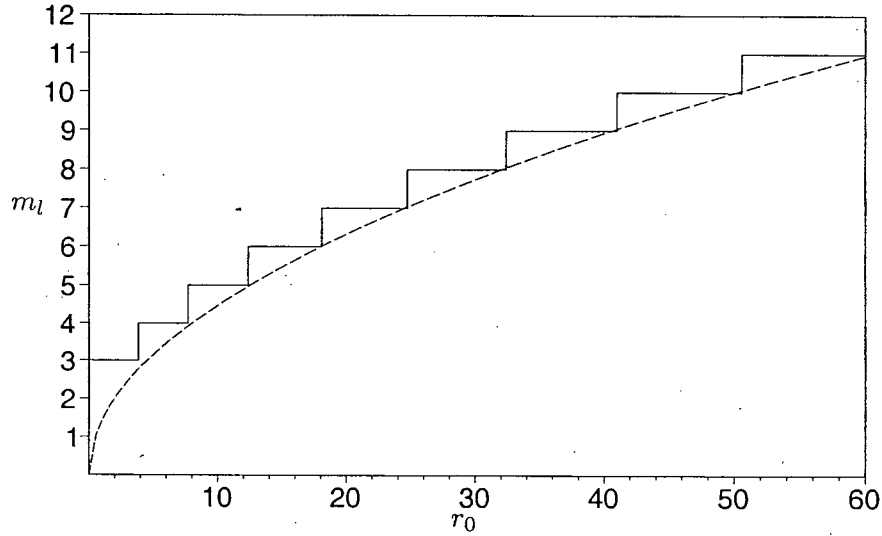
Figure 2.7: The graph of the first unstable mode m_l versus the ring radius r_0 when $\tau = O(1)$. The dotted line is the asymptotic curve (2.99).

We cannot analytically determine m_l for arbitrary R. However, by considering the two limiting cases $R \ll 1$ and $R \gg 1$, we can obtain the following limit results:

Proposition 2.3.3 *The following asymptotic formulae relate the domain radius R and the equilibrium ring radius r_0, as defined by the solution to (2.78):*

$$R \sim \sqrt{2}r_0, \qquad R \to 0, \tag{2.96}$$

$$R \sim r_0 + \frac{1}{2}\ln(2r_0), \qquad R \to \infty. \tag{2.97}$$

Suppose that $\tau = O(1)$, and let m_l be the smallest value of m for which the eigenvalue of Proposition 2.3.2 is unstable. Then

$$m_l = 3, \qquad R \to 0, \tag{2.98}$$

$$m_l \sim \sqrt{2r_0}, \qquad R \to \infty. \tag{2.99}$$

By calculating r_0 in terms of R from (2.97), (2.99) can be written as $m \sim \sqrt{2(R - \frac{1}{2}\ln(2R) + \cdots)}$.

We now derive this result. We first consider the case $R \to 0$. A simple calculation using (2.13d) shows that the equilibrium condition (2.78) for r_0 can be written as

$$\frac{K_0(r_0)}{I_0(r_0)} - \frac{K_0'(R)}{I_0'(R)} = \frac{1}{2r_0 I_0(r_0)I_0'(r_0)}. \tag{2.100}$$

83

For $R \to 0$, with $0 < r_0 < R$, we use the small argument expansions of I_0 and K_0 to obtain that

$$2r_0 I_0(r_0) I_0'(r_0) \sim r_0^2\,, \qquad \frac{K_0'(R)}{I_0'(R)} \sim -2R^{-2}\,, \qquad \frac{K_0(r_0)}{I_0(r_0)} \sim -\ln r\,.$$

Therefore, (2.100) reduces to $2R^{-2} \sim r^{-2}$. This yields $R \sim \sqrt{2}r_0$, which establishes (2.96).

Next, we determine the stability threshold m_l for $R \to 0$. Using the small argument expansions of I_0 and K_0, we readily obtain that

$$J_1(r_0) J_2(r_0) \sim \frac{2}{R^2} \sim r_0^{-2}\,. \tag{2.101}$$

Using (2.32), and the small argument expansions

$$K_m(r_0) \sim \frac{1}{2}\Gamma(m)\left(\frac{r_0}{2}\right)^{-m} \qquad I_m(r_0) \sim \frac{1}{\Gamma(m+1)}\left(\frac{r_0}{2}\right)^{m}\,, \tag{2.102}$$

we calculate for $R \ll 1$ and $r \ll 1$ that

$$J_{1,m}(r_0) J_{2,m}(r_0) = I_m(r_0) K_m(r_0) - \frac{K_m'(R)}{I_m'(R)}\left(I_m(r_0)\right)^2 \sim \frac{1}{2}\frac{\Gamma(m)}{\Gamma(m+1)}\left(1 + \frac{1}{2^m}\right)\,. \tag{2.103}$$

Here $\Gamma(m)$ is the Gamma function. Therefore, substituting (2.101) and (2.103) into (2.95), we have instability when $R \ll 1$ if and only if

$$\frac{m}{1 + 2^{-m}} - 2 > 0\,. \tag{2.104}$$

The first integer for which (2.104) holds is $m_l = 3$, which establishes (2.98).

Next, we derive the results in Proposition 2.3.3 for $R \gg 1$. To do so, we need the following standard asymptotic formulae (cf. [1]):

$$K_0(z) \sim \sqrt{\frac{\pi}{2z}}e^{-z}\left(1 - \frac{1}{8z}\right)\,, \qquad I_0(z) \sim \sqrt{\frac{1}{2\pi z}}e^{z}\left(1 + \frac{1}{8z}\right)\,. \tag{2.105}$$

Therefore, we get

$$\frac{K_0(r_0)}{I_0(r_0)} \sim \frac{\pi}{e^{2r_0}}\left(1 - \frac{1}{4r_0}\right)\,, \qquad \frac{K_0'(R)}{I_0'(R)} \sim -\frac{\pi}{e^{2R}}\left(1 - \frac{3}{4R}\right)\,, \qquad I_0(r_0) I_0'(r_0) \sim \frac{e^{2r_0}}{2\pi r_0}\left(1 - \frac{1}{4r_0}\right)\,.$$

Substituting these formulae into (2.100), we get that

$$\frac{\pi}{2r_0}e^{-2r_0} \sim \pi e^{-2R}\left(1 - \frac{3}{4R}\right)\,.$$

84

Solving this equation asymptotically, we get $R \sim r_0 + \frac{1}{2}\ln(2r_0)$ as $R \to \infty$, which establishes (2.97).

Finally, we establish the stability threshold (2.99) for $R \gg 1$. Using (2.105) and (2.97), we readily estimate that

$$J_1(r_0)J_2(r_0) \sim \frac{1}{2}\left(1 + e^{2r_0 - 2R}\right) \sim \frac{1}{2r_0}\left(1 + \frac{1}{2r_0}\right). \qquad (2.106)$$

Next, we must calculate $J_{1,m}(r_0)J_{2,m}(r_0)$. Since, we have $m_l \gg 1$ and $r_0 \gg 1$, we must use the following *uniform* expansions of $K_m(mz)$ and $I_m(mz)$ for $m \to \infty$ as given in [1]:

$$K_m(mz) \sim \sqrt{\frac{\pi}{2m}}\frac{e^{-m\beta(z)}}{(1+z^2)^{1/4}}, \qquad I_m(mz) \sim \frac{1}{\sqrt{2\pi m}}\frac{e^{m\beta(z)}}{(1+z^2)^{1/4}}, \qquad (2.107)$$

where $\beta(z)$ is defined by

$$\beta(z) \equiv \sqrt{1+z^2} + \ln z - \ln\left(1 + \sqrt{1+z^2}\right). \qquad (2.108)$$

Defining z and z_1 by

$$z = \frac{r_0}{m}, \qquad z_1 = \frac{R}{m},$$

we get using (2.107) that

$$J_{1,m}(r_0)J_{2,m}(r_0) \sim \frac{1}{2m\sqrt{1+z^2}}\left(1 + e^{2m[\beta(z)-\beta(z_1)]}\right). \qquad (2.109)$$

Since $R = r_0 + \frac{1}{2}\ln(2r_0)$, we have that $z - z_1 \to 0$ provided that $\ln(r_0)/m \ll 1$. Assuming for the moment that this condition is true, we can then use $\beta'(z) = z^{-1}\sqrt{1+z^2}$ to estimate

$$\beta(z) - \beta(z_1) \sim \beta'(z)(z - z_1) \sim -\frac{1}{2mz}\ln(2r_0)\sqrt{1+z^2}.$$

Substituting this expression into (2.109), and using (2.106), the stability threshold condition defined by $4r_0^2 J_1(r_0)J_2(r_0)J_{1,m}(r_0)J_{2,m}(r_0) = 1$ becomes

$$\frac{z}{\sqrt{1+z^2}}\left(1 + \frac{1}{2r_0}\right)\left(1 + e^{-\ln(2r_0)z^{-1}\sqrt{1+z^2}}\right) \sim 1, \qquad (2.110)$$

where $z \equiv r_0/m$. If we assume that $z = O(1)$ and $r \gg 1$, then it is easy to see that there is no root to (2.110). Therefore, we must assume that $z \gg 1$. In this limit, (2.110) reduces to

$$\frac{z}{\sqrt{1+z^2}}\left(1 + \frac{1}{2r_0}\right)^2 \sim 1.$$

Squaring both sides, we readily obtain that $r_0 \sim 2z^2$. Since $z = r_0/m$, we get that $m = \sqrt{2r_0}$, which establishes (2.99). The consistency condition $\ln(2r_0)/m \ll 1$ needed above is indeed satisfied.

The upper instability threshold in estimated in the same way as was done for a stripe in §2.2.1. The only difference is that m gets replaced by $\frac{m}{r_0}$. Therefore, we obtain the following results for intermediate and high-feed regimes:

Proposition 2.3.4 *Consider an equilibrium ring solution of radius r_0 for the Gray-Scott model in a disk of radius R as constructed in Proposition 2.3.1. Then, all zigzag perturbations of the form (2.85) are unstable in the zone $m_l < m < m_u$, and are stable outside of this zone. Here m_l is the root of $4r_0^2 J_1(r_0) J_2(r_0) J_{1,m}(r_0) J_{2,m}(r_0) = 1$, which depends on R.*

In the high-feed case $A = O(1)$, we have $m_u = \frac{m_{0u} r_0}{\varepsilon}$ where the threshold m_{0u}, plotted in Fig. 2.5, is independent of R but depends on the value of B along the primary branch of the γ versus B bifurcation diagram.

In the intermediate regime $B = 3\delta$ with $O(\varepsilon^{1/2}) \ll \delta \ll O(1)$, m_u is determined explicitly as

$$m_u = \frac{6 r_0 \delta^2}{\varepsilon}.$$

As with the stripe, we find that the instability band can dissapear in the intermediate regime for a small domain size. As found in Proposition 2.3.3, $m_l = 3$ when $R \ll 1$. On the other hand, assuming $r_0 \ll 1$, $A \leq O(1)$, and using (2.81), (2.13) and (2.106) we obtain:

$$3\delta = B = r_0 \frac{A}{2},$$

$$m_u = \frac{r_0^3 A^2}{6\varepsilon}.$$

On the other hand we must have $\varepsilon \ll R = O(r_0)$. In addition, the intermediate regime must satisfy $\delta \gg O(\varepsilon^{1/2})$. This yields the following stability result:

Proposition 2.3.5 *Suppose $R \ll 1$. Then the equilibrium ring solution in the intermediate regime is stable with respect to zigzag instabilities provided that*

$$r_0^3 A^2 < 18\varepsilon \ll r_0. \quad \text{and} \quad O(\varepsilon^{1/2}) \ll r_0 A \ll O(1).$$

In particular, the zigzag instabilties are stable provided that

$$A = O(1) \quad and \quad O(R^3) \ll \varepsilon \ll O(R^2).$$

Here, $r_0 \sim \frac{R}{\sqrt{2}}$ is the ring radius as derived in Proposition 2.3.3.

Finally, the stability property of a ring with respect to a breakup instability is very similar to that of a stripe. We have,

Proposition 2.3.6 *Consider an equilibrium ring solution given in Proposition 2.1.1, in the intermediate regime $B = 3\delta \ll 1$. Such a solution is unstable with respect to the large eigenvalues, if and only if the following inequality holds:*

$$3\delta^2 r_0 < \varepsilon m < \frac{\sqrt{5}}{2} r_0 \,. \tag{2.111}$$

In the high-feed-rate regime, the instability band is given by

$$\sqrt{\mu_1} r_0 < \varepsilon m < \sqrt{\mu_2} r_0 \,, \tag{2.112}$$

where $\mu_1 = \mu_1(B)$ and $\mu_2 = \mu_2(B)$ are given in Table 2.1 and plotted in Fig. 2.6.

The result (2.112) follows immediately by noting that when $m_0 = m\varepsilon = O(\varepsilon)$, the leading-order problem for (2.88) become:

$$(\lambda + \frac{m_0^2}{r_0^2})\Phi_0 = \Phi_0'' - \Phi_0 + V_0^2 N_0 + 2V_0 U_0 \Phi_0 \,, \tag{2.113a}$$

$$\frac{m_0^2}{r_0^2} N_0 = N_0'' - V_0^2 N_0 - 2V_0 U_0 \Phi_0 \,. \tag{2.113b}$$

But these equations are the same as (2.59) upon relabelling εm by $\frac{\varepsilon m}{r_0}$. The result (2.111) is also readily obtained by a slight modification of the analysis in §4. To obtain (2.111), we repeat the analysis of (2.60)–(2.72). The upper bound in (2.111) follows from (2.61). Then, to determine the lower bound in (2.111), we re-derive the nonlocal eigenvalue problem (2.71), where the multiplier χ in (2.72) is to be replaced with

$$\chi = 2 \left[1 + \frac{\varepsilon \delta^{-2}}{6G_m(r_0; r_0)} \right]^{-1} \,, \qquad G_m(r_0; r_0) \equiv r_0 J_{1,m}(r_0) J_{2,m}(r_0) \,. \tag{2.114}$$

Here $G_m(r_0; r_0)$ is the Green's function, evaluated at $r = r_0$, for the operator $\eta'' + r^{-1}\eta' - m^2 r^{-2}\eta = -\delta(r - r_0)$ with $\eta'(0) = \eta'(R) = 0$. In (2.114), $J_{1,m}$ and $J_{2,m}$ are defined in (2.32). From Lemma 1.1.3, the stability threshold occurs when $\chi = 1$. Since $\varepsilon\delta^{-2} \ll 1$ in the intermediate regime where $\delta \gg O(\varepsilon^{1/2})$, we conclude that all modes with $m = O(1)$ are stable. However, since $J_{1,m}J_{2,m} \sim (2m)^{-1}$ as $m \to \infty$ for fixed r_0, we have that χ will decrease below unity when m is below the lower bound in (2.111).

2.4 Numerical Examples

In this section we give a few numerical examples to support the results of this chapter. For a rectangular domain, the computations have been done with the software package "VLUGR" [6]. For a disk domain, we wrote our own code. We used a 2nd order finite difference uniform discretization in r and θ, combined with the forward Euler method in time. Matlab was used for visualization.

Experiment 1: ring breakup and splitting instabilities. For this experiment we chose a disk domain of radius $R = 3$, with $\varepsilon = 0.05$, $\tau = 1$, and discretized the radial and anglular direction into 60 and 30 intervals, respectively. The time step was taken to be 0.00005. For initial conditions, we chose a ring of radius $r_0 = 1.5$ of width ε, and with very small, random perturbations in the angular direction. Note from Proposition 2.3.1 we expect the ring to have the equilibrium radius of $r_R = 2.238$. Also, from Proposition 2.3.1, the equilibrium exists only when $A < 1.837$.

Figure 2.8 shows a simulation for $A = 2.0$. The initial ring at $r_0 = 1.5$ starts to expand until its radius reaches about 2.25. It then breaks into many spots. This implies that all lower-modes are stable, but a very high instability mode is triggered. Moreover, the spots form both at the outside and at the inside of the ring – thus the splitting instability is triggered at about the same time as the breakup instability. The ring breakup occurs at about $r = 2.25$ which is close to the equilibrium ring radius $r_R = 2.238$.

In Figure 2.9 we take $A = 2.5$. In this case the ring first splits into two. The two resulting

t=20, A=2.0   t=60, A=2.0   t=70, A=2.0

t=80, A=2.0   t=290, A=2.0   t=1000, A=2.0
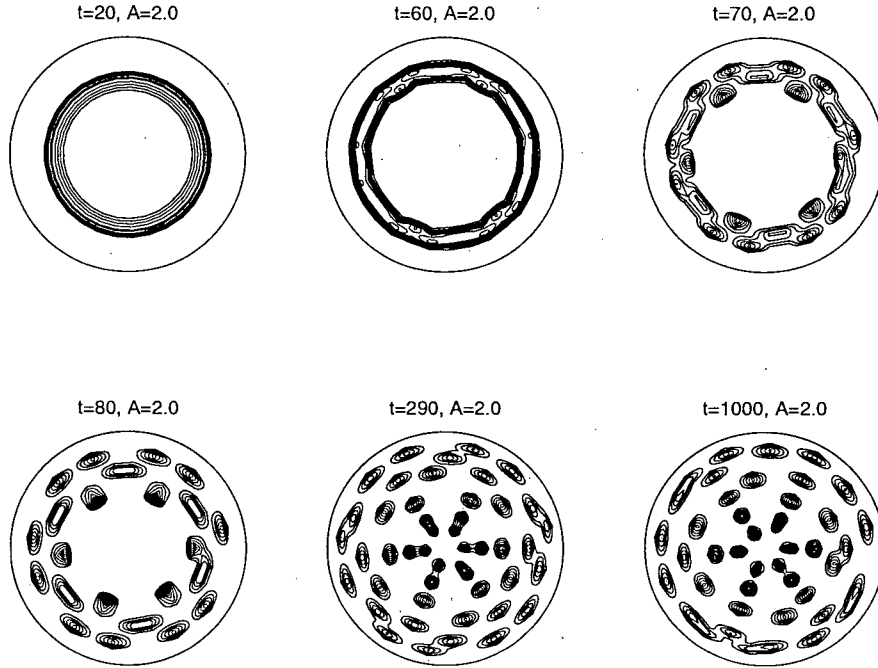
Figure 2.8: Contour plot of v for $A = 2.0$.

t=10, A=2.5   t=20, A=2.5   t=80, A=2.5

t=340, A=2.5   t=480, A=2.5   t=600, A=2.5
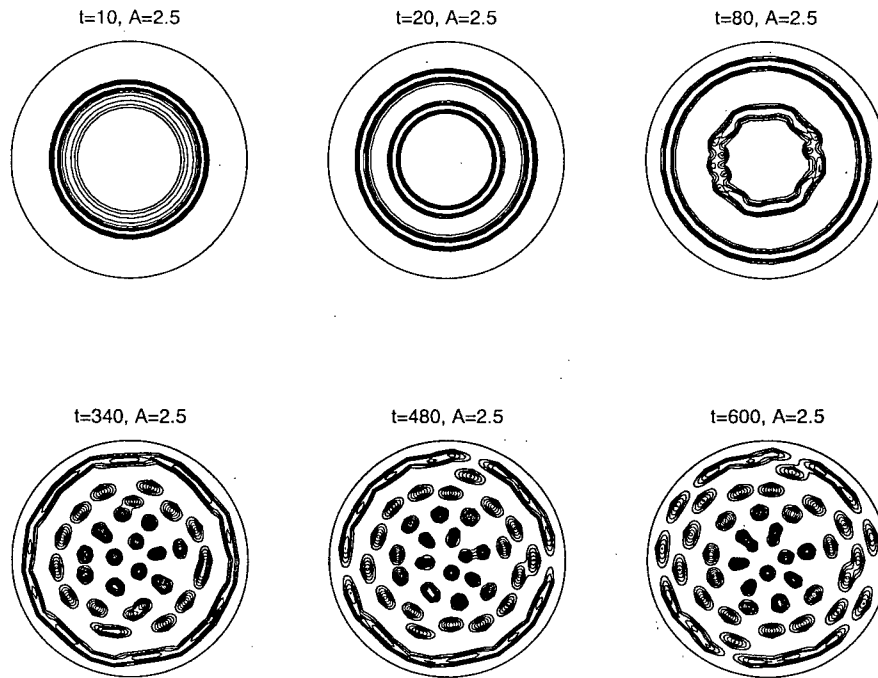
Figure 2.9: Contour plot of v for $A = 2.5$.
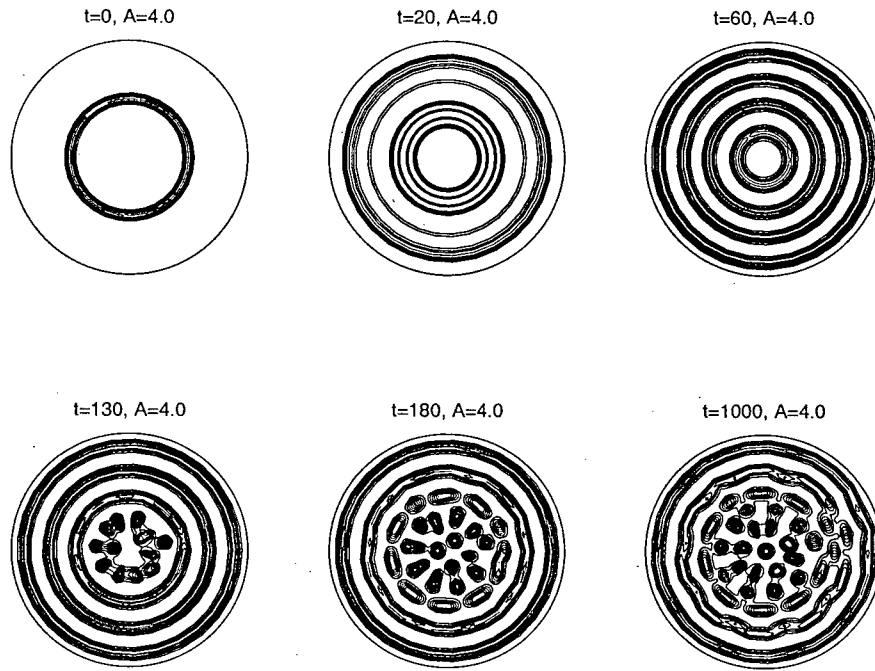
Figure 2.10: Contour plot of v for $A = 4.0$.

rings then start travelling apart. Some time later, the inner ring breaks up. Then much later the outer ring also breaks.

Finally, in Figure 2.10 we take $A = 4$. As a result, a single ring eventually splits into four. The resulting rings then lose their stability, one-by-one, starting from the innermost ring, and progressing towards the outermost ring. Note however that the outer ring can remain stable for a very long time, and becomes unstable only after the adjacent ring has been broken up.

Example 1: Zigzag Instability of a Stripe: In order to observe zigzag instabilities, one must choose parameters and initial conditions carefully so that these instabilities are not dominated by breakup instabilities that occur on shorter timescales. In this example, we consider a stripe equilibrium with $\varepsilon = 0.004$, $A = 1.7$, and $\tau = 1.0$, in the rectangular domain $[-1, 1] \times [0, 1]$ so that $d = l = 1$. For this value of A, we compute that $B = A \tanh 1 = 1.3 < 1.35$. Hence, by Proposition 1.2.1, there is a stripe equilibrium solution centered along $x_1 = 0$. For these parameter values, we obtain from Proposition 2.2.2 that the unstable modes m satisfy $m_b < m < m_{0u}/\varepsilon$, where $m_l \approx 1.05$ when $l = 1$, and $m_{0u} \approx 0.72$ when $B = 1.3$. This yields the

instability zone $1.05 < m < 180$ when $\varepsilon = .004$.

The meshsize in the x_1 direction must be finer than ε in order to resolve the stripe. With $\varepsilon = 0.004$, the computation would be quite prohibitive for most uniform-grid codes. Fortunately, VLUGR uses an adaptive mesh-refinement algorithm, which captures the localized structure of the stripe without the need for a huge number of grid points.

For the initial conditions for (2.1) we took $v = \frac{1}{\varepsilon} w \left(\frac{x_1 + 10^{-4} \cos(10\pi x_2)}{\varepsilon} \right)$ and $u = \varepsilon$, where $w(y) = \frac{3}{2} \mathrm{sech}^2(y/2)$ satisfies (1.7). Therefore, the preference for a zigzag instability corresponding to the mode $m = 10\pi$, which lies within the instability zone, is built in. The resulting numerical simulation is shown in Fig. 2.11. The system does indeed develop a zigzag instability corresponding to this mode.
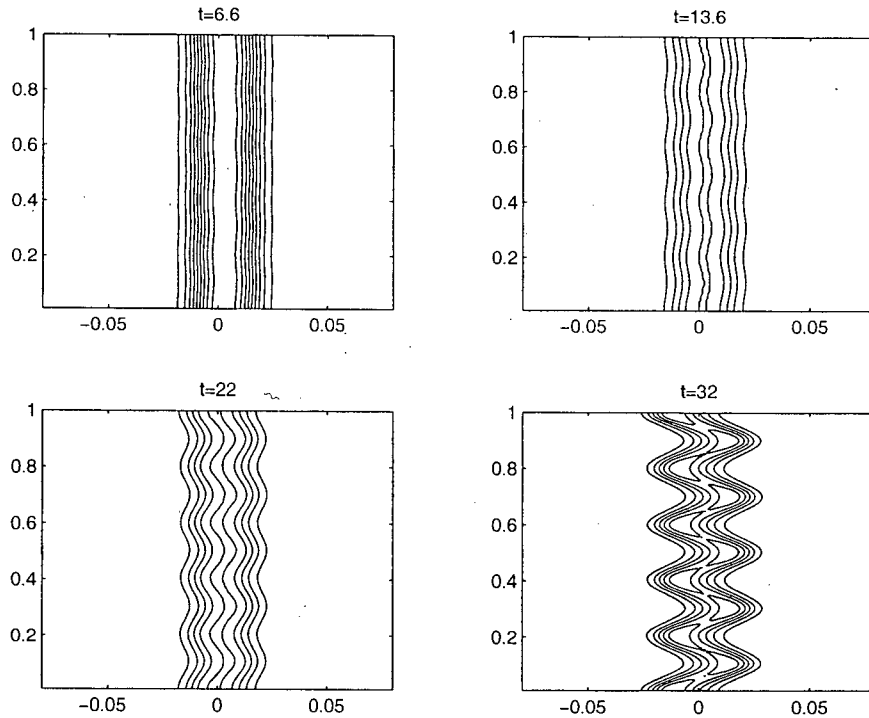
Figure 2.11: Contour plot of v obtained from the full numerical solution of (2.1). The parameters are $\varepsilon = 0.004$, $A = 1.7$, $\tau = 1.0$, and the domain size was set to $[-1, 1] \times [0, 1]$. The initial condition was taken to be $v = \frac{1}{\varepsilon} w \left(\frac{x_1 + 10^{-4} \cos(2\pi 5 x_2)}{\varepsilon} \right)$, $u = \varepsilon$, where $w(y) = \frac{3}{2} \mathrm{sech}^2(y/2)$. Outside the region shown, v is exponentially small.

Numerically, we can also validate the theoretically predicted form of the zigzag instability. From

the theory of §3, we would expect that the eigenfunction ϕ has the form

$$\phi = \frac{d}{dx_1} v_e(x_1) \cos mx_2 , \qquad (2.115)$$

where v_e is the equilibrium stripe. Since $v \sim v_e + Ce^{\lambda t}\phi$ and $\lambda = O(\varepsilon) \ll 1$, we have that ϕ is well-approximated by the difference in the numerical solution at two different times. From results obtained from our numerical simulations, we plot $v_{t=22} - v_{t=18}$ in Fig. 2.12. From this figure we observe that the shape of the resulting perturbation is indeed of the form (2.43a)
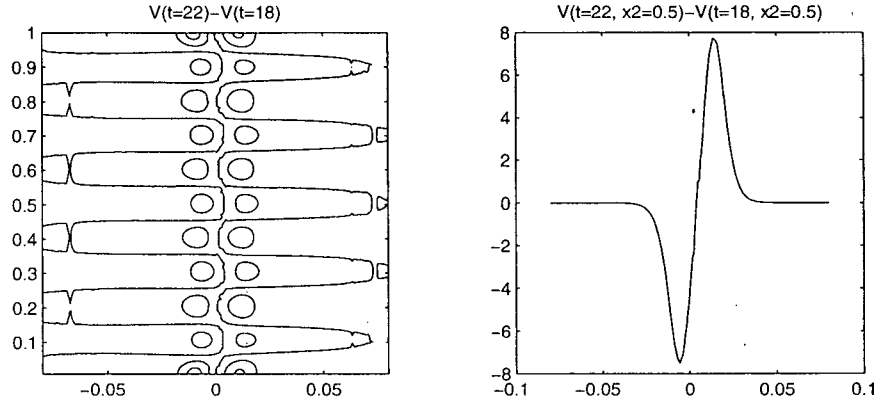
Figure 2.12: Left: contour plot of $v_{t=22} - v_{t=18}$ for the data of Fig. 2.11. Right: The horizontal slice of the figure on the left at $x_2 = 0.5$.

The onset of a breakup instability for this example is visible in Fig. 2.11 at time $t = 32$, when the wiggled stripe starts to develop an instability. Shortly after this time, the stripe breaks up into spots, which then self-replicate until the entire rectangle is full of spots.

Example 2: Breakup Instability of a Stripe: Next, we verify Proposition 2.2.6 for the parameter set $\varepsilon = 0.004$, $A = 1.313$, $l = 1$, and $d = 2$. For this value of A, we compute that $B = A \tanh(1) = 1$. From Table 2.1, we have have $\mu_1 = 0.0659, \mu_2 = 0.9208$. Therefore, from Proposition 2.2.6, the instability zone is $64.2 \leq m \leq 239.9$. To check this, we start with the following initial condition for v that has a built-in preference for the the mode $m = 20\pi = 62.8$:

$$v = \frac{1}{\varepsilon}(1 + 10^{-4}\cos(20\pi x_2))w\left(\frac{x_1}{\varepsilon}\right) , \qquad u = \varepsilon , \qquad (2.116)$$

where $w(y) = \frac{3}{2}\mathrm{sech}^2(y/2)$ is given by (1.7). Note that this mode is *stable*. Indeed, in the

92
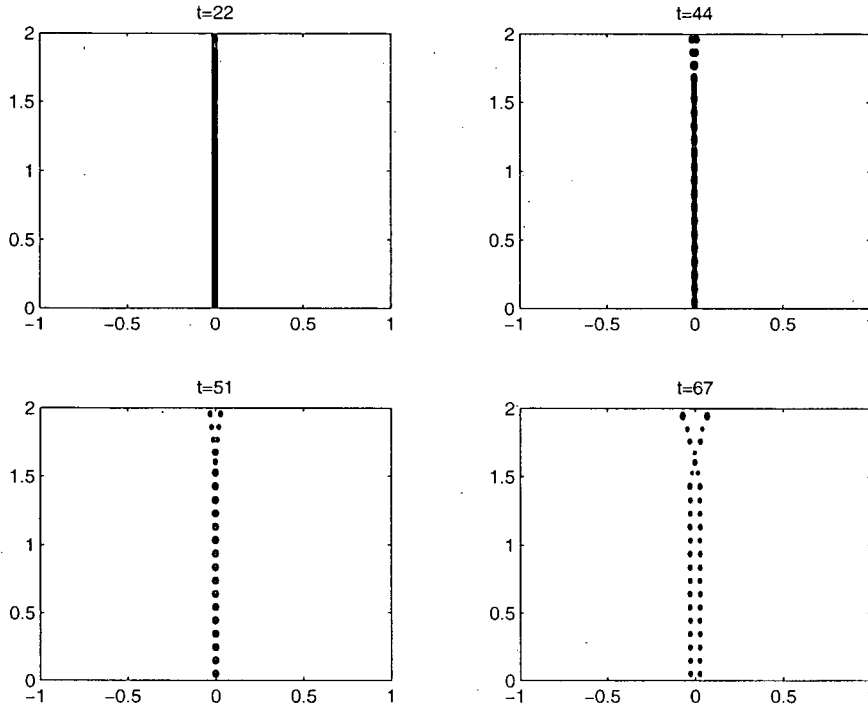
Figure 2.13: Contour plot of v computed from the full numerical simulation of (2.1). The domain size was set to $[-1, 1] \times [0, 1]$, and the parameter values are $\varepsilon = 0.004$, $A = 1.313$, and $\tau = 1.0$. The initial condition was taken to be (2.116).

resulting simulation shown in Fig. 2.13, the stripe breaks up into 21 and not 20 spots. This corresponds to $m = 21\pi = 66$, which lies just within the theoretical instability band.

Example 3: Space-Filling Curve: In this example, we numerically show the development of a zigzag instability in the weak interaction regime, where both u and v are localized near $x_1 = 0$. For convenience, we introduce an extra parameter D to be the diffusivity coefficient of u. In this way, (2.1) is replaced by

$$\begin{cases} v_t = \tilde{\varepsilon}^2 \triangle v - v + Av^2 u, \\ \tau u_t = D \triangle u - u + 1 - v^2 u. \end{cases} \tag{2.117}$$

For this computation we take $\tilde{\varepsilon} = 0.05$, $D = 0.01$, $A = 2.0$, $l = 1$, and $d = 5$. This corresponds to the weak interaction regime, whereby both u and v are localized near the stripe, and is similar to parameter regimes studied in [63], [64], and [72]. Notice that by re-scaling, these parameter values are equivalent to taking $\varepsilon = 0.5$ $D = 1$, $l = 10$, and $d = 50$, in (2.1). Therefore, since ε is

93

rather large, the theoretical analysis of §3 and §4 is not applicable. The numerical results are shown in Fig. 2.14 and Fig. 2.15. The zigzag instability corresponding to the mode $\cos\left(\frac{3}{2\pi5}x_2\right)$ becomes unstable and, in contrast to Example 2, we do not observe any instabilities that lead to the development of spots. The end state seems to be a domain-filling curve. We ran the simulation to about $t = 10000$; the solution seems to have reached a steady state at this time, since no changes in the solution were observed between $t = 8000$ and $t = 10000$.
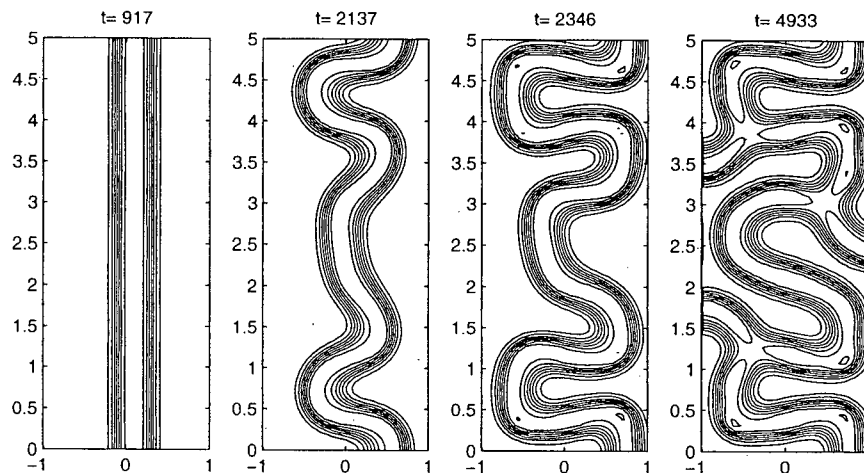
Figure 2.14: Contour plot of v for Example 3 at the times indicated.

Example 4: Zigzag Instability of a Ring: In this example, we consider (2.117) and we take the parameter values $\tilde{\varepsilon} = 0.05$, $D = 0.01$, $A = 2.0$, in a rectangular domain $\Omega = [-2, 2] \times [0, 4]$, so that $l = 2$ and $d = 4$. Since this parameter set again corresponds to the weak interaction regime, it is not in the scope of our theoretical analysis. We take the initial condition to be a spot at the center of the domain. After a short time, the spot grows into an expanding ring. Some time later, this ring develops a zigzag instability corresponding to the mode $m = 4$. The end state of this computation is again a complicated domain-filling curve as shown in Fig. 2.16.

2.5 Discussion

The results of §2.1 were previously presented in [48]. In a related work [56], Morgan and Kaper have also performed a similar analysis of ring-like solutions on Gray-Scott model. Below we review and compare their results with ours. They used the following scaling of the Gray-Scott
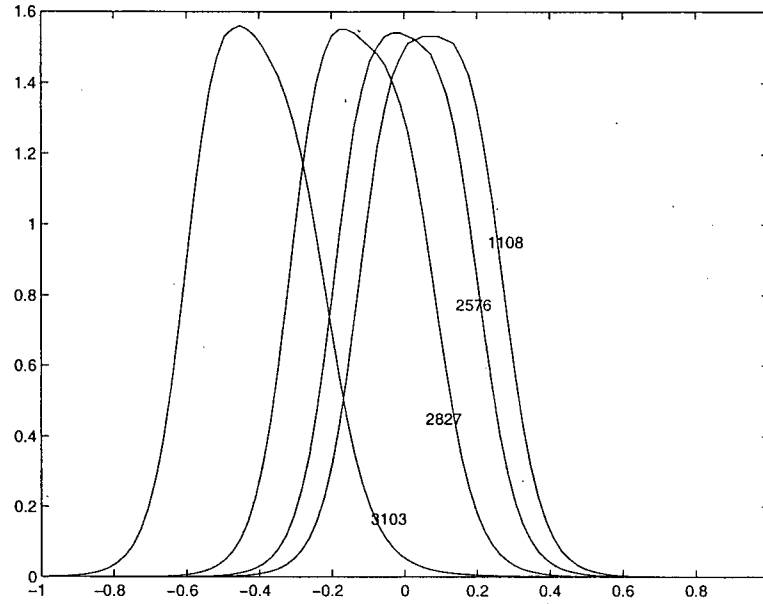
Figure 2.15: Plots of $v(x_1, x_2)$ versus x_1 with $x_2 = 2.5$.

model:

$$\frac{dV(y,s)}{ds} = D_{mk}\triangle V - BV + UV^2$$

$$\frac{dU(y,s)}{ds} = \triangle U + A_{mk}(1 - U) - UV^2$$

By scaling the variables as follows:

$$V = \sqrt{A_{mk}}v, \quad U = u, \quad s = \frac{1}{B}t, \quad y = \frac{1}{\sqrt{A_{mk}}}x$$

we re-obtain our system (2.1) with

$$\tau = \frac{B}{A_{mk}}, \quad \varepsilon = \sqrt{\frac{D_{mk}A_{mk}}{B}}, \quad A = \frac{\sqrt{A_{mk}}}{B}$$

or

$$A_{mk} = \frac{1}{\tau^2 A^2}, \quad B = \frac{1}{\tau A^2}, \quad D_{mk} = \varepsilon^2\tau.$$

The paper [56] obtains results for the ring location and its stability. In addition, Morgan and Kaper also perform a linear Turing analysis for the radially-symmetric solutions and full numerical simulations.
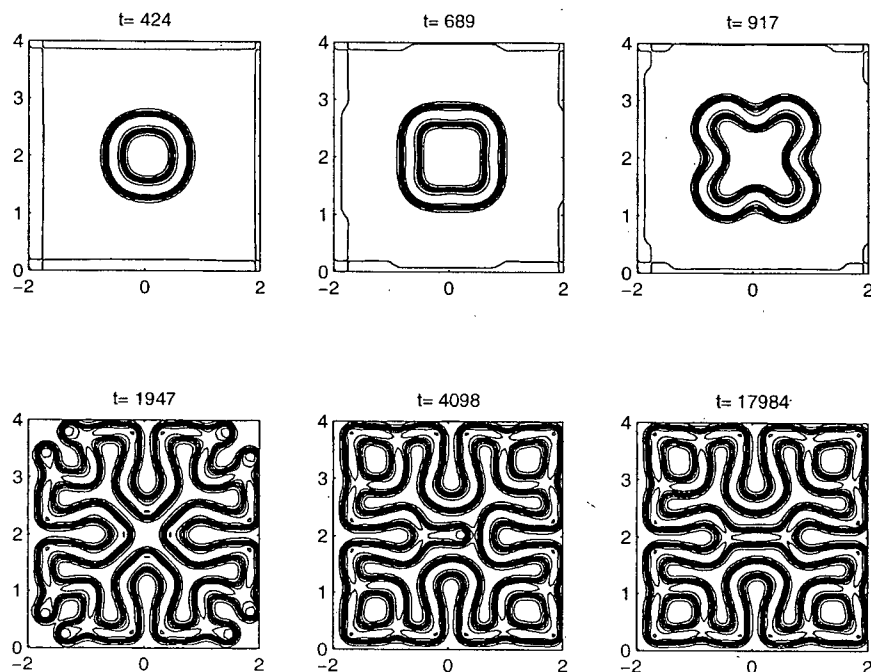
Figure 2.16: Contour plot of v for Example 4 showing the zigzag instability of a ring and the labyrinthine pattern that results at later time.

For the location of the ring, Morgan and Kaper obtain the same formula (equation (2.35) of [56]) as we obtain in Proposition 2.1.2 (see also (2.19)). However, they do not have any analytical results on the existence of solution to equation (2.35) of [56]. Indeed, they consider only a bounded domain – in which case a ring solution exists for any choice of $\hat{A}$. Our result on existence of the bound $\hat{A}_c$ on $\hat{A}$ in case of the *unbounded* domain is new. In the case of the boudned domain, we rigorously show the existence of $r_R < R$, which has the property that the radius of the ring $r_0 \rightarrow r_R$ as $\hat{A} \rightarrow \infty$. This is also a new result. Another new result that we have obtained using the comparison principle, is the existence of $\hat{A}$ for any given ring radius r_0 in the case of the unbounded domain.

For the stability analysis with respect to angular perturbations, we obtain a simple sufficient condition (see Proposition 2.1.3) for when the ring is unstable with respect to node m. This condition is also necessary when $\tau = 0$. Our condition involves only Bessel functions of order m and the ring radius r_0. Our proof involves no numerical computations. By contrast, the stability criteria for the m-th mode in [56] is implicitly contained in integrals of hypergeometric

functions which is then solved by mathematica. In both cases, the stability analysis is reduced to a non-local eigenvalue problem. We also find that all nodes $1 \ll m \ll O(\frac{1}{\varepsilon})$ are unstable for any $\tau \leq O(1)$, and all nodes $m > \frac{\sqrt{5}}{2}\frac{r_0}{\varepsilon}$ are stable (Proposition 2.1.7). These results are new.

For the ring-splitting regime $A = O(1)$, we use formal asymptotics and one-dimensional numerics to derive an explicit bound A_c in terms of R (see Proposition 2.3.1) such that the ring-splitting occurs when $A > A_c$. This is a new result. We then use full numerical simulation to confirm existence of the ring-splitting regime. Morgan and Kaper also observe ring splitting numerically, but they do not perform any analysis of this regime.

We have analyzed zigzag and breakup instabilities of stripes and rings for the Gray-Scott model (2.1). For the breakup instabilities, we have established the presence of instability band in either low-feed or high-feed regimes. For the zigzag instabilities, we have analysed only intermediate and high-feed regimes. In the intermediate regime, we have shown that it is possible for a stripe or a ring to be stable with respect to all zigzag modes, when the domain is small enough (with $D = 1$). Altenatively, this is equivalent to fixing the domain size and taking the limit $D \gg 1$. In particular, we expect the stripes to be stable with respect to zigzag instabilities in the well-known shadow limit $D \to \infty$.

A natural extension of this work is to determine whether there is a parameter regime where the breakup instability band disappears. One way to stabilize a stripe is to take the domain width d to be very small. Indeed, since the upper bound of the instability band is $O(\varepsilon^{-1})$, a stripe can be stable if we take the domain width to be of order $O(\varepsilon)$. Such an analysis was performed in [21]. A different possibility is to analyze zigzag and breakup instabilities of a stripe and ring solution in the weak interaction regime of [63], [64], [72], and [35], where u and v are both exponentially localized near a stripe or a ring. This regime corresponds to taking $D_v = O(D_u) \ll 1$ in (7). The numerical computations of Examples 3 and 4 of §6 indicate that there exists values of $D \equiv D_v/D_u = O(1)$, with $D_v = O(D_u) \ll 1$, so that a stripe or ring is stable with respect to breakup instabilities, but is unstable with respect to zigzag instabilities. We conjecture that in the absence of such breakup instabilities a zigzag instability leads to a

labyrinthine pattern such as shown in §2.4. An open problem is to study zigzag and breakup instabilities of stripes and rings for the Gray-Scott model in the weak interaction regime.

Chapter 3
Gierer-Meinhard model in two dimensions

In this chapter we concentrate on the study of the Gierer-Meinhardt (GM) model [26] in two dimensions. In its dimensionless form, the system is:

$$A_t = \varepsilon^2 \triangle A - A + \frac{A^p}{H^q}, \qquad x \in \Omega, \quad t > 0, \tag{3.1a}$$

$$\tau H_t = D \triangle H - H + \frac{A^r}{H^s}, \qquad x \in \Omega, \quad t > 0, \tag{3.1b}$$

$$\partial_n A = \partial_n H = 0, \qquad x \in \partial\Omega. \tag{3.1c}$$

Here Ω is a bounded two-dimensional domain, A and H represent the activator and the inhibitor concentrations, ε^2 and D represent the diffusivity of the activator and inhibitor, τ is the inhibitor time constant, and the exponents (p, q, r, s) satisfy

$$p > 1, \qquad q > 0, \qquad r > 0, \qquad s \geq 0, \qquad \frac{p-1}{q} < \frac{r}{s+1}. \tag{3.2}$$

As in the Gray Scott model, we assume that he activator diffuses more slowly than does the inhibitor, so that

$$\varepsilon^2 \ll D.$$

The GM system exhibits surprisingly rich dynamics for various parameter ranges. Large amplitude spike solutions have been studied intensively using numerical methods since the 1970's (cf. [26], [54], [33] and references therein), but only relatively recently from an analytical viewpoint.

In this chapter we study asymptotically the dynamics of a one-spike solution to the GM system with $\tau = 0$ in the limit $\varepsilon \to 0$. A one-spike solution has the form shown in Figure 3.1.
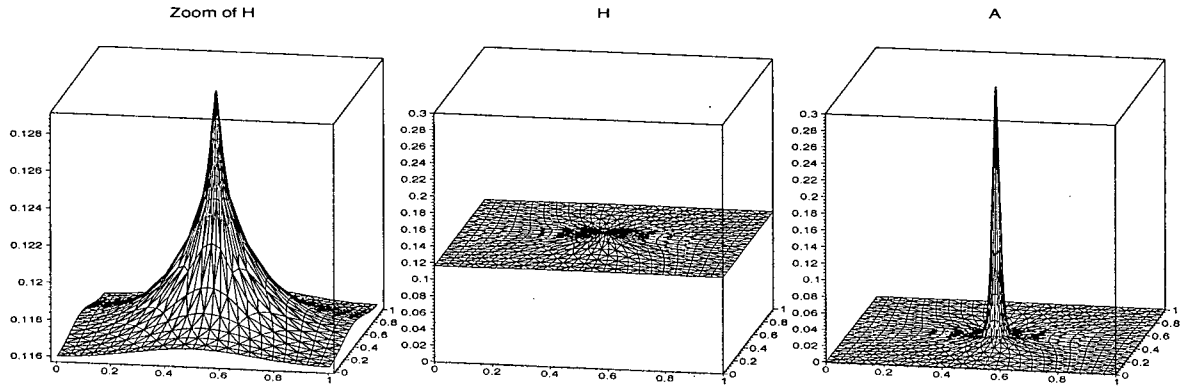
Figure 3.1: A spike for the Gierer-Meinhardt system (3.1) with $\tau = 0$ in a square domain with $(p, q, r, s) = (2, 1, 2, 0)$ (with A, H rescaled so that both are $O(1)$ as $\varepsilon \to 0$). Here, $\varepsilon = 0.01$, $D = 5$. Note that the inhibitor H does not change very much compared to A at the center of the spike.

Before describing our specific results for (3.1), we survey some previous results on spike solutions to the GM system in a two-dimensional domain.

When $\tau = 0$ and D is infinite, (3.1) reduces to the well-known shadow system involving a non-local scalar partial differential equation for the activator concentration A. The behavior of spike solutions to this shadow problem is now well understood (see [37], [10], [78]). As $\varepsilon \to 0$, the equilibrium location of the spike for a one-spike solution is at the center of the largest ball that can be inserted into the domain (cf. [73], [81]). This solution is metastable in the sense that a single spike located in the domain moves exponentially slowly towards the boundary of the domain (cf. [37]). For the equilibrium shadow problem solutions with multiple spikes are possible. The locations of these spikes were found in [5], [27] and [49] to be related to a ball-packing problem. Equilibrium solutions for the shadow problem with two or more spikes are unstable on an $O(1)$ time scale.

In the regime where D is at least logarithmically large as $\varepsilon \to 0$, but not exponentially large, i.e.

$$-\ln \varepsilon \leq D \ll O(\varepsilon^2 e^{2d/\varepsilon}),$$

where d is the distance of the spike center from the boundary, the stability of an equilibrium n-

spike pattern was analyzed rigorously in [83]. It was found that for $\varepsilon \ll 1$ there exists threshold values $D_1 < D_2 < ...$ such that an n-spike equilibrium solution is stable if and only if $D < D_n$. For the case of a one-spike solution, a differential equation for the dynamics of the center of the spike was derived in [14] and [76].

When D is very small, so that $D = O(\varepsilon^2)$, the motion of two spikes in $\mathbb{R}^2$ was analyzed in [24]. In this case, both the activator and the inhibitor concentrations are localized near the core of the spikes, with A and H decaying exponentially away from the spike cores. It was found in [24] that the interaction between the spikes is exponentially weak and that the spikes move away from each other with a speed that is exponentially decreasing with the distance between the spike centers. An explicit differential equation for the distance between the spike centers was derived.

In this chapter, in addition to $\varepsilon^2 \ll D$, we will also always assume:

$$D \ll O(\varepsilon^2 e^{2d/\varepsilon}). \tag{3.3}$$

where d is the distance of the spike from the boundary. The case of exponentially large D will be discussed in the following chapter. The results of this and the following chapter were previously reported in [46] and [47], respectively. We start by deriving a unified dynamical law that determines the motion of a single spike inside a two-dimensional bounded domain for *any* D with $D \gg O(\varepsilon^2)$. The previous results for large D found in [14] and [76], as well as results for small D, are then obtained as limiting cases. The motion of the spike is found to depend critically on various Green's functions and their gradients.

The equation of motion for a spike for (3.1) when $D = O(1)$ and $\tau = 0$ differs significantly from the case when $D \gg -\ln \varepsilon$, since for $D \gg -\ln \varepsilon$ only the gradient of the regular part of a modified Green's function for the Laplacian is involved (cf. [76]). However, when $D = O(1)$, we find that the differential equation for the spike motion involves both the regular part of a certain reduced-wave Green's function and its gradient. This complication results in part because of the presence of the two different scales, ε and $-\frac{1}{\ln \varepsilon}$, that arise due to the logarithmic point-source behavior of the two-dimensional Green's function. The presence of these two scales
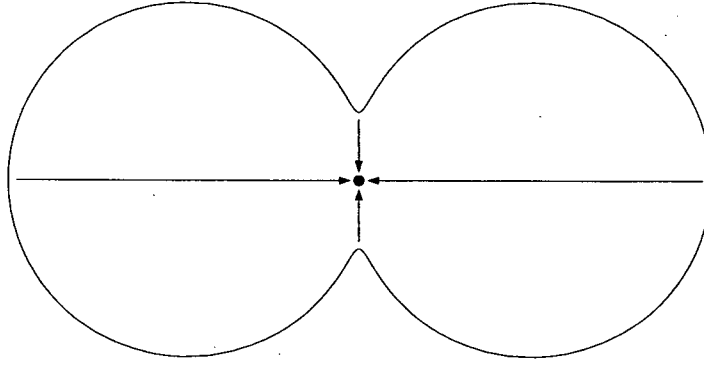
Figure 3.2: A dumbell-shaped domain and its unique spike equilibrium location in the case $D = O(-\frac{1}{\ln \varepsilon})$.

makes the asymptotic analysis of the spike motion rather delicate.

The second goal of this chapter is to examine how both the shape of the domain and the inhibitor diffusivity constant D determine the possible equilibrium locations for a one-spike solution. We find that for D small, the stable equilibrium spike locations tend to the centers of the disks of largest radii that can fit within the domain. Hence, for D small, there are two stable equilibrium locations for a dumbell-shaped domain. In contrast, we find that for a certain dumbell-shaped domain, there is only one possible equilibrium location when D is sufficiently large. Such a domain is shown in Figure 3.2. To obtain this latter result, we use complex analysis to derive an exact expression for the gradient of the modified Green's function for the Laplacian. While this result is obtained for a very specific dumbell-shaped domain, we conjecture that it is true more generally. More specifically, we conjecture that when D is sufficiently large there is only one possible equilibrium spike location for any connected domain. This conjecture is further supported through numerical experiments.

The outline of this chapter is as follows. In §3.1 we introduce an appropriate scaling of (3.1), and we derive the equation of motion for a single spike, which is valid for any D satisfying $D \gg O(\varepsilon^2)$. In §3.2.1 and §3.2.2, we then derive limiting results of this evolution for the special cases where $D \ll 1$ and $D \gg -\ln \varepsilon$, respectively. The exact solution for the modified Green's function of the Laplacian on a domain that is an analytic mapping of the unit disk is derived

in §3.3. This result is then applied in §3.3.1 to a specific dumbell-shaped domain. In §3.3.1, a conjecture regarding the uniqueness of the equilibrium spike location for large D is proposed. Numerical evidence supporting this conjecture is given in §3.4. In §3.4 we also compare our asymptotic results for the spike motion with corresponding full numerical results.

3.1 Dynamics Of A One-Spike Solution

In this section we study the dynamics of a one-spike solution to (3.1) when $\tau = 0$. We assume that the spike is centered at some point $x = x_0 \in \Omega$. The goal is to derive a differential equation for the dynamics of $x_0(t)$ for any D with $D \gg O(\varepsilon^2)$.

We begin by introducing a rescaled version of (3.1) as was done in [84]. This scaling ensures that the rescaled inhibitor field h is $O(1)$ as $\varepsilon \to 0$ at $x = x_0 \in \Omega$. To find such a scaling, we let $A(x) = \xi a(x)$ and $H = \xi^{\frac{p-1}{q}} h(x)$, for some constant ξ to be found. With this change of variables, and setting $\tau = 0$ in (3.1b), (3.1) becomes

$$a_t = \varepsilon^2 \triangle a - a + \frac{a^p}{h^q}, \qquad x \in \Omega, \quad t > 0, \tag{3.4a}$$

$$0 = D \triangle h - h + \xi^\gamma \frac{a^r}{h^s}, \qquad x \in \Omega, \quad t > 0, \tag{3.4b}$$

where γ is defined by

$$\gamma = r + \frac{1}{q}(1 - p)(1 + s). \tag{3.4c}$$

The parameter ξ will be chosen so that

$$h(x_0) = 1 + o(1), \quad \text{as} \quad \varepsilon \to 0. \tag{3.5}$$

Since $D \gg O(\varepsilon^2)$, a spike core of extent $O(\varepsilon)$ will be formed near $x = x_0$. In the core, we define a new inner variable $y = \varepsilon^{-1}(x - x_0)$. Outside of the spike core, where $|y| \to \infty$, the linear terms in (3.4a) dominate, and a decays exponentially as

$$a \sim C\varepsilon^{1/2}|x - x_0|^{-1/2}e^{-|x-x_0|/\varepsilon}, \tag{3.6}$$

for $\varepsilon^{-1}|x - x_0| \to \infty$. In the core of the spike, we assume that h changes more slowly as $\varepsilon \to 0$ than does a. This arises from the assumption that $D \gg O(\varepsilon^2)$. In other words, for $\varepsilon \to 0$, we

103

assume that to a leading order approximation

$$\frac{a(x_0 + \varepsilon y)^r}{h(x_0 + \varepsilon y)^s} \sim \frac{a(x_0 + \varepsilon y)^r}{h(x_0)^s} \sim a(x_0 + \varepsilon y)^r, \qquad \frac{a(x_0 + \varepsilon y)^p}{h(x_0 + \varepsilon y)^q} \sim a(x_0 + \varepsilon y)^p. \tag{3.7}$$

Under this assumption, the equilibrium solution to (3.4a) in the limit $\varepsilon \to 0$ is

$$a(x) \sim w\left(\varepsilon^{-1}|x - x_0|\right), \tag{3.8}$$

for some x_0, where $w(\rho)$ is the unique positive solution of

$$w'' + \frac{1}{\rho}w' - w + w^p = 0, \qquad \rho \geq 0, \tag{3.9a}$$

$$w(0) > 0, \qquad w'(0) = 0, \qquad w \sim c\rho^{-1/2}e^{-\rho}, \quad \text{as} \quad \rho \to \infty. \tag{3.9b}$$

Here c is a positive constant.

Let $G(x, x_0)$ be the Green's function satisfying

$$\triangle G - \frac{1}{D}G = -\delta(x - x_0), \quad x \in \Omega; \qquad \partial_n G = 0, \quad x \in \partial\Omega. \tag{3.10}$$

Let R be the regular part of G defined by

$$R(x, x_0) = G(x, x_0) + \frac{1}{2\pi}\ln|x - x_0|. \tag{3.11}$$

Then, the solution to (3.4b) is

$$h(x_0) = \int_\Omega G(x, x_0)\frac{\xi^\gamma}{D}\frac{a^r(x)}{h^s(x)}\,dx. \tag{3.12}$$

Since the integrand in (3.12) is exponentially small except in an $O(\varepsilon)$ region near $x = x_0$, we get from (3.7), (3.8), (3.11) and (3.12), that, as $\varepsilon \to 0$,

$$h(x_0) \sim \frac{\xi^\gamma \varepsilon^2}{D} \int_{\mathbb{R}^2} \left(-\frac{1}{2\pi}\ln(\varepsilon|y|) + R\right) w^r(|y|)\,dy = \frac{\xi^\gamma \varepsilon^2 \ln(\frac{1}{\varepsilon})}{2\pi D} \int_{\mathbb{R}^2} w^r(|y|)\,dy + o(1). \tag{3.13}$$

Thus, to ensure that $h(x_0) = 1 + o(1)$ as $\varepsilon \to 0$, we must choose ξ as

$$\xi^\gamma = \frac{D\nu}{\varepsilon^2 b}, \tag{3.14}$$

where b and ν are defined as

$$b = \int_0^\infty w^r(\rho)\rho\,d\rho, \qquad \nu = \frac{1}{\ln(\frac{1}{\varepsilon})} \gg \varepsilon, \quad \text{as} \quad \varepsilon \to 0. \tag{3.15}$$

104

Substituting (3.14) into (3.4) we obtain the scaled system

$$a_t = \varepsilon^2 \triangle a - a + \frac{a^p}{h^q}, \qquad x \in \Omega, \quad t > 0, \tag{3.16a}$$

$$0 = D\triangle h - h + \frac{D\nu}{b\varepsilon^2} \frac{a^r}{h^s}, \qquad x \in \Omega, \quad t > 0. \tag{3.16b}$$

Next, we derive a differential equation for the motion of the center x_0 of the spike. Our main result is the following:

Proposition 3.1.1 *Suppose that $D \gg O(\varepsilon^2)$. Then, the trajectory $x = x_0(t)$ of the center of a one-spike solution to (3.16) satisfies the differential equation*

$$\frac{dx_0}{dt} \sim -\left(\frac{4\pi q}{p-1}\right) \frac{\varepsilon^2}{\ln(\frac{1}{\varepsilon}) + 2\pi R_0} \nabla R_0, \qquad as \quad \varepsilon \to 0, \tag{3.17}$$

where R_0 and its gradient are defined by

$$R_0 \equiv R(x_0, x_0), \qquad \nabla R_0 \equiv \nabla_x R(x, x_0)|_{x=x_0}. \tag{3.18}$$

Here R is the regular part of the reduced wave Green's function defined by (3.10) and (3.11).

We now derive this result using the method of matched asymptotic expansions. Assuming that a decays exponentially away from $x = x_0$, we have that a^r/h^s decays exponentially away from x_0. Thus, from (3.16b), we obtain that the outer solution for h satisfies

$$\triangle h - \frac{h}{D} \sim -2\pi\nu B\delta(x - x_0), \qquad B = \frac{1}{2\pi b}\int_{\mathbb{R}^2} \frac{a^r(x_0 + \varepsilon y)}{h^s(x_0 + \varepsilon y)}\, dy, \tag{3.19}$$

where $B \to 1$ as $\varepsilon \to 0$. The solution to (3.19) is

$$h \sim 2\pi B\nu G(x, x_0) = B\nu \left[-\ln(\varepsilon|y|) + 2\pi R(x_0 + \varepsilon y, x_0)\right], \tag{3.20}$$

where $y = \varepsilon^{-1}(x - x_0)$ and G satisfies (3.10). The local behavior of the outer solution near the core of the spike is

$$h \sim B + 2\pi\nu B R_0 - \nu B \ln|y| + 2\pi\varepsilon\nu B\nabla R_0 \cdot y + O(\varepsilon^2|y|^2\nu), \qquad as \quad x \to x_0. \tag{3.21}$$

The difficulty in matching an inner solution to the local behavior of the outer solution given in (3.21) is that there are two scales, ν and ε, to consider. To allow for these two scales, we must

expand the inner solution in a generalized asymptotic expansion of the form

$$a = a_0(|y|; \nu) + \varepsilon \nu a_1(y; \nu) + \cdots, \qquad h = h_0(|y|; \nu) + \varepsilon \nu h_1(y; \nu) + \cdots, \qquad (3.22)$$

where

$$y = \varepsilon^{-1} \left[x - x_0(\tau) \right], \qquad \tau = \varepsilon^2 \nu t. \qquad (3.23)$$

Generalized asymptotic expansions of the form (3.22) have been used in [70] and [75] to treat related singularly perturbed problems involving the two scales ν and ε.

Substituting (3.22) and (3.23) into (3.16), and collecting powers of ε, we obtain

$$\triangle a_0 - a_0 + \frac{a_0^p}{h_0^q} = 0, \qquad \triangle h_0 + \frac{\nu}{b} \frac{a_0^r}{h_0^s} = 0, \qquad |y| \geq 0, \qquad (3.24)$$

and

$$\triangle a_1 - a_1 + \frac{p a_0^{p-1}}{h_0^q} a_1 = \frac{q a_0^p}{h_0^{q+1}} h_1 - a_0' \frac{y \cdot x_0'(\tau)}{|y|}, \qquad (3.25a)$$

$$\triangle h_1 + \frac{\nu}{b} \left(\frac{r a_0^{r-1}}{h_0^s} a_1 - \frac{s a_0^r}{h_0^{s+1}} h_1 \right) = 0. \qquad (3.25b)$$

Here the prime on a_0 indicates differentiation with respect to $|y|$. The matching condition is that $a_i \to 0$ exponentially as $|y| \to \infty$ and that h satisfies (3.21) as $|y| \to \infty$.

We first study the problem (3.24) for the radiallly symmetric solution a_0 and h_0. Since the outer inhibitor field is to satisfy $h(x_0) = 1 + o(1)$ as $\varepsilon \to 0$, we expand the solution to (3.24) as

$$h_0 = 1 + \nu h_{01}(|y|) + O(\nu^2), \qquad a_0 = w(|y|) + \nu a_{01}(|y|) + O(\nu^2). \qquad (3.26)$$

Here w is defined in (3.9). Substituting (3.26) into (3.24), we obtain for $|y| \geq 0$ that

$$\triangle a_{01} - a_{01} + p w^{p-1} a_{01} = q w^p h_{01}, \qquad (3.27a)$$

$$\triangle h_{01} + \frac{1}{b} w^r = 0. \qquad (3.27b)$$

The matching process then proceeds as in [70] (see also [75]). Since $\nu \gg \varepsilon$, we treat ν as a constant of order one in the local behavior of the outer solution given in (3.21). We now match

the constant term of the inner solution h_0 to the constant term of the local behavior of the outer solution (3.21). This yields $1 = B + \nu 2\pi B R_0$, so that

$$B = \frac{1}{1 + 2\pi R_0 \nu}\,. \tag{3.28}$$

Substituting this value of B back into (3.21), we then obtain the revised matching condition

$$h \sim 1 - \frac{\nu}{1 + 2\pi\nu R_0}\ln|y| + 2\pi\varepsilon\nu B\nabla R_0 \cdot y + \cdots\,, \qquad \text{as } y \to \infty\,, \tag{3.29}$$

where B is given in (3.28). Expanding (3.29) in a Taylor series in ν, and comparing with the expansion of h_0 in (3.26), we conclude that h_{01} must satisfy (3.27b) subject to the far-field asymptotic behavior

$$h_{01} = -\ln|y| + o(1)\,, \quad \text{as} \quad |y| \to \infty\,. \tag{3.30}$$

Recalling the definition of b in (3.15), it easily follows that there is a unique solution to (3.27b) with asymptotic behavior (3.30). Solving for h_{01}, and then substituting into (3.27a), we can then in principle determine a_{01}. Higher order terms in the logarithmic expansion of a_0 and h_0 can be obtained in the same way.

We now study the problem (3.25) for a_1 and h_1. From the matching condition (3.29) it follows that we must have $h_1 = 2\pi B\nabla R_0 \cdot y + o(1)$ as $|y| \to \infty$. Thus, we introduce $\tilde{h}_1$ by

$$h_1 = 2\pi B\nabla R_0 \cdot y + \tilde{h}_1\,, \tag{3.31}$$

where $\tilde{h}_1 \to 0$ as $|y| \to \infty$. Substituting (3.31) into (3.25), we can write the resulting system in matrix form as

$$L\phi + \mathcal{M}\phi = f\,, \qquad \mathcal{M} \equiv \begin{pmatrix} m_{11} & m_{12} \\ m_{21} & m_{22} \end{pmatrix}\,, \qquad \phi \equiv \begin{pmatrix} a_1 \\ \tilde{h}_1 \end{pmatrix}\,, \qquad f \equiv \begin{pmatrix} f_1 \\ f_2 \end{pmatrix}\,, \tag{3.32}$$

where L is the Laplacian operator $L\phi \equiv \triangle\phi$, and

$$m_{11} = -1 + \frac{pa_0^{p-1}}{h_0^q}\,, \qquad m_{12} = -\frac{qa_0^p}{h_0^{q+1}}\,, \tag{3.33a}$$

$$m_{21} = \frac{\nu r a_0^{r-1}}{bh_0^s}\,, \qquad m_{22} = -\frac{\nu s a_0^r}{bh_0^{s+1}}\,, \tag{3.33b}$$

$$f_1 = 2\pi q B\nabla R_0 \cdot y\frac{a_0^p}{h_0^{q+1}} - a_0'\frac{y \cdot x_0'(\tau)}{|y|}\,, \qquad f_2 = 2\pi\nu s B\nabla R_0 \cdot y\frac{a_0^r}{bh_0^{s+1}}\,. \tag{3.33c}$$

The solution to (3.32) must satisfy $\phi \rightarrow 0$ as $|y| \rightarrow \infty$.

To derive the differential equation for $x_0(t)$ we impose a solvability condition on (3.32). Let ψ be any solution to the homogeneous adjoint problem associated with (3.32). Thus, ψ satisfies,

$$L\psi + \mathcal{M}^t\psi = 0\,, \tag{3.34}$$

with $\psi \rightarrow 0$ as $|y| \rightarrow \infty$, where $\mathcal{M}^t$ indicates the transpose of $\mathcal{M}$. Multiplying (3.32) by ψ^t, we integrate by parts over $\mathbb{R}^2$ to obtain

$$\int_{\mathbb{R}^2} \left(\psi^t L\phi + \psi^t \mathcal{M}\phi\right) dy = \int_{\mathbb{R}^2} \phi^t \left(L\psi + \mathcal{M}^t\psi\right) dy = \int_{\mathbb{R}^2} \psi^t f\, dy\,. \tag{3.35}$$

Since ψ satisfies the homogeneous adjoint problem, we conclude from (3.34) and (3.35) that (3.32) must satisfy the solvability condition

$$\int_{\mathbb{R}^2} \psi^t f\, dy = 0\,. \tag{3.36}$$

We now obtain a more convenient form for this solvability condition. Setting $\psi = (\psi_1, \psi_2)^t$, and using (3.33a) and (3.33b), we write the adjoint problem (3.34) as

$$\triangle\psi_1 + \left(-1 + \frac{pa_0^{p-1}}{h_0^q}\right)\psi_1 + \frac{\nu r a_0^{r-1}}{bh_0^s}\psi_2 = 0\,, \tag{3.37a}$$

$$\triangle\psi_2 - \frac{qa_0^p}{h_0^{q+1}}\psi_1 - \frac{\nu s a_0^r}{bh_0^{s+1}}\psi_2 = 0\,, \tag{3.37b}$$

where $\psi_j \rightarrow 0$ as $|y| \rightarrow \infty$ for $j = 1, 2$. Using (3.33c), the solvability condition (3.36) can be written as

$$x_0' \cdot \int_{\mathbb{R}^2} \frac{y}{|y|} a_0'\psi_1\, dy = 2\pi B \nabla R_0 \cdot \int_{\mathbb{R}^2} y\left(\frac{qa_0^p}{h_0^{q+1}}\psi_1 + \frac{\nu s a_0^r}{bh_0^{s+1}}\psi_2\right) dy\,. \tag{3.38}$$

Equation (3.38) is simplified further by using (3.37b) to replace the right-hand side of (3.38). This yields,

$$x_0' \cdot \int_{\mathbb{R}^2} \frac{y}{|y|} a_0'\psi_1\, dy = 2\pi B \nabla R_0 \cdot \int_{\mathbb{R}^2} y\,\triangle\psi_2\, dy\,, \tag{3.39}$$

where B is defined in (3.28). Equation (3.39) is an ordinary differential equation for the motion of the center of the spike.

108

We note that the derivation of (3.39) has not used any expansion of a_0 or h_0 in powers of the logarithmic gauge function ν. In principle, to determine an explicit form for the ODE (3.39) for $x_0(t)$, which contains all the logarithmic terms, we must solve (3.24) for a_0 and h_0 and then compute non-trivial solutions to the adjoint problem (3.37). This is a difficult task. Instead, we will only calculate the leading order term in an infinite logarithmic expansion of ψ_1 and ψ_2. This requires only the leading order term in the infinite logarithmic expansion of a_0 and h_0 given in (3.26). Therefore, substituting (3.26) and

$$\psi_1 = \psi_{10} + \nu\psi_{11} + O(\nu^2), \qquad \psi_2 = \psi_{20} + \nu\psi_{21} + O(\nu^2), \tag{3.40}$$

into (3.37), we obtain the leading order adjoint problem

$$\triangle\psi_{10} + \left(-1 + pw^{p-1}\right)\psi_{10} = 0, \tag{3.41a}$$

$$\triangle\psi_{20} - qw^p\psi_{10} = 0. \tag{3.41b}$$

There are two linearly independent solutions to (3.41a). They are

$$\psi_{10} = \partial_{y_j}w, \qquad j = 1, 2. \tag{3.42}$$

Substituting (3.42) into (3.41b), we obtain

$$\triangle\psi_{20} = \frac{q}{p+1}\left[w^{p+1}(|y|)\right]'\frac{y_j}{|y|}, \qquad j = 1, 2. \tag{3.43}$$

The solution to (3.43) is

$$\psi_{20} = \frac{q}{\rho(p+1)}\left(\int_0^\rho s\left[w(s)\right]^{p+1}ds\right)\frac{y_j}{|y|}, \tag{3.44}$$

where $\rho = |y|$. Substituting $a_0 \sim w$, (3.42), and (3.43), into the solvability condition (3.39), we obtain

$$x_0' \cdot \int_{\mathbb{R}^2}\frac{y}{|y|}w'\partial_{y_j}w\,dy = \frac{2\pi Bq}{p+1}\nabla R_0 \cdot \int_{\mathbb{R}^2}y\left[w^{p+1}(|y|)\right]'\frac{y_j}{|y|}\,dy, \qquad j = 1, 2. \tag{3.45}$$

The integrals in (3.45) are evaluated using

$$\int_{\mathbb{R}^2}\frac{y_iy_j}{|y|^2}\left[w'(|y|)\right]^2dy = \pi\delta_{ij}\int_0^\infty\rho\left[w'(\rho)\right]^2d\rho, \tag{3.46a}$$

$$\int_{\mathbb{R}^2}\frac{y_iy_j}{|y|}\left[w^{p+1}(|y|)\right]'dy = \pi\delta_{ij}\int_0^\infty\rho^2\left[w^{p+1}(\rho)\right]'d\rho = -2\pi\delta_{ij}\int_0^\infty\rho\left[w(\rho)\right]^{p+1}d\rho, \tag{3.46b}$$

109

where δ_{ij} is the Kronecker symbol. Substituting (3.46) into (3.45), we obtain

$$x_0'(\tau) = -\frac{4\pi Bq}{p+1}\nabla R_0 \left(\frac{\int_0^\infty [w(\rho)]^{p+1}\rho\,d\rho}{\int_0^\infty [w'(\rho)]^2\rho\,d\rho}\right). \tag{3.47}$$

In Appendix B of [76], equation (3.9) was used to calculate the ratio

$$\frac{\int_0^\infty [w(\rho)]^{p+1}\rho\,d\rho}{\int_0^\infty [w'(\rho)]^2\rho\,d\rho} = \frac{p+1}{p-1}. \tag{3.48}$$

Hence (3.47) reduces to

$$x_0'(\tau) = -\frac{4\pi qB}{p-1}\nabla R_0. \tag{3.49}$$

Substituting (3.28) for B into (3.49), and recalling the definition of ν given in (3.15), we recover the main result (3.17) for $x_0(t)$.

There are two important remarks. Firstly, from (3.49) it follows that the center of the spike moves towards the location of a local minimum of R_0. This minimum depends only on D and not on ε. In the following sections we will explore how this location depends on D. Secondly, as seen from the analysis above, since we have only used the leading order term in the logarithmic expansion of the homogeneous adjoint eigenfunction, the error in (3.17) is of order $O(\nu)$. This error, however, is still proportional to ∇R_0. In fact, the two integrals in the solvability condition (3.39) are independent of x_0 and the shape of the domain. Thus, even if we had retained higher order terms in the logarithmic expansion of the adjoint eigenfunction, we would still conclude that the equilibrium locations of the spike are at local minima of ∇R_0, and the spike would follow the same path in the domain as that described by (3.17). The higher order terms in the logarithmic expansion of a_0, h_0 and the adjoint eigenfunction, only change the time-scale of the motion. However, at first glance, an error proportional to $O(\nu)$ in the time-scale of the asymptotic dynamics seems rather large. This is not as significant a concern as it may appear, as from the numerical experiments performed in §3.4 we show that it is the dependence of B on ν as given in (3.28) that allows for a close agreement between the asymptotic and full numerical results for the spike motion.

To derive Proposition 3.1.1, we had to expand the a_0, h_0 in ν as in (3.26). But this is only valid when ν is small, i.e. ε is exponentially small. To derive more accurate dynamics for a more realistic case of ε polynomially small, we need to work directly with adjoint equations (3.37).

Let $r = |y|$. Direct computation yields, for any function $f(r)$,

$$\triangle(y_j f(r)) = y_j \left(f''(r) + \frac{3}{r} f'(r) \right).$$

Letting

$$\psi_1(x) = \frac{y_j}{r} f(r), \quad \psi_2(x) = \frac{y_j}{r} g(r), \tag{3.50a}$$

we obtain

$$f'' + \frac{1}{r} f' - \frac{1}{r^2} f + \left(-1 + \frac{p a_0^{p-1}}{h_0^q} \right) f + \frac{\nu r a_0^{r-1}}{b h_0^s} g = 0, \tag{3.50b}$$

$$g'' + \frac{1}{r} g' - \frac{1}{r^2} g - \frac{q a_0^p}{h_0^{q+1}} f - \frac{\nu s a_0^r}{b h_0^{s+1}} g = 0, \tag{3.50c}$$

and

$$\int_{\mathbb{R}^2} \frac{y_i}{y} a_0' \psi_1 dy = \delta_{ij} \pi \int_0^\infty r a_0'(r) f(r) dr \tag{3.51}$$

$$\int_{\mathbb{R}^2} y \left(\frac{q a_0^p}{h_0^{q+1}} \psi_1 + \frac{\nu s a_0^r}{b h_0^{s+1}} \psi_2 \right) dy = \delta_{ij} \pi \int_0^\infty r^2 \left(\frac{q a_0^p}{h_0^{q+1}} f + \frac{\nu s a_0^r}{b h_0^{s+1}} g \right) dr. \tag{3.52}$$

Therefore we obtain:

$$x_0' \sim 2\pi B \nabla R_0 \frac{\int_0^\infty r^2 \left(\frac{q a_0^p}{h_0^{q+1}} f + \frac{\nu s a_0^r}{b h_0^{s+1}} g \right) dr}{\int_0^\infty r a_0'(r) f(r) dr} \tag{3.53}$$

The integral on the right hand side is to be evaluated numerically. The functions a_0, h_0, f, g are solved numerically using a boundary value solver `colsys` [3]. We approximate the infinite line by $[0, L]$ where L was taken to be 15. Note that f and g are determined only up to an arbitrary scaling. For f, g we use the following boundary conditions:

$$f(0) = 0, \ g'(0) = 1, \ f'(L) = 0, \ g'(L) = 0.$$

These conditions assure decay at infinity and the solution being odd. The remaining conditions are: $a_0'(L) = 0, h_0'(0) = a_0'(0) = 0$, and $h(0) = 1$.

Next we consider an example. We take $\Omega = [0,1]^2$, $\varepsilon = 0.01, (p,q,r,s) = (2,1,2,0)$. Taking an initial spike to be at $x_0 = (0.4, 0)$ we obtain numerically that $R_0 = 0.7598$ and $\nabla R_0 = $

$(-0.09137, 0)$ (see Section 3.2.1.) From a full numerical simulation of the system, we obtain $\frac{|x_0'(\varepsilon^2 t)|}{|\nabla R_0|} = 7.057$. On the other hand, using (3.28) we obtain $B = 0.491$ and $\frac{|x_0'(\varepsilon^2 t)|}{|\nabla R_0|} = 6.170$, with an error of about 10%. Using `colsys` obtain numerically,

$$\frac{\int_0^\infty r^2 \frac{a_0^2}{h_0^2} f}{\int_0^\infty r a_0' f} = -2.566$$

which yields from (3.53), $\frac{|x_0'(\varepsilon^2 t)|}{|\nabla R_0|} = 7.92$. This method also give an error of about 10%. However we expect that the latter method is more accurate for smaller values of ε.

3.2 Limiting Cases Of The Dynamics

In this section we consider two limiting cases of result (3.17) for the motion of a spike. In §3.2.1 we consider the case where $\varepsilon^2 \ll D \ll 1$ and in §3.2.2 we consider the case $D \gg 1$.

3.2.1 Dynamics For Small D

In this section we assume that $\varepsilon^2 \ll D \ll 1$. The inequality $\varepsilon^2 \ll D$ was crucial to the derivation of (3.17) in §2. When $D \ll 1$ we can treat D as a small parameter and obtain limiting results from (3.17).

We begin by introducing $\widetilde{R}$ defined by

$$\widetilde{R}(x, x_0) = G(x, x_0) - V(x), \tag{3.54}$$

where G satisfies (3.10), and V is the free-space Green's function in $\mathbb{R}^2$ satisfying

$$\triangle V - \lambda^2 V = -\delta(x - x_0), \qquad \lambda \equiv \frac{1}{\sqrt{D}}. \tag{3.55}$$

The solution to (3.55) is

$$V(x) = \frac{1}{2\pi} K_0(\lambda |x - x_0|). \tag{3.56a}$$

The asymptotic behavior of $K_0(r)$ for $r \ll 1$ is

$$K_0(r) \sim -\ln r + \ln 2 - \gamma + O\left(r^2 \ln r\right), \qquad \text{as } r \to 0. \tag{3.56b}$$

Here γ is Euler's constant. In terms of $\widetilde{R}$, the regular part R_0 defined in (3.18) is

$$R_0 = \widetilde{R}(x_0, x_0) - \frac{1}{2\pi}(\ln \lambda - \ln 2 + \gamma), \qquad \nabla R_0 = \nabla \widetilde{R}(x, x_0)|_{x=x_0}. \tag{3.57}$$

112

To obtain some insight into the dynamics when D is small, we first consider the case where $\Omega = [0,1]^2$ is a unit square. Then, using the method of images, we can solve (3.10) explicitly for G for any value of D. This yields

$$\widetilde{R}(x, x_0) = \left(\sum_{n=-\infty}^{\infty} \sum_{m=-\infty}^{\infty} V\left[v_m(h_n(x))\right] \right) - V(x), \tag{3.58a}$$

where

$$h_n(x) = \begin{cases} (x_1 - n, x_2) & \text{if } n \text{ is even} \\ (n + 1 - x_1, x_2) & \text{if } n \text{ is odd} \end{cases}, \quad v_m(x) = \begin{cases} (x_1, x_2 - m) & \text{if } m \text{ is even} \\ (x_1, m + 1 - x_2) & \text{if } m \text{ is odd} \end{cases}. \tag{3.58b}$$

For D small, such that $\lambda|x - x_0| \gg 1$, the function V decays exponentially as

$$V(x) \sim \frac{1}{2} \frac{1}{\sqrt{2\pi}} \left[\lambda|x - x_0|\right]^{-\frac{1}{2}} e^{-\lambda|x-x_0|}, \quad \text{for } \lambda|x - x_0| \gg 1. \tag{3.59}$$

Now suppose that the spike is located at $x_0 = (\frac{1}{2}, \xi)$ with $O\left(\frac{1}{\lambda}\right) \ll \xi < \frac{1}{2} - O\left(\frac{1}{\lambda}\right)$. Then, for $D \ll 1$, we need only retain the two terms $(n, m) = (0, 0)$ and $(n, m) = (0, -1)$ in the series (3.58a). The other terms are exponentially small at the point x_0 in comparison with these terms. Thus, for $\lambda \to \infty$, we obtain from (3.58a) that

$$\widetilde{R}(x, x_0) \sim \frac{1}{2\pi} K_0 \left[\lambda|\tilde{x} - x_0|\right], \quad \tilde{x} = (x_1, -x_2), \quad x = (x_1, x_2). \tag{3.60a}$$

Now substituting (3.60a) into (3.57), and using the large argument expansion (3.59), we obtain

$$R_0 \sim \frac{1}{4\sqrt{\pi\lambda\xi}} e^{-2\lambda\xi} + \frac{1}{2\pi} \left(\ln 2 - \gamma - \ln\lambda\right), \quad 2\nabla R_0 \sim -\frac{1}{2}\sqrt{\frac{\lambda}{\pi\xi}} e^{-2\lambda\xi} \hat{\jmath}, \tag{3.60b}$$

where $\hat{\jmath}$ is a unit vector in the positive x_2 direction. Substituting (3.60b) into (3.17), we obtain an evolution equation for ξ

$$\frac{d\xi}{dt} \sim \frac{q}{p-1} \left(\frac{\varepsilon^2 \sqrt{\pi\lambda}}{\ln 2 - \gamma - \ln[\varepsilon\lambda]} \right) \frac{e^{-2\lambda\xi}}{\sqrt{\xi}}. \tag{3.61}$$

We now make a few remarks. The ODE (3.61) breaks down when $\varepsilon\lambda = O(1)$. This occurs when $D = O(\varepsilon^2)$. Thus, we require that $\varepsilon \ll 1$ and $\lambda \gg 1$, but $\varepsilon\lambda \ll 1$. In this limit, (3.61) shows that ξ is increasing exponentially slowly without bound as t increases. The ODE, however, was
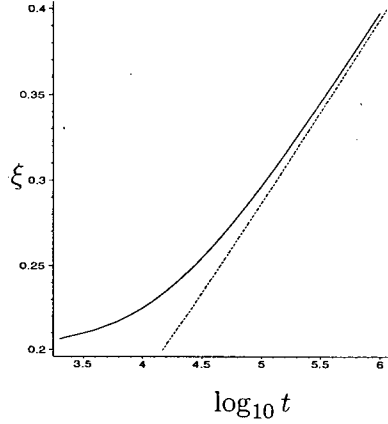
Figure 3.3: Movement of the center $(0.5, \xi(t))$ of a single spike of (3.16) within a unit box $[0,1]^2$ versus $\log_{10} t$, with $\varepsilon = D = 0.01$. The solid curve is the numerical solution to (3.61) with $\xi(0) = 0.2$. The broken curve is the approximation (3.63).

derived under the assumption that $O\left(\frac{1}{\lambda}\right) \ll \xi < \frac{1}{2} - O\left(\frac{1}{\lambda}\right)$. When ξ is near the value $\xi = 1/2$, the ODE must be rederived by retaining an additional image point in the infinite sum in (3.58a) corresponding to $(n, m) = (0, 1)$. The effect of this additional term is to ensure that $\xi \to 1/2$ as $t \to \infty$. This implies that the spike tends to the center of the square as $t \to \infty$.

Consider (3.61) with the initial condition $\xi(0) = \xi_0$. To determine the time T for which $\xi(T) = \xi_1$, where $O\left(\frac{1}{\lambda}\right) \ll \xi_0 < \xi_1 < \frac{1}{2} - O\left(\frac{1}{\lambda}\right)$, we integrate (3.61) to obtain

$$\int_{\xi_0}^{\xi_1} \sqrt{\xi}\, e^{2\lambda\xi}\, d\xi = \frac{q}{p-1}\left(\frac{\varepsilon^2\sqrt{\pi\lambda}}{\ln 2 - \gamma - \ln[\varepsilon\lambda]}\right) T\,. \tag{3.62}$$

Evaluating the integral asymptotically for $\lambda \gg 1$ we get

$$T \sim \frac{p-1}{q}\left(\frac{\ln 2 - \gamma - \ln[\varepsilon\lambda]}{2\varepsilon^2\sqrt{\pi}\lambda^{3/2}}\right)\sqrt{\xi_1}\, e^{2\lambda\xi_1}\,, \qquad \lambda \gg 1\,. \tag{3.63}$$

Thus, when $D \ll 1$, the motion of the spike is *metastable*. The spike moves exponentially slowly with time (see Fig. 3.3) as it approaches the center of the square. Indeed, this behavior is not specific to a square domain as we will now demonstrate.

More generally, consider any domain Ω with smooth boundary. Let $\widetilde{R}(x, x_0)$ be defined as in (3.54). Then, $\widetilde{R}$ satisfies

$$\triangle\widetilde{R} - \lambda^2\widetilde{R} = 0 \qquad x \in \Omega\,; \qquad \partial_n\widetilde{R} = -\partial_n V\,, \qquad x \in \partial\Omega\,, \tag{3.64}$$

114

where $V(x)$ is given in terms of x_0 by (3.56a). To obtain a representation formula for $\widetilde{R}$, we apply Green's theorem to $\widetilde{R}$ and V. This yields,

$$\widetilde{R}_0 \equiv \widetilde{R}(x_0, x_0) = \int_{\partial\Omega} \left[V(x')\partial_n \widetilde{R}(x', x_0) - \widetilde{R}(x', x_0)\partial_n V(x') \right] dx' . \qquad (3.65)$$

The only term in the integrand of (3.65) that we still need to calculate is $\widetilde{R}(x', x_0)$ for $x' \in \partial\Omega$. We now calculate this term for $\lambda \gg 1$ using a boundary layer analysis on (3.64). Since $\lambda \gg 1$, the solution to (3.64) has a boundary layer of width $O\left(\lambda^{-1}\right)$ near $\partial\Omega$. Thus, it suffices to estimate $\widetilde{R}$ inside the boundary layer. Let $\eta = \lambda|x' - x|$ where x' is the point on $\partial\Omega$ closest to x (one can always find such an x' assuming that x is within the boundary layer and λ is sufficiently large). Let ξ represent the other coordinate orthogonal to η. Then, using this coordinate change in (3.64), we have to leading order that

$$\widetilde{R}_{\eta\eta} - \widetilde{R} = 0, \qquad \eta \geq 0; \qquad \lambda \widetilde{R}_\eta|_{\eta=0} \sim \partial_n V(x') . \qquad (3.66)$$

Since x_0 is assumed to be strictly in the interior of Ω, we can estimate V on $\partial\Omega$ using the far field behavior (3.59). This yields, for $\lambda \gg 1$, that

$$\partial_n V(x') \sim -\lambda V(x')\langle \hat{r}', \hat{n} \rangle , \qquad \hat{r}' \equiv \frac{x' - x_0}{|x' - x_0|} , \qquad (3.67)$$

where $\hat{n}$ is the unit outward normal to $\partial\Omega$ at x', and the angle brackets denote the scalar dot product. The solution to (3.66) that is bounded as $\eta \to +\infty$ is proportional to $e^{-\eta}$. Therefore,

$$\widetilde{R} \sim -\lambda^{-1}\partial_n V(x')e^{-\eta} . \qquad (3.68)$$

Using (3.67), and evaluating (3.68) on $\partial\Omega$ where $\eta = 0$, we obtain the following key results for $\lambda \gg 1$:

$$\widetilde{R}(x', x_0) \sim V(x')\langle \hat{r}', \hat{n} \rangle , \qquad x' \in \partial\Omega , \qquad (3.69a)$$

$$\partial_n \widetilde{R}(x', x_0) \sim \lambda V(x')\langle \hat{r}', \hat{n} \rangle , \qquad x' \in \partial\Omega . \qquad (3.69b)$$

Next, we substitute (3.69) and (3.67) into (3.65). This yields, for $\lambda \gg 1$, that

$$\widetilde{R}_0 \equiv \widetilde{R}(x_0, x_0) \sim \lambda \int_{\partial\Omega} \left[V(x') \right]^2 \left(\langle \hat{r}', \hat{n} \rangle^2 + \langle \hat{r}', \hat{n} \rangle \right) dx' . \qquad (3.70)$$

We now evaluate this integral asymptotically for $\lambda \gg 1$. To do so we use Laplace's formula (see [86]),

$$\int_{\partial\Omega} \frac{1}{r'} F(r') e^{-2\lambda r'} dx' \sim \left(\frac{\pi}{\lambda r_m}\right)^{\frac{1}{2}} e^{-2\lambda r_m} \sum F(r_m) \left(1 - \frac{r_m}{\kappa_m}\right)^{-\frac{1}{2}} . \qquad (3.71)$$

Here $r_m = \text{dist}(\partial\Omega, x_0)$, $\kappa_m \geq 0$ is the curvature of $\partial\Omega$ at x_m, and the sum is taken over all $x_m \in \partial\Omega$ that are closest to x_0. Comparing (3.70) with (3.71), we get

$$F(r') \equiv \frac{1}{8\pi} \left(\langle \hat{r}', \hat{n}\rangle^2 + \langle \hat{r}', \hat{n}\rangle\right) . \qquad (3.72)$$

At the points $x_m \in \partial\Omega$ closest to x_0, we have that $r' = r_m$ and $\hat{r}' = \hat{n}$. This yields, $F(r_m) = 1/4\pi$. Therefore, for $\lambda \gg 1$, the estimate (3.71) for (3.70) becomes

$$\widetilde{R}_0 \sim \frac{1}{4\sqrt{\lambda\pi r_m}} e^{-2\lambda r_m} \sum \left(1 - \frac{r_m}{\kappa_m}\right)^{-\frac{1}{2}} . \qquad (3.73)$$

Finally, to calculate ∇R_0 needed in (3.17), we use (3.57) and the reciprocity relation $\widetilde{R}(x, x_0) = \widetilde{R}(x_0, x)$ to get

$$\nabla R_0 = \nabla \widetilde{R}(x, x_0)|_{x=x_0} = \frac{1}{2}\frac{d}{dx_0}\widetilde{R}(x_0, x_0) = \frac{1}{2}\frac{d}{dx_0}\widetilde{R}_0 . \qquad (3.74)$$

Differentiating (3.73), and substituting into (3.74), we obtain

$$2\nabla R_0 \sim -\frac{1}{2}\sqrt{\frac{\lambda}{\pi r_m}} e^{-2\lambda r_m} \sum \left(1 - \frac{r_m}{\kappa_m}\right)^{-\frac{1}{2}} \hat{r}_m , \qquad (3.75)$$

where $\hat{r}_m \equiv (x_m - x_0)/|x_m - x_0|$. Substituting (3.75) and (3.57) into (3.17), we obtain the following proposition:

Proposition 3.2.1 *For $\varepsilon^2 \ll D \ll 1$ and $\varepsilon \ll 1$, the trajectory of the center of a one-spike solution to (3.16) satisfies the differential equation*

$$\frac{dx_0}{dt} \sim \frac{\sqrt{\pi\lambda}\, q}{p-1} \left(\frac{\varepsilon^2}{\ln 2 - \gamma - \ln[\varepsilon\lambda]}\right) \frac{1}{\sqrt{r_m}} e^{-2\lambda r_m} \sum \left(1 - \frac{r}{\kappa_m}\right)^{-\frac{1}{2}} \hat{r}_m . \qquad (3.76)$$

Here $\lambda \equiv D^{-\frac{1}{2}}$, $\hat{r}_m$ is defined following (3.75), and the other symbols are defined in the sentence following (3.71).

The formula (3.76) agrees with (3.61) when Ω is a unit box. Moreover, we have the following result:

116

Proposition 3.2.2 *Let $r(x) = \text{dist}(\partial\Omega, x)$. Suppose that x_0 is a local minimum of $f(x_0) \equiv R(x_0, x_0)$ as $\lambda \to \infty$. Then, for $\lambda \to \infty$, x_0 is a local maximum of $r(x)$.*

Proof. The proof is by contradiction. Suppose that x_0 is not a local maximum of $r(x)$. Since r is continuous, we can find x_1 with $|x_1 - x_0| > 0$ arbitrary small, with $r(x_1) - r(x_0) > 0$. However, (3.73) yields

$$\frac{\widetilde{R}(x_1, x_1)}{\widetilde{R}(x_0, x_0)} \sim C e^{-2\lambda[r(x_1)-r(x_0)]}, \tag{3.77}$$

where $C = C(x_0, x_1)$ is independent of λ. Hence, for λ sufficiently large, $\frac{\widetilde{R}(x_1,x_1)}{\widetilde{R}(x_0,x_0)} < 1$. This implies that $\widetilde{R}(x_1, x_1) < \widetilde{R}(x_0, x_0)$ for λ large enough. Hence, x_0 is not a local minimizer of $\widetilde{R}$ as $\lambda \to \infty$. Using (3.57) to relate $\widetilde{R}$ to R completes the proof. $\qquad\Box$

It follows that for $D \ll 1$ and for convex domains, the center of the spike moves towards a point within the domain located at the center of the largest disk that can be inserted into the domain.

3.2.2 Dynamics For Large D

The dynamics for the limiting case where $D \gg 1$ is significantly different from the previous analysis where $D \ll 1$.

When D is large, we may expand G defined in (3.10) as

$$G = DG_0 + G_m + \frac{1}{D}G_2 + \cdots. \tag{3.78}$$

Substituting (3.78) into (3.10), and collecting powers of D, we obtain

$$\triangle G_0 = 0, \qquad x \in \Omega; \qquad \partial_n G_0 = 0, \qquad x \in \partial\Omega, \tag{3.79a}$$

$$\triangle G_m = G_0 - \delta(x - x_0), \qquad x \in \Omega; \qquad \partial_n G_m = 0, \qquad x \in \partial\Omega. \tag{3.79b}$$

From (3.79a) we conclude that G_0 is a constant. The solvability condition for (3.79b) then yields

$$G_0 = \frac{1}{\text{vol}\,\Omega}, \tag{3.80}$$

where $\text{vol}\,\Omega$ is the area of Ω. The solvability condition for the problem for G_2 also yields that $\int_\Omega G_m\,dx = 0$. Hence, G_m is the modified Green's function for Ω satisfying

$$\triangle G_m = \frac{1}{\text{vol}\,\Omega} - \delta(x - x_0)\,, \quad x \in \Omega\,; \quad \partial_n G_m = 0\,, \quad x \in \partial\Omega\,; \qquad \int_\Omega G_m\,dx = 0\,. \quad (3.81)$$

Let R_m be the regular part of G_m defined by

$$R_m(x, x_0) = \frac{1}{2\pi}\ln|x - x_0| + G_m(x, x_0)\,. \quad (3.82)$$

Combining (3.11), (3.78), (3.80), and (3.82), we conclude that for $D \gg 1$

$$R(x, x_0) \sim \frac{D}{\text{vol}\,\Omega} + R_m(x, x_0) + O\,(1/D)\,. \quad (3.83)$$

Substituting (3.83) into (3.17), we obtain the following proposition:

Proposition 3.2.3 *If $D \gg 1$ and $\varepsilon \ll 1$, the trajectory of a one-spike solution of (3.16) satisfies*

$$\frac{dx_0}{dt} = -\frac{4\pi q\varepsilon^2}{p-1}\left(\frac{1}{-\ln\varepsilon + 2\pi\frac{D}{\text{vol}\,\Omega} + 2\pi R_{m0}}\right)\nabla R_{m0}\,, \quad (3.84\text{a})$$

where R_{m0} and its gradient are defined by

$$R_{m0} \equiv R_m(x_0, x_0), \qquad \nabla R_{m0} = \nabla_x R_m(x, x_0)|_{x = x_0}\,. \quad (3.84\text{b})$$

As a corollary, we obtain the following proposition, which was originally derived in [14] and [76]:

Proposition 3.2.4 *(Ward et al, [76], Proposition 3.2) Let $\varepsilon \ll 1$ and assume that $D \gg -\ln\varepsilon$. Then, the trajectory of a one-spike solution of (3.16) satisfies*

$$\frac{dx_0}{dt} = -\left(\frac{2q\,\text{vol}\,\Omega}{p-1}\right)\frac{\varepsilon^2}{D}\nabla R_{m0}\,, \quad (3.85)$$

where R_{m0} and ∇R_{m0} are defined in (3.84b).

Several general observations can be made by comparing (3.17), (3.76), and (3.85). In all three cases, the activator diffusivity ε only controls the timescale of the motion. The precise trajectory traced by x_0 as t increases depends only on D and on the shape of the domain inherited through the terms ∇R_0 and ∇R_{m0}. For the case of small D, where $\varepsilon^2 \ll D \ll 1$, the motion is exponentially slow, or *metastable*, and D controls the dynamics. In contrast, when $D = O(1)$, the speed of the spike is of the order $\frac{\varepsilon^2}{-\ln \varepsilon}$, with a complicated dependence on D through R_0. Finally for $D \gg -\ln \varepsilon$, the speed is controlled by both ε and D and is of order $\frac{\varepsilon^2}{D}$. In the limit $D \to \infty$ and $\tau = 0$, the system (3.1) is approximated by the so-called *shadow system* (see [37], [10]). In this case the motion of the spike is again metastable. However, for the shadow system a one-spike interior equilibrium solution is unstable and the spike moves towards the closest point on the boundary of the domain. This behavior is in direct contrast to what we have found for small D, whereby by Propositions 3.2.1 and 3.2.2 the spike moves exponentially slowly towards a point that is the furthest away from the boundary. This suggests that as D is increased, the number of possible equilibria for x_0 may decrease. In §3.3 we will show that for a certain dumbell-shaped domain, there is only one possible stable equilibrium location for D sufficiently large, whereas there are two stable equilibrium locations when D is sufficiently small.

The analysis of this chapter breaks down in the *near-shadow system* when D is exponentially large, i.e. when (3.3) fails. In such a case, there is an exponentially weak boundary effect that must be taken into account, since it becomes of the same order as the effect due to ∇R_m. The near-shadow system will be considered in detail in the next chapter.

3.3 Exact Calculation Of The Modified Green's Function

In this section we will use complex analysis to derive an exact formula for ∇R_{m0} defined in (3.84b) for domains of the form

$$\Omega = f(B), \tag{3.86}$$

where B is the unit circle, and f is a rather general class of analytic functions. We will then use this formula to further explore the dynamics of a spike for the GM system on a certain

dumbell-shaped domain. Our main result here is the following:

Theorem 3.3.1 *Let $f(z)$ be a complex mapping of the unit disk B satisfying the following conditions:*

(i) f is analytic and is invertible on $\overline{B}$. Here $\overline{B}$ is B together with its boundary ∂B.

(ii) f has only simple poles at the points $z_1, z_2, .., z_k$, and f is bounded at infinity.

(iii) $f = g/h$ where both g and h are analytic on the entire complex plane, with $g(z_i) \neq 0$.

(iv) $\overline{f(z)} = f(\overline{z})$.

On the image domain $\Omega = f(B)$, let G_m and R_m be the modified Green's function and its regular part, as defined in (3.81) and (3.82), respectively. Let R_{m0} and ∇R_{m0} be the value of R_m and its gradient evaluated at x_0, as defined in (3.84b). Then, we have

$$\nabla R_{m0} = \frac{\nabla s(z_0)}{f'(z_0)}, \tag{3.87}$$

where $z_0 \in B$ satisfies $x_0 = f(z_0)$, and $\nabla s(z_0)$ is given by

$$\nabla s(z_0) = \frac{1}{2\pi} \left(\frac{z_0}{1-|z_0|^2} + \frac{f''(\overline{z}_0)}{2f'(\overline{z}_0)} \right)$$

$$- \frac{f'(\overline{z}_0)\left(f(z_0) - f(\frac{1}{\overline{z}_0}) \right) + \sum_j \frac{g(z_j)f'(\frac{1}{z_j})}{z_j^2 h'(z_j)} \left(\frac{1}{z_j - \overline{z}_0} + \frac{z_j}{1-z_j\overline{z}_0} \right)}{2\pi \sum_j \frac{g(z_j)f'(\frac{1}{z_j})}{z_j^2 h'(z_j)}}. \tag{3.88}$$

In the equation above, and for the rest of this section, we will treat vectors $v = (v_1, v_2)$ as complex numbers $v_1 + iv_2$. Thus vw is assumed to be complex multiplication. The dot product will be denoted by $\langle v, w \rangle \equiv \frac{1}{2}(v\overline{w} + \overline{v}w)$.

Proof. Given $x, x_0 \in \Omega$, choose z, z_0 such that $x = f(z), x_0 = f(z_0)$. We will use $\hat{n}$ and $\hat{N}$ to denote the normal to ∂B at a point z and the normal to $\partial \Omega$ at $x = f(z)$, respectively. Since f is analytic on $\overline{B}$ we obtain

$$\hat{N} = \frac{\hat{n}f'(z)}{|f'(z)|} = \frac{zf'(z)}{|f'(z)|}, \qquad d\sigma(z) = \frac{dz}{iz}, \tag{3.89}$$

120

where $d\sigma$ is the length element on ∂B.

We now define $S(x)$ by

$$S(x) = G_m(x, x_0) + \frac{1}{2\pi} \ln|x - x_0| - \frac{1}{4 \operatorname{vol} \Omega}|x - x_0|^2 \,. \tag{3.90}$$

Substituting (3.90) into (3.81), we find that S satisfies

$$\begin{cases} \triangle S = 0, & \text{in} \quad \Omega \,, \\ \langle \nabla S, \hat{N} \rangle = \langle x - x_0, \hat{N} \rangle \left(\frac{1}{2\pi|x-x_0|^2} - \frac{1}{2\operatorname{vol}\Omega} \right), & \text{on} \quad \partial\Omega \,, \end{cases} \tag{3.91a}$$

with

$$\int_\Omega S \, dx = \frac{1}{2\pi} \int_\Omega \ln|x - x_0| - \frac{1}{4 \operatorname{vol} \Omega} \int_\Omega |x - x_0|^2 \, dx \,. \tag{3.91b}$$

Combining (3.90) and (3.82), we relate ∇R_m to ∇S as

$$\nabla R_m(x, x_0)|_{x=x_0} = \nabla S(x_0) \,. \tag{3.92}$$

The problem (3.91a) determines S up to an additive constant. This constant is determined by (3.91b). However, the precise value of this additive constant does not influence ∇R_{m0}, since this term depends only on the gradient of S. Hence, without loss of generality, in the derivation below we only calculate S up to an additive constant.

Let $s(z) = S(f(z))$. Since f is analytic and S is harmonic, s satisfies Laplaces's equation. Using (3.89), and the fact that f is analytic, we get $\langle \nabla s, \hat{n} \rangle = \langle \nabla S, \hat{N} \rangle |f'(z)|$. Hence, (3.91a) transforms to

$$\begin{cases} \triangle s = 0, & \text{in} \quad B \,, \\ \langle \nabla s, \hat{n} \rangle = \chi(z, z_0) \equiv \langle x - x_0, z f'(z) \rangle \left(\frac{1}{2\pi|x-x_0|^2} - \frac{1}{2\operatorname{vol}\Omega} \right), & \text{on} \quad \partial B \,. \end{cases} \tag{3.93}$$

On the unit ball $\Omega = B$, let $g_m(z, \xi)$ be the solution to the modified Green's function problem (3.81), with singular point at $z = \xi$. It [76] it was shown that

$$g_m(z, \xi) = \frac{1}{2\pi} \left(\frac{|z|^2}{2} - \ln|z - \xi| - \ln\left|z - \frac{\xi}{|\xi|^2}\right| \right) + C(\xi) \,, \tag{3.94}$$

where C is a constant depending on ξ. Notice that if $|z| = 1$ then $|z - \frac{\xi}{|\xi|^2}|^2 = \frac{|z-\xi|^2}{|\xi|^2}$. Hence,

$$\nabla_\xi g_m(z, \xi)|_{z \in \partial B} = \frac{1}{\pi} \frac{z - \xi}{|z - \xi|^2} + C_1(\xi) \,, \tag{3.95}$$

121

where C_1 is another constant.

Next, we use Green's identity to represent the solution to (3.93) as the boundary integral

$$s(\xi) = \int_{\partial B} g_m(z, \xi)\chi(z, z_0)\,d\sigma(z) + C_2\,, \qquad \chi(z, z_0) \equiv \langle \nabla s, \hat{n} \rangle\,, \qquad (3.96)$$

where C_2 is a constant. Since $s(z) = S(f(z))$, we get from (3.92) that

$$\nabla R_{m0} \equiv \nabla R_m(x, x_0)|_{x=x_0} = \left.\frac{\nabla s(z)}{f'(z)}\right|_{z=z_0}\,. \qquad (3.97)$$

Differentiating (3.96) with respect to ξ and using (3.95), we evaluate the resulting expression at $\xi = z_0$ to get

$$\nabla s(z_0) = \int_{\partial B} \nabla_\xi g_m(z, z_0)\chi(z, z_0)\,d\sigma = \frac{1}{\pi}\int_{\partial B} \frac{z - z_0}{|z - z_0|^2}\chi(z, z_0)\,d\sigma + C_1\int_{\partial B}\chi(z, z_0)\,d\sigma\,. \quad (3.98)$$

From (3.93) it follows that $\int_{\partial B}\chi(z, z_0)\,d\sigma(z) = 0$. Then, using (3.93) for $\chi(z, z_0)$ and (3.89) for $d\sigma(z)$, (3.98) becomes

$$\begin{aligned}
\nabla s(z_0) &= \int_{\partial B} \langle x - x_0, zf'(z)\rangle \left(\frac{1}{2\pi|x - x_0|^2} - \frac{1}{2\,\mathrm{vol}\,\Omega}\right)\frac{1}{\pi}\frac{z - z_0}{|z - z_0|^2}\frac{dz}{iz} \\
&= \frac{1}{2\pi i}\int_{\partial B}\left((x - x_0)\overline{zf'(z)} + \overline{x - x_0}zf'(z)\right)\left(\frac{1}{2\pi|x - x_0|^2} - \frac{1}{2\,\mathrm{vol}\,\Omega}\right)\frac{1}{1 - z\overline{z}_0}\,dz \\
&= \frac{1}{4\pi^2 i}\int_{\partial B}\overline{\left(\frac{zf'(z)}{x - x_0}\right)}\frac{1}{1 - z\overline{z}_0}\,dz + \frac{1}{4\pi^2 i}\int_{\partial B}\frac{zf'(z)}{x - x_0}\frac{1}{1 - z\overline{z}_0}\,dz \\
&\quad - \frac{1}{4\pi i\,\mathrm{vol}\,\Omega}\int_{\partial B}(x - x_0)\overline{zf'(z)}\frac{1}{1 - z\overline{z}_0}\,dz - \frac{1}{4\pi i\,\mathrm{vol}\,\Omega}\int_{\partial B}\overline{x - x_0}zf'(z)\frac{1}{1 - z\overline{z}_0}\,dz\,.
\end{aligned}$$
$$(3.99\mathrm{a})$$

This equation is written concisely as

$$\nabla s(z_0) = J_1 + J_2 + J_3 + J_4\,, \qquad (3.99\mathrm{b})$$

where the J_k are, consecutively, the four integrals in the last equality in (3.99a). We now calculate each of these terms.

We first calculate J_2. Using the residue theorem, the relations $x = f(z)$ and $x_0 = f(z_0)$, and the invertibility of f, we readily calculate that

$$J_2 \equiv \frac{1}{4\pi^2 i}\int_{\partial B}\frac{zf'(z)}{x - x_0}\frac{1}{1 - z\overline{z}_0}\,dz = \frac{z_0}{2\pi\left[1 - |z_0|^2\right]}\,. \qquad (3.100)$$

122

To calculate J_1 we use an identity. For any function $H(z)$, it is easy to show that

$$\overline{\frac{1}{2\pi i} \int_{\partial B} H(z)\,dz} = \frac{1}{2\pi i} \int_{\partial B} \overline{H(z)} \frac{1}{z^2}\,dz\,. \tag{3.101}$$

This determines J_1 as

$$J_1 \equiv \frac{1}{4\pi^2 i} \int_{\partial B} \overline{\left(\frac{zf'(z)}{x-x_0}\right)} \frac{1}{1-z\bar{z}_0}\,dz = \frac{f''(\bar{z}_0)}{4\pi f'(\bar{z}_0)}\,. \tag{3.102}$$

To show this, we use $z\bar{z}=1$ for $z \in \partial B$, and (3.101) and (3.102), to get

$$J_1 = \frac{1}{4\pi^2 i} \int_{\partial B} \overline{\left(\frac{f'(z)}{(x-x_0)(z-z_0)}\right)} \frac{1}{z^2}\,dz = \overline{\frac{1}{4\pi^2 i} \int_{\partial B} \frac{f'(z)}{(x-x_0)(z-z_0)}\,dz}\,. \tag{3.103}$$

Using $x = f(z)$ and $x_0 = f(z_0)$, we write (3.103) as

$$J_1 = \overline{\frac{1}{4\pi^2 i} \int_{\partial B} \frac{\phi(z)}{(z-z_0)^2}\,dz}\,, \qquad \phi(z) \equiv \frac{f'(z)(z-z_0)}{f(z)-f(z_0)}\,. \tag{3.104}$$

The function $\phi(z)$ is analytic in B and $\phi'(z_0) = f''(z_0)/\left[2f'(z_0)\right]$. Thus, using the residue theorem, and property (iv) of Theorem 4.1, we get

$$J_1 = \frac{1}{2\pi}\overline{\phi'(z_0)} = \frac{1}{4\pi}\frac{f''(\bar{z}_0)}{f'(\bar{z}_0)}\,. \tag{3.105}$$

This completes the derivation of (3.102).

To calculate J_3 and J_4, we need to evaluate $\text{vol}\,\Omega$ given by

$$\text{vol}\,\Omega = \int_\Omega dx = \int_{\partial\Omega} \frac{1}{2}\langle x, \hat{N}\rangle\,d\Sigma\,. \tag{3.106}$$

Using $d\Sigma = |f'(z)|d\sigma$, $x = f(z)$, $z\bar{z}=1$ on ∂B, and (3.89) for $\hat{N}$ and $d\sigma$, we get

$$\text{vol}\,\Omega = \frac{1}{4i} \int_{\partial B} \overline{f(z)}f'(z)\,dz + \frac{1}{4i} \int_{\partial B} \overline{f'(z)}\frac{f(z)}{z^2}\,dz\,. \tag{3.107}$$

To evaluate (3.107), J_3, and J_4, we need another identity. Let $F(z)$ be any function analytic inside and on the unit disk, and assume that $\overline{F(z)} = F(\bar{z})$. Then

$$I \equiv \frac{1}{2\pi i} \int_{\partial B} \overline{f(z)}F(z)\,dz = -\sum_j \frac{g(z_j)}{z_j^2 h'(z_j)}F(\frac{1}{z_j})\,. \tag{3.108}$$

To show this result, we use (3.101) to write I as

$$I = \frac{1}{2\pi i} \int_{\partial B} \overline{\bar{z}^2 f(z)\overline{F(z)}}\frac{1}{z^2}\,dz = \overline{\frac{1}{2\pi i} \int_{\partial B} \bar{z}^2 f(z)\overline{F(z)}\,dz}\,. \tag{3.109}$$

Since $z\bar{z} = 1$ and $\overline{F(z)} = F(\bar{z}) = F(1/z)$ on ∂B, we get

$$I = \overline{J}, \qquad \text{where} \qquad J \equiv \frac{1}{2\pi i} \int_{\partial B} \frac{f(z) F(1/z)}{z^2} \, dz. \qquad (3.110)$$

Then, since $F(1/z)$ is analytic in $|z| \geq 1$ and $f(z)$ is bounded at infinity by property (ii) of Theorem 4.1, we can evaluate J by integrating the integrand of J over the boundary of the annulus $1 \leq |z| \leq R$ and letting $R \to \infty$. By properties (ii) and (iii) of Theorem 4.1, $f(z) = g(z)/h(z)$ has simple poles at $z = z_j$ with $|z_j| > 1$. Using the residue theorem over the annulus, and letting $R \to \infty$, we obtain

$$J = -\sum_j \frac{g(z_j)}{z_j^2 h'(z_j)} F\left(\frac{1}{z_j}\right). \qquad (3.111)$$

Substituting (3.111) into (3.110) and using $\overline{f(z)} = f(\bar{z})$, $\overline{F(z)} = F(\bar{z})$, and the fact that z_j is a pole of $f(z)$ if and only if $\bar{z}_j$ is, we obtain the result (3.108) for I.

Next, we use (3.101) to write $\text{vol}\,\Omega$ in (3.107) as

$$\text{vol}\,\Omega = \frac{\pi}{2} \left[\frac{1}{2\pi i} \int_{\partial B} \overline{f(z)} f'(z) \, dz + \overline{\frac{1}{2\pi i} \int_{\partial B} \overline{f(z)} f'(z) \, dz} \right]. \qquad (3.112)$$

Then, using (3.108), we can calculate the two integrals in (3.112) to get

$$\text{vol}\,\Omega = -\frac{\pi}{2} \sum_j \left(\frac{g(z_j) f'(\frac{1}{z_j})}{z_j^2 h'(z_j)} + \frac{g(\bar{z}_j) f'(\frac{1}{\bar{z}_j})}{\bar{z}_j^2 h'(\bar{z}_j)} \right) = -\pi \sum_j \frac{g(z_j) f'(\frac{1}{z_j})}{z_j^2 h'(z_j)}. \qquad (3.113)$$

The last equality above follows from property (iv) of Theorem 4.1, which implies that z_j is a pole of $f(z)$ if and only if $\bar{z}_j$ is.

Next, we evaluate J_4 of (3.99a). We calculate that

$$J_4 \equiv -\frac{1}{4\pi i \, \text{vol}\,\Omega} \int_{\partial B} \overline{f(z) - f(z_0)} \, z f'(z) \frac{1}{1 - z\bar{z}_0} \, dz = \frac{1}{2\,\text{vol}\,\Omega} \sum_j \frac{g(z_j) f'(\frac{1}{z_j})}{z_j^2 h'(z_j)(z_j - \bar{z}_0)}. \qquad (3.114)$$

To obtain this result, we use the fact that $z f'(z)/(1 - z\bar{z}_0)$ is analytic in B to get

$$J_4 = -\frac{1}{2\,\text{vol}\,\Omega} \left(\frac{1}{2\pi i} \int_{\partial B} \overline{f(z)} \frac{z f'(z)}{1 - z\bar{z}_0} \, dz \right). \qquad (3.115)$$

The result (3.114) then follows by using the identity (3.108) in (3.115).

124

Lastly, we calculate J_3 of (3.99a). We find,

$$J_3 \equiv -\frac{1}{4\pi i \operatorname{vol}\Omega} \int_{\partial B} [f(z) - f(z_0)] \overline{z f'(z)} \frac{1}{1 - z\bar{z}_0}\, dz$$

$$= \frac{1}{2 \operatorname{vol}\Omega} \sum_j \frac{g(z_j) f'(\frac{1}{z_j})}{h'(z_j) z_j (1 - z_j \bar{z}_0)} + \frac{1}{2 \operatorname{vol}\Omega} f'(\bar{z}_0) \left[f(z_0) - f(\frac{1}{\bar{z}_0}) \right]. \qquad (3.116)$$

To obtain this result, we use (3.101) to rewrite J_3 as

$$\bar{J}_3 = -\frac{1}{2 \operatorname{vol}\Omega} \left(\frac{1}{2\pi i} \int_{\partial B} \overline{f(z) - f(z_0)}\, F(z)\, dz \right), \qquad F(z) \equiv \frac{f'(z)}{z - z_0}. \qquad (3.117)$$

Now we repeat the steps (3.109)–(3.111) used in the derivation of (3.108), except that here we must include the contribution from the simple pole of $F(z)$ at $z = z_0$, which lies inside B. Analogous to (3.110), we obtain

$$J_3 = -\frac{1}{2 \operatorname{vol}\Omega} \left(\frac{1}{2\pi i} \int_{\partial B} \frac{[f(z) - f(z_0)]\, f'(1/z)}{z^2 (z^{-1} - \bar{z}_0)}\, dz \right). \qquad (3.118)$$

Outside the unit disk the integrand has simple poles at $z = z_j$ and at $z = 1/\bar{z}_0$. Integrating over the annulus $1 \le |z| \le R$, using the residue theorem, and then letting $R \to \infty$, we obtain (3.116).

Finally, combining (3.99b) and (3.97), we obtain our result for the gradient of the modified Green's function

$$\nabla R_{m0} \equiv \nabla R_m(x, x_0)|_{x=x_0} = \frac{1}{f'(z_0)} \sum_{k=1}^{4} J_k. \qquad (3.119)$$

Substituting the results for J_k and $\operatorname{vol}\Omega$ given by (3.100), (3.102), (3.113), (3.114), and (3.116), into (3.119), we obtain our main result (3.87) and (3.88). $\qquad \square$

3.3.1 Uniqueness Of The One-Spike Equilibrium Solution For Large D

Consider the following example from [30]:

$$f(z) = \frac{(1 - a^2)z}{z^2 - a^2}. \qquad (3.120)$$

Here a is real and $a > 1$. The resulting domain $\Omega = f(B)$ for several values of a is shown in Fig. 3.4. Notice that $\Omega \to B$ as $a \to \infty$. One can also show that as $\varepsilon \equiv a - 1 \to 0^+$, Ω
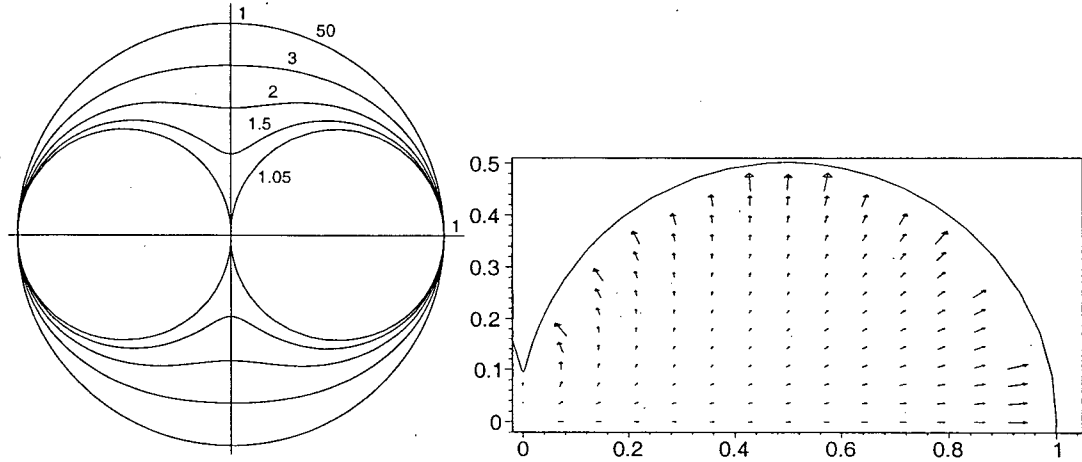
Figure 3.4: Left: The boundary of $\Omega = f(B)$, with $f(z)$ as given in (3.120), for the values of a as shown. Right: The vector field ∇R_{m0} in the first quadrant of Ω with $a = 1.1$.

approaches the union of two circles centered at $(\pm\frac{1}{2}, 0)$, with radius $\frac{1}{2}$, which are connected by a narrow channel of length $2\varepsilon + O(\varepsilon^2)$. From Theorem 3.3.1, we calculate

$$\nabla s(z_0) = \frac{1}{2\pi}\left(\frac{z_0}{1 - |z_0|^2} - \frac{(\bar{z}_0^2 + 3a^2)\,\bar{z}_0}{\bar{z}_0^4 - a^4} + \frac{a^2\bar{z}_0}{\bar{z}_0^2 a^2 - 1} + \frac{\bar{z}_0}{\bar{z}_0^2 - a^2}\right.$$
$$\left. - \frac{(a^4 - 1)^2(|z_0|^2 - 1)(z_0 + a^2\bar{z}_0)(\bar{z}_0^2 + a^2)}{(a^4 + 1)(\bar{z}_0^2 a^2 - 1)(z_0^2 - a^2)(\bar{z}_0^2 - a^2)^2}\right) . \tag{3.121}$$

In the limit $a \to \infty$, $\Omega \to B$, $x_0 \to z_0$, and $f'(0) \to 1$. In this limit, we calculate from (3.87) and (3.121) that

$$\nabla R_{m0} = \frac{1}{2\pi}\left(\frac{2 - |x_0|^2}{1 - |x_0|^2}\right) x_0 . \tag{3.122}$$

This is precisely the formula for ∇R_{m0} on the unit disk, which can be derived readily from (3.94) as was done in [76]. This provides an independent verification of a limiting case of Theorem 3.3.1. We have also verified the formula (3.121) by using the boundary element method to compute ∇R_{m0} for Ω as obtained by the mapping (3.120). The two solutions are graphically indistinguishable.

Next, we calculate from (3.121) that

$$\nabla s(z_0)\big|_{a \to 1^+} = \frac{Re(z_0)}{\pi(1 - |z_0|^2)(\bar{z}_0^2 + 1)} . \tag{3.123}$$

126

In the limit $a \to 1^+$, Ω becomes the union of two disks of radius $1/2$ centered at $(\pm\frac{1}{2}, 0)$. Thus, the unique root of $\nabla s(z_0)|_{a \to 1+} = 0$ in Ω is $z_0 = 0$. This root is easily verified to be a simple root. Hence, it follows from the implicit function theorem that $\nabla s(z_0)$ has a unique root for any $\varepsilon = a - 1 > 0$ small enough. By symmetry, this root must be at the origin. We summarize our result as follows:

Proposition 3.3.2 *Consider a domain $\Omega = f(B)$ with f given by (3.120) as shown in Fig. 3.4. Then for $\varepsilon = a-1 > 0$ small enough, Ω is approximately a union of two disks of radius $\frac{1}{2}$ centered at $(\pm\frac{1}{2}, 0)$, connected by a narrow channel of size $2\varepsilon + O(\varepsilon^2)$. Furthermore, ∇R_{m0} given by (3.84b) has a unique root located at the origin. Thus, in this case, there is a unique equilibrium location for the single-spike solution of (3.16).*

We now show that there are no roots $\nabla s(z_0)$ along the real axis when $a > 1$, except the one at $z_0 = 0$. Thus, there are no equilibrium spike-layer locations in the lobes of the dumbell for any $a > 1$. In (3.121) we let $z_0 = \overline{z}_0 = \xi$, where $-1 < \xi < 1$. After a tedious but straightforward calculation, we get

$$\nabla s(z_0) = \frac{\xi}{2\pi}\mu(\xi), \tag{3.124a}$$

$$\mu(\xi) \equiv \frac{2a^2(a^2+1) - (\xi^2 + a^2)^2}{(a^4 - \xi^4)(1 - \xi^2)} + \frac{1}{a^2\xi^2 - 1}\left[a^2 + \frac{(a^4-1)^2(a^2+1)(\xi^2 + a^2)(\xi^2 - 1)}{(a^4 + 1)(a^2 - \xi^2)^3}\right]. \tag{3.124b}$$

The function μ is even. Thus, to establish our result, we need only show that $\mu(\xi)$ is of one sign on the interval $0 \le \xi \le 1$ for any $a > 1$. A simple calculation shows that the term in the square brackets in (3.124b) vanishes at $\xi = 1/a$. In fact, $\xi = 1/a$ is a removable singularity of μ. It is also easy to show that $\mu(0) > 0$ for any $a > 1$, $\mu \to +\infty$ as $\xi \to 1^-$, and $\mu'(\xi) > 0$ on $0 < \xi < 1$. Hence, for any $a > 1$, $\mu(\xi) > 0$ on $0 \le \xi < 1$. Thus, $\nabla s(z_0)$ has a unique root at $z_0 = 0$. Consequently, there is only one equilibrium spike location, and it is at $z_0 = 0$. This leads us to propose the following conjecture:

Conjecture 3.3.3 *Let Ω be any simply-connected domain, not necessarily convex. Then the gradient ∇R_{m0} of the regular part of the modified Green's function given in (3.84b) has a unique*

127

root inside Ω. Thus, there is a unique equilibrium location of a one-spike solution of (3.16).

In experiments 3 and 4 of §3.4 we consider another example of a non-convex domain that adds further support to this conjecture.

To illustrate the novelty of our conjecture, we consider a similar problem for the conventional Green's function G_d with Dirichlet boundary conditions satisfying

$$\triangle G_d = -\delta(x - x_0) \qquad x \in \Omega\,, \tag{3.125a}$$

$$G_d = 0\,, \qquad x \in \partial\Omega\,. \tag{3.125b}$$

The regular part of G_d and its gradient are defined by

$$R_d(x, x_0) = G_d(x, x_0) + \frac{1}{2\pi} \ln |x - x_0|\,, \qquad \nabla R_{d0} = \nabla R_d(x, x_0)|_{x=x_0}\,. \tag{3.126}$$

It was shown in [30] that

$$f'(z_0) \nabla R_{d0} = -\frac{1}{2\pi} \left(\frac{z_0}{1 - |z_0|^2} + \frac{f''(\overline{z}_0)}{2f'(\overline{z}_0)} \right)\,, \tag{3.127}$$

where $x_0 = f(z_0)$ (compare this result with Theorem 3.3.1). Unlike computing the modified Green's function R_{m0} with Neumann boundary conditions, no knowledge of the singularities of $f(z)$ outside the unit disk is required to compute $R_{d0} = R_d(x_0, x_0)$.

It was shown by several authors (cf. [30], [7]) that for a *convex* domain Ω, the function R_{d0} is convex. Thus, for convex domains, its gradient has a unique root. However the derivation of this result explicitly uses the convexity of the domain. For non-convex domains generated by the mapping (3.120), it was shown in [30] that ∇R_{d0} can have multiple roots. Thus, the Neumann boundary conditions are essential for Conjecture 3.3.3.

From Conjecture 3.3.3 together with (3.85), it follows that for D large enough, there is exactly one possible location for a one-spike equilibrium solution. On the other hand, for a dumbell-shaped domain such as in Fig. 3.4, we know from Proposition 3.2.2, that when D is small enough, the only possible minima of the regular part R_0 of the reduced wave Green's function are near the centers of the lobes of the two dumbells. In Appendix 3.5, we show that $R_0 \to +\infty$

128

as x_0 approaches the boundary of the domain. Hence, R_0 must indeed have a minimum inside the domain. By symmetry, it follows that for D small enough, the centers of both lobes of the dumbell correspond to stable equilibrium locations for the spike dynamics. In addition, it also follows by symmetry and by Proposition 3.2.2 that the origin is an unstable equilibria. Hence, this suggests that a pitchfork bifurcation occurs as D is increased past some critical value D_c. As D approaches D_c from below, the two equilibria in the lobes of the dumbell should simultaneously merge into the origin. For the non-convex domain of experiment 4 in §3.4, this qualitative description is verified quantitatively by using a boundary element method to compute R_0.

3.4 Numerical Experiments and Discussion

In this section we perform numerical experiments to verify the results of this chapter.

In experiments 1 and 2 we compare the asymptotic formulas (3.17), (3.84) and (3.85) with corresponding full numerical solutions of (3.16). In experiment 3 we provide some further numerical evidence for Conjecture 3.3.3. Finally in experiment 4 we will study the effect of the shape of the domain and the constant D on the the existence of spike equilibria location.

The asymptotic results require us to compute R_0, R_{m0}, and their gradients. For experiments 1 and 2 we restrict ourselves to a square domain. For this case R_0 can be computed using the method of images solution (3.58). Equation (3.58) also works well for $D = O(1)$. However, note that the number of terms needed in (3.58) to achieve a specified error bound is directly proportional to D. Therefore the time cost is given by $O(D)$ (the storage cost being constant).

To compute R_0 on a non-square domain (or on a square domain when D is large) as well as to compute R_{m0} on any domain to which Theorem 3.3.1 does not apply, we have adopted a Boundary Element algorithm as described in §8.5 of [4]. Details are given in §3.4.1

To compare with our asymptotic results we use a finite element method to solve (3.16). A standard numerical finite element method code does not perform well over long time intervals due to the very slow movement of the spike and the very steep gradients near the core of

the spike. To overcome this, we have collaborated with Neil Carlson who kindly provided us with his moving-mesh program, `mfe2ds` with adaptive time step (cf. [8], [9]). This has reduced the computer time dramatically, because much fewer mesh nodes or time steps were required. However, the solution obtained from the current version of `mfe2ds`, tends to deviate from the expected solution after a long time period. This is because as the spike moves, it moves the mesh along with it, until eventually the mesh is overstretched (see Fig. 3.5). In spite of this limitation for long-time computations, full numerical results for (3.16) are computed using `mfe2ds`.

3.4.1 Boundary Element method

We now describe the Boundary Element method (BEM) used to compute the regular part $R(x, x_0)$. We write:

$$G(x, x_0) = V(x, x_0) + \tilde{R}(x, x_0) , \qquad V(x, x_0) \equiv \frac{1}{2\pi} K_0 \left(\lambda |x - x_0| \right) . \qquad (3.128)$$

where $K_0(z)$ is the modified Bessel function of order zero. From (3.10) we obtain

$$\tilde{R}(x, x_0) = R(x, x_0) + \frac{1}{2\pi} \left[\log |x - x_0| + K_0 \left(\lambda |x - x_0| \right) \right] \qquad (3.129)$$

Using the local behavior of $K_0(z)$, (3.56b) we obtain

$$\tilde{R}(x, x_0) = R(x, x_0) - \frac{1}{2\pi} \left(\log 2 - \gamma - \log \lambda \right) + o(1) , \quad \text{as} \quad x \to x_0 , \qquad (3.130)$$

where γ is Euler's constant. Therefore, since $\nabla \tilde{R}(x; x_0)|_{x=x_0} = \nabla R(x; x_0)|_{x=x_0}$, it suffices to compute $\tilde{R}(x, x_0)$.

Substituting (3.128) into (3.10), we obtain that $\tilde{R}(x, \xi)$ satisfies

$$\triangle \tilde{R}(x, \xi) - \lambda^2 \tilde{R}(x, \xi) = 0 , \qquad x \in \Omega , \qquad (3.131a)$$

$$\partial_n \tilde{R}(x, \xi) = -\partial_n V(x, \xi) , \qquad x \in \partial\Omega \qquad (3.131b)$$

where $\lambda = \frac{1}{\sqrt{D}}$. The integral representation for $\tilde{R}$ is

$$\tilde{R}(x, \xi) = - \int_{\partial\Omega} G(x, \eta) \partial_n V(\eta, \xi) \, dS(\eta) . \qquad (3.132a)$$

Using (3.128), this can be written as

$$\tilde{R}(x,\xi) = -\int_{\partial\Omega} \tilde{R}(x,\eta)\partial_n V(\eta,\xi)\, dS(\eta) - \int_{\partial\Omega} V(x,\eta)\partial_n V(\eta,\xi)\, dS(\eta)\,. \tag{3.132b}$$

Next, we discretize the boundary $\partial\Omega$ into n pieces $\partial\Omega_1, \cdots, \partial\Omega_n$, and approximate $\tilde{R}(x,\xi) = \tilde{R}(x,\xi_i)$ for $\xi_i \in \partial\Omega_i$, where ξ_i is the midpoint of the arc $\partial\Omega_i$. Letting $\tilde{R}_j = \tilde{R}(x,\xi_j)$, we can then approximate (3.132b) by the dense linear system

$$\tilde{R}_j = \sum_{i=1}^{n} \left(a_{ij}\tilde{R}_i + b_{ij}\right)\,, \tag{3.133a}$$

where

$$a_{ij} = -\int_{\partial\Omega_i} \partial_n V(\eta,\xi_j)dS(\eta)\,, \qquad b_{ij} = -\int_{\partial\Omega_i} V(x,\eta)\partial_n V(\eta,\xi_j)\, dS(\eta)\,. \tag{3.133b}$$

After calculating the solution to (3.133a), we can determine $\tilde{R}(x,x_0)$ by discretizing (3.132b). This leads to

$$\tilde{R}(x,x_0) = -\sum_{i=1}^{n} \left(V(x,\eta_i) + \tilde{R}_i\right)\partial_n V(\eta_i,x_0)l_i\,. \tag{3.134}$$

Here l_i is the length of $\partial\Omega_i$.

It remains to compute the coefficients a_{ij} and b_{ij} in (3.133b). When $i \neq j$ we have

$$a_{ij} = -l_i\partial_n V(\eta_i,\xi_j)\,, \qquad b_{ij} = -l_i V(x,\eta_i)\partial_n V(\eta_i,\xi_j)\,. \tag{3.135}$$

The case $i = j$ requires a special treatment because of the logarithmic singularity of the free-space Green's function V. Let r be the radius of curvature of $\partial\Omega_i$ at ξ_i, and set $\kappa_i = 1/r$. Let $l = l_i$ be the length of $\partial\Omega_i$. Since $\partial\Omega_i$ is small, we may assume that $\partial\Omega_i$ is parametrized for $t \ll 1$ as

$$\eta(t) = r(\cos t, \sin t), \quad -\frac{l}{2r} \leq t \leq \frac{l}{2r}\,, \tag{3.136a}$$

with

$$\xi = \xi_i = (r,0)\,. \tag{3.136b}$$

The asymptotic behavior $V(\eta,\xi) \sim -\frac{1}{2\pi}\log|\eta-\xi| + O(1)$ as $|\eta-\xi| \to 0$ yields

$$\partial_n V(\eta,\xi) \sim -\frac{1}{2\pi}\frac{\eta-\xi}{|\eta-\xi|^2}\cdot\hat{n}\,. \tag{3.137}$$
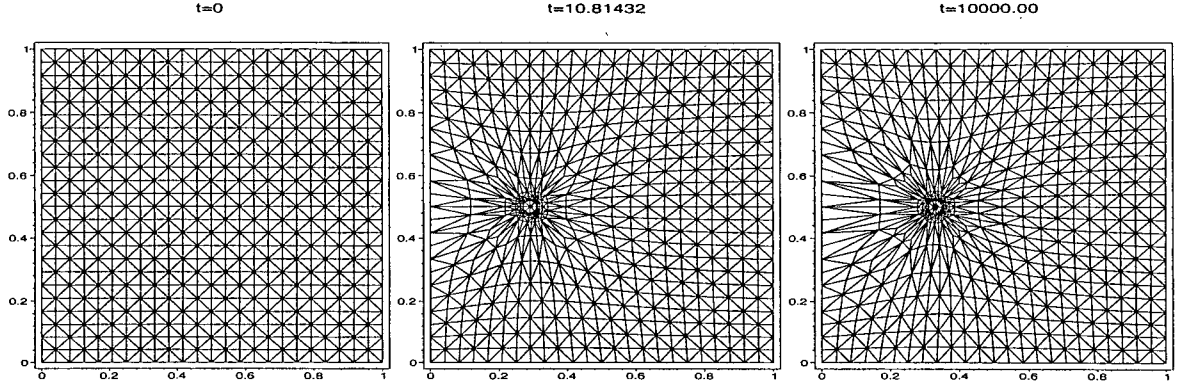
131

Figure 3.5: Numerical solution using the moving mesh method. At the beginning, the mesh vertices concentrate at the spike. Then they move along with the spike, eventually overstretching the mesh geometry and resulting in a loss of precision over a long time period. In this example, $\varepsilon = 0.01, D = 5$, and the initial conditions at $t = 0$ were $a = \text{sech}(|x - (0.3, 0.5)|)$ and $h = 1$.

Since $\hat{n} = (\cos t, \sin t)$ we calculate $(\eta - \xi) \cdot \hat{n} = r(1 - \cos t)$, and $|\eta - \xi|^2 = r^2(2 - 2\cos t)$. Hence, from (3.137),

$$\partial_n V(\eta, \xi) \sim -\frac{1}{4\pi r}, \quad \text{as} \quad r \to 0, \tag{3.138}$$

Therefore, the coefficients a_{ii} and b_{ii} in (3.133b) are

$$a_{ii} = \frac{\kappa_i}{4\pi} l_i, \qquad b_{ii} = a_{ii} V(x, \eta_i). \tag{3.139}$$

3.4.2 Experiment 1: Effect Of ε With $D = 1$.

Fig. 3.6 shows the the peak location $(x(t), 0.5)$ versus time for a unit box $[0, 1]^2$, with $D = 1$ at several values of ε. It shows that the asymptotic approximation (3.17) is very close to the full numerical results when $\varepsilon = 0.01$, and it still gives a reasonable approximation even when $\varepsilon = 0.1$. Presumeably, we would have a much closer agreement at $\varepsilon = 0.1$ if we had retained higher order terms in the infinite logarithmic expansion of a_0, h_0, and the adjoint eigenfunction ψ, in the derivation of (3.17) from (3.39). From Fig. 3.6 we note that the full numerical solution for $x(t)$ seems to settle at something less than 0.5. This is a numerical artifact of the current implementation of the moving mesh code. We think that this is caused by the over-stretching of the mesh topology.
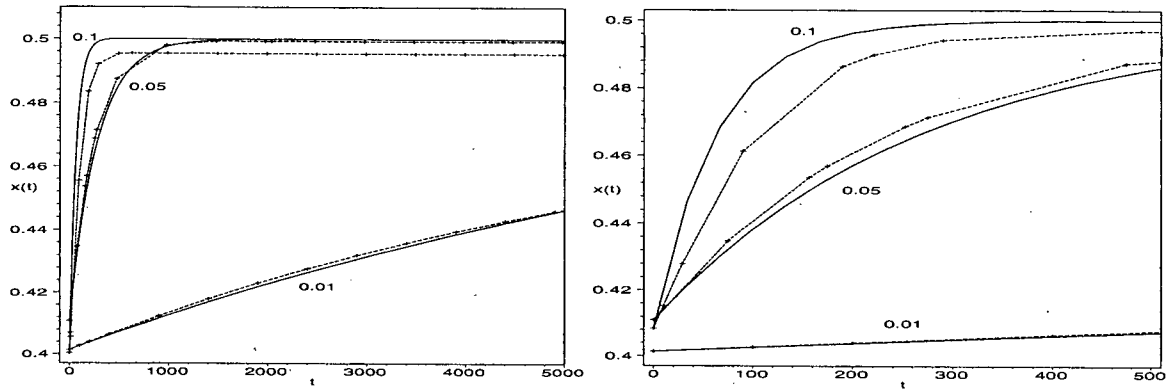
Figure 3.6: Movement of the center $(x(t), 0.5)$ of a single spike of (3.16) within a unit box $[0,1]^2$ versus time t. Here $D = 1$ and $\varepsilon = 0.01, 0.05, 0.01$ as shown. The solid lines show the asymptotic approximation (3.17). The broken lines show the full numerical solution computed using mfe2ds. The figure on the right compares the asymptotic and numerical results on a smaller time interval than the figure on the left.

3.4.3 Experiment 2: Effect Of D With $\varepsilon = 0.01$

Fig. 3.7 shows the peak location $(x(t), 0.5)$ versus time for a unit box $[0,1]^2$, with $\varepsilon = 0.01$ and $D = 1, 3, 5$. For each value of D, the full numerical solution as well as the asymptotic approximations (3.17), (3.84) and (3.85) are shown.

While we assumed in the derivation of (3.84) that $D \gg 1$, the simulation shows that even for $D = 1$, the approximation (3.84) is rather good. Notice that the approximation (3.85), which does not involve any terms involving $-\ln \varepsilon$ and the modified Green's function in the denominator, provides a significantly worse approximation to the spike dynamics than either (3.84) or (3.17). This point was mentioned at the end of §2.

As before, the numerical solution given by mfe2ds seems to deviate from the expected solution after a long time due to excessive mesh stretching. This effect is especially pronounced for larger D. We are currently working with Neil Carlson to address this problem by combining moving mesh with mesh refinement algorithms.
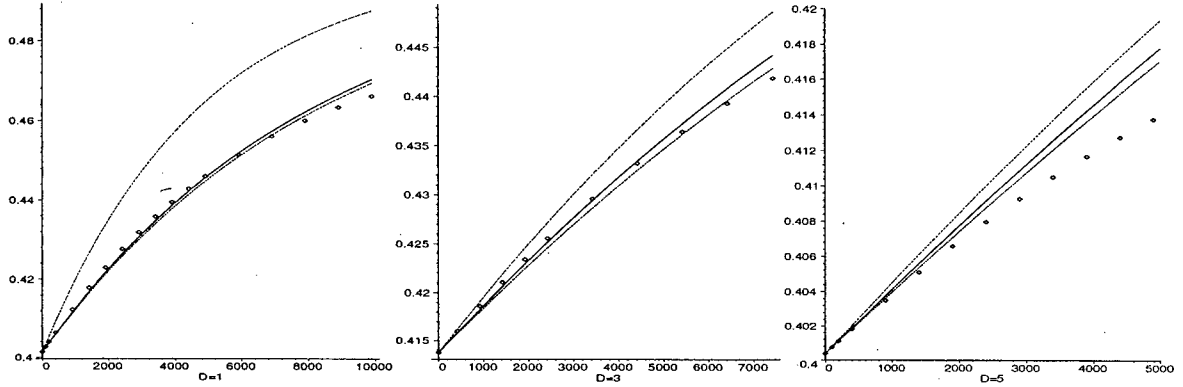
133

Figure 3.7: Movement of the center $(x(t), 0.5)$ of a single spike of (3.16) within a unit box $[0, 1]^2$ versus time t, with $\varepsilon = 0.01$ and $D = 1, 3, 5$. The solid curves show the asymptotic approximation (3.17). The bottom and and top curves show the approximations (3.84) and (3.85), respectively. The diamonds show the results from the full numerical simulation.

3.4.4 Experiment 3: Uniqueness Of Equilibria For Large D

We have used a boundary element method to numerically compute ∇R_{m0} for the non-convex domain Ω shown in Fig. 3.8. There is only one equilibrium solution in Ω and it lies along the imaginary axis as indicated in the figure caption. This provides more evidence for Conjecture 3.3.3.

3.4.5 Experiment 4: A Pitchfork Bifurcation.

In this experiment we consider the dumbell-shaped domain $\Omega = f(B)$ as given by (3.120), and we study the effect of the neck width as well as D on the roots of ∇R_0. To compute ∇R_0 we used the boundary element method described in §3.4.1, discretising the boundary into 200 elements. Since Ω is symmetric we look for spike equilibria that are along the x-axis.

When the dumbbell shape-parameter is $b = 1.2$, and for the values of λ as shown, in Fig. 3.9a we plot R_x along the segment of the positive x-axis that lies within the dumbbell. Notice that there are either one, two, or three spike equilibria on $x \geq 0$ depending on the range of $\lambda = D^{-1/2}$. The resulting subcritical pitchfork bifurcation diagram for the spike equilibria is shown in Fig. 3.9b. Our computations show that there is a pitchfork bifurcation at $\lambda \approx 3.74$, where $\lambda = D^{-1/2}$. Furthermore, there is a fold-point bifurcation of spike equilibria when $\lambda \approx 2.59$. The spike at
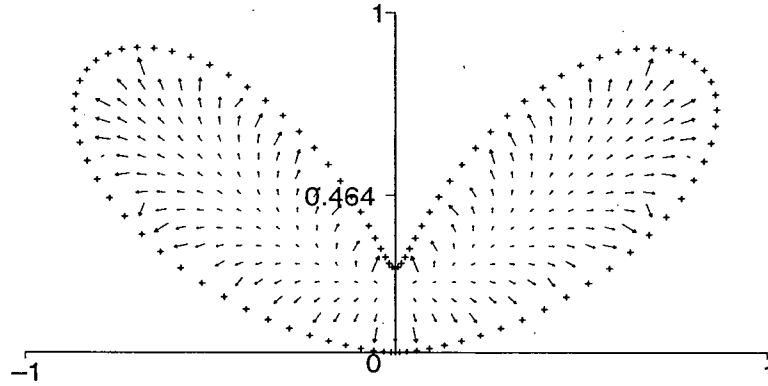
134

Figure 3.8: Plot of ∇R_{m0} for a non-convex domain whose boundary is given by $(x, y) = (\sin^2 2t + \frac{1}{4}\sin t)(\cos(t), \sin(t)), t \in [0, \pi]$. Its center of mass is at about $(0, 0.464)$, which lies outside the domain. The resulting vector field has only one equilibrium, at approximately $(0, 0.2)$. The discretization of the boundary that was used for the boundary element method is also shown.

the origin is stable when $\lambda < 3.74$, and is unstable for $\lambda > 3.74$. In Fig. 3.9b, the upper branch of spike equilibria is stable, while the middle branch is unstable. A subcritical bifurcation diagram of this type has not computed previously. Notice that as $\lambda \to \infty$ $(D \to 0)$, the upper branch corresponds to stable spike equilibria that tend to the lobes of the dumbbell as $D \to 0$.

(a) R_x versus x for $x > 0$
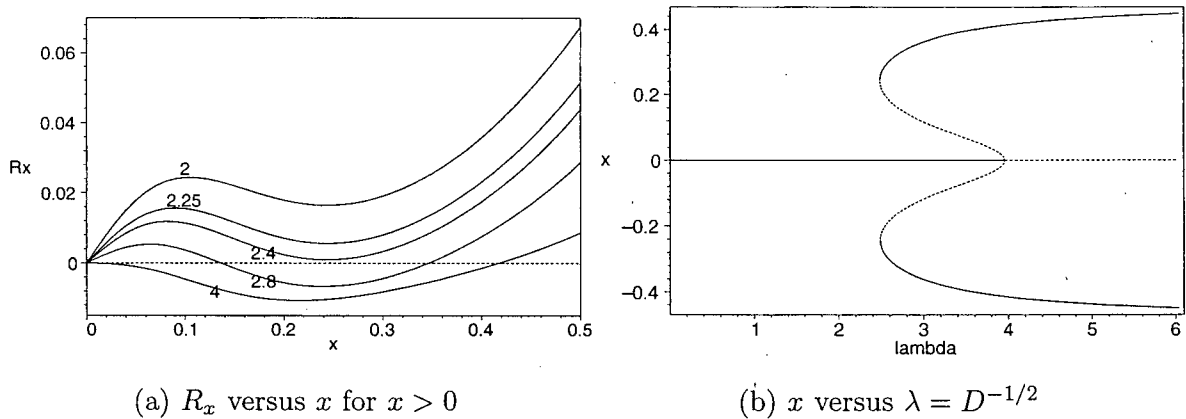
(b) x versus $\lambda = D^{-1/2}$

Figure 3.9: (a) Plot of R_x when x is along the positive real axis, for the values of λ as indicated. The dumbbell shape-parameter is $b = 1.2$. (b) The subcritical bifurcation diagram of the roots of $R_x = 0$ versus $\lambda = D^{-1/2}$ when $b = 1.2$.

Next, we investigate numerically the effect of changing the dumbbell shape-parameter b. In Fig. 3.10 we plot the numerically computed bifurcation diagram of spike equilibria for nine

different values of b. The leftmost curve in this figure correspond to $b = 1.15$. Successive curves, from left to right in Fig. 3.10, correspond to an increment in b of 0.05. Qualitatively, we observe from this figure that the equilibrium spike at the origin has a subcritical bifurcation in λ only when $1 < b < b_c$. For $b > b_c$, the origin has a more conventional supercritical pitchfork bifurcation. We estimate numerically that $b_c \approx 1.4$. Since for $b \to 1^+$ the domain Ω reduces to the union of two disconnected circles each of radius 1/2, Fig. 3.10 suggests that the bifurcation of spike equilibria at the origin is subcritical when the neck of the dumbbell is sufficiently narrow, and is supercritical when the domain is close to a unit circle (b large). It would be interesting to investigate more generally whether certain broad classes of dumbbell-shaped domains with thin necks will always yield subcritical pitchfork bifurcations for a one-spike equilibrium of (3.1) when $D = O(1)$. We remark that the stability properties of the branches of equilibria in Fig. 3.10 are precisely the same as described previously for Fig. 3.10. For each $b > 1$, there is still a stable spike equilibrium that tends to a lobe of the dumbbell as $\lambda \to \infty$ ($D \to 0$).
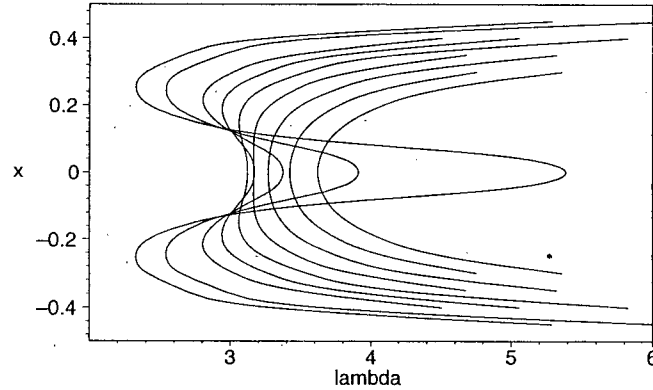
Figure 3.10: Plot of the bifurcation diagram for the spike equilibria versus $\lambda = D^{-1/2}$ for various values of the dumbbell shape-parameter b. The curves from left to right correspond to $b = 1.15$, $b = 1.2$, $b = 1.25$, $b = 1.3$, $b = 1.35$, $b = 1.4$, $b = 1.45$, $b = 1.5$, and $b = 1.55$.

In Fig. 3.11a we plot the bifurcation diagram in the λ versus b parameter plane. From this figure we observe that when $b > 1.4$, there is only one bifurcation value of λ, and it corresponds to the pitchfork bifurcation point for the equilibrium $x_0 = 0$. For $1.15 < b < 1.4$, there are two bifurcation values for λ. The larger value of λ corresponds to the pitchfork bifurcation value, and

the smaller value of λ corresponds to the fold-point value where the middle and upper branches of spike equilibria associated with the subcritical bifurcation coincide. Finally, in Fig. 3.11b, we plot the fold-point value for the spike equilibria as a function of b for $1.15 < b < 1.4$. The non-smoothness of this curve reflects the fact that, due to computational resource limitations, we only had nine data points to fit with a spline interpolation.

(a) $\lambda = D^{-1/2}$ versus b

(b) Fold-point locations x_f versus b

Figure 3.11: (a) Curves of λ versus b where the spike equilibria have either a pitchfork bifurcation or a fold-point bifurcation. (b) Locations x_f of the fold-point bifurcation versus b.
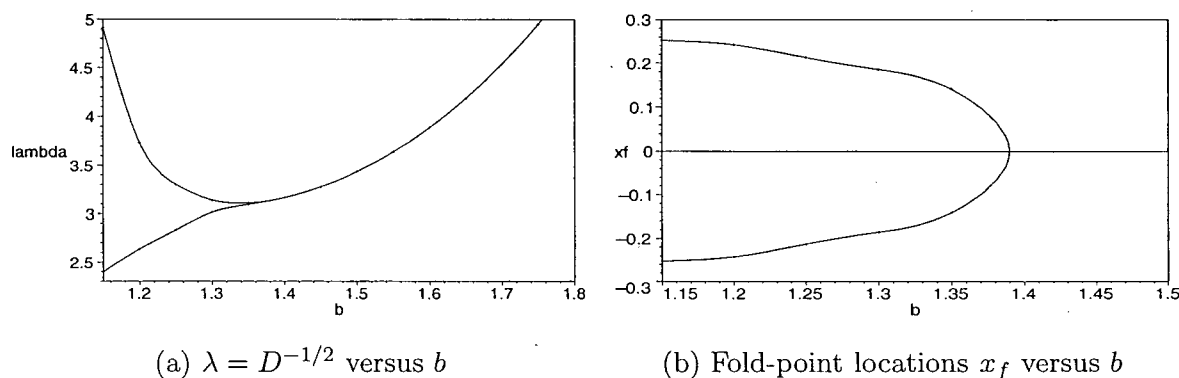
3.4.6 Discussion

There are several open problems that await a rigorous proof. A main conjecture 3.3.3, is that the gradient ∇R_m of the regular part of the modified Green's function with *Neumann* boundary conditions has a unique root in an arbitrary, possibly non-convex, simply-connected bounded domain. In contrast, as was shown in [30], this is not true if Dirichlet boundary conditions are used instead. Many properties of the gradient of the regular part of the Green's function for the Laplacian with Dirichlet boundary condition have been given in the survey [4]. The uniqueness of a root to this gradient with Dirichlet boundary conditions in a *convex* domain is established in [30] and [7]. Our conjecture shows that further work is needed to understand the properties of the regular part of the Green's function associated with a Neumann boundary condition.

A second conjecture, based on §6, is that the zeroes of the gradient ∇R of the reduced wave Green's function will have a subcritical bifurcation with respect to $\lambda = D^{-1/2}$ in a dumbbell-shaped domain, whenever the neck of the dumbbell is sufficiently thin. Alternatively, we conjecture that the zeroes of ∇R will have a supercritical bifurcation in λ when a dumbbell-shaped

137

domain is sufficiently close to a circular domain.

3.5 Appendix: The Behavior Of R_0 On The Boundary

Theorem 3.5.1 *Suppose $\partial\Omega$ is C^2 smooth. Let $x' \in \partial\Omega$ and let $x_0(d) = x' - d\hat{n}$ be the point a distance d away from x' and $\partial\Omega$. Then there exist positive constants C_1, C_2, ε such that*

$$R(x_0, x_0) \geq C_1 \ln\frac{1}{d} + C_2, \qquad (3.140)$$

for all $d \leq \varepsilon$ sufficiently small, where R is given by (3.18).

Proof. When Ω is convex, this theorem was proven in the Appendix of [84]. However, the convexity assumption was critical in their proof. Our proof below does not require this assumption. The proof in [84] utilized a boundary integral representation of R. We use the comparison principle instead.

It suffices to prove this result for R replaced by $\widetilde{R}$. From (3.10) and (3.54), $\widetilde{R}$ satisfies

$$\triangle\widetilde{R}(x, x_0) - \lambda^2\widetilde{R}(x, x_0) = 0, \qquad x \in \Omega; \qquad \partial_n\widetilde{R}(x, x_0) = -\partial_n V(|x - x_0|), \qquad x \in \partial\Omega,$$

where $\lambda \equiv 1/\sqrt{D}$, and

$$V(r) = \frac{1}{2\pi}K_0(\lambda r).$$

By rotating and translating, we may assume that $x_0 = (d, 0)$ and $x' = 0$. We parametrize $\partial\Omega$ by its arclength $x(s)$ with $x(0) = x'$. We let $x_0^r = (-d, 0)$ be the reflection of x_0 in x' and define κ be the curvature of $\partial\Omega$ at x'.

Step 1. Show that

$$\partial_n V(|x - x_0^r|) - C \leq -\partial_n V(|x - x_0|), \qquad (3.141)$$

for some constant C, for all $s, d < \varepsilon$, and ε small enough.

If $\kappa > 0$, then it follows geometrically that for ϵ small enough, $|x - x_0^r| \geq |x - x_0|$ and $-\frac{\langle x - x_0^r, \hat{n}\rangle}{|x - x_0^r|} \leq \frac{\langle x - x_0, \hat{n}\rangle}{|x - x_0|}$. Hence (3.141) follows with $C = 0$ from the monotonicity of V.

138

The case $\kappa < 0$ is more involved. We have,

$$x(s) = \left(\frac{\kappa}{2}s^2 + o(s^3), s + o(s^3)\right), \qquad \hat{n} = \left(-1 + o(s^2), \kappa s + o(s^2)\right),$$

where κ is the curvature at x'. Here and below, $o(s^p, d^q)$ is some function such that $o(s^p, d^q) \leq C(|s|^p + |d|^q)$ for some constant C and for all $|s|, |d| \leq \varepsilon$. For $x = x(s)$, we have

$$\langle x - x_0(d), \hat{n} \rangle = \frac{\kappa}{2}s^2 - d + o(s^2)d + o(s^3),$$

and

$$|x - x_0|^2 = d^2 + s^2(1 - \kappa d) + o(s^3).$$

Next, we calculate that

$$
\begin{aligned}
-\partial_n V(|x - x_0|) &= \frac{1}{2\pi}\frac{\langle x - x_0, \hat{n}\rangle}{|x - x|^2} + o(|x - x_0|) \quad \text{by (3.3b)}, \\
&= \frac{1}{2\pi}\frac{\frac{\kappa}{2}s^2 - d + o(s^2)d + o(s^3)}{d^2 + s^2(1 - \kappa d) + o(s^3)} + o(s, d), \\
&= \frac{1}{2\pi}\frac{\frac{\kappa}{2}s^2 - d + o(s^2)d + o(s^3)}{d^2 + s^2(1 - \kappa d)}\left(1 - \frac{o(s^3)}{d^2 + s^2(1 - \kappa d)} + \dots\right) + o(s, d), \\
&= \frac{1}{2\pi}\left(\frac{\frac{\kappa}{2}s^2 - d}{d^2 + s^2(1 - \kappa d)} + o(s)\right)(1 + o(s)) + o(s, d), \\
&= \frac{1}{2\pi}\frac{\frac{\kappa}{2}s^2 - d}{d^2 + s^2(1 - \kappa d)} + o(s)\frac{d}{d^2 + s^2(1 - \kappa d)} + o(s, d), \\
&= \frac{1}{2\pi}\frac{\frac{\kappa}{2}s^2 - d}{d^2 + s^2}(1 + o(d)) + o(s)\frac{d}{d^2 + s^2} + o(s, d), \\
&= \frac{1}{2\pi}\frac{\frac{\kappa}{2}s^2 - d}{d^2 + s^2} + \frac{o(sd)}{d^2 + s^2} + o(s, d), \\
&= \frac{1}{2\pi}\frac{\frac{\kappa}{2}s^2 - d}{d^2 + s^2} + o(1) + o(s, d).
\end{aligned}
$$

In a similar way, we get

$$\partial_n V(|x - x_0^\tau|) = \frac{1}{2\pi}\frac{-\frac{\kappa}{2}s^2 - d}{d^2 + s^2} + o(1) + o(s, d).$$

Therefore,

$$-\partial_n V(|x - x_0|) \geq \frac{1}{2\pi}\frac{\frac{\kappa}{2}s^2 - d}{d^2 + s^2} + C_1,$$

$$\partial_n V(|x - x_0^\tau|) \leq \frac{1}{2\pi}\frac{-\frac{\kappa}{2}s^2 - d}{d^2 + s^2} + C_2,$$

for some constants C_1, C_2 independent of d, s. Notice that

$$\frac{-\frac{\kappa}{2}s^2 - d}{d^2 + s^2} + \kappa \leq \frac{\frac{\kappa}{2}s^2 - d}{d^2 + s^2} + |\kappa| \, .$$

Hence,

$$\partial_n V(|x - x_0^\tau|) + \frac{\kappa - |\kappa|}{2\pi} + C_1 - C_2 \leq -\partial_n V(|x - x_0|) \, ,$$

which completes the proof of Step 1.

Step 2. By the compactness of the set $(\partial\Omega \backslash \{x(s), |s| < \epsilon\}) \times \{x_0(d), 0 \leq d \leq \varepsilon\}$, the continuity of $V(|x - x_0|)$ on this set, and (3.141), it follows that (3.141) holds for all $x \in \partial\Omega$ and all $d < \epsilon$ if the constant C is large enough.

Step 3. Let $u(x)$ be the solution of

$$\triangle u - \lambda^2 u = 0, \qquad x \in \Omega \, ; \qquad \partial_n u = -C, \qquad x \in \partial\Omega \, ,$$

where C is as in step 2. Then $v = V(|x - x_0^\tau|) + u$ also satisfies $\triangle v - \lambda^2 v = 0$ and $\partial_n v(x) < \partial_n R(x, x_0)$ for $x \in \partial\Omega$ and any d, ϵ. By the maximum principle, it follows that $v(x) < R(x, x_0)$ for $x \in \Omega$. Recalling (3.56b) completes the proof. $\qquad \square$

Chapter 4

Bifurcation of spike equilibria in the near-shadow Gierer-Meinhardt model and near-boundary spikes

In this chapter we continue the study of (3.1), but in the regime where the diffusivity coefficient D becomes exponentially large. The motivation for this is as follows. It is known (see for instance [37]) that when $D = \infty$, a single interior spike will drift exponentially slowly towards the nearest boundary. As such, there is no stable spike equilibria in the interior of the domain. On the other hand, as shown in §3, when D is large enough (but not not exponentially large), there is a unique stable interior equilibrium. The reason for this apparent discrepancy is that the motion of the spike is driven by the superposition of two fields: an exponentially small boundary field which is of $O(\varepsilon^2 e^{-2d/\varepsilon})$ where d is the distance of the spike to the nearest boundary, and the field due to the Green's function whose strength is of $O(\frac{1}{D})$. Thus the boundary only starts to have an effect when $D = O(\varepsilon^{-2} e^{2d/\varepsilon})$. In such a regime, there is a transition between the dynamics driven by the Green's function as discussed in §3, and the dynamics driven by the boundary, as discussed in [37]. The primary purpose of this chapter is to study this transition and the bifurcations that occur therein.

As an example of the complicated bifurcation structure that results, we again consider the dumbell-shaped domain discussed in §3. In Figure 4.1 we schematically illustrate the various bifurcations that occur as D is decreased from infinity to $O(\varepsilon^2)$. Note that the unstable equilibria at $D = \infty$ undergoes a complicated bifurcation structure, resulting in a single stable equilibria at the origin as D is decreased to $1 \ll D \ll \exp(d/\varepsilon)$.

(a) $D = \infty$

(b) $D = O(\varepsilon^2 e^{2d/\varepsilon})$

(c) $-\log \varepsilon \ll D \ll O(\varepsilon^2 e^{2d/\varepsilon})$

(d) $D = O(1)$
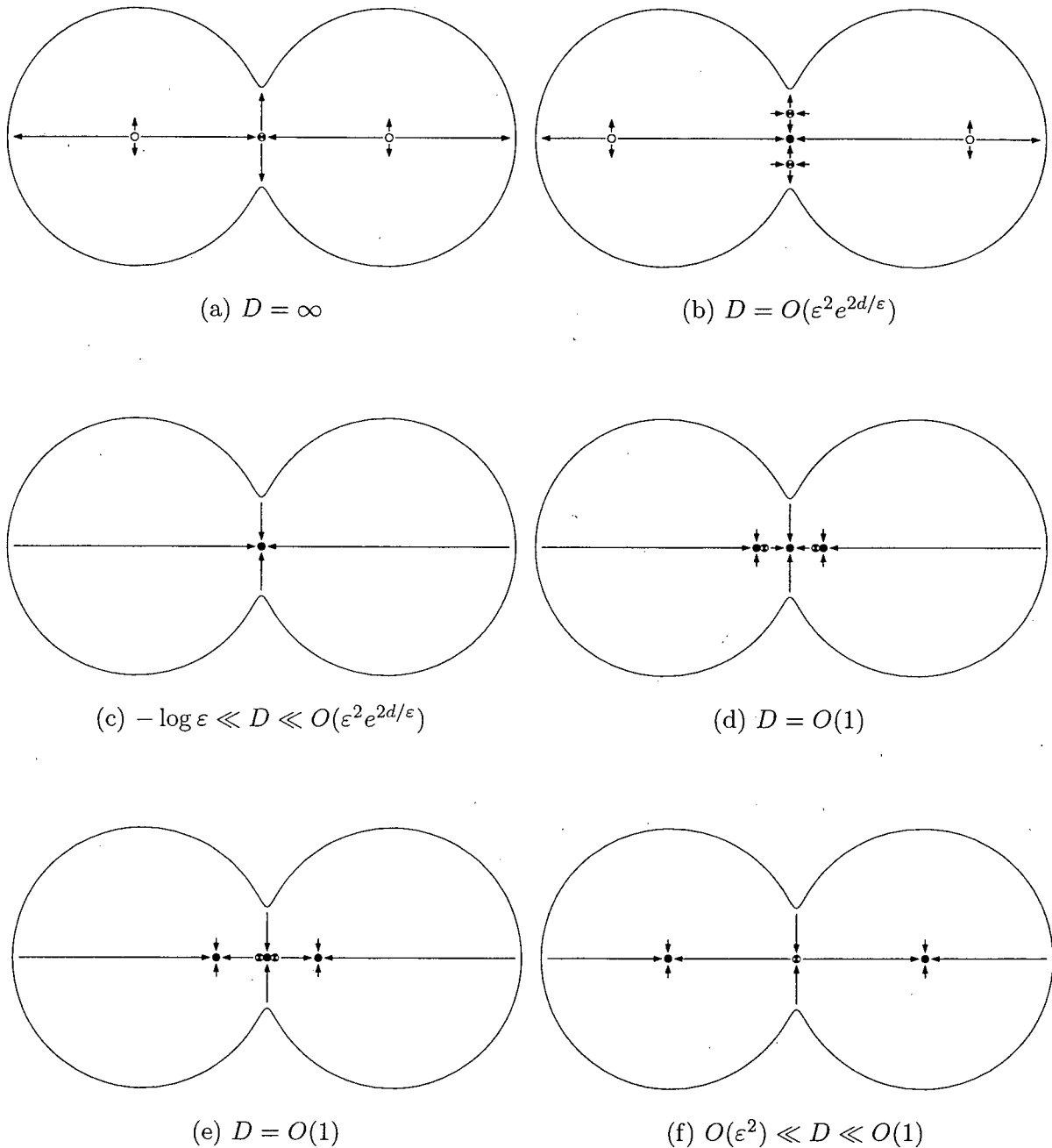
(e) $D = O(1)$

(f) $O(\varepsilon^2) \ll D \ll O(1)$

Figure 4.1: Schematic representations of vector fields and the bifurcations that occur for interior spike solutions in a dumbbell-shaped domain as D is decreased from ∞ to $O(\varepsilon^2)$. Stable equilibria, saddle points, and unstable equilibria correspond to black dots, hatched dots, and white dots, respectively. (a) For the shadow system all equilibria are unstable and correspond to critical points of the distance function from the center of the spike to the boundary. (b) In the intermediate regime, a competition between ∇R_m and the distance function determines the locations of an equilibrium interior spike. (c) For D large, but not exponentially large, there is a unique (stable) spike equilibrium inside the domain located where $\nabla R_m = 0$. (d) For $D = O(1)$ and $O(\varepsilon^2) \ll D \ll O(1)$, an interior spike is located where $\nabla R = 0$. (e) An intricate bifurcation structure may be present in the intermediate regime between (c) and (f). (f) On the range $O(\varepsilon^2) \ll D \ll O(1)$, R can be approximated by the distance function. Thus, in (f) the field is the the same as (a), except that the direction is reversed.

This transition, from a stable interior spike when D is large, to the dynamics driven by the nearest boundary in the case $D = \infty$, is made possible by the existence of what we call *near boundary* spikes, in the transition regime when D is exponentially large. More precisely, we show that there exists a spike equilibria location, at a distance σ from the boundary, whenever $\varepsilon \ll \sigma \ll 1$ and

$$D \sim C(p)q \left(\frac{\varepsilon}{\pi\sigma}\right)^{1/2} |\Omega| e^{2\sigma/\varepsilon}, \tag{4.1}$$

where $C(p)$ is some positive constant depending only on p. We find that such a near-boundary equilibria is always unstable in the radial direction. Its stability in the tangential direction, as well as its location, depends on the behaviour of the modified Green's function at the boundary. For the dumbell example above, we show that there are four such equilibria, two of them stable and two unstable, as shown on Figure 4.2.

We further conjecture that these near-boundary spikes are related to the boundary spike solutions. For the case $D = \infty$, such solution was derived in [38]. There, it was found that a single boundary spike is located at the minimum of the curvature of the boundary. For the case of exponentially large D, we expect that the Green's function on the boundary will also play a role in determining the boundary spike location.
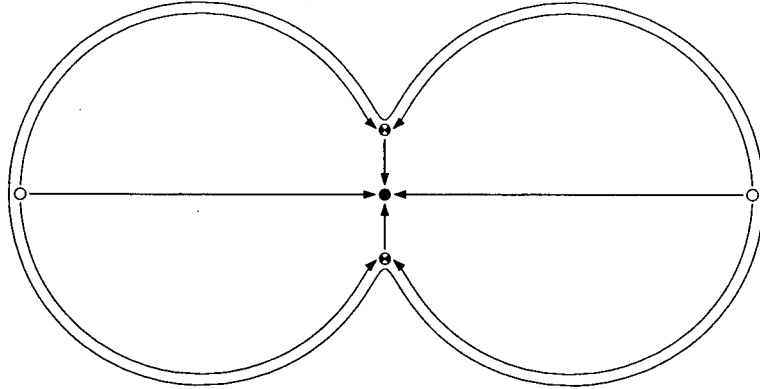

Figure 4.2: Plot of local vector field associated with near-boundary spikes for the transition regime (4.1).

The results of this chapter first appeared in [47].

143

4.1 The dynamics of a spike for exponentially large D

We now outline the derivation of the equation of motion for a spike solution to (3.1) in $\Omega \in \mathbb{R}^2$. We will use the following scaling of (3.1):

$$a_t = \varepsilon^2 \triangle a - a + \frac{a^p}{h^q}, \qquad x \in \Omega, \quad t > 0, \tag{4.2a}$$

$$\tau h_t = D \triangle h - h + \varepsilon^{-2} \frac{a^m}{h^s}, \qquad x \in \Omega, \quad t > 0, \tag{4.2b}$$

$$\partial_n a = \partial_n h = 0, \qquad x \in \partial\Omega. \tag{4.2c}$$

For the shadow problem where $D = \infty$, the spike motion is metastable and is determined by the exponentially weak interaction between the far-field behavior of the spike and the boundary $\partial\Omega$ (cf. [37]). For $D \gg 1$, but with D not exponentially large as $\varepsilon \to 0$, the exponentially weak interaction of the spike with the boundary is insignificant in comparison to the local behavior of the inhibitor field near $x = x_0$, which is determined by the Green's function G_m of (3.81). When D is exponentially large, the dynamics of x_0 is determined by a competition between the exponentially weak interaction of the spike with the boundary and the gradient of the regular part of the modified Green's function. Since this competition is essentially a superposition of the previous results in [37] and §3 (also [46]), we only outline the key steps in the derivation of the dynamics for x_0.

Let $x_0 \in \Omega$, with $\text{dist}(x_0; \partial\Omega) \gg O(\varepsilon)$. For $D \gg 1$, we get from (4.2) that $h \sim \mathcal{H}$ on Ω, and that

$$a \sim \mathcal{H}^\gamma w \left(\varepsilon^{-1} |x - x_0| \right), \qquad \gamma \equiv \frac{q}{p-1}. \tag{4.3}$$

Here the radially symmetric solution $w(\rho)$, with $\rho \equiv |y|$, satisfies

$$w'' + \frac{1}{\rho} w' - w + w^p = 0, \qquad \rho \geq 0, \tag{4.4a}$$

$$w(0) > 0, \quad w'(0) = 0; \quad w(\rho) \sim \alpha \rho^{-1/2} e^{-\rho}, \qquad \text{as} \quad \rho \to \infty, \tag{4.4b}$$

for some $\alpha > 0$. Substituting (4.3) and the expansion $h = \mathcal{H} + h_1/D + \cdots$ into (4.2b), we find

that h_1 satisfies

$$\triangle h_1 = \mathcal{H} - b_m \mathcal{H}^{\gamma m - s} \delta(x - x_0), \qquad x \in \Omega; \qquad \partial_n h = 0, \qquad x \in \partial \Omega, \qquad (4.5)$$

where $b_m \equiv \int_{\mathbb{R}^2} w^m \, dy$. This problem has a solution only when $\mathcal{H}$ satisfies $\mathcal{H}^{\gamma m - (s+1)} = |\Omega|/b_m$, where $|\Omega|$ is the area of Ω. The solution for h_1 is $h_1 = \mathcal{H}|\Omega|G_m$, where G_m satisfies (3.81).

To determine an equation of motion for x_0, we substitute $a = \mathcal{H}^\gamma w(y) + v$ and $h = \mathcal{H} + h_1/D + \cdots$ into (4.2a), where $y = \varepsilon^{-1}[x - x_0(t)]$. Assuming that $v \ll 1$, we then obtain the following quasi steady-state problem for v:

$$L_\varepsilon v \equiv \varepsilon^2 \triangle v - v + p w^{p-1} v = \frac{q|\Omega|\mathcal{H}^\gamma}{D} w^p G_m - \varepsilon^{-1} \frac{(x - x_0)}{|x - x_0|} \cdot x_0' \mathcal{H}^\gamma w', \qquad x \in \Omega, \qquad (4.6a)$$

$$\partial_n v = -\mathcal{H}^\gamma \partial_n w, \qquad x \in \partial \Omega. \qquad (4.6b)$$

As shown in [37], the eigenvalue problem $L_\varepsilon \phi = \lambda_0 \phi$ in Ω, together with $\partial_n \phi = 0$ on $\partial \Omega$, has two exponentially small eigenvalues λ_i, with $i = 1, 2$. The corresponding eigenfunctions have the boundary layer form

$$\phi_i \sim \partial_{x_i} w + \hat{\phi}_i. \qquad (4.7)$$

Here $x = (x_1, x_2)$, and $\hat{\phi}_i$ is a boundary layer function localized near $\partial \Omega$ that allows the no-flux condition for ϕ_i on $\partial \Omega$ to be satisfied. Multiplying (4.6a) by ϕ_i, and integrating over Ω, we let $\varepsilon \to 0$ to get the limiting solvability condition

$$\varepsilon^{-1} x_0' \cdot \int_\Omega \frac{(x - x_0)}{|x - x_0|} w' \partial_{x_i} w \, dx = \frac{q|\Omega|}{D} \int_\Omega G_m w^p \partial_{x_i} w \, dx + \int_{\partial \Omega} \varepsilon^2 \phi_i \partial_n w \, dS, \qquad (4.8)$$

for $i = 1, 2$. Since w is localized near $x = x_0$, we let $y = \varepsilon^{-1}(x - x_0)$ in (4.8), and use the following local behavior for G_m:

$$G_m(x_0 + \varepsilon y, x_0) = -\frac{1}{2\pi} \log(\varepsilon|y|) + R_m(x_0, x_0) + \varepsilon y \cdot \nabla R_{m0} + O(|y|^2). \qquad (4.9)$$

Here $\nabla R_{m0} \equiv \nabla R_m|_{x=x_0}$. In this way, we obtain from (4.8) that

$$x_0' \cdot \int_{\mathbb{R}^2} \frac{y y_i}{|y|^2} \left[w'(|y|) \right]^2 dy = \frac{\varepsilon^2 q|\Omega|}{D(p+1)} \nabla R_{m0} \cdot \int_{\mathbb{R}^2} \frac{y y_i}{|y|} \left[w^{p+1}(y) \right]' dy + \int_{\partial \Omega} \varepsilon^2 \phi_i \partial_n w \, dS, \qquad (4.10)$$

for $i = 1, 2$, where $y = (y_1, y_2)$. The integrals over $\mathbb{R}^2$ in (4.10) were calculated in (3.48). The integral in (4.10) over $\partial \Omega$ was calculated in [37] (see §3.3 of [37]). In this way, we obtain the following main result:

Proposition 4.1.1 *Let $\varepsilon \ll 1$, and assume that $x_0 \in \Omega$ with $dist(x_0; \partial\Omega) \gg O(\varepsilon)$. Then, for D exponentially large as $\varepsilon \to 0$, the spike location x_0 satisfies the differential equation*

$$\frac{dx_0}{dt} \sim \frac{2\varepsilon q}{p-1}\left[\frac{\alpha^2}{2\pi\beta}\left(\frac{p-1}{q}\right)J - \frac{\varepsilon|\Omega|}{D}\nabla R_{m0}\right], \qquad (4.11a)$$

where the vector boundary integral J is defined by

$$J = \int_{\partial\Omega} \frac{\hat{r}}{r}e^{-2r/\varepsilon}\left(1 + \hat{r}\cdot\hat{n}\right)\hat{r}\cdot\hat{n}\,dS\,. \qquad (4.11b)$$

Here $r = |x - x_0|$, and $\hat{r} = (x - x_0)/r$. The constant α is defined in (4.4b) and β is defined by

$$\beta \equiv \int_0^\infty \rho\left[w'(\rho)\right]^2 d\rho\,. \qquad (4.12)$$

The dynamics (4.11) for x_0 expresses a competition between ∇R_{m0}, inherited from the local inhibitor field, and the boundary integral J, representing the exponentially weak interaction between the tail of the spike and the boundary $\partial\Omega$. The dynamics depends on the constants α and β, defined in (4.4b) and (4.12). For several values of p, these constants were computed numerically in [73], with the result

$$
\begin{aligned}
\alpha &= 10.80, & \beta &= 2.47, & p &= 2; \\
\alpha &= 3.50, & \beta &= 1.86, & p &= 3; \\
\alpha &= 2.12, & \beta &= 1.50, & p &= 4.
\end{aligned}
\qquad (4.13)
$$

When $D \gg 1$, but with D not exponentially large as $\varepsilon \to 0$, (4.11) reduces to the gradient flow

$$\frac{dx_0}{dt} \sim -\frac{2\varepsilon^2 q|\Omega|}{D(p-1)}\nabla R_{m0}\,. \qquad (4.14)$$

This limiting result was derived independently in [76] and [14], and was also obtained in §3.2.2. The conjecture 3.3.3 is that $\nabla R_{m0} = 0$ has exactly one root in the interior of an arbitrary, possibly non-convex, bounded and simply-connected domain Ω.

4.2 A Radially Symmetric Domain: D Exponentially Large

In this section we analyze the dynamics and equilibria of a spike solution to the Gierer-Meinhardt model (4.2) in a two-dimensional unit disk $\Omega = \{x : |x| < 1\}$ when D is exponentially large.

We look for a solution to (4.2) that has an interior spike centered at $x_0 \in \Omega$. Since $|\Omega| = \pi$, we obtain from (4.11) that the dynamics of the spike satisfies

$$\frac{dx_0}{dt} \sim \frac{2\varepsilon q}{p-1} \left[\frac{\alpha^2}{2\pi\beta} \left(\frac{p-1}{q} \right) J - \frac{\varepsilon\pi}{D} \nabla R_{m0} \right] , \tag{4.15}$$

where J was defined in (4.11b), and the constants α and β were defined in (4.4b) and (4.12), respectively. For such a ball domain, the gradient of R_{m0} was calculated previously in [76] as

$$\nabla R_{m0} = \frac{1}{2\pi} \left(\frac{2 - |x_0|^2}{1 - |x_0|^2} \right) x_0 . \tag{4.16}$$

By symmetry, we need only look for an equilibrium solution to (4.15) on the segment $x_0 \in [0, 1)$ of the positive real axis. To do so, we need Laplace's formula (cf. [86]) valid for $\varepsilon \ll 1$,

$$\int_{\partial\Omega} r^{-1} F(r) e^{-2r/\varepsilon} \, dS \sim \sum \left(\frac{\pi\varepsilon}{r_m} \right)^{1/2} F(r_m) \left(1 - \kappa_m r_m \right)^{-1/2} e^{-2r_m/\varepsilon} . \tag{4.17a}$$

Comparing (4.11b) with (4.17a), we take

$$F(r) \equiv \hat{r} \left(1 + \hat{r} \cdot \hat{n} \right) \hat{r} \cdot \hat{n} . \tag{4.17b}$$

In (4.17a), $r_m = \text{dist} \left(x_0; \partial\Omega \right)$, κ_m is the curvature of $\partial\Omega$ at x_m, and the sum is taken over all $x_m \in \partial\Omega$ that are closest to x_0. The sign convention is such that $\kappa_m > 0$ if Ω is convex at x_m.

We first suppose that $x_0 \gg O(\varepsilon)$ and that $1 - x_0 \gg O(\varepsilon)$. In this case, the point $(1, 0)$ on $\partial\Omega$ is the unique point closest to x_0. Using (4.17) with $\hat{r} = (1, 0)$, $\hat{n} = (1, 0)$, and $\kappa_m = 1$, we get for $\varepsilon \ll 1$ that

$$J \sim 2 \left(\frac{\pi\varepsilon}{x_0(1 - x_0)} \right)^{1/2} e^{-2\varepsilon^{-1}(1-x_0)} \hat{\imath} , \tag{4.18}$$

where $\hat{\imath} = (1, 0)$.

Next, suppose that $x_0 > 0$ with $x_0 = O(\varepsilon)$. In this case, Laplace's formula (4.17) fails since the asymptotic contribution to J arises from the entire integral over the boundary rather than from a discrete set of points. Parameterizing $\partial\Omega$ by $x = \cos t$ and $y = \sin t$, we calculate for $x_0 \ll 1$ that

$$r = 1 - x_0 \cos t + O \left(x_0^2 \right) ;$$

$$\hat{r} = (\cos t, \sin t) + x_0 \left(-\sin^2 t, \sin t \cos t \right) + O \left(x_0^2 \right) ; \tag{4.19}$$

$$\hat{r} \cdot \hat{n} = 1 + O \left(x_0^2 \right) .$$

Substituting (4.19) into (4.11b), we obtain to leading order that

$$J \sim 2\hat{\imath}\, e^{-2/\varepsilon} \int_0^{2\pi} (\cos t)\, e^{2\varepsilon^{-1} x_0 \cos t}\, dt \,. \tag{4.20}$$

Since the modified Bessel function I_1 of the first kind of order one has the integral representation (cf. [1]),

$$I_1(x) = \frac{1}{2\pi} \int_0^{2\pi} (\cos \theta)\, e^{x \cos \theta}\, d\theta \,, \tag{4.21}$$

we obtain that

$$J \sim 4\pi \hat{\imath}\, e^{-2/\varepsilon} I_1 \left(2x_0/\varepsilon\right) \,. \tag{4.22}$$

This expression is valid for $x_0 = O(\varepsilon)$. When $x_0 \ll O(\varepsilon)$, the asymptotic evaluation of J is obtained by using the local behavior $I_1(z) \sim z/2$ as $z \to 0$ in (4.22). This yields,

$$J \sim 4\pi \varepsilon^{-1} \hat{\imath}\, x_0 e^{-2/\varepsilon} \,. \tag{4.23}$$

Using $I_1(z) \sim (2\pi z)^{-1/2} e^z$ in (4.22), we obtain that the far-field form of (4.22) for $x_0 \gg O(\varepsilon)$ agrees with the leading order behavior of (4.18) as $x_0 \to 0$. Combining (4.18) and (4.22), we can write a uniformly valid leading order approximation to J as

$$J \sim \frac{4\pi \hat{\imath} e^{-2/\varepsilon}}{\sqrt{1 - x_0}} I_1 \left(2x_0/\varepsilon\right) \,. \tag{4.24}$$

This formula is valid for $x_0 \geq 0$, with $1 - x_0 \gg O(\varepsilon)$.

The origin $x_0 = 0$ is an equilibrium point for (4.15) for any $D > 0$. Using (4.23) and (4.16) we can write the local behavior for (4.15) when $x_0 \ll 1$ as

$$\frac{dx_0}{dt} \sim \frac{2\varepsilon^2 q}{(p-1)D} \left(\frac{D}{D_c} - 1 \right) x_0 \,, \tag{4.25a}$$

where D_c is defined by

$$D_c = \frac{\varepsilon^2 q \beta}{2\alpha^2 (p-1)} e^{2/\varepsilon} \,. \tag{4.25b}$$

Hence, the equilibrium $x_0 = 0$ is unstable when $D > D_c$, and is stable when $D < D_c$. The constants α and β in (4.25b) are given for various p in (4.13). Substituting (4.16) and (4.24) into (4.15), we obtain the following main result:

148

Proposition 3.1: *Let $\varepsilon \ll 1$ and assume that the spike location x_0 within the unit ball is along the segment of the real axis satisfying $x_0 \geq 0$ with $1 - x_0 \gg O(\varepsilon)$. Then, the trajectory $x_0(t)$ of an interior spike solution satisfies*

$$\frac{dx_0}{dt} \sim \frac{2\varepsilon^2 q}{(p-1)D}\left[\frac{D}{D_c} - \frac{1}{H(x_0)}\right] \frac{\varepsilon I_1(2x_0/\varepsilon)}{\sqrt{1-x_0}}, \tag{4.26a}$$

where D_c is defined in (4.25b), and $H(x_0)$ is defined by

$$H(x_0) \equiv \frac{\varepsilon\sqrt{1-x_0}(1+x_0)I_1\left(2x_0/\varepsilon\right)}{x_0\left(1 - x_0^2/2\right)}. \tag{4.26b}$$

Since $H(0) = 1$, the equilibrium location $x_0 = 0$ is stable when $D < D_c$ and is unstable when $D > D_c$. On the range $x_0 > 0$ with $1 - x_0 \gg O(\varepsilon)$, for each $D < D_c$ there is a unique unstable equilibrium solution to (4.26a) satisfying

$$\frac{D_c}{D} = H(x_0). \tag{4.27}$$

The local behavior of the bifurcating branch, obtained by setting $y = x_0/\varepsilon$ in (4.27), is given by

$$\frac{D}{D_c} = \frac{y}{I_1(2y)}. \tag{4.28}$$

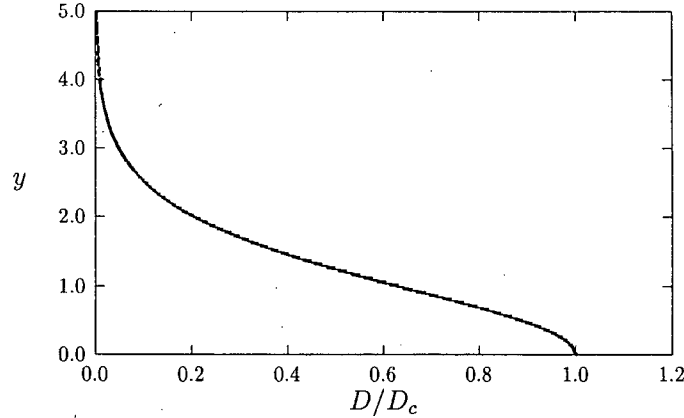Figure 4.3: Plot of the local bifurcation diagram (4.28) where $y = x_0/\varepsilon$.

In Fig. 4.3 we plot the local bifurcation behavior (4.28). Qualitatively, we see that, except within an $O(\varepsilon)$ neighborhood of $x_0 = 1$ where (4.27) is not valid, (4.27) shows that the ratio D_c/D increases as x_0 increases. Therefore, the unstable spike, which bifurcated from $x_0 = 0$ at

149

the value $D = D_c$, moves towards the boundary of the circle as D decreases below D_c. From (4.25b), the critical value D_c is exponentially large as $\varepsilon \to 0$ and depends on the parameters α and β given numerically in (4.13).

Since our analysis has only considered interior spike solutions that interact exponentially weakly with the boundary, we cannot describe the process by which the unstable interior spike merges onto the boundary of the unit ball at some further critical value of D. However, using (4.27) we can give an estimate of the value of D for which a spike approaches to within an $O(\sigma)$ neighborhood of the boundary, where $\varepsilon \ll \sigma \ll 1$. Let $x_0 = 1 - \sigma$ in (4.27). A simple calculation using (4.25b), (4.26b), and the large argument expansion of $I_1(z)$, yields

$$D \sim \frac{\beta\sqrt{\pi}}{4\alpha^2} \left(\frac{q}{p-1} \right) \left(\frac{\varepsilon}{\sigma} \right)^{1/2} e^{2\sigma/\varepsilon} . \tag{4.29}$$

Since we have specified $x_0 \in (0, 1]$ at the outset of the analysis, our bifurcation analysis cannot determinine the direction in which the equilibrium spike moves towards the boundary as D is decreased. This degeneracy in the fundamental problem can be broken by a slight perturbation in the shape of the domain. A resulting imperfection senstitivity analysis would presumeably be able to resolve the degeneracy and determine a unique direction for the bifurcating spike.

4.3 A Dumbbell-Shaped Domain: D Exponentially Large

When D is exponentially large, we now analyze the dynamics and equilibria of a one-spike solution to (4.2) with $\tau = 0$ in a one-parameter family of dumbbell-shaped domains introduced in [30] and studied further in §3.3.1. There, we considered a family of domains given by $\Omega = f(\mathcal{B})$ where $\mathcal{B} = \{z : |z| < 1\}$ is the unit disk in a complex plane and

$$w = f(z) = \frac{(1 - b^2)z}{z^2 - b^2} . \tag{4.30}$$

Here b is real and $b > 1$. The resulting domain $\Omega = f(\mathcal{B})$ is shown in Figure 3.4 for several values of b. Notice that $\Omega \to \mathcal{B}$ as $b \to \infty$. Moreover, as $\delta \equiv b - 1 \to 0^+$, Ω approaches the union of two circles centered at $(\pm 1/2, 0)$, with radius $1/2$, that are connected by a thin neck region of width $2\delta + O(\delta^2)$. This class of dumbbell-shaped domains is symmetric with respect

to both the x and y axes. Therefore, when $D = \infty$, and for a certain range of b, we expect that there will be three equilibrium one-spike solutions, one centered at the origin and the other two centered on the x-axis in the lobes of the dumbbell. It is easy to show that Ω is non-convex only when $1 < b < b_c \equiv 1 + \sqrt{2}$.

Let x_0 be the location of a one-spike solution to (4.2) in Ω, with pre-image point $z_0 \in \mathcal{B}$ satisfying $x_0 = f(z_0)$. Recall from 3.3.1 that ∇R_{m0} as defined in (4.9) is given by:

$$\nabla R_{m0} = \frac{\nabla s(z_0)}{\overline{f'(z_0)}}, \tag{4.31a}$$

where

$$\nabla s(z_0) = \frac{1}{2\pi} \left(\frac{z_0}{1 - |z_0|^2} - \frac{2b^2 \bar{z}_0}{\bar{z}_0^4 - b^4} + \frac{b^2 \bar{z}_0}{\bar{z}_0^2 b^2 - 1} - \frac{(b^4 - 1)^2 (|z_0|^2 - 1)(z_0 + b^2 \bar{z}_0)(\bar{z}_0^2 + b^2)}{(b^4 + 1)(\bar{z}_0^2 b^2 - 1)(z_0^2 - b^2)(\bar{z}_0^2 - b^2)^2} \right), \tag{4.31b}$$

and

$$f'(z_0) = (b^2 - 1)\frac{(z_0^2 + b^2)}{(z_0^2 - b^2)^2}, \qquad x_0 = f(z_0). \tag{4.31c}$$

In (4.31), we interpret vectors as complex numbers so that $\nabla R_{m0} = \partial_x R_{m0} + i \partial_y R_{m0}$. The area $|\Omega|$ of Ω, which is needed below, was also derived in 3.3.1 to be

$$|\Omega| = \pi \frac{(b^4 + 1)}{(b^2 + 1)^2}. \tag{4.32}$$

Note that $|\Omega| \to \pi$ as $b \to \infty$, and $|\Omega| \to \pi/2$ as $b \to 1^+$, when Ω reduces to two circles each of radius $1/2$.

The dynamics and equilibria of a one-spike solution to (4.2) in Ω is obtained by substituting (4.31) and (4.32) into (4.11). We show below that the bifurcation behavior of equilibria to (4.11) is as sketched in Figure 4.1. In §4.3.1 we analyze this behavior for the equilibrium spike located at the origin $(0,0)$ in the neck region of the dumbbell. In §4.3.2 we analyze equilibrium spikes in the lobes of the dumbbell.

4.3.1 The Neck Region of the Dumbbell

When $D = \infty$, the equilibrium spike solution at the origin is unstable. However, as we show below, as D decreases below some critical value D_c this equilibrium solution regains its stability,

151

and new unstable equilibria appear at the points $(0, \pm y_0)$ in Ω for some $y_0 > 0$. These equilibria move along the vertical axis towards the boundary $\partial\Omega$ as D is decreased below D_c (see Figure 4.1(b)).

To analyze the spike behavior, we must calculate the integral J in (4.11) asymptotically. To do so, we parameterize $\partial\Omega$ by letting $z = e^{it}$, for $-\pi \le t < \pi$, and $w(t) = f\left(e^{it}\right) = \xi(t) + i\eta(t)$. Using (4.30), we calculate

$$\xi(t) = \frac{(b^2 - 1)^2 \cos t}{b^4 + 1 - 2b^2 \cos 2t}, \qquad \eta(t) = \frac{(b^4 - 1)\sin t}{b^4 + 1 - 2b^2 \cos 2t} . \tag{4.33}$$

For a spike located at $(0, y_0)$ in Ω, with $y_0 > 0$ but small, the dominant contribution to J arises from the points corresponding to $t = \pm\pi/2$, labelled by $(0, \pm y_m)$, where

$$y_m = \left(\frac{b^2 - 1}{b^2 + 1}\right) . \tag{4.34}$$

A simple calculation using (4.33) shows that the curvature κ_m of $\partial\Omega$ at $(0, \pm y_m)$ is

$$\kappa_m = \frac{\xi'\eta'' - \eta'\xi''}{[\eta'^2 + \xi'^2]^{3/2}}\bigg|_{t=\pm\pi/2} = \left(\frac{b^2 + 1}{b^2 - 1}\right)^3 \left[1 - \frac{8b^2}{(b^2 + 1)^2}\right] . \tag{4.35}$$

By symmetry, the vector integral J in (4.11) has the form $J = (0, J_2)$. When $y_0 \ll y_m - \varepsilon$, we evaluate the integral J asymptotically in (4.11) for $\varepsilon \to 0$, to obtain

$$J_2 \sim 2\sqrt{\pi\varepsilon}\, e^{-2y_m/\varepsilon} \left[\frac{e^{2y_0/\varepsilon}}{\sqrt{r_{m1}(1 - \kappa_m r_{m1})}} - \frac{e^{-2y_0/\varepsilon}}{\sqrt{r_{m2}(1 - \kappa_m r_{m2})}}\right] , \tag{4.36a}$$

where

$$r_{m1} = y_m - y_0 , \qquad r_{m2} = y_m + y_0 . \tag{4.36b}$$

When $|y_0| = O(\varepsilon)$, we calculate

$$J_2 \sim 4\left(\frac{\pi\varepsilon}{y_m(1 - \kappa_m y_m)}\right)^{1/2} e^{-2y_m/\varepsilon} \sinh\left(2y_0/\varepsilon\right) . \tag{4.37}$$

Next, we calculate ∇R_{m0} near the origin. Let $z_0 = iv_0 \in \mathcal{B}$, and $w_0 = iy_0 \in \Omega$. Since $w = f(z)$, we calculate that

$$v_0 = \frac{(b^2 - 1)}{2y_0} - \left[\left(\frac{b^2 - 1}{2y_0}\right)^2 - b^2\right]^{1/2} , \tag{4.38a}$$

152

and

$$y_0 \sim f'(0)v_0, \qquad \text{where} \qquad f'(0) = \frac{(b^2 - 1)}{b^2}, \qquad \text{as} \quad v_0 \to 0. \qquad (4.38b)$$

Using (4.32) and (4.38b), we can calculate $|\Omega|\partial_y R_{m0}$ in (4.31) in terms of y_0 for $|y_0| \ll 1$. A simple, but lengthy, calculation yields that

$$|\Omega|\partial_y R_{m0} = y\mathcal{G}(b), \qquad \mathcal{G}(b) = \frac{(b^2 - 1)}{2(b^4 - 1)^2} \left[2b^6 + 3b^4 + 2b^2 - 1\right]. \qquad (4.39)$$

Substituting (4.37) and (4.39) into (4.11a), we obtain the following main result:

Proposition 4.3.1 *Let $\varepsilon \ll 1$ and assume that the spike location $(0, y_0)$ on the y-axis satisfies $y_0 = O(\varepsilon)$. Then, the local trajectory $y_0(t)$ satisfies*

$$\frac{dy_0}{dt} \sim \varepsilon^{1/2} \mu_0 e^{-2y_m/\varepsilon} \left[\frac{\sinh(2y_0/\varepsilon)}{(2y_0/\varepsilon)} - \frac{D_c}{D}\right] y_0, \qquad (4.40a)$$

where D_c and μ_0 satisfy

$$D_c = \frac{\varepsilon^2 \beta}{4\alpha^2} \left(\frac{q}{p-1}\right) \left(\frac{\pi}{\varepsilon}\right)^{1/2} [y_m(1 - \kappa_m y_m)]^{1/2} \mathcal{G}(b)e^{2y_m/\varepsilon}, \qquad (4.40b)$$

$$\mu_0 = \frac{8\alpha^2}{\sqrt{\pi}\beta} [y_m(1 - \kappa_m y_m)]^{-1/2}. \qquad (4.40c)$$

When $D > D_c$, $y_0 = 0$ is the unique, and unstable, equilibrium solution for (4.40a). For $D < D_c$, $y_0 = 0$ is stable, and there are two unstable equilibria with $|y_0| = O(\varepsilon)$, satisfying

$$\frac{2\zeta}{\sinh(2\zeta)} = \frac{D}{D_c}, \qquad \zeta = y_0/\varepsilon. \qquad (4.41)$$

The bifurcation value D_c depends on the dumbbell shape-parameter b, and on α and β defined in (4.4b) and (4.12), respectively. The values α and β were computed numerically in (4.13) for a few exponents p. In the limiting case $b - 1 = \delta \to 0^+$, we calculate from (4.34), (4.35), and (4.39), that

$$y_m \to \delta, \qquad \kappa_m \to -\delta^{-3}, \qquad \mathcal{G} \to 3\delta^{-1}/8, \qquad \text{as} \quad \delta \to 0^+. \qquad (4.42)$$

Substituting (4.42) into (4.40b), we obtain

$$D_c \sim \frac{3\beta\sqrt{\pi}}{32\alpha^2} \left(\frac{q}{p-1}\right) \left(\frac{\varepsilon}{\delta}\right)^{3/2} e^{2\delta/\varepsilon}, \qquad \text{as} \quad \delta \to 0^+. \qquad (4.43)$$

153

This limiting formula for the bifurcation point is valid for $0 < \varepsilon \ll \delta \ll 1$.

Next, we determine the global bifurcation branch for $y_0 > 0$ with $O(\varepsilon) \ll y_0 \ll y_m - O(\varepsilon)$. We set $z_0 = iv_0$ in (4.31b) with $0 < v_0 < 1$. From (4.31b) and (4.32), we then obtain

$$|\Omega|\partial_y R_{m0} = v_0 \chi_I(b; v_0),$$ (4.44)

where $\chi_I(b; v_0)$ is defined by

$$\chi_I(b; v_0) \equiv \frac{(b^4 + 1)(b^2 - 1)}{2(b^4 - 1)^2} \frac{(b^2 + v_0^2)^2}{(b^2 - v_0^2)}$$
$$\times \left[\frac{(1 + b^2)}{(1 - v_0^2)(1 + b^2 v_0^2)} + \frac{2b^2}{v_0^4 - b^4} - \frac{(b^4 - 1)^2(b^2 - 1)(1 - v_0^2)(b^2 - v_0^2)}{(b^4 + 1)(1 + b^2 v_0^2)(b^2 + v_0^2)^3} \right].$$ (4.45)

Here $v_0 = v_0(y_0)$ is given by (4.38a). Comparing (4.44) with the local behavior (4.39), and using $y_0 \sim f'(0)v_0$ for $v_0 \ll 1$, it follows that

$$\chi_I(b; 0) = \mathcal{G}(b)f'(0),$$ (4.46)

where $\mathcal{G}(b)$ is defined in (4.39). As $v_0 \to 1^-$, or equivalently $y_0 \to y_m^-$, $\partial_y R_{m0} \to +\infty$. From (4.45), we calculate

$$\chi_I(b; v_0) \sim \frac{(b^4 + 1)}{4(b^2 - 1)^2}(1 - v_0)^{-1}, \qquad \text{as} \quad v_0 \to 1^-.$$ (4.47)

On the range $y_0 > 0$ with $O(\varepsilon) \ll y_0 \ll y_m - O(\varepsilon)$, the term in (4.36a) proportional to $e^{-2y_0/\varepsilon}$ can be neglected. To determine the dynamics of y_0 on this range, we substitute (4.36a), and (4.45), into (4.11). After some algebra, we get

$$\frac{dy_0}{dt} \sim \varepsilon^{1/2} \mu_0 e^{-2y_m/\varepsilon} \left[\left(\frac{C(y_m)}{C(r_m)} \right) \frac{e^{2y_0/\varepsilon}}{(4v_0/\varepsilon)} - \frac{D_c}{D} \left(\frac{\chi_I(b; v_0)}{\mathcal{G}(b)} \right) \right] v_0,$$ (4.48a)

where $r_m = y_m - y_0$. Here D_c and μ_0 are defined in (4.40), and the function $C(s)$ is defined by

$$C(s) = [s(1 - \kappa_m s)]^{1/2}.$$ (4.48b)

The equilibria of (4.48a) satisfy

$$\frac{D}{D_c} = 4v_0 \varepsilon^{-1} \left(\frac{C(r_m)}{C(y_m)} \right) \left(\frac{\chi_I(b; v_0)}{\mathcal{G}(b)} \right) e^{-2y_0/\varepsilon}.$$ (4.49)

Using the formula (4.38a) for $v_0 = v_0(y_0)$, we can write D/D_c as a function of y_0. For $\varepsilon \ll 1$, the right-hand side of (4.49) is a decreasing function of y_0. Thus, D is a decreasing function of y_0.

154

4.3.2 The Lobe Region of the Dumbbell

Next, we analyze the behavior of an equilibrium spike in the right lobe $\mathcal{L}$ of the dumbbell as D is decreased from infinity. Let $\mathcal{R}$ denote the largest inscribed circle within $\mathcal{L}$. Let x_{in} and r_{in} denote the center and radius of $\mathcal{R}$, respectively. For $b = 1.8$, in Fig. 4.4 we show the right lobe $\mathcal{L}$ and the largest inscribed circle $\mathcal{R}$, with center on the x-axis.

When $D = \infty$, the location x_0 of an equilibrium spike satisfies $J = 0$, where J is defined in (4.11). To leading order as $\varepsilon \to 0$, $x_0 \sim x_{\mathrm{in}}$ satisfies $J = 0$. The correction term is of $O(\varepsilon)$ and may also be computed as in [73]. Therefore, to leading order, it suffices to determine x_{in}.
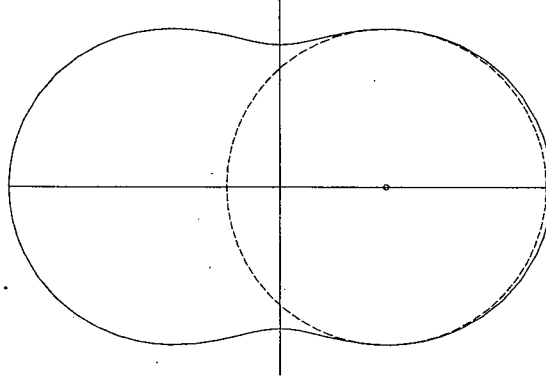

Figure 4.4: The domain Ω with $b = 1.8$ and the largest inscribed circle $\mathcal{R}$ inside its right lobe $\mathcal{L}$.

The largest inscribed circle $\mathcal{R}$ makes two-point contact with $\partial\Omega$ at $x_c = (\xi_c, \pm\eta_c)$, with $\eta_c > 0$. These points are such that the normal to $\partial\Omega$ at x_c is parallel to the y-axis. From (4.33), this implies that $\eta' = 0$. We write (4.33) as

$$\xi(t) = \frac{(b^2 - 1)^2}{\chi} \cos t, \qquad \eta(t) = \frac{(b^4 - 1)}{\chi} \sin t, \tag{4.50a}$$

where

$$\chi \equiv b^4 + 1 - 2b^2 \cos(2t) = (b^2 + 1)^2 - 4b^2 \cos^2 t. \tag{4.50b}$$

Setting $\eta' = 0$, we get

$$\sin^2 t = \frac{\chi}{8b^2}, \qquad \text{or} \qquad \cos t = 0. \tag{4.51}$$

Two roots are $t = \pm\pi/2$. Combining (4.51) and (4.50b), we get $\chi = 2(b^2 - 1)^2$, and that the

155

other root satisfies

$$\cos^2 t = \frac{[6b^2 - (b^4 + 1)]}{4b^2} .$$

(4.52)

Substituting (4.52) into (4.50), we obtain that the contact points satisfy

$$(\xi_c, \pm \eta_c) = \left(\frac{1}{4b} \left[6b^2 - (b^4 + 1) \right]^{1/2} , \pm \frac{(b^2 + 1)}{4b} \right) .$$

(4.53)

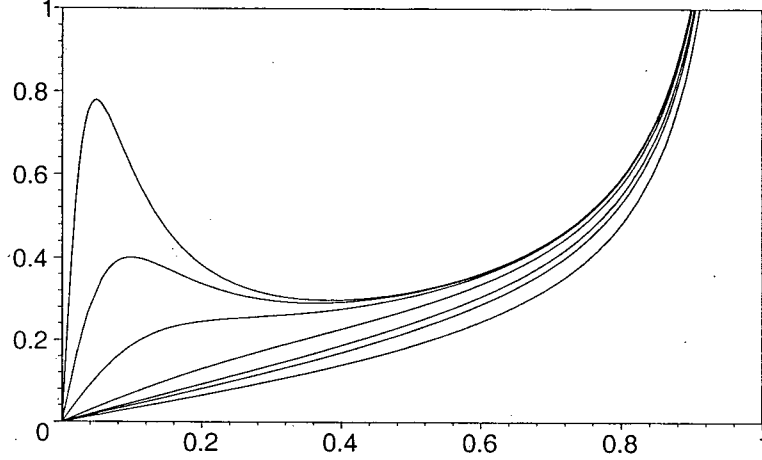Hence, $x_{in} = (\xi_c, 0)$, and $r_{in} = \eta_c$.

Figure 4.5: Plot of $\partial_x R_{m0}(x, 0)$ versus x for $b = 1.05, 1.1, 1.2, 1.5, 2, 2.5, \infty$. The top (bottom) curve corresponds to $b = 1.05$ (∞), respectively. Note that $\partial_x R_{m0}(x, 0)$ is positive on the positive x-axis.

The formula (4.53) is valid only when $6b^2 - (b^4 + 1) > 0$. Therefore, we require that $1 < b < b_c \equiv 1 + \sqrt{2}$. In order to show, that r_{in} is the radius of the largest inscribed circle for this range of b, we must verify that a circle centered at x_{in} will lie strictly inside the domain, and will only touch the boundary at $(\xi_c, \pm \eta_c)$. This global verification has been done numerically.

As $b \to b_c^-$, we have $x_{in} \to (0, 0)$ and $r_{in} \to 1/\sqrt{2}$. Alternatively as $b \to 1^+$, we have $x_{in} \to \left(\frac{1}{2}, 0 \right)$ and $r_{in} \to 1/4$. From (4.35) we conclude that the curvature κ_m of $\partial \Omega$ at the point $x = 0$ tends to zero as $b \to b_c^-$, Moreover, more algebra shows that the domain is convex when $b > b_c$. The convexity of the domain for $b > b_c$ explains the nonexistence of a largest inscribed circle in the right lobe of the dumbbell for this range of b.

156

Next, we determine the equilibrium point x_0 of (4.11a) in the right lobe of the dumbbell when D is exponentially large. In Fig. 4.5, we use (4.31) to plot $\partial_x R_{m0}$ along the positive x-axis. Note that $\partial_x R_{m0} > 0$ for $x > 0$. This inequality was shown in §3.3.1. Therefore, as D decreases, the equilibrium location $(x_0, 0)$ tends to the point $(1, 0) \in \partial\Omega$. When D is sufficiently small, the point $(1, 0)$ will be the closest point on the boundary to $(x_0, 0)$. In this range of D, we conclude from (4.11) that the location of the spike is determined by a balance between $\partial_x R_{m0}$ and the dominant contribution to the x-component J_1 of the integral J obtained from the closet point $(1, 0) \in \partial\Omega$. From (4.11), this unstable equilibrium satisfies

$$\frac{\alpha^2}{2\pi\beta}\left(\frac{q}{p-1}\right) J_1 = \frac{\varepsilon}{D}|\Omega|\partial_x R_{m0}\,.\tag{4.54}$$

Calculating J_1 asymptotically as in (4.17), we get

$$J_1 \sim 2\left(\frac{\pi\varepsilon}{1-x_0}\right)^{1/2}\frac{e^{-2(1-x_0)/\varepsilon}}{[1-\kappa_1(1-x_0)]^{1/2}}\,,\tag{4.55}$$

where κ_1 is the curvature at the point $(1, 0)$ given by

$$\kappa_1 = 1 + 4b^2/(b^2+1)^2\,.\tag{4.56}$$

4.4 Spike Equilibria Near the Boundary

In this section we will compute the leading-order behavior of ∇R_{m0} near the boundary of the dumbbell-shaped domains of §4.3. We then use this formula to analyze equilibrium spike locations near the boundary. We begin with the following result, which describes the behavior of the Green's function near the boundary.

Proposition 4.4.1 *Let $\Omega = f(B)$, where B is the unit ball and f is given by (4.30). Let z be a point on the boundary ∂B and let $x = f(z)$ be the corresponding point on the image boundary $\partial\Omega$. Let $\hat{N}$ be the outward pointing normal at x. Let*

$$x_0 = x - \sigma\hat{N}\,,\qquad 0 < \sigma \ll 1\,,\tag{4.57}$$

and z_0 satisfy $x_0 = f(z_0)$. Then

$$\nabla R_{m0}(x_0) = \frac{\hat{N}}{4\pi\sigma} + \frac{\hat{N}}{2\pi|f'(z)|}\left[\frac{\bar{z}^2 b^2}{\bar{z}^2 b^2 - 1} - \frac{(\bar{z}^4 + 5b^2\bar{z}^2)}{\bar{z}^4 - b^4} - \frac{1}{4}\right] + O(\sigma)\,.\tag{4.58}$$

Here and below, ab denotes complex multiplication and $\langle a, b \rangle = \text{Re}(a\overline{b})$ will denote a vector dot product.

Proof.

We calculate $\hat{N}$ as

$$\hat{N} = \frac{-i\frac{d}{dt}f(e^{it})}{\left|\frac{d}{dt}f(e^{it})\right|} = \frac{zf'(z)}{|f'(z)|} = \frac{z|f'(z)|}{f'(z)}. \tag{4.59}$$

From (4.57) and (4.59) we have:

$$f(z_0) = x_0 = f(z) - \frac{\sigma z f'(z)}{|f'(z)|} \sim f\left(z - \frac{\sigma z}{|f'(z)|}\right). \tag{4.60}$$

Thus, for $0 < \sigma \ll 1$, we obtain

$$z_0 \sim z - \frac{\sigma z}{|f'(z)|} = z\left(1 - \frac{\sigma}{|f'(z)|}\right). \tag{4.61}$$

For $\sigma \ll 1$, we calculate from (4.31b) that

$$\nabla s(z_0) \sim \frac{1}{2\pi}\left(\frac{z_0}{1 - |z_0|^2}\right) + \frac{\overline{z}_0 b^2}{2\pi}\left(\frac{1}{\overline{z}_0^2 b^2 - 1} - \frac{2}{\overline{z}_0^4 - b^4}\right) + O(\sigma). \tag{4.62}$$

Substituting (4.61) into (4.62), and using $|z| = 1$, we obtain

$$\frac{1}{2\pi}\left(\frac{z_0}{1 - |z_0|^2}\right) = \frac{|f'(z)|z}{4\pi\sigma}\left(1 - \frac{\sigma}{2|f'(z)|}\right) + O(\sigma). \tag{4.63}$$

Next, we note that

$$\frac{1}{f'(z_0)} = \frac{1}{f'(z)}\left[1 + \frac{\sigma z}{|f'(z)|f'(z)}f''(z) + O(\sigma^2)\right]. \tag{4.64}$$

Therefore, using (4.30) for $f(z)$, we get

$$\frac{1}{\overline{f'(z_0)}}\frac{1}{2\pi}\left(\frac{z_0}{1 - |z_0|^2}\right) = \frac{|f'(z)|z}{4\pi\sigma\overline{f'(z)}}\left(1 - \frac{\sigma}{2|f'(z)|}\right)\left(1 + \frac{\sigma\overline{z}\overline{f''(z)}}{|f'(z)|\overline{f'(z)}}\right) + O(\sigma), \tag{4.65a}$$

$$= \hat{N}\left(\frac{1}{4\pi\sigma} - \frac{1}{8\pi|f'(z)|} + \frac{1}{4\pi}\frac{\overline{z}\overline{f''(z)}}{|f'(z)|\overline{f'(z)}}\right) + O(\sigma), \tag{4.65b}$$

$$= \hat{N}\left(\frac{1}{4\pi\sigma} - \frac{1}{8\pi|f'(z)|} + \frac{1}{4\pi|f'(z)|}\left[\frac{-2\left(\overline{z}^2 + 3b^2\right)\overline{z}^2}{\overline{z}^4 - b^4}\right]\right) + O(\sigma). \tag{4.65c}$$

158

Finally, substituting (4.65c) and the second term of (4.62) into (4.31a), we obtain

$$\nabla R = \frac{\nabla s(z_0)}{f'(z_0)} \tag{4.66a}$$

$$= \frac{\hat{N}}{2\pi}\left(\frac{1}{2\sigma} - \frac{1/4}{|f'(z)|} - \frac{1}{|f'(z)|}\left[\frac{\left(\bar{z}^2 + 3b^2\right)\bar{z}^2}{\bar{z}^4 - b^4}\right]\right.$$
$$\left. + \frac{1}{|f'(z)|}\left[\frac{\bar{z}^2 b^2}{\bar{z}^2 b^2 - 1} - \frac{2\bar{z}^2 b^2}{\bar{z}^4 - b^4}\right]\right) + O(\sigma), \tag{4.66b}$$

$$= \frac{\hat{N}}{2\pi}\left(\frac{1}{2\sigma} - \frac{1}{4|f'(z)|} + \frac{1}{|f'(z)|}\left[\frac{\bar{z}^2 b^2}{\bar{z}^2 b^2 - 1} - \frac{\left(\bar{z}^4 + 5b^2\bar{z}^2\right)}{\bar{z}^4 - b^4}\right]\right) + O(\sigma). \tag{4.66c}$$

This completes the proof. ∎

We now use this proposition to describe the spike dynamics and equilibria near the boundary. Let $x_0 = x_0(t)$ be $O(\sigma)$ close to the boundary, as defined in (4.57), and assume that $\varepsilon \ll \sigma \ll 1$. We then use Laplace's method to calculate the integral J in (4.11a) as

$$J \sim 2\sqrt{\frac{\pi\varepsilon}{\sigma}}e^{-2\sigma/\varepsilon}\hat{N}, \tag{4.67}$$

where J is defined in (4.11b). In deriving (4.67) we have assumed that $\kappa\sigma \ll 1$, where κ is the curvature of $\partial\Omega$. Substituting (4.67) and (4.66c) into (4.11a), we obtain

$$\frac{dx_0}{dt} \sim \frac{2\varepsilon q}{p-1}\left[\frac{\alpha^2}{\pi\beta}\left(\frac{p-1}{q}\right)\sqrt{\frac{\pi\varepsilon}{\sigma}}e^{-2\sigma/\varepsilon}\hat{N}\right.$$
$$\left. - \frac{\varepsilon|\Omega|}{D}\left\{\frac{\hat{N}}{4\pi\sigma} - \frac{\hat{N}}{8\pi|f'(z)|} + \frac{\hat{N}}{2\pi|f'(z)|}\left(\frac{\bar{z}^2 b^2}{\bar{z}^2 b^2 - 1} - \frac{\bar{z}^4 + 5b^2\bar{z}^2}{\bar{z}^4 - b^4}\right)\right\}\right]. \tag{4.68}$$

Note that the first three terms on the right hand side of (4.68) point in the direction of $\hat{N}$. Therefore, a necessary condition for x_0 to be in equilibrium is that the last term on the right hand-side of (4.68) also points in the normal direction, i.e.

$$\text{Im}\left(\frac{\bar{z}^2 b^2}{\bar{z}^2 b^2 - 1} - \frac{\bar{z}^4 + 5b^2\bar{z}^2}{\bar{z}^4 - b^4}\right) = 0. \tag{4.69}$$

This condition is clearly satisfied when $z = \pm 1$ and when $z = \pm i$. Next we show that there are no other solutions to (4.69). Setting $w = z^2$ and using $2\,\text{Im}(x) = x - \bar{x}$, (4.69) becomes

$$-\frac{\left(\bar{w}^2 + 5b^2\bar{w}\right)}{\bar{w}^2 - b^4} + \frac{\bar{w}b^2}{\bar{w}b^2 - 1} + \frac{w^2 + 5b^2 w}{w^2 - b^4} - \frac{wb^2}{wb^2 - 1} = 0. \tag{4.70}$$

159

Using the relation $w\overline{w} = 1$, (4.70) simplifies to

$$4(1 + b^4)b^2 \frac{w(w-1)(w+1)}{(b^4w^2-1)(b^4-w^2)} = 0. \tag{4.71}$$

It follows $z = \pm 1, \pm i$. are the only possible equilibria.

When the condition (4.69) is satisfied, we obtain to leading order from (4.68) that the equilibrium location for σ is related to D by

$$D \sim \frac{\beta}{4\alpha^2}\left(\frac{q}{p-1}\right)\left(\frac{\varepsilon}{\pi\sigma}\right)^{1/2}|\Omega|\,e^{2\sigma/\varepsilon}. \tag{4.72}$$

Notice that this relation is the same for any equilibrium location. Moreover, (4.72) involves only the leading order behavior of $\nabla R \sim \frac{\hat{N}}{4\pi\sigma}$ near the boundary, which is independent of the shape of the boundary. Therefore, the result (4.72) is also independent of the domain shape. Notice also that (4.72) with $|\Omega| = \pi$ agrees with the result (4.29) derived earlier for an equilibrium spike near the boundary of a circular cylindrical domain of radius one.

Next, we analyze the stability of these equilibria with respect to the direction normal to the boundary. Notice that $D = D(\sigma)$ has a minimum at $\sigma_m = \frac{\varepsilon}{4}$. At this point, $D(\sigma_m) \equiv D_m = \sqrt{2}e^{\frac{1}{2}}\frac{|\Omega|q\beta}{4\alpha^2\sqrt{\pi}(p-1)}$. However, since we have assumed that $\sigma \gg \varepsilon$, we have $D \gg D_m$. Furthermore, for any given D with $D \gg D_m$, (4.72) has two solutions for σ: $\sigma_1 \ll \varepsilon$ and $\sigma_2 \gg \varepsilon$. By examining the sign of the right hand side of (4.68), we conclude that the equilibrium at σ_2 is *unstable* with respect to the normal direction. Alternatively, σ_1 is stable with respect to the normal direction. However, our analysis is invalid for the root σ_1, since $\sigma_1 \ll \varepsilon$. Nevertheless, this formal analysis may suggest the existence of boundary spike equilibria located on the boundary of $\partial\Omega$ at $f(z)$, where $z = \pm 1$ or $z = \pm i$. See Conjecture 4.5.1 below. We summarize:

Proposition 4.4.2 *For an arbitrary smooth domain Ω, let D be given by (4.72), where $\varepsilon \ll \sigma \ll 1$. Then there exists a spike equilibria location at a distance σ away from the boundary. Such an equilibria is unstable in the direction normal to the boundary.*

Next, we analyze the stability of these equilibria with respect to the tangential direction. The unit tangent vector to $\partial\Omega$, measured in the counterclockwise direction, is

$$\hat{T}(t) = i\frac{zf'(z)}{|f'(z)|} \quad \text{where} \quad z = e^{it}. \tag{4.73}$$

The stability in the tangential direction is controlled by the last term on the right hand side of (4.68). The direction of this term, up to a positive constant scalar multiple, is given by

$$\vec{v}(t) = -\frac{1}{|f'(z)|}\hat{N}\left(\frac{\bar{z}^2 b^2}{\bar{z}^2 b^2 - 1} - \frac{(\bar{z}^4 + 5b^2\bar{z}^2)}{\bar{z}^4 - b^4}\right), \tag{4.74a}$$

$$= -\frac{f'(z)}{|f'(z)|^2}\left(\frac{\bar{z}b^2}{\bar{z}^2 b^2 - 1} - \frac{(\bar{z}^3 + 5b^2\bar{z})}{\bar{z}^4 - b^4}\right), \tag{4.74b}$$

where $z = e^{it}$.

The differential equation (4.68) can be written in the form

$$\frac{dx_0}{dt} \sim a_1\hat{N} + \omega\vec{v}, \tag{4.75}$$

where a_1 and $\omega > 0$ are real. Multiplying (4.75) by $\hat{T}$ and taking real parts of the resulting expression we get

$$\text{Re}\left(x_0'\overline{\hat{T}}\right) = \omega\,\text{Re}\left(\vec{v}\overline{\hat{T}}\right). \tag{4.76}$$

We decompose the velocity field as $x_0' = s_N\hat{N} + s_T\hat{T}$, and we let θ denote the angle between the tangential direction and $\vec{v}$. Using the identity $< a, b >= \text{Re}(a\bar{b})$ for the dot product, we then reduce (4.76) to

$$s_T = \omega|\vec{v}|\cos\theta, \tag{4.77}$$

where

$$\cos\theta = \frac{1}{|\vec{v}|} < \hat{T}, \vec{v} >, \tag{4.78a}$$

$$= \frac{1}{|\vec{v}|}\text{Re}\left[i\frac{zf'(z)\overline{f'(z)}}{|f'(z)||f'(z)|^2}\left(\frac{z^3 + 5b^2z}{z^4 - b^4} - \frac{zb^2}{z^2b^2 - 1}\right)\right], \tag{4.78b}$$

$$= -C(t)\text{Im}\left(\frac{z^4 + 5b^2z^2}{z^4 - b^4} - \frac{z^2b^2}{z^2b^2 - 1}\right). \tag{4.78c}$$

Here $C(t)$ is some irrelevant positive scalar.

At the equilibrium points $z = \pm 1$ and $z = \pm i$ we have that $\vec{v}$ points in the normal direction. Therefore, at these points, we have $< \hat{T}, \vec{v} > = 0$ and $\cos\theta = 0$. From (4.77) we observe that if $\frac{d\cos\theta}{dt} < 0$ at the equilibrium position, then we have stability in the tangential direction. At the equilibrium positions, where $\sin\theta = 1$, we calculate from (4.78) that

$$\frac{d\theta}{dt} = C(t)\,\mathrm{Im}\left[\frac{d}{dt}\mathcal{F}(e^{it})\right], \qquad \text{where} \quad \mathcal{F}(z) \equiv \frac{z^4 + 5b^2 z^2}{z^4 - b^4} - \frac{z^2 b^2}{z^2 b^2 - 1}. \qquad (4.79)$$

At $t = 0$ and $t = \pi/2$ where $z = 1$ and $z = i$, respectively, we obtain from (4.79) that

$$\left.\frac{d\theta}{dt}\right|_{t=0} = C(0)\,\mathrm{Re}\left[\mathcal{F}'(0)\right], \qquad \left.\frac{d\theta}{dt}\right|_{t=\frac{\pi}{2}} = -C\left(\frac{\pi}{2}\right)\mathrm{Im}\left[\mathcal{F}'(i)\right]. \qquad (4.80)$$

From (4.79) and (4.80), we calculate

$$\left.\frac{d\theta}{dt}\right|_{t=0} = -C(0)\left(\frac{8b^2(1+b^4)}{(b^2+1)^2(b^2-1)^2}\right) < 0, \qquad (4.81a)$$

$$\left.\frac{d\theta}{dt}\right|_{t=\frac{\pi}{2}} = C\left(\frac{\pi}{2}\right)\left(\frac{8b^2(1+b^4)}{(b^2+1)^2(b^2-1)^2}\right) > 0. \qquad (4.81b)$$

Since $\frac{d\cos\theta}{dt} = -\frac{d\theta}{dt}$ at the equilibrium positions, we conclude from (4.77) and (4.81) that the equilibrium position near $f(\pm i)$ (near $f(\pm 1)$) is stable (unstable) in the tangential direction, respectively. We summarize our results in the following proposition.

Proposition 4.4.3 *For the dumbbell-shaped domain $\Omega = f(\mathcal{B})$, where f is given by (4.30), let σ be such that $\varepsilon \ll \sigma \ll 1$. For the value of D given by (4.72), there are precisely four equilibrium spike locations, all at a distance σ away from the boundary. They are given by $x_s^\pm = f(\pm i) - \hat{N}\sigma$ and $x_u^\pm = f(\pm 1) - \hat{N}\sigma$, where $\hat{N}$ is the normal to the boundary $\partial\Omega$ at $f(\pm i)$ and $f(\pm 1)$, respectively. All four equilibria are unstable in the direction $\hat{N}$ normal to the boundary. Moreover, $x_s^\pm$ ($x_u^\pm$) are stable (unstable) in the tangential direction, respectively.*

In Figure 4.2 we illustrate the local vector field and stability properties of near-boundary spikes. Our results suggest that the unstable manifold of the equilibrium near-boundary spike along the x-axis connects with the stable manifold of the near-boundary spike along the y-axis in the neck region of the dumbbell.

162

Our analysis has been restricted to the case where the distance σ between the spike and the boundary satisfies $\sigma \gg \varepsilon$. We expect that the equilibrium locations of spikes that are located on the boundary of the domain should result from a competition between the zeroes of the derivative of the curvature (as for the shadow problem where $D = \infty$) and the local behavior of the gradient of the regular part R_m of the Green's function on the boundary. To this end, we define R_b by

$$R_b(x) = \lim_{y \to x} \left[R_m(x, y) + \frac{1}{4\pi} \ln |x - y| \right]. \tag{4.82}$$

We now show that for the dumbbell-shaped domain of §4 that the minimum of R_b occurs at that point of the boundary where the curvature is at its minimum.

For the dumbbell-shaped domains of §4 we obtain the following result:

Proposition 4.4.4 *Let $\Omega = f(B)$ where f is given by (4.30) and B is the unit ball. Then R_b defined in (4.82) is given by:*

$$R_b(x) = \frac{1}{4\pi} \ln \left(\frac{b^4 + 2b^2 \cos 2t + 1}{b^4 - 2b^2 \cos 2t + 1} \right) + C, \qquad where \quad x = f(e^{it}). \tag{4.83}$$

Here C is some constant independent of x.

The proof of this result is given in Appendix §4.6. Notice that the expression inside the log term of (4.83) has its maximum at $t = 0, \pi$ and its minimum at $t = \frac{\pi}{2}, \frac{3\pi}{2}$. Therefore, R_b has a minimum on the y axis in the neck of the dumbbell, where the curvature of $\partial \Omega$ is at its minimum.

4.5 Discussion

For different ranges of the inhibitor diffusivity D, we have described the bifurcation behavior of an equilibrium one-spike solution to the GM model (4.2) in a radially symmetric domain, and in a class of dumbbell-shaped domains. In a radially symmetric domain, we have calculated the bifurcation value $D_c = O(\varepsilon^2 e^{2d/\varepsilon})$, where d is the distance of the spike to the boundary, for which an equilibrium spike at the midpoint of the domain becomes stable as D decreases below D_c. For a dumbbell-shaped domain of Figure 4.1, the center at the neck also bifurcates

as D is increased beyond some exponentially large value; however the bifurcation occurs along the y axis, as shown in Figure 4.1(b). Since this bifurcation occurs when D is exponentially large as $\varepsilon \to 0$, a main conclusion of our study is that spike behavior for the shadow system corresponding to $D = \infty$, has very different properties from that of spike solutions to (4.2) when D is large, but independent of ε. Moreover, in §3.4, we showed that when D decreases below some $O(1)$ value, the spike in the neck of the dumbbell loses its stability through a pitchfork bifurcation to two stable spike locations that tend to the lobes of the dumbbell as $D \to 0$.

Although there have been many studies of the existence and stability of boundary spikes for the shadow GM system with $D = \infty$, the problem of constructing equilibrium boundary spike solutions for different ranges of D is largely open. The analysis in this paper has been restricted to the situation where the spike is away from the boundary, i.e. the distance σ of a spike to the boundary is such that $\sigma \gg O(\varepsilon)$. Therefore, we have not described boundary spikes or spikes that are $O(\varepsilon)$ close to the boundary. Some work on equilibrium boundary spikes for the case where D is algebraically large as $\varepsilon \to 0$ is given in [11].

For the case where $D = \infty$, the dynamical behavior of a boundary spike was derived in [38]. The equilibrium case was studied in [81] and [82] (see also the references therein). From these studies, it is well-known that the dynamics and equilibrium locations depend only on the curvature of the boundary of the domain. For the domain in Fig. 4.1, the boundary spike located on the y-axis is stable when $D = \infty$. For asymptotically large values of D, we expect that the dynamics of a boundary spike depends on both the derivative of the curvature of the boundary and on the behavior of the gradient of the regular part of the Green's function R_m on the boundary. For the dumbbell-shaped domain of in Fig. 4.1, we showed in §4.sec:4.5 that this gradient vanishes at the same points where the curvature of the boundary has a local maxima or minima. This suggests the following conjecture:

Conjecture 4.5.1 *Suppose that $O(1) \ll D \ll O(\varepsilon^q e^{c/\varepsilon})$ for some q and c to be found. Then, a boundary spike for the domain $\Omega = f(B)$ shown in Figure 4.1 is at equilibrium if and only if its center is located on either the x or the y-axes. Furthermore, the equilibrium locations on*

the y and the x-axes are stable and unstable, respectively.

Finally, it is well-known (cf. [5], [49], [27]) that the shadow system admits unstable multi-spike equilibrium solutions where the locations of the spikes satisfy a ball-packing problem. These solutions are unstable with respect to both the large $O(1)$ and the exponentially small eigenvalues of the linearization. Since when $D \ll 1$, the distance function plays a central role, the locations of the spikes should also satisfy a ball packing problem. However, in a strictly convex domain these solutions should be stable. It would be interesting to extend the analysis given here to determine the bifurcation properties, and the exchange of stability, of multi-spike solutions as D is decreased.

4.6   Appendix: The Proof of Proposition 5.3

Here we prove Proposition 5.3. Let $x = x(t) = f(e^{it})$, $\widehat{N}$ be the normal at x, and label $y(t) = x(t) - \sigma \widehat{N}(t)$. We define $h(t)$ by

$$h(t) = R_m(y(t), y(t)), \tag{4.84}$$

and calculate

$$h'(t) = \nabla R_m(y(t), y(t)) \cdot y'(t). \tag{4.85}$$

Note that $x'(t) = \widehat{T}|f'(z)|$, where $z = e^{it}$ and $\widehat{T} = i\widehat{N}$ is the tangential direction at $x = f(z)$. Therefore, we have

$$y'(t) = |f'(z)|\widehat{T} - \sigma c \widehat{T}, \tag{4.86}$$

where $c(t) = \frac{d}{dt}|\widehat{N}|$ is some irrelevant function. From Proposition 5.1 and using $a \cdot b = \mathrm{Re}(\overline{a}b)$, we obtain

$$h'(t) = \left(\frac{\widehat{N}}{4\pi\sigma} + \frac{\widehat{N}}{2\pi|f'(z)|} \left[\frac{\overline{z}^2 b^2}{\overline{z}^2 b^2 - 1} - \frac{(\overline{z}^4 + 5b^2\overline{z}^2)}{\overline{z}^4 - b^4} - \frac{1}{4} \right] + O(\sigma) \right)$$

$$\cdot \left(\widehat{T}|f'(z)| - \sigma c \widehat{T} \right) \tag{4.87}$$

$$= -\frac{1}{2\pi} \mathrm{Im} \left[\frac{z^2 b^2}{z^2 b^2 - 1} - \frac{(z^4 + 5b^2 z^2)}{z^4 - b^4} \right] + O(\sigma) = \frac{1}{2\pi} \mathrm{Im}\, \mathcal{F}(z),$$

165

where $\mathcal{F}$ is given by (4.79). Note that the singular part $\frac{\hat{N}}{4\pi\sigma}$ does not enter into $h'(t)$ since it is perpendicular to the tangent direction.

Integrating (4.87), we obtain

$$h(t) = \int h'(t)dt = \frac{1}{2\pi} \int \operatorname{Im} \mathcal{F}(z) \frac{dz}{iz} . \tag{4.88}$$

Therefore,

$$\operatorname{Im} \mathcal{F}(z) = \frac{\mathcal{F}(z) - \mathcal{F}(\frac{1}{z})}{2i} \tag{4.89a}$$

$$= \frac{1}{i} 2(1+b^4)b^2 \frac{w(w^2-1)}{(b^4 w^2 - 1)(w^2 - b^4)} , \tag{4.89b}$$

$$= \frac{-1}{i} w \left(\frac{b^2}{wb^2 + 1} - \frac{b^2}{wb^2 - 1} + \frac{1}{w + b^2} - \frac{1}{w - b^2} \right) . \tag{4.89c}$$

Here $w = z^2$. In addition, $\frac{dz}{z} = \frac{1}{2}\frac{dw}{w}$ so that

$$h(t) = \frac{1}{4\pi} \int \left(\frac{b^2}{wb^2 + 1} - \frac{b^2}{wb^2 - 1} + \frac{1}{w + b^2} - \frac{1}{w - b^2} \right) dw , \tag{4.90a}$$

$$= \frac{1}{4\pi} \ln \left| \frac{(wb^2 + 1)(w + b^2)}{(wb^2 - 1)(w - b^2)} \right| + C . \tag{4.90b}$$

This result can be simplified as

$$h(t) = \frac{1}{4\pi} \ln \left| \frac{(wb^2 + 1)(w + b^2)}{(wb^2 - 1)(w - b^2)} \right| + C , \tag{4.91a}$$

$$= \frac{1}{8\pi} \ln \frac{(wb^2 + 1)(\overline{w}b^2 + 1)(w + b^2)(\overline{w} + b^2)}{(wb^2 - 1)(\overline{w}b^2 - 1)(w - b^2)(\overline{w} - b^2)} + C , \tag{4.91b}$$

$$= \frac{1}{8\pi} \ln \frac{\left(1 + b^4 + 2b^2 \cos 2t\right)^2}{\left(1 + b^4 - 2b^2 \cos 2t\right)^2} + C , \tag{4.91c}$$

$$= \frac{1}{4\pi} \ln \left(\frac{1 + b^4 + 2b^2 \cos 2t}{1 + b^4 - 2b^2 \cos 2t} \right) + C . \tag{4.91d}$$

The constant $C = C(\sigma)$ depends on the distance from the boundary but not on x. Finally, for $x \in \partial\Omega$ and $y \in \Omega$, we define the regular part of the boundary Green's function by

$$S(x, y) = R_m(x, y) + \frac{1}{4\pi} \ln |x - y| . \tag{4.92}$$

Note that S is smooth and bounded for all $y \in \Omega$. Therefore, we have

$$R_b(x) = \lim_{y \to x} S(x,y) = \lim_{y \to x} [S(y,y) + O(x-y)] = \lim_{y \to x} S(y,y), \qquad (4.93\text{a})$$

$$= \lim_{\sigma \to 0} h(t) + \frac{1}{4\pi} \ln \sigma \qquad (4.93\text{b})$$

$$= \frac{1}{4\pi} \ln \left(\frac{1 + b^4 + 2b^2 \cos 2t}{1 + b^4 - 2b^2 \cos 2t} \right) + C. \qquad (4.93\text{c})$$

Since we are only concerned with determining points on the boundary where R_b has minima and maxima, the constant C is irrelevant. This completes the proof. ∎

Chapter 5

Q-switching instability in passively mode-locked lasers

One of the applications of where pulse-like structures occur is in the field of nonlinear optics. In this chapter we consider a model arising in lasers, which exhibits localized spike-like structures. The following equations have been proposed as a continuous model of the mode-locked lasers (see [31], [41], [23]):

$$E_T = \left(N - 1 - \frac{a}{1 + b|E|^2} \right) E + E_{\theta\theta} \tag{5.1a}$$

$$N_T = \gamma \left[A - N - NL^{-1} \int_0^L |E|^2 d\theta \right]. \tag{5.1b}$$

Here, θ represents the time describing a single laser pulse and T is a slow time variable describing the modulation of its amplitude. $E(\theta, T)$ represents the field satisfying the periodic boundary condition $E(\theta, T) = E(\theta + L, T)$, and $N(T)$ is the inversion of population. In addition, $\gamma = O(10^{-4} - 10^{-3})$ is the relaxation rate of the upper level relative to the coherence lifetime. The constant A is the pump parameter defined so that $A = 1$ is the lasing threshold if $a = 0$. The saturation term in (5.1) is the same as the one used by Kärtner et al [42]. This model has been studied numerically in [41]. Taking a as a bifurcation parameter, the following typical parameter values have been considered in [41]:

$$A = 8, \quad L = 3800, \quad \gamma = 0.00014, \quad b = 0.01. \tag{5.2}$$

Using numerical simulations, it was reported in [41] that for $a = 0.0025$, the solution $E(\theta)$ settles to a steady state in the form of a spike. However as a was increased past 0.003, fast-scale oscillations in the steady-state solution were observed. Such oscillations are called Q-switch

instabilities, and are undesired for most of the applications. In this chapter, we use stability analysis to predict the onset of a Q-switch instability via a Hopf bifurcation. The results of this chapter have been previously reported in [23].

From the mathematical viewpoint, we consider the following generalization of (5.1):

$$E_T = -(1 + a(1 - (b|E|^2)^{\frac{p-1}{2}} k(b|E|^2))E + N(E + E_{\theta\theta}), \tag{5.3a}$$

$$N_T = \gamma \left[A - \left(1 + \frac{1}{L} \int_0^L |E|^2 d\theta \right) N \right] \tag{5.3b}$$

Here, k is a nonlinearity with $k(0) = 1$, $p > 1$, and where T is the time variable. Equation (5.1) corresponds to choosing

$$k(t) = \frac{1}{1+t}, \quad p = 3. \tag{5.4}$$

We will also study in more detail the case of no saturation,

$$k(t) = 1, \quad p > 0, \tag{5.5}$$

for which more explicit results are possible.

We scale (5.3) as follows:

$$N = 1 + \omega x, \quad E = \sqrt{A-1}u \tag{5.6a}$$

$$t = \omega T, \quad z = \sqrt{\omega}\theta \tag{5.6b}$$

where

$$\omega = \sqrt{2\gamma(A-1)} \tag{5.6c}$$

this yeilds,

$$u_t = u_{zz}(1 + \varepsilon_2 x) - u(\alpha - x) + \alpha\beta^{\frac{p-1}{2}} u^p k(\beta u^2)) \tag{5.7a}$$

$$x_t = \frac{1}{2}(1 - 2\varepsilon_1 x) - \frac{1}{2}(1 + \varepsilon_2 x)\frac{1}{l} \int_0^l u^2 \tag{5.7b}$$

where

$$\alpha = a\frac{1}{\omega}, \quad \beta = b(A-1), \quad l = \sqrt{\omega}L, \quad \varepsilon_1 = \frac{\omega}{2A}, \quad \varepsilon_2 = \omega. \tag{5.8a}$$

169

The typical values (5.2) then become

$$\beta = 0.07, \quad \varepsilon_1 = 0.0032, \quad \varepsilon_2 = \omega = 0.044, \quad l = 800. \tag{5.9}$$

The numerical result from [41] is that for k and p as given in (5.4), there is a Hopf bifurcation as α passes through $\alpha_c = 0.068$.

We will treat $\varepsilon_1, \varepsilon_2$ as small parameters in this problem. Our goal is to study the asymptotic stability in terms of these parameters.

5.1 Stability analysis

Let $u = u^*, x = x^*$ be the steady state solution. It is convenient to further rescale the space variable as follows:

$$\overline{z} = dz, \quad u = h\overline{z}, \quad x = \overline{x} \tag{5.10a}$$

where

$$d^2 = \frac{\alpha - x^*}{1 + \varepsilon_2 x^*}, \quad h = (\alpha - x^*)^{\frac{1}{p-1}} \alpha^{-\frac{1}{p-1}} \beta^{-\frac{1}{2}}. \tag{5.10b}$$

Dropping the bars, (5.7) becomes

$$u_t = u_{zz}(1 + \varepsilon_2 x)\frac{\alpha - x^*}{1 + \varepsilon_2 x^*} - u(\alpha - x) + (\alpha - x^*)u^p k(cu^2), \tag{5.11a}$$

$$x_t = \frac{1}{2}(1 - 2\varepsilon_1 x) - \frac{1}{2}(1 + \varepsilon_2 x)\frac{h^2}{ld}\int_0^{ld} u^2 \tag{5.11b}$$

where

$$c = (\alpha - x^*)^{\frac{2}{p-1}} \alpha^{-\frac{2}{p-1}}. \tag{5.11c}$$

The steady-state equations therefore become

$$0 = u_{zz}^* - u^* + u^{*p} k(cu^{*2}) \tag{5.12a}$$

$$\frac{h^2}{ld}\int_0^{ld} u^{*2} = \frac{1 - 2\varepsilon_1 x^*}{1 + \varepsilon_2 x^*} = 1 - x^*(2\varepsilon_1 + \varepsilon_2). \tag{5.12b}$$

170

Next we examine the stability. Letting

$$u = u^* + e^{\lambda t}\phi(z), \quad x = x^* + e^{\lambda t}\psi(z) \tag{5.13}$$

we obtain, up to $O(\varepsilon_1, \varepsilon_2)$, the following eigenvalue problem:

$$\frac{\lambda}{\alpha - x^*}\phi = \phi'' - \phi + \frac{d}{du^*}\left(u^{*p}k(cu^{*2})\right)\phi + \psi\left[\frac{u^*}{\alpha - x^*} + u_{zz}^*\varepsilon_2\right] \tag{5.14}$$

$$\lambda\psi = -\varepsilon_1\psi - \frac{1}{2}\varepsilon_2\psi\frac{h^2}{ld}\int_0^{ld} u^{*2} - (1 + \varepsilon_2 x^*)\frac{h^2}{ld}\int_0^{ld}\phi u^* \tag{5.15}$$

Using (5.15) to solve for ψ and substituting it into (5.15) we obtain

$$\frac{\lambda}{\alpha - x^*}\phi = L_0\phi - \left[\frac{u^*}{\alpha - x^*} + u_{zz}^*\varepsilon_2\right]\frac{1 + \varepsilon_2 x^*}{\lambda + \varepsilon_1 + \frac{1}{2}\varepsilon_2}\frac{h^2}{ld}\int_0^{ld}\phi u^* \tag{5.16}$$

where

$$L_0\phi \stackrel{def}{=} \phi'' - \phi + \frac{d}{du^*}\left(u^{*p}k(cu^{*2})\right)\phi. \tag{5.17}$$

For convenience we rescale

$$\overline{\lambda} = \frac{\lambda}{\alpha - x^*} \tag{5.18}$$

Dropping bars we obtain

$$\lambda\phi = L_0\phi - \chi(u^* + 0(\varepsilon_2))\frac{h^2}{ld}\int_0^{ld}\phi u^*, \quad \chi \stackrel{def}{=} \frac{1 + \varepsilon_2 x^*}{(\alpha - x^*)\left((\alpha - x^*)\lambda + \varepsilon_1 + \frac{1}{2}\varepsilon_2\right)} \tag{5.19}$$

Since this equation is linear in ϕ, we may scale it to obtain

$$\frac{1}{\chi} = \frac{h^2}{ld}\int_0^{ld}\phi u^*, \tag{5.20a}$$

$$(L_0 - \lambda)\phi = u^* + 0(\varepsilon_2) \tag{5.20b}$$

We now look for a hopf bifurcation. That is assume that λ is purely imaginary. We let

$$\lambda = i\lambda_I, \quad \phi = \phi_R + i\phi_I. \tag{5.21}$$

to obtain

$$L_0\phi_R + \lambda_I\phi_I = u^* + O(\varepsilon_2), \qquad L_0\phi_I - \lambda_I\phi_R = 0 \tag{5.22}$$

This equation decouples:

$$L_0^2\phi_I + \lambda_I^2\phi_I = \lambda_I u^* + O(\varepsilon_2), \qquad L_0^2\phi_R + \lambda_I^2\phi_R = L_0 u^* \tag{5.23}$$

171

and hence (5.20a) becomes

$$\frac{ldh^{-2}(\alpha - x^*)\left((\alpha - x^*)\lambda_I\right)}{1 + \varepsilon_2 x^*} = \int_0^{ld} u^* \phi_I \overset{def}{=} \mu_I(\lambda_I) \tag{5.24a}$$

$$\frac{ldh^{-2}(\alpha - x^*)\left(\varepsilon_1 + \frac{1}{2}\varepsilon_2\right)}{1 + \varepsilon_2 x^*} = \int_0^{ld} u^* \phi_R \overset{def}{=} \mu_R(\lambda_I) \tag{5.24b}$$

Together, equations (5.24), (5.12) and (5.11c) yield a system of three equations for three unknowns λ_I, x^* and α which determine the hopf bifurcation. However the solution of this system requires extensive computations since ϕ_I, ϕ_R have to be determined numerically for any given α, λ_I as a solution to the boundary value problem of fourth order.

In practice, for reasonable nonlinearity k such as of type (5.4) or (5.5), we may assume that $c = O(1)$, or equivalently

$$\alpha - x^* = O(\alpha). \tag{5.25}$$

It then follows that $d = O(\sqrt{\alpha}), h^{-2} = O(\beta)$. Furthermore, from (5.12b) we obtain

$$\int_0^{dl} u^{*2} = O(l\beta\sqrt{\alpha}), \tag{5.26}$$

from where we conclude that $dl = O(l\sqrt{\alpha}) \gg 1$, since otherwise $\int_0^{dl} u^{*2} = O(l\sqrt{\alpha})$, which contradicts (5.26) and the fact that $\beta \ll 1$. Therefore,

$$u^* \sim w, \quad \int_0^{dl} u^{*2} \sim \int w^2, \tag{5.27}$$

where w satisfies the same ODE (5.12a) as u^*, but on the whole space:

$$0 = w_{zz} - w + w^p k(cw^2), \tag{5.28a}$$

$$w(z) = ae^{-|z|} \quad \text{as} \quad |z| \to \infty \tag{5.28b}$$

Furthermore $ldh^{-2} = O(l\sqrt{\alpha}\beta)$ and $\int w^2 = O(1)$ and hence it follows from (5.27) and (5.26) that $ldh^{-2} = O(1)$. Thus the left hand side of (5.24b) is of $O(\alpha\varepsilon_1)$, and therefore small. On the other hand expanding ϕ_R, ϕ_I as a series in $\frac{1}{\lambda_I}$ and using (5.22) we obtain

$$\mu_R(\lambda_I) = \frac{1}{\lambda_I^2} \int wL_0w + O(\frac{1}{\lambda_I^4}), \tag{5.29a}$$

$$\mu_I(\lambda_I) = \frac{1}{\lambda_I} \int w^2 + O(\frac{1}{\lambda_I^3}). \tag{5.29b}$$

172

Since the left hand side of (5.24b) is small, we may assume that ϕ_R is small and therefore the expansion (5.29a) is valid. Thus λ_I is big and therefore the expansion (5.29b) is also valid. Substituting (5.29) into (5.24) and eliminating λ_I, then using the approximation (5.27) we obtain

$$\frac{\varepsilon_1 + \frac{1}{2}\varepsilon_2}{\alpha - x^*} = \frac{\int wL_0w}{\int w^2}. \tag{5.30}$$

From (5.12b) and (5.11c) we obtain

$$\alpha - x^* = \left(\frac{c\int w^2}{l\beta}\right)^2. \tag{5.31}$$

Combining this with (5.30) we obtain an equation involving only c:

$$(l\beta)^2\left(\varepsilon_1 + \frac{1}{2}\varepsilon_2\right) = c^2\left(\int w^2\right)\left(\int wL_0w\right) \tag{5.32a}$$

$$\gamma L^2 b^2 A(A-1)^2 = c^2\left(\int w^2\right)\left(\int wL_0w\right). \tag{5.32b}$$

Once c is so determined, we may finally determine α from (5.31),(5.32a) and (5.11c):

$$\alpha = c^{\frac{5-p}{2}}(\beta l)^{-2}\left(\int_{-\infty}^{\infty} w^2\right)^2 \tag{5.33a}$$

$$= (l\beta)^{\frac{5-p}{2}-2}\left(\varepsilon_1 + \frac{1}{2}\varepsilon_2\right)^{\frac{5-p}{4}}\left(\int w^2\right)^{\frac{p-5}{4}+2}\left(\int wL_0w\right)^{\frac{p-5}{4}} \tag{5.33b}$$

Using (5.8) we finally obtain

$$a = \gamma^{\frac{5-p}{4}}(A-1)^{\frac{1-p}{2}}A^{\frac{5-p}{4}}(Lb)^{\frac{1-p}{2}}F(c,p) \tag{5.34a}$$

where

$$F(c,p) = \left(\int w^2\right)^{\frac{p+3}{4}}\left(\int wL_0w\right)^{\frac{p-5}{4}} \tag{5.34b}$$

Thus we obtain the following characterisation of the Hopf bifurcation of (5.7):

Proposition 5.1.1 *Let w be the entire solution to (5.28) where c satisfies (5.32b), with $c = O(1)$. Then there is a Hopf bifurcation that occurs for the system (5.3) for the value of a given by (5.34).*

173

5.2 Hopf bifurcation for for $p = 3$, $k(t) = \frac{1}{1+t}$

To find c of Proposition 5.1.1 we need to be able to evaluate $\int_{-\infty}^{\infty} w^2$ and $\int_{-\infty}^{\infty} w L_0 w$ for various values of c. There are two ways of doing this efficiently. Note that (5.28) admits a first integral

$$\frac{w'^2}{2} - \frac{w^2}{2} + f(w,c) = 0 \quad \text{where} \quad f(w,c) = \int_0^w t^p k(ct^2) dt \tag{5.35}$$

Thus $dt = w^2 \frac{dw}{\sqrt{w^2 - 2f(w,c)}}$ and so

$$\int w^2 = 2 \int_0^{w_m} w^2 \frac{dw}{\sqrt{w^2 - 2f(w,c)}}, \quad \int w L_0 w = 2 \int_0^{w_m} w L_0 w \frac{dw}{\sqrt{w^2 - 2f(w,c)}}, \tag{5.36}$$

where w_m is the maximum of w given by

$$w_m{}^2 - 2f(w_m, c) = 0. \tag{5.37}$$

However, the integral on the right hand side of (5.36) is singular at the right endpoint and a numerical approximation on a uniform grid using for example Simpson's method gives a very bad approximation. This can be overcome by developing this integral in Taylor series at the singular endpoint.

A simpler and a numerically cheap approach is to instead integrate the initial value problem $w(0) = w_m$, $A(0) = 0$, $A' = 2w^2$, $w'' - w + w^p k(cw^2) = 0$, where w_m and c are related by (5.37), using a standard Runga-Kutta method from zero until t_1 where say $w(t_1) < 10^{-8}$ (in typical examples we tried, t_1 was about 10-15). Then $\int_{-\infty}^{\infty} w^2$ is numerically approximated by $A(t_1)$. The integral $\int_{-\infty}^{\infty} w L_0 w$ is analogously evaluated.

A physically relevant case studied in [41] is $p = 3$, $k(t) = \frac{1}{1+t}$. Then we compute:

$$L_0 w = \frac{2w^3}{(1 + cw^2)^2}$$

and

$$w^2 - 2f(w,c) = \left(1 - \frac{1}{c}\right) w^2 + \frac{1}{c^2} \ln(1 + cw^2). \tag{5.38}$$

For parameter values (5.2) used in [41], we used the method outlined above to numerically obtain $c = 0.580$ (which is of O(1)), $w_m = 2.515$, $\int_{-\infty}^{\infty} w^2 = 18.78$, $\int_{-\infty}^{\infty} w L_0 w = 12.60$ which

174

yields the predicted bifurcation value of $\alpha = 0.065$ or $a = 0.0029$. This agrees to all significant digits with the value of $a_c = 0.003$ reported in [41], as observed from a full numerical simulation of (5.3). Figure 5.1 lists the threhold value a at which the hopf bifurcation occurs, as a function of b.
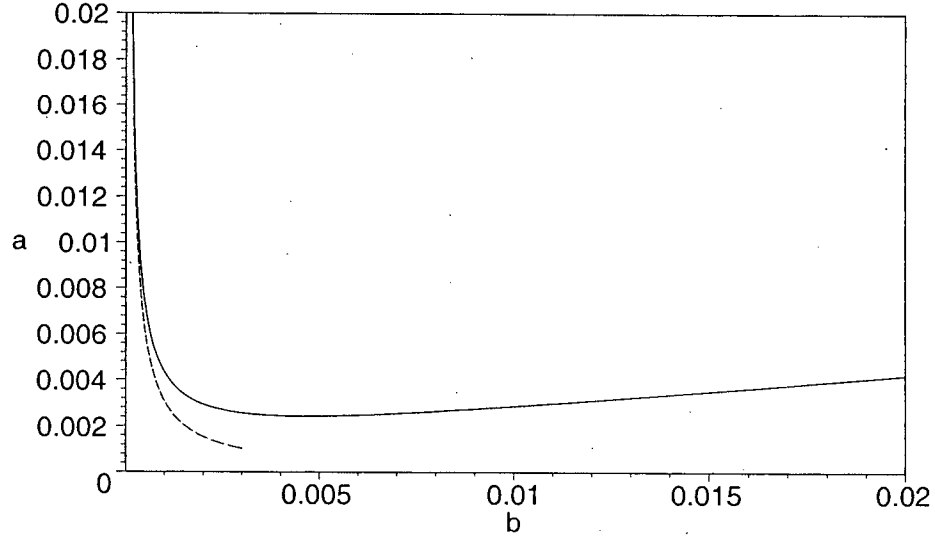

Figure 5.1: The hopf bifurcation diagram in the $b - a$ plane. The solid curve is the numerically computed bifurcation threshold from Proposition 5.1.1. Instability occurs above the solid curve. The dashed curve is the asymptotic approximation valid for small b, given by (5.46a).

5.3   Hopf bifurcation without saturation

Next, we examine the case $k = 1$ for arbitrary p. Equations (5.37) and (5.36) then become

$$w_m = \left(\frac{p+1}{2}\right)^{\frac{1}{p-1}}, \tag{5.39}$$

$$\int w^2 = 2 \int_0^{w_m} w \frac{dw}{\sqrt{1 - 2\frac{w^{p-1}}{p+1}}} = 2\left(\frac{p+1}{2}\right)^{\frac{2}{p-1}} \int_0^1 \frac{v\,dv}{\sqrt{1 - v^{p-1}}}. \tag{5.40}$$

To evaluate $\int wL_0 w$, note that $L_0 w = (p-1)w^p$. From (5.35) we have

$$\int w'^2 - \int w^2 + \frac{2}{p+1} \int w^{p+1} = 0. \tag{5.41}$$

Multiplying (5.28a) by w, integrating, and using integration by parts on the first term we obtain

$$-\int w'^2 - \int w^2 + \int w^{p+1} = 0. \tag{5.42}$$

175

Thus we obtain

$$\int w L_0 w = \frac{2(p+1)(p-1)}{p+3} \int w^2. \tag{5.43}$$

For the cases $p = 2, 3, 5$, the integral (5.40) is easily evaluated using elementary techniques. More generally, we have

$$\int_0^1 \frac{v}{\sqrt{1 - v^{p-1}}} = \frac{\Gamma(\frac{1}{2})\Gamma(\frac{2}{p-1})}{(p-1)\Gamma(\frac{1}{2} + \frac{2}{p-1})}. \tag{5.44}$$

In particular it is possible to to evaluate this integrals in terms of elementary functions when the argument to Γ is of the form $n/2$ with n an integer. This happens when p is of the form $\frac{2+m}{m}$ or $\frac{4+m}{m}$ with m an integer.

We summarize these results below.

Proposition 5.3.1 *Suppose that $k = 1$ in (5.3). Then a Hopf bifurcation occurs in (5.3) for the value of a given by*

$$a = (\gamma A)^{\frac{5-p}{4}} ((A-1)Lb)^{\frac{1-p}{2}} F(p), \tag{5.45a}$$

where

$$F(p) = 2^{\frac{3p-11}{4}} (p+1)^{\frac{p-1}{4}} (p-1)^{\frac{-3-p}{4}} (p+3)^{\frac{5-p}{4}} \left(\frac{\Gamma(\frac{1}{2})\Gamma(\frac{2}{p-1})}{\Gamma(\frac{1}{2} + \frac{2}{p-1})} \right)^{\frac{p-1}{2}}. \tag{5.45b}$$

For special values of p we have the following:

$$p = 3: \quad a = \frac{\sqrt{6\gamma A}}{(A-1)Lb}, \quad F = \sqrt{6} \tag{5.46a}$$

$$p = 5: \quad a = \frac{3}{4}\pi^2 \frac{1}{[(A-1)Lb]^2}, \quad F = \frac{3}{4}\pi^2 = 7.402 \tag{5.46b}$$

$$p = \frac{7}{3}: \quad a = 15^{\frac{1}{3}} \left(\frac{\pi\gamma A}{4(A-1)Lb} \right)^{\frac{2}{3}}, \quad F = \pi^{\frac{2}{3}} 15^{\frac{1}{3}} 2^{\frac{-4}{3}} = 2.099 \tag{5.46c}$$

$$p = \frac{3}{4}: \quad a = 2.89(\gamma A)^{\frac{17}{16}} [(A-1)Lb]^{\frac{1}{8}}, \quad F = \frac{3}{14} 5^{-\frac{1}{8}} 42^{\frac{3}{4}} = 2.89 \tag{5.46d}$$

$$p = 2: \quad a = 2.136(\gamma A)^{\frac{3}{4}} ((A-1)Lb)^{-\frac{1}{2}}, \quad F = 5^{\frac{3}{4}} 6^{-\frac{1}{4}} = 2.136 \tag{5.46e}$$

When $p = 5$, the value of a at which the Hopf bifurcation occurs does not depend on γ. When $p = \frac{7}{3}$, it does not depend on A if A is large.

176

5.4 Discussion

An open problem is to study how Hopf bifurcation behaves as we change the saturation parameter b. For very small b, which corresponds to the limit of no saturation, the asymptotic expression for the Hopf bifurcation was derived in (5.46a). It would be also interesting to find an asymptotic expression for large b. This corresponds to the case c near 1 in (5.38). Setting $c = 1 - \delta$, where $0 < \delta \ll 1$, we then obtain

$$g(w) = w^2 - 2f(w, c) \sim -\delta w^2 + (1 + 2\delta) \ln(1 + w^2).$$

Then setting $g = 0$ we obtain

$$\delta \sim \frac{\ln w_m^2}{w_m^2}, \quad w_m \gg 1.$$

This gives an expression for the height of the spike. To compute the hopf bifurcation in this case, we need to evaluate the integrals in (5.36) asymptotically. It is an open question to complete this computation.
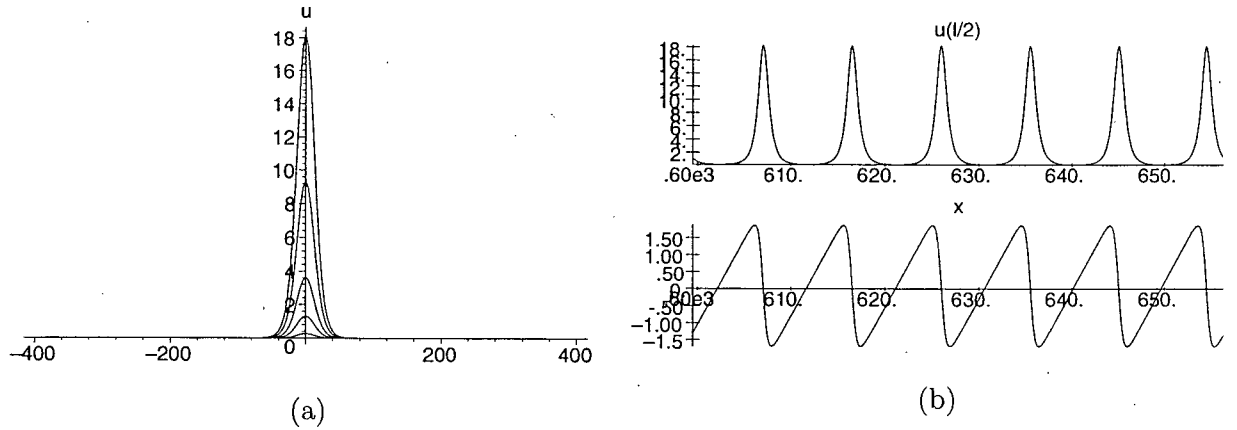

(a)

(b)

Figure 5.2: (a) Solution profile $u(z)$ at different times. (b) Height of the spike and $x(t)$ vs. time. Here, $\alpha = 0.1, \beta = 0.07, l = 800, p = 3, k(t) = \frac{1}{1+t}, \varepsilon_1 = 0.0032$ and $\varepsilon_2 = 0.044$.

Another open question is to study the dynamics of an oscillating spike away from the Hopf bifurcation, where the oscillations become strongly pulsating. Numerically, the oscillation consists of a long, "pulse-building" phase, where the spike height $N(L/2)$ is exponentially small; followed by a short "pulse-firing" phase (see Figure 5.2).

177

Finally, the analytical method could be used for more complicated situations such as taking into account the finite relaxation time of the absorber, which is important for semiconductor devices [22].

Bibliography

[1] M. Abramowitz and I.A. Stegun, *Handbook of Mathematical Functions with Formulas, Graphs, and Mathematical Tables*, Washington, National Bureau of Standards Applied Mathematics, 1964.

[2] E. Anderson et al. *LAPACK User's Guide: Third Edition*, SIAM Publications (1999).

[3] U. Ascher, R. Christiansen, R. Russel, *Collocation Software for Boundary value ODE's*, Math. Comp., **33** (1979) 659-579.

[4] C. Bandle, M. Flucher, *Harmonic Radius and Concentration of Energy; Hyperbolic Radius and Liouville's Equations $\triangle U = e^U$ and $\triangle U = U^{(n+2)/(n-2)}$*, SIAM Rev., **38**, No. 2, (1996), pp. 191-238.

[5] P. Bates, N. Fusco, *Equilibria with Many Nuclei for the Cahn-Hilliard Equation*, J. Diff. Eq. **162**, (2000), pp. 283-356.

[6] J.G. Bom, R.A. Trompert and J.G. Verwer, *Algorithm 758: VLUGR2: A Vectorizable Adaptive Grid Solver for PDEs in 2D*, Association for Computing Machinery Transactions on Mathematical Software, 22 (1996) 302-328.

[7] L. A. Caffarelli, A. Friedman, *Convexity of Solutions of Semilinear Elliptic Equations*, Duke Math. J., **52**, No. 2, (1985), pp. 431-456.

[8] N. N. Carlson, K. Miller, *Design and Application of a Gradient-Weighted Moving Finite Element Code I: in One Dimension*, SIAM J. Sc. Comput., **19**, No. 3, (1998), pp. 728-765.

[9] N. N. Carlson, K. Miller, *Design and Application of a Gradient-Weighted Moving Finite Element Code II: in Two Dimensions*, SIAM J. Sc. Comput., **19**, No. 3, (1998), pp. 766-798.

[10] X. Chen, M. Kowalczyk, *Slow Dynamics of Interior Spikes in the Shadow Gierer-Meinhardt System*, Adv. in Diff. Equat., **6**, No. 7, (2001), pp. 847-872.

[11] M. Del Pino, P. Felmer, M. Kowalczyk *Boundary Spikes in the Gierer-Meinhardt System*, Commun. Pure Appl. Anal., **1**, No. 1 (2002), pp. 137-156

[12] M. Del Pino, M. Kowalczyk, X. Chen, *The Gierer Meinhardt System: The Breaking of Homoclinics and Multi-Bump Ground States*, Commun. Contemp. Math., **3**, No. 3, (2001), pp. 419-439.

[13] A. De Wit, *Spatial Patterns and Spatiotemporal Dynamics in Chemical Systems*, Advances in Chemical Physics, 109. I. Prigogine and S.A. Rice, editors.

[14] X. Chen, M. Kowalcyzk, *Dynamics of an Interior Spike in the Gierer-Meinhardt System*, SIAM. J. Math. Anal., to appear, (2002).

[15] E. J. Crampin, P. K. Maini, *Reaction-Diffusion Models for Biological Pattern Formation*, Methods and Appl. of Analysis, 8, No. 2, (2001), pp. 415-428.

[16] A. Doelman, W. Eckhaus, T. J. Kaper, *Slowly Modulated Two-Pulse Solutions in the Gray-Scott Model I: Asymptotic Construction and Stability*, SIAM J. Appl. Math., **61**, No. 3, (2000), pp. 1080-1102.

[17] A. Doelman, W. Eckhaus, T. J. Kaper, *Slowly Modulated Two-Pulse Solutions in the Gray-Scott Model II: Geometric Theory, Bifurcations, and Splitting Dynamics*, SIAM J. Appl. Math., **61**, No. 6, (2000), pp. 2036-2061.

[18] A. Doelman, A. Gardner and T.J. Kaper, *Stability analysis of singular patterns in the 1-D Gray-Scott model: A matched asymptotic approach*, Physica D. 122 (1998), 1-36.

[19] A. Doelman, R. A. Gardner, T. Kaper, *A Stability Index Analysis of 1-D Patterns of the Gray Scott Model*, Memoirs of the AMS, **155**, No. 737, (2002).

[20] A. Doelman, T. Kaper, and P. A. Zegeling, *Pattern formation in the one-dimensional Gray-Scott model*, Nonlinearity 10 (1997), 523-563.

[21] A. Doelman, H. van der Ploeg, *Homoclinic stripe patterns*, SIAM J. Appl. Dyn. Syst. 1 (2002) 65-104.

[22] J.L.A. Dubbeldam, J.A. Leegwater, and D. Lenstra, *Theory of mode-locked semiconductor lasers with finite absorber relaxation times*, Appl. Phys. Lett. **70**, 1938-1940 (1997)

[23] T. Erneux, T. Kolokolnikov, N. Joly and S. Bielawski, *The Q-switching instability in passively mode-locked lasers*, preprint.

[24] S. I. Ei, J. Wei, *Dynamics of Metastable Localized Patterns and its Application to the Interaction of Spike Solutions for the Gierer-Meinhardt System in Two Spatial Dimensions*, Japan J. Ind. Appl. Math., to appear, (2002).

[25] R.J. Field and R.M. Noyes, *A model illustrating amplification of perturbation in an excitable medium*, Symp. Faraday Soc. 9, 21-7 (1974).

[26] A. Gierer, H. Meinhardt, *A Theory of Biological Pattern Formation*, Kybernetik, **12**, (1972), pp. 30–39.

[27] C. Gui, J. Wei, *Multiple Interior Peak Solutions for Some Singularly Perturbed Neumann Problems*, J. Diff. Eq. **158**, No. 1, (1999), pp. 1-27.

[28] P. Gray and S.K. Scott, *Autocatalytic reactions in the isothermal, continuous stirred tank reactor: isolas and other forms of multistability*, Chem. Eng. Sci. 38 (1983), 29-43.

[29] P. Gray and S.K. Scott, *Autocatalytic reactions in the isothermal, continuous stirred tank reactor: oscillations and instabilities in the system $A + 2B \rightarrow 3B, B \rightarrow C$*, Chem. Eng. Sci. 39 (1984), 1087-1097.

[30] B. Gustafsson, *On the Convexity of a Solution of Liouville's Equation*, Duke Math. J., **60**, No. 2, (1990), pp. 303-311.

[31] H.A. Haus, *Theory of mode locking with a slow saturable absorber*, IEEE J. Quantum Electronics **11**, 736-746 (1975)

[32] H.A. Haus, *Theory of modelocking with a fast saturable absorber*, J. Appl. Phys., **46**, 3049-3058 (1975)

[33] L. Harrison, D. Holloway, *Order and Localization in Reaction-Diffusion Pattern*, Physica A, **222**, (1995), pp. 210-233.

[34] E. Hairer, S.P. Norsett and G. Wanner, *Solving ordinary differential equations I. Nonstiff problems. 2nd Edition*, Springer series in computation mathematics, Spring-verlag (1993).

[35] J.K. Hale, L.A. Peletier and W.C. Troy, *Exact homoclinic and heteroclinic solutions of the Gray-Scott model for autocatalysis*, SIAM J. Appl. Math. 61 (2000), 102-130.

[36] J.K. Hale, L.A. Peletier and W.C. Troy, *Stability and instability in the Gray-Scott model: The case of equal diffusivities*, Appl. Math. Lett. 12 (1999), 59-65.

[37] D. Iron, M. J. Ward, *A Metastable Spike Solution for a Non-Local Reaction-Diffusion Model*, SIAM J. Appl. Math., **60**, No. 3, (2000), pp. 778-802.

[38] D. Iron, M. J. Ward, *The Dynamics of Boundary Spikes for a Non-local Reaction-Diffusion Model* , Europ. J. Appl. Math., **11**, No. 5, (2000), pp. 491-514

[39] D. Iron, M. J. Ward, *The dynamics of multi-spike solutions to the one-dimensional Gierer-Meinhardt Model* , SIAM J. Appl. Math., **62** No. 6, (2002), pp. 1924-1951. (electronic)

[40] D. Iron, M. J. Ward, J. Wei, The Stability of Spike Solutions to the One-Dimensional Gierer-Meinhardt Model, *Physica D*, 150 (2001), 25-62.

[41] N. Joly and S. Bielawski, *Suppression of Q-switch instabilities by feedback control in passively mode-locked lasers*, Opt. Lett. **26**, 692-694 (2001)

[42] F.X. Kärnter, J. Aus der Au, and U. Keller, Mode-locking with slow and fast saturable absorbers – what's the difference?, IEEE J. of Select. Topics in QUantum Electronics 4, 159-168 (1998)

[43] A.J. Koch and H. Meinhardt, *Biological pattern formation: from basic mechanisms to complex structures*, Reviews of Modern Physics, Vol. 66 No. 4, 1481-1507 (1994)

[44] T. Kolokolnikov, M.J. Ward, and J. Wei,*The existence and stability of spike equilibria in the one-dimensional Gray-Scott model: the pulse-splitting regime*, preprint.

[45] T. Kolokolnikov, M.J. Ward, and J. Wei,*Zigzag and breakup instabilities of stripes and rings in the two-dimensional Gray-Scott model*, preprint.

[46] T. Kolokolnikov, and M.J. Ward, *Reduced Wave Green's functions and their effect on the dynamics of a spike for the Gierer-Meinhard model*, Euro. J. Appl. Math. **14** (2003) no. 5, 513-545.

[47] T. Kolokolnikov, and M.J. Ward, *Bifurcation of spike equilibria in the near-shadow Gierer-Meinhard model, to appear*, Discrete and Continuous Dynamical Systems B (2002), 32 pages.

[48] T. Kolokolnikov, and J. Wei, *On ring-like solutions for the Gray-Scott Model: existence, instability and self-replicating rings*, submitted, Nonlinearity (2003).

[49] M. Kowalczyk, *Multiple Spike Layers in the Shadow Gierer-Meinhardt System: Existence of Equilibria and Approximate Invariant Manifold*, Duke Math. J., **98**, No. 1, (1999), pp. 59-111.

[50] G.L. Lamb, *Elements of Soliton theory*, Willey Interscience, (1980).

[51] F. H. Lin, Q. Du, *Ginzburg-Landau Vortices: Dynamics, Pinning and Hysteresis*, SIAM J. Math. Anal., **28**, (1997), pp. 1265-1293.

[52] K. J. Lee, W. D. McCormick, J. E. Pearson, and H. L. Swinney, *Experimental observation of self-replicating spots in a reaction-diffusion system*, Nature 369 (1994), 215-218.

[53] K. J. Lee, W. D. McCormick, Q. Ouyang, and H. L. Swinney, *Pattern formation by interacting chemical fronts*, Science 261 (1993), 192-194.

[54] H. Meinhardt, *Models of Biological Pattern Formation*, Academic Press, London, (1982).

[55] D. Morgan, A. Doelman, T. Kaper, *Stationary periodic patterns in the 1D Gray-Scott model*, Methods and Applications of Analysis 7 (2000), 105-150.

[56] D. Morgan, T. Kaper, *Axisymmetric ring solutions of the 2-D Gray-Scott model and their destabilization into spots*, submitted, Physica D.

[57] C.B. Muratov, V.V. Osipov, *Static spike autosolitons in the Gray-Scott model*, J. Phys. A 33 (2000), 8893-8916.

[58] C.B. Muratov, V.V. Osipov, *Stability of the static spike autosolitons in the Gray-Scott model*, SIAM J. Appl. Math., **62**, No. 5, (2002), pp. 1463-1487.

[59] C.B. Muratov, V.V. Osipov, *Spike autosolitons and pattern formation scenarios in the two-dimensional Gray-Scott model*, Eur. Phys. J. B **22** (2001) 213-221

[60] C.B. Muratov, V.V. Osipov, *Traveling spike autosolitons in the Gray-Scott model*, Physical D, 155 (2002), 1463-1487.

[61] J.D. Murray, *Mathematical Biology*. Berlin, Springer-Verlag (1989).

[62] G. Nicolis and I. Prigogine, *Self-Organization in Nonequilibrium Systems*. Wiley, New York, 1977

[63] Y. Nishiura and D. Ueyama, *A skeleton structure of self-replicating dynamics*, Physica D 130 (1999), 73-104.

[64] Y. Nishiura and D. Ueyama , *Spatio-temporal chaos for the Gray-Scott model*, Physica D 150(2001) 137-162.

[65] J.E. Pearson , *Complex patterns in a simple system*, Science 261 (1993), 189-192.

[66] J. Reynolds, J. Pearson and S. Ponce-Dawson , *Dynamics of self-replicating spots in reaction-diffusion systems*, Phy. Rev. E 56 (1)(1997),185-198.

[67] J. Reynolds, J. Pearson and S. Ponce-Dawson, *Dynamics of self-replicating patterns in reaction diffusion systems*, Phy. Rev. Lett. 72 (1994), 2797-2800.

[68] L.A. Segel and J.L. Jackson, *Dissipative structure: an explanation and an ecological example*, J. Theor. Biol. 37 (1972), 545-549

[69] W. Sun, T. Tang, M. J. Ward and J. Wei *Numerical Challenges for Resolving Spike Dynamics for Two Reaction-Diffusion Systems*, Studies in Applied Math, Vol. 111, No. 1, (2003), pp. 41-84.

[70] M. Titcombe, M. J. Ward, *Summing Logarithmic Expansions for Elliptic Equations in Multiply-Connected Domains with Small Holes*, 7, No. 3, (1999), pp. 313-343.

[71] A. Turing, *The Chemical Basis of Morphogenesis*, Phil. Trans. Roy. Soc. B, **237**, (1952), pp. 37-72.

[72] D. Ueyama, *Dynamics of Self-Replicating Patterns in the One-Dimensional Gray-Scott Model*, Hokkaido Math J., **28**, No. 1, (1999), pp. 175-210.

[73] M. J. Ward, *An Asymptotic Analysis of Localized Solutions for Some Reaction-Diffusion Models in Multi-Dimensional Domains*, Stud. Appl. Math., **97**, No. 2, (1996), pp. 103-126.

[74] M. Ward, T. Kolokolnikov and J. Wei, *The stability of spike equilibria in the one-dimensional Gray-Scott model: the low feed-rate regime*, submitted, AMS Monographs (2003).

[75] M. J. Ward, W. D. Henshaw, J. B. Keller, *Summing Logarithmic Expansions for Singularly Perturbed Eigenvalue Problems*, SIAM J. Appl. Math., **53**, No. 3, (1993), pp. 799-828.

[76] M. J. Ward, D. McInerney, P. Houston, D. Gavaghan, P. Maini, *The Dynamics and Pinning of a Spike for a Reaction-Diffusion System*, SIAM J. Appl. Math., to appear, (2002).

[77] M. J. Ward, J. Wei, *Hopf Bifurcations and Oscillatory Instabilities of Spike Solutions for the One-Dimensional Gierer-Meinhardt Model*, Journal of Nonlinear Science, **13**, No. 2, (2003), pp. 209-264.

[78] J. Wei, *On single interior spike solutions of the Gierer-Meinhardt system: uniqueness and spectrum estimate*, Euro. Journal Appl. Math. 10 (1999), 353-378.

[79] J. Wei, *Existence, stability and metastability of point condensation patterns generated by Gray-Scott system*, Nonlinearity 12 (1999), 593-616.

[80] J. Wei, *Pattern formations in two-dimensional Gray-Scott model: existence of single-spot solutions and their stability*, Physica D 148 (2001), 20-48.

[81] J. Wei, *On the Interior Spike Layer Solutions to a Singularly Perturbed Neumann Problem*, Tohoku Math. J., **50**, (1998), pp. 159-178.

[82] J. Wei, *Uniqueness and Critical Spectrum of Boundary Spike Solutions*, Proc. Royal Soc. Edinburgh, Section A (Mathematics), **131**, No. 6, (2001), pp. 1457–1480.

[83] J. Wei, M. Winter, *Spikes for the Two-Dimensional Gierer-Meinhardt System: the Weak Coupling Case*, J. Nonlinear Science, to appear, (2002).

[84] J. Wei, M. Winter, *Spikes for the Two-Dimensional Gierer-Meinhardt System: the Strong Coupling Case*, J. Diff. Eq, to appear, (2002).

[85] J. Wei and M. Winter, *Asymmetric spotty patterns for the Gray-Scott model in R^2*, Stud. Appl. Math. 110 (2003), no. 1, 63-102.

[86] R. Wong, *Asymptotic Approximations of Integrals*, Academic Press, (1989).